Structure Functions of the Nucleon in a Soliton Model

by

Ishmael Takyi

Dissertation presented for the degree of Doctor of Philosophy in the Faculty of Science at Stellenbosch University

Supervisor: Prof. Herbert Weigel

Co-supervisor: Prof. Frederik G. Scholtz

April 2019

Declaration

By submitting this dissertation electronically, I declare that the entirety of the work contained therein is my own, original work, that I am the sole author thereof (save to the extent explicitly otherwise stated), that reproduction and publication thereof by Stellenbosch University will not infringe any third party rights and that I have not previously in its entirety or in part submitted it for obtaining any qualification.

Date: April 2019

Abstract

Structure Functions of the Nucleon in a Soliton Model

I. Takyi

Department of Physics
Merensky Building, Merriman Ave.
Stellenbosch University
Private Bag X1, Matieland, 7602, South Africa.

Dissertation: PhD (Theoretical Physics)

April 2019

We study nucleon structure functions (both polarized and unpolarized functions) within the Nambu-Jona-Lasinio (NJL) model, in which the nucleons emerge as solitons. In particular we investigate the polarized vacuum contribution to the nucleon structure functions. Rather than copying the quark distribution interpretation from QCD, we start from a fully regularized action functional to establish an intrinsically consistent formulation of the structure functions. For that matter we will employ the Pauli-Villars subtraction scheme to incorporate the vacuum polarization effects within the bosonized NJL model. Using Cutkosky's rules the structure functions are extracted from the imaginary part of the Compton tensor. The structure functions are then evaluated numerically which includes a perturbative DGLAP evolution calculation before comparing our results with empirical data.

Uittreksel

Struktuurfunksies van die Nukleon binne 'n Soliton Model

I. Takyi

Department Fisika
Merenskygebou, Merrimanlaan
Universiteit Stellenbosch
Privaatsak X1, Matieland, 7602, Suid-Afrika.

Proefskrif: PhD (Teoretiese Fisika)

April 2019

Ons bestudeer kern struktuurfunksies (beide gepolariseerd en ongepolariseerd) binne die Nambu-Jona-Lasinio (NJL) model, waarin die nukleone as soliton oplossings verskyn. In besonder ondersoek ons die gepolariseerde vakuumbydra tot die nukleon struktuurfunksies. Eerder as om die kwark-verdeling interpretasie van KCD te gebruik, begin ons vanaf 'n volledig geregulariseerde aksiefunksionaal om 'n intern konsekwente formulering van die struktuurfunksies te vestig. Hiervoor sal ons die Pauli-Villars-aftrekskema gebruik om die vakuumpolarisasie-effekte binne die gebosoniseerde NJL-model in te sluit. Met behulp van Cutkosky se reëls word die struktuurfunksies uit die imaginêre deel van die Compton tensor verkry. Die struktuurfunksies word dan numeries geëvalueer, wat 'n steuringsteoretiese implementasie van 'n DGLAP evolusie berekening insluit voordat ons resultate met empiriese data vergelyk word.

Acknowledgements

I am grateful to the Almighty God who is the source of my inspiration, strength and provider and without whom this project would not have been accomplished.

I will like to express my profound gratitude to my supervisor Professor Herbert Weigel, who has journeyed with me through my masters to this level. He has been my mentor and motivator in carrying out this work. I will also like to thank Stellenbosch Institute for Advance Studies (STIAS) for financing my studies.

And finally I am pleased to thank my mother, Margaret Nti and sister, Abigail Takyi for their encouragement in carrying out this project. I am highly indebted to my friends Kenneth Dadedzi, Paul Williams, Stanard Mebwe, Somialo Azote, George Dwapanyin and the Stellenbosch Physics Department for their love and support.

Contents

List of Figures

List of Tables

Chapter 1

Introduction

One of the most challenging problems in particle physics is to understand the relation between the fundamental degrees of freedom in strong interactions (quarks and gluons) and the observed hadrons (pions, nucleons etc.). In this respect structure functions play a key role. They describe the distribution of quarks and gluons inside hadrons. Colloquially speaking, structure functions are the hadron wave-functions. Quantitative information on structure functions are obtained in the deep inelastic scattering of leptons on hadrons. Evolution of these functions at high Q^2 values has been proven successful in the field of perturbative quantum chromodynamics (QCD) when compared to empirical data. However, at low Q^2 values the physics behind it is highly nonperturbative. The nonperturbative treatment of QCD is essentially inaccessible and requires the use of effective models. Beforehand the discrete lattice gauge theory has been used in nonperturbative treatment of hadron properties in QCD. However, computation of the structure function (especially inclusion of the Dirac sea contribution) using the lattice gauge theory becomes a challenge. In this thesis we compute (the evolution of) these structure functions (including the Dirac sea contributions) by employing an effective chiral soliton model.

In the remainder of this chapter we review some essential features of QCD at low energies and how we want to implement them in an effective theory. The outline of this thesis is presented at the end of this chapter.

1.1 QCD as Strong Interaction

The quest to find the fundamental structure (elementary particles) of matter led to the discovery of the atom by Joseph John Thomson in 1897, Ernest Rutherford in 1911 and subsequently James Chadwick in 1932. Their studies revealed that the atom is made of a central nucleus (consisting of positively charged protons (p) and neutral neutrons (n)) with negatively charged electrons (e) (classically) orbiting around it and held in place by an attractive electrical force which emanates from their respective charges[1]. At this stage the nucleus and electrons were

[1]Here we refrain from the detailed discussion of the atom and its properties.

considered as the elementary particles of nature that are bound to the atom by the electrostatic force. The question, what holds the nucleus together, as the closely packed positively charged protons repel each other, led to the discovery of quarks; which are the constituents components of protons and neutrons and are bound together by a strong force.

Subsequent studies revealed that aside from electrons there are the muons (μ), tau (τ) and their neutrinos (ν); collectively called leptons. These leptons together with quarks form the fundamental structure of matter. The weak and electromagnetic forces are the interactions of leptons. Quarks and leptons are spin-$\frac{1}{2}$ fermions. Along strong, weak, and electromagnetic forces there is the gravitational force - together these four form the fundamental forces of nature. On the level of elementary particle physics the gravitational force is so weak that it may be safely ignored.

Once the elementary particles have been identified their interactions must be clarified. The gauge field theory has proven successful in describing the interaction of particles. In these theories forces are described by (virtual) gauge bosons propagating between the fermions. The gauge is typically represented by a unitary ($U(N)$) or special unitary ($SU(N)$) Lie group. The fermions and gauge bosons are elements of the fundamental and adjoint representations. (The role of the Higgs boson need not be discussed here). The dimension, N, of the Lie group is the number of elementary fermions. Then there are N^2 and N^2-1 gauge bosons for unitary and special unitary gauge theories, respectively. For example in electromagnetic interaction between the leptons is mediated by a gauge boson called photon, the quantized electromagnetic field and the gauge theory is called Quantum electrodynamics (QED) which is a $U(1)$ gauge symmetry. For strong interactions, the forces between quarks are mediated by the gluon gauge field and the gauge theory is known as Quantum chromodynamics (QCD) with its gauge symmetry given as $SU(N_c)$, where $N_c = 3$ are the color charges of the quarks. Like the electromagnetic charge in QED, color is conserved in QCD. While the photon has no electromagnetic charge, the gluons do have color charge and interact directly with each other. This makes QCD much more complicated than QED.

QCD is defined by the Lagrangian[5]

$$\mathcal{L}_{QCD} = \bar{q}\left(\imath\partial\!\!\!/ - m^0\right)q - \frac{1}{4}F^{a\mu\nu}F^a_{\mu\nu} + g_{QCD}\bar{q}\gamma^\mu A^a_\mu \frac{\lambda^a}{2}q, \tag{1.1.1}$$

which describes the structure and dynamics of hadrons (we will discuss this in the next section) by an interaction that mediates gluon gauge fields (A^a_μ) between the color degrees of the quarks (q) with the coupling strength g_{QCD}. The color quantum numbers of the quark takes three different values, which conveniently are named as red(R), green(G) and blue(B). The eight (for $N_c = 3$) Gell-Mann matrices λ^a are the generators of the gauge group in the fundamental representation. They are hermitian and traceless with the commutation relation

$$\left[\frac{\lambda^a}{2}, \frac{\lambda^b}{2}\right] = \imath f^{abc}\frac{\lambda^c}{2}, \tag{1.1.2}$$

where f^{abc} are the structure constants of the color gauge group.

In addition the quarks posses a flavor quantum number (up, down, strange, charm, bottom, top) that eventually dictate the observable quantum numbers of hadrons. However, the color interaction is flavor-blind so that in the Lagrangian different flavors are reflected by the mass term

$$m^0 = \text{diag}\left(m_u^0, m_d^0, m_s^0, m_c^0, m_b^0, m_t^0\right). \tag{1.1.3}$$

The second term in the Lagrangian is the Yang - Mills Lagrangian with the non - Abelian field strength tensor

$$F_{\mu\nu}^a = \partial_\mu A_\nu^a - \partial_\nu A_\mu^a + g_{QCD} f^{abc} A_\mu^b A_\nu^c. \tag{1.1.4}$$

The non-Abelian nature of the theory is described by the term quadratic in A_μ^a with $f_{abc} \neq 0$. This non-Abelian feature of the field strength tensor causes the gluons not only to couple with the quarks but also with themselves (in cubic and quartic self-interactions); as such provide anti-screening of color charges in QCD. The last term denotes the coupling of gluons to the color currents,

$$j_\mu^a = \bar{q}\frac{\lambda^a}{2}\gamma_\mu q, \tag{1.1.5}$$

of the quarks.

One uniqueness of the strong interaction is that, the total amount of observed color is either zero or the three colors occur in equal proportions. As a results of this, all hadron states and physical observables are invariant under the color $SU(3)$ transformation, with the only colorless combinations being $q\bar{q}$ (mesons), qqq (baryons) and $\bar{q}\bar{q}\bar{q}$ (antibaryons). The phenomenon of non observability of colored states is phrased as the quark confinement which states that

one cannot observe a single quark on its own.

This can be thought of as follows: The quarks in a given hadron are bound together by the strong force. Hence pulling the quarks apart requires an energy to break the strong force of interaction. Eventually the energy needed to pull the quarks apart becomes large enough to create a new quark anti-quark pair. That is, instead of separating the colored quarks to build asymptotic states, new colorless hadrons are formed.

In particle physics, the coupling constant (dependent on the energy scale) determines the strength of the interactive force. When this coupling constant is small, a perturbative expansion is appropriate. For example in QED the coupling constant in the e^+e^- annihilation into $\mu^+\mu^-$ is of order

$$\alpha_{QED} = \frac{e^2}{4\pi} = \frac{1}{137} \tag{1.1.6}$$

which is small and hence perturbation theory can be applied in this QED process. To investigate the applicability of perturbation theory to QCD it is illuminating to apply renormalization group techniques and scale momentum variables $p \to \mu p$. Renormalization calculations [6]

transfer that scaling into a scale dependence of the coupling constant via the so-called β-function

$$\beta = \mu \frac{\mathrm{d}g_{QCD}}{\mathrm{d}\mu}. \tag{1.1.7}$$

At one loop order one finds $\beta = -\beta_0 g_{QCD}^3$ which $\beta_0 > 0$ unless there are more than 16 quark flavors. The positivity of β_0 in QCD is due to the gluon self-interactions and thus opposite to QED. As a result the coupling constant scales as

$$g_{QCD}^2 = \frac{g_0}{1 + 2\beta_0 g_0^2 \ln \frac{\mu}{\mu_0}}, \tag{1.1.8}$$

with μ_0 being the reference scale such that $g_{QCD}(\mu_0) = g_0$. At large momentum scales g_{QCD} becomes small (feature called asymptotic freedom) and perturbation techniques can be applied. Comparison with data this gives $\mu_0 \sim \Lambda_{QCD} \sim 200\,\mathrm{MeV}$. But for small momentum scales g_{QCD} becomes large and this requires inclusion of higher powers of g_{QCD} in its perturbation expansion. Eventually the perturbation expansion fails. There are attempts to compute low energy hadron properties in QCD using discrete lattice theory with non-perturbative techniques. However, calculations of hadron properties from this approach become difficult for small (realistic) quark masses. It is therefore unavoidable to analyze effective models of the strong interaction that mimic some properties of the low-energy dynamics of QCD reflected by particular symmetries. We will discuss an example of these models in the next chapter.

1.2 Hadrons

We have seen that, quarks (and leptons) are the fundamental building blocks of matter. The quarks come in six flavors, namely, up (u), down (d), strange (s), charm (c), bottom (b) and top (t). Table 1.1 shows the charges and current masses of these flavor quarks. To each of these flavored quark (q) corresponds an anti-quark($\bar{q}$) with opposite charge. As mentioned quarks must combine to color neutral bound states. Two types of low-lying color neutral bound states are observed

- mesons, these are an antisymmetric combination of a quark and an anti-quark.
- baryons, these are bound states of three quarks.

Collectively these baryons and mesons are called hadrons.

At higher energies also tetraquarks (two quarks - two anti-quarks) and pentaquarks (four quarks- one anti-quark) have recently been established, cf. Ref [7]. They will not be the subject of the current project. Rather the objects of interest are the protons and neutrons, generically called nucleons. These fermions are the lightest baryons, as their quantum numbers are made of up (u) and down (d) quarks. The proton has the quantum numbers (flavors) of two up (u) quarks and one down (d) quark, uud, with an integer charge of one and mass,

Flavor	Charge	Mass(MeV)
up (u)	$\frac{2}{3}$	2.3
down (d)	$-\frac{1}{3}$	4.8
strange (s)	$-\frac{1}{3}$	95
charm (c)	$\frac{2}{3}$	1275
bottom (b)	$-\frac{1}{3}$	4180
top (t)	$\frac{2}{3}$	173500

Table 1.1: The six flavor quarks with their charges and masses.

$m = 938.272\,\text{MeV}$, whilst the neutron has one up (u) quark and two down (d) quarks, udd, with zero charge and mass, $m = 939.565\,\text{MeV}$[8].

1.2.1 Nucleon and Isospin

Since the masses of proton and neutron are essentially the same, they are regarded as two 'states' of the same particle called the 'nucleon' (N). Proton and neutron are the two components of the nucleon

$$N = \begin{pmatrix} p \\ n \end{pmatrix}. \tag{1.2.1}$$

In analogy to spin, $\vec{S}$, the mathematical structure used to describe the nucleon is called isospin, $\vec{I} = \frac{1}{2}\vec{\tau}$, satisfying the commutation relation

$$[I_i, I_j] = \imath\epsilon_{ijk} I_k \tag{1.2.2}$$

where the components of the isovector $\vec{\tau}$ are the isospin versions of the Pauli matrices with

$$\tau_1 = \begin{pmatrix} 0 & 1 \\ 1 & 0 \end{pmatrix}, \quad \tau_2 = \begin{pmatrix} 0 & -\imath \\ \imath & 0 \end{pmatrix} \quad \text{and} \quad \tau_3 = \begin{pmatrix} 1 & 0 \\ 0 & -1 \end{pmatrix}. \tag{1.2.3}$$

The nucleon is assigned with an isospin of $I = \frac{1}{2}$ and its states are differentiated by the isospin projection, I_3. The proton state is assigned with the isospin projection $I_3 = \frac{1}{2}$ and that of the neutron state as $I_3 = -\frac{1}{2}$. As the strong interaction does not (or almost not) distinguish protons and neutrons, isospin should indeed be a symmetry, at least approximately. On the QCD level this is reflected by the fact that the corresponding quark mass difference is significantly smaller than the interaction scale $|m_u - m_d| \ll \Lambda_{QCD}$.

1.3 Chiral Symmetry

In this section we discuss the symmetry properties of the QCD Lagrangian (1.1.1). We consider the Dirac equation for the quark fields

$$\left(\not{p} + g_{QCD}\not{A} + m\right) q = 0. \tag{1.3.1}$$

This equation does not change when multiply by γ_5

$$\gamma_5 \left(\not{p} + g_{QCD}\not{A} + m\right) q = 0. \tag{1.3.2}$$

Using the commutation relation $\{\gamma_\mu, \gamma^5\} = 0$ one obtains

$$\left(\not{p} + g_{QCD}\not{A} - m\right) (\gamma_5 q) = 0. \tag{1.3.3}$$

But when restricted to up and down quarks, the mass term m in (1.3.1) is negligible compared to the energy scale of the QCD interaction rate. For example in the e^+e^- annihilation to hadrons the energy scale of the interaction rate is of order $\Lambda_{QCD} = 200\,\text{MeV}$ as compared to a mass of $m \approx 9\,\text{MeV}$. Thus, in QCD one can consider $m = 0$ as an appropriate approximation. This means that, for a free quark ($m = 0$) both q and its helicity partner $\gamma_5 q$ are eigenstates of its Hamiltonian

$$H = \vec{\alpha} \cdot \vec{p} + g_{QCD}\not{A}. \tag{1.3.4}$$

Thus, QCD exhibits chiral symmetry, at least approximately.

Furthermore, one can easily verify that for $m = 0$, the QCD Lagrangian is invariant under the global flavor rotations

$$q \to U_V(N_f)q, \quad U_V(N_f) = e^{\imath\theta_V^a \left(\frac{\lambda_a}{2}\right)_f} \tag{1.3.5}$$

and axial-vector (chiral) flavor transformation

$$q \to U_A(N_f)q, \quad U_A(N_f) = e^{\imath\gamma_5\theta_A^a \left(\frac{\lambda_a}{2}\right)_f} \tag{1.3.6}$$

respectively, where N_f is the number of flavors and $\left(\frac{\lambda_a}{2}\right)_f$ are generators of the flavor group $U(N_f)$. The above transformations correspond to the

$$U_V(N_f) \otimes U_A(N_f) \tag{1.3.7}$$

symmetry.

In the next step, we define two-component spinors

$$q_R = \frac{1}{2}(1 + \gamma_5)q = P_R q \quad \text{and} \quad q_L = \frac{1}{2}(1 - \gamma_5)q = P_L q \tag{1.3.8}$$

as linear combinations of the two eigenstates q and $\gamma_5 q$. Here $P_{R,L}$ are the orthogonal chiral projection operators satisfying

$$P_R + P_L = 1, \quad P_{R,L}^2 = P_{R,L} \quad \text{and} \quad P_R P_L = P_L P_R = 0. \tag{1.3.9}$$

Let $\theta_A = \theta_A^a \left(\frac{\lambda_a}{2}\right)_f$ and $\theta_V = \theta_V^a \left(\frac{\lambda_a}{2}\right)_f$ then we have that under the chiral transformation (1.3.7), the infinitesimal transformation of the quark fields read

$$q \to (1 + \theta_V + \gamma_5 \theta_A)\, q = (1 + P_R(\theta_V + \theta_A) + P_L(\theta_V - \theta_A))\, q. \tag{1.3.10}$$

Upon exponentiation this yields

$$q_L \to e^{\imath\theta_L} q_L \quad \text{and} \quad q_R \to e^{\imath\theta_R} q_R, \tag{1.3.11}$$

with $\theta_{L,R} = \theta_V \mp \theta_A$. Thus, left-and right-handed flavor transformations independently act on the left- and right- handed quark fields, respectively. Furthermore they decouple as

$$\bar{q}\left(\imath\partial\!\!\!/ + g_{QCD}A\!\!\!/\right) q = \bar{q}_L \left(\imath\partial\!\!\!/ + g_{QCD}A\!\!\!/\right) q_L + \bar{q}_R \left(\imath\partial\!\!\!/ + g_{QCD}A\!\!\!/\right) q_R. \tag{1.3.12}$$

1.4 Dynamical Chiral Symmetry Breaking

Since equation (1.3.7) is only an approximate symmetry, it is suggestive to write the strong interaction Hamiltonian as

$$h = h_0 + \lambda h_1. \tag{1.4.1}$$

The Hamiltonian h_0 is invariant under this symmetry transformation, while h_1 describes the perturbation of the system. In the limit of $\lambda = 0$, all generators of the symmetry algebra are conserved[2]. In general the particle content of this symmetry forms degenerate multiplets, which correspond to irreducible representations of the group algebra of this symmetry. For the present case this would imply that parity doublets are (approximately) degenerate. This is not observed and can be understood by the vacuum configuration (of the Hamiltonian h_0) not being invariant under the symmetry transformation. Thus, the chiral symmetry is spontaneously broken.

In this case the symmetry operators do not transform to singlet states but rather develop non-zero vacuum expectation values (VEV). Moreover, massless particles are excited when (some of) the symmetry generators act on these VEV. These massless particles are the so-called Goldstone bosons. A study of the low-lying meson spectrum[9] reveals the pseudoscalar mesons as the Goldstone particles. Spontaneous symmetry breaking requires a non-zero order parameter. To relate to massless pseudoscalar mesons this order parameter must have the structure of a mass term. And indeed it is the quark condensate

$$\langle \bar{q} q \rangle \neq 0. \tag{1.4.2}$$

For $m \neq 0$ the mass term of the QCD Lagrangian breaks the chiral symmetry explicitly as its couples right-to left-handed quark field

$$\mathcal{L}_{\text{mass}} = -\bar{q} m^0 q = -\left(\bar{q}_R m^0 q_L + \bar{q}_L m^0 q_R\right). \tag{1.4.3}$$

[2]We will explore an example of such algebra conservation in the next chapter.

This mass term represents the explicit breaking of chiral symmetry and is reflected by the observed pseudoscalar mesons not being exactly massless.

We will take into account the above chiral symmetry and both its explicit and spontaneous breaking when analyzing effective models for low-energy QCD dynamics, whose mechanism yields the VEV of equation (1.4.2).

1.5 The $\frac{1}{N_c}$ Expansion

In this section we discuss how baryons emerge as solitons in the limit of $N_c \to \infty$, especially in the low-energy QCD dynamics [10, 11] where the perturbation expansion is out of reach as discussed in section 1.1. Here N_c is the number of colors and appears as a combinatorial factor. In Feynman diagrams, following Ref. [10] we will use combinatorics when discussing the underlying physics, in particular in the determination of Green functions, of the large-N_c limit of QCD. In our early discussion we have seen that QCD is a gauge theory of quark interactions, where each quark is equipped with a single color, with their interactions mediated by gauge bosons called gluons. This field carries two color charges, where one of these color charges couples to the quark spinor and the other couples to the conjugated spinor. The additional restriction that the color generators λ_i are traceless is subleading for large N_c. Thus, the gluon field appears as a combination of quark and anti-quark pair with N_c^2 color degrees. Hence, when considering the combinatorics of Feynman diagrams the gluon line is drawn as two lines; one for the quarks and other for the anti-quarks as shown in Figure 1.1.

Having clarified this, we consider as an example, the combinatorial factors associated with the one-loop gluon interaction in Figure 1.2, which must be of the order unity to ensure that an expansion in $\frac{1}{N_c}$ converges. On the right hand side of Figure 1.2 the color index of the outer quark line contracts with those of the initial and final states. Its quantum numbers are specified once the final and initial states are known. But the closed color line in the center of the figure contracts with itself with an unspecified quantum number. Summing over this undetermined color contributes a factor of N_c to the diagram. On the other hand each of the three-gluon interaction vertices contributes a factor of g_{QCD}, this gives an overall factor of g_{QCD}^2 to the diagram. But for a smooth large-N_c limit, the diagram in Figure 1.2 must be of order unity, this requires

$$g_{QCD} = \mathcal{O}\left(\frac{1}{\sqrt{N_c}}\right). \tag{1.5.1}$$

In what follows, we consider higher order QCD diagrams and compute the associated combina-

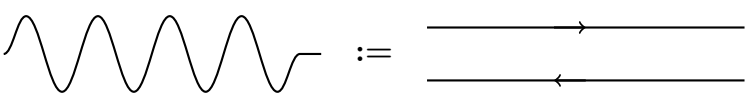

Figure 1.1: Double-line Feynman diagram for the gluon.

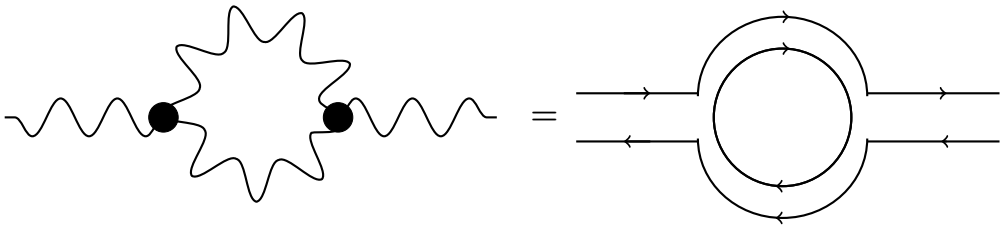

Figure 1.2: The double-line notation for the gluon vacuum polarization.

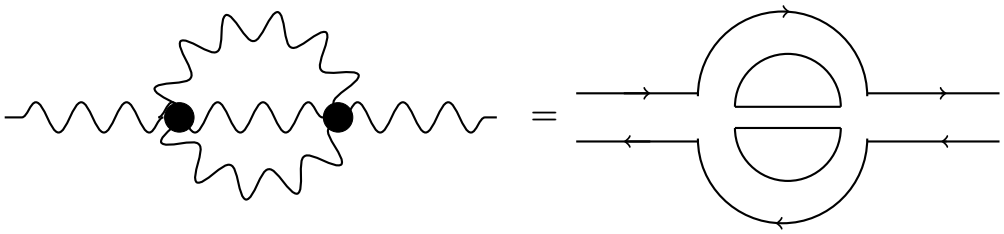

Figure 1.3: Feynman diagram for the two-loop gluon self interaction.

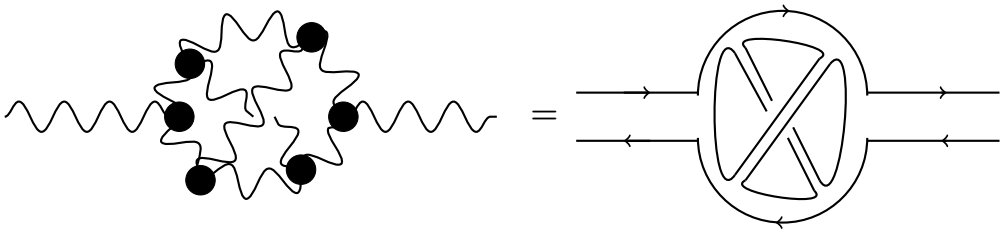

Figure 1.4: Non-planar diagram of gluon self-interaction.

toric factors. We seek to determine whether a given diagram will be of the order unity in the limit of $N_c \to \infty$. Consider the diagram in Figure 1.3. This has two color loops each having a combinatoric factor of N_c in its double-line notation with contributing factors of g^4_{QCD} from the interaction vertices, altogether the diagram is of order $g^4_{QCD}N_c^2 = 1$ and does survive in the large-N_c limit. This is a typical planar diagram because all quark lines and vertices can be drawn in a single plane. In contrast the diagram in Figure 1.4 is non planar (in the sense that the internal gluon lines crosses each other when drawn in a plane). The (tangled closed) color loop lines produces a combinatorial factor N_c to the diagram. However, it has six interaction vertices that produce the factor of g^6_{QCD}. Thus the full diagram is of order $g^6_{QCD}N_c = \dfrac{1}{N_c^2}$ and in the large-N_c limit its vanishes like $\dfrac{1}{N_c^2}$. In general, for large-N_c, all non-planar diagrams are suppressed by factors of $\dfrac{1}{N_c^2}$.

1.5.1 An Effective Theory for QCD in the Large-N_c limit

We have seen that all hadronic states are color singlets and their quantum numbers are determined entirely by their flavor content. Hence, in applications of the large-N_c limit to hadrons we consider matrix elements of color singlet quark bilinears, examples of which are $\bar{q}\gamma^\mu q$ and $\bar{q}\left(\imath\partial_\mu - g_{QCD}A_\mu\right)q$, where A_μ is the gluon field. Broadly we denote such quark bilinear operators as $J(x)$. This requires considering Feynman diagrams in which these bilinears couple to

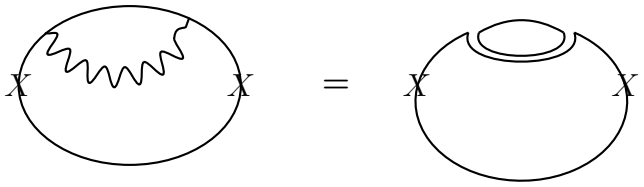

Figure 1.5: The coupling of quark bilinear J (coupling indicated by "X") loops in QCD.

gluons (loops). An example for such a Feynman diagram is shown in Figure 1.5. This diagram is of order $g^2_{QCD}N_c^2 = N_c$, which is the leading order coupling to quark bilinears. In general the leading order diagrams of Figure 1.5, possess the following properties[10]

- Internal lines of the diagram consist of only gluons.
- The diagrams are planar.
- Their edges are only made up of quark lines.

In what follows, we consider intermediate states between the quark bilinears in the large-N_c limit. These intermediate states are identified by cutting through diagrams that satisfy the above conditions using Cutkosky's rules. Since in the large-N_c limit planar diagrams with only quarks at the edges contribute to the matrix elements of the quark bilinears, the color indices along any cut combine to a single trace resulting to a single hadron (presuming the confinement hypothesis). For non-planar diagrams, the color indices along any cut form separated saturated sums. This corresponds to products of at least two color singlet hadrons. Hence, in the limit of $N_c \to \infty$ all intermediate states are quark bilinear color singlets, i.e one-meson intermediate states.

The fact that, these intermediate states are one-meson states, means that for large-N_c the bilinear quark operator $J(x)$ can be decomposed as

$$\langle J(x)J(y)\rangle = \int \frac{\mathrm{d}^4k}{(2\pi)^4} e^{\imath k(x-y)} \sum_j \frac{a_j(k)a_j^\dagger(k)}{k^2 - m_j^2}, \tag{1.5.2}$$

the sum goes over all meson states that couple to $J(x)$ and $a_j = \langle 0|J|j\rangle$ is the matrix element for J to create the j^{th} meson (mass m_j) from the vacuum. Using the properties of planar diagrams above, the following deductions can be made from equation (1.5.2):

- The right hand side is the sum of all planar diagrams for any N_c. The left hand side has a smooth limit as $N_c \to \infty$. Hence $m_j \sim \mathcal{O}(N_c^0)$.
- Also due to asymptotic freedom nature of QCD, one notices that equation (1.5.2) is logarithmically divergent for large k^2, as such there must be an infinite number of meson states. Equation (1.5.2) is formally a spectral representation. Hence the m_j must be real. This causes the mesons to be stable.

- Lastly, from the properties of planar diagrams, equation (1.5.2) should be of order N_c, which implies that the meson amplitude a_j should be of order $\sqrt{N_c}$.

Accordingly any interaction of n mesons is described by the product of n such operators and their vertex functions. Like before this product must be of order N_c i.e

$$\underbrace{\langle 0|J|j_1\rangle \cdot \cdots \cdot \langle 0|J|j_n\rangle}_{n \quad \text{factors}} \Gamma^{(n)}_{j_1 \cdots j_n} = N_c = N_c^{\frac{n}{2}} \times \Gamma^{(n)}_{j_1 \cdots j_n}, \tag{1.5.3}$$

here $\Gamma^{(n)}_{j_1 \cdots j_n}$ is the vertex contribution for the interaction of n mesons. Therefore the coupling constant of their interaction is of order

$$\Gamma^{(n)}_{j_1 \cdots j_n} = \mathcal{O}\left(N_c^{1-n/2}\right). \tag{1.5.4}$$

For example, meson-meson scattering is described by an $n = 4$ vertex function and thus scales like $\frac{1}{N_c}$. The decay of a single meson into m other mesons scales like $N_c^{1-\frac{m+1}{2}} = N_c^{\frac{1-m}{2}} \to 0$ as $N_c \to \infty$. The above results leads to the conjecture that at large-N_c, QCD is equivalent to a meson theory, with meson loops and coupling constants being suppressed as N_c becomes large [10, 11].

1.5.2 Properties of Baryons in large-N_c Limit

We now look at a (non-relativistic constituent picture of) baryon properties in the leading order of N_c. We first study the behavior of baryon masses in the large-N_c limit before discussing their interactions. This will give us a fair idea of the behavior of effective models for low-energy QCD.

1.5.2.1 Baryon Masses in Large-N_c Limit

In contrast to mesons which consist of quark anti-quark pairs ($\bar{q}q$), baryons are totally antisymmetric color singlets of N_c quarks. Therefore the shape of Feynman diagrams that describe any baryon property varies with N_c. Hence the large-N_c limit requires the combined N_c dependence coming from N_c quarks as well as their vertex contributions. As an example we consider two quarks inside a baryon that interact via the exchange of a virtual gluon. A typical diagram is shown in the left panel of Figure 1.6. Of course, there are $\frac{1}{2}N_c(N_c-1) \sim \frac{N_c^2}{2}$ such diagrams. The diagram has two interaction vertices producing a factor $g^2_{QCD} \sim \frac{1}{N_c}$. Putting things together gives a combinatoric factor of

$$\frac{1}{2}N_c^2\left(\frac{1}{N_c}\right) = \mathcal{O}(N_c). \tag{1.5.5}$$

Thus, it seems unpromising to have a smooth N_c-limit for baryons. Even for higher order diagrams like the right panel of Figure 1.6, we have the total vertex contribution $g^4_{QCD} = \frac{1}{N_c^2}$,

since there are two gluon exchanges. Also, the four quarks that exchange the gluons scales like $\frac{1}{4}N_c^4$. Altogether this gives a combinatoric factor of

$$\frac{1}{4}N_c^4\left(\frac{1}{N_c^2}\right) = \mathcal{O}(N_c^2), \tag{1.5.6}$$

and diverges as N_c grows. Thus studying of Feynman diagrams in the large-N_c limit of baryons is not convenient as they diverge when N_c becomes large.

For this reason we look at the behavior of the baryon mass in the limit of $N_c \to \infty$ as a many-body problem in a non-relativistic framework. Following the arguments of [10], we assume that the N_c quarks bound to the baryon are heavy. In the case of light quarks, the relativistic effects do not change the large-N_c results qualitatively. In what follows, we apply the Hartree-Fock approximation in treating the non-relativistic many-body problem by assuming that the quark interaction is small. Of course this is the case as any one quark interacts with $N_c - 1$ remaining ones with strength $\dfrac{1}{N_c}$ and the mean field potential is of order one. Thus, the Hamiltonian including the quark mass (M) after taking Fourier transform of the gluon propagator in the static approximation (since the quarks are heavy) to coordinate space reads

$$H = N_c M + \sum_{i=1}^{N_c}\frac{-\vec{\partial}_i^2}{2M} - \frac{g^2}{N_c}\sum_{i>j}^{N_c}\frac{1}{|\vec{r}_i - \vec{r}_j|}. \tag{1.5.7}$$

Here $g = \sqrt{N_c}g_{QCD}$ and is of the order unity for large N_c. To have a valid description of the Hamiltonian (1.5.7) requires to symmetrize it with respect to space and spin, hence we omit spin-dependence forces. The construction of the ground state wave-function requires to place each quark in the ground state of a mean field potential. This motivates to write the many-body wave function as a product of the normalized one-particle wave function ϕ of the quarks, i.e

$$\Psi\left(\vec{r}_1, \cdots, \vec{r}_{N_c}\right) = \prod_{i=1}^{N_c}\phi(\vec{r}_i). \tag{1.5.8}$$

To determine ϕ, we write the total energy $E = N_c\epsilon$, where ϵ is the energy of each quark. Ultimately we apply the variational principle to

$$\langle\Psi|H - E|\Psi\rangle = -N_c\epsilon + N_c M + \frac{N_c}{M}\int \mathrm{d}^3 r\, \vec{\partial}\phi^*(\vec{r})\cdot\vec{\partial}\phi(\vec{r}) - \frac{N_c(N_c-1)}{2}\frac{g^2}{N_c}\int \mathrm{d}^3 r_1 \int \mathrm{d}^3 r_2\, \frac{|\phi(\vec{r}_1)|^2|\phi(\vec{r}_2)|^2}{|\vec{r}_1 - \vec{r}_2|}. \tag{1.5.9}$$

yielding, for $N_c \to \infty$

$$-\frac{\vec{\partial}^2}{2M}\phi(\vec{r}_1) - g^2\phi(\vec{r}_1)\int \mathrm{d}^3 r_2\, \frac{|\phi(\vec{r}_2)|^2}{|\vec{r}_1 - \vec{r}_2|} - \epsilon\phi(\vec{r}_1) = 0. \tag{1.5.10}$$

Obviously the common factor N_c has canceled showing that ϕ and ϵ are $\mathcal{O}(N_c^0)$. Hence the baryon masses are of order N_c. It can be deduced from the above argument that the baryon radius

$$\langle r^2\rangle = \frac{1}{N_c}\langle\Psi|\sum_i r_i^2|\Psi\rangle \tag{1.5.11}$$

is of the order unity since ϕ is $\mathcal{O}(N_c^0)$. In our later discussion we will see that indeed soliton models for baryons predict their total energy to be of order N_c.

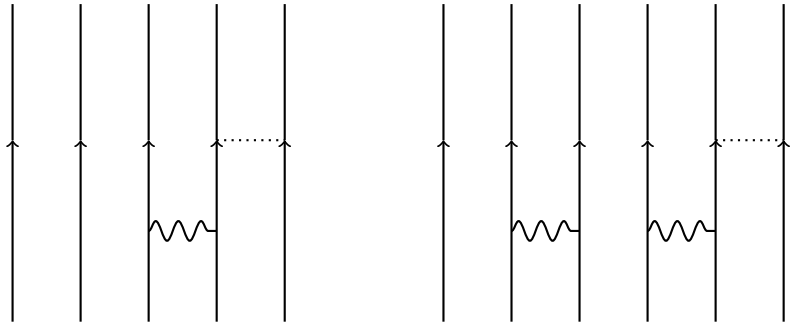

Figure 1.6: Left panel: Feynman diagram for propagating N_c quarks inside baryons with one gluon exchange. Right panel: Feynman diagram for propagating N_c quarks inside baryons with two gluon exchange.

1.5.2.2 Scattering Processes of Hadrons in Large-N_c Limit

Here using non-relativistic theory, we discuss hadron scattering processes and the large N_c limit of their scattering amplitudes. Hadron scattering processes can either be baryon-baryon, baryon-antibaryon and baryon-meson scatterings.

As before, we will first visualize the combinatoric factors associated with such interactions before applying the Hartree-Fock approximation. We first consider baryon-baryon scattering. The leading order (in g_{QCD}) diagram is shown in the left panel of Figure 1.7: a gluon is exchanged between quarks from the two baryons. The one-gluon exchange has the combinatoric factor N_c^2. The two vertices contribute $g_{QCD}^2 = \frac{1}{N_c}$. Hence the one-gluon exchange in baryon-baryon scattering scales as

$$N_c^2 \left(\frac{1}{N_c}\right) = N_c. \tag{1.5.12}$$

This is the same as for the baryon mass. In what follows we will adopt the approach to the baryon mass by considering the $2N_c$ quarks to be heavy and using the non-relativistic many-body theory in Hartree approximation. A few remarks are in order for the baryon-baryon interaction: the two baryons either repel or attract each other, therefore we will make use of the time-dependent Schrödinger equation for the $2N_c$ quarks. Since there are $2N_c$ quarks with only N_c colors for this system, the Pauli-exclusion principle forbids us to place the $2N_c$ quarks in one space-spin wave function. Instead we consider time-dependent normalized space-spin wave functions $\phi_i(\vec{r}, t), i = 1, 2$, one for each of the N_c quarks in the $2N_c$ quarks system.

Having made this clarification the ansatz for the many-body wave function becomes

$$\Psi\left(\vec{r}_1, \cdots, \vec{r}_{2N_c}, t\right) = \sum_p (-1)^p \prod_{i=1}^{N_c} \phi_1(\vec{r}_i, t) \prod_{j=1}^{N_c} \phi_2(\vec{r}_{N_c+j}, t). \tag{1.5.13}$$

This wave function is anti-symmetrized between the quarks from the two baryons. In the next step, we apply the time dependent variational principle, i.e $\left\langle \Psi | H - \imath \frac{\partial}{\partial t} | \Psi \right\rangle$, to determine the normalized wave functions ϕ_i. We then obtain the variational equation [10]

$$g^2 \phi_1(\vec{r}_1, t) \int \mathrm{d}^3 r_2 \, \frac{|\phi_1(\vec{r}_2, t)|^2}{|\vec{r}_1 - \vec{r}_2|} + g^2 \phi_2(\vec{r}_1, t) \int \mathrm{d}^3 r_2 \, \frac{\phi_2^*(\vec{r}_2, t)\phi_1(\vec{r}_2, t)}{|\vec{r}_1 - \vec{r}_2|} + \frac{\vec{\partial}^2}{2M} \phi_1(\vec{r}_1, t) + \imath \frac{\partial}{\partial t} \phi_1(\vec{r}_1, t) = 0, \tag{1.5.14}$$

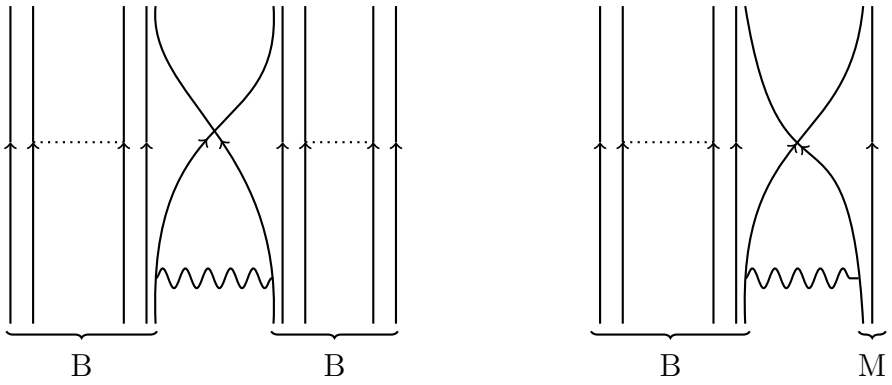

Figure 1.7: Left Panel: Baryon-baryon scattering by a single exchange of gluon. Right panel: Baryon-meson scattering by a single exchange of gluon

for the single quark wave-function ϕ_1 and a similar one for ϕ_2. Obviously this equation does not contain N_c. We then conclude that the scattering wave-function (1.5.13) has a smooth large N_c limit; so does the baryon-baryon scattering amplitude. For the meson-baryon scattering (right panel of Figure 1.7) the vertices contributes $\frac{1}{N_c}$. Since the mesons contain only one quark, the combinatoric factor is N_c. Altogether, this diagram is $\mathcal{O}(N_c^0)$. Thus in the limit of $N_c \to \infty$, the baryon-baryon scattering is stronger as compared to that of the meson-baryon system. Since the baryon is infinitely heavy in the large-N_c limit, only the mesons react in the scattering process leaving the baryons unaffected. Thus meson-baryon scattering can be viewed as mesons scattering off a static potential.

To set up the mean field formulation we consider N_c+1 quarks and one anti-quark. The baryon wave function is again a product of single quark wave-function $\phi(\vec{r}_i)$. The meson is described by a single wave-function $u(\vec{r},\vec{y},t)$ for the quark at position $\vec{r}$ and the anti-quark at $\vec{y}$. The many-body wave function for the system becomes

$$\Psi\left(\vec{r}_1,\cdots,\vec{r}_{N_c},\vec{r},\vec{y},t\right)=\sum_p(-1)^p\prod_{i=1}^{N_c}\Big[\phi(\vec{r}_i,t)\Big]u(\vec{r},\vec{y},t). \tag{1.5.15}$$

As before, this wave function is anti-symmetrized with respect to the colors of the quarks in ϕ and u respectively. Applying the time dependent variational principle, we find the wave-equation without any factors N_c [10]

$$\imath\frac{\partial}{\partial t}u(\vec{r}\,',\vec{y},t)=-\frac{1}{2M}\left(\vec{\partial}^2_{r'}+\vec{\partial}^2_{y}\right)u(\vec{r}\,',\vec{y},t)-g^2\frac{u(\vec{r}\,',\vec{y},t)}{|\vec{r}\,'-\vec{y}|}-g^2\phi(\vec{r}\,')\int \mathrm{d}^3z\,\phi^*(\vec{z},t)u(\vec{z},\vec{y},t)\Big[\frac{1}{|\vec{z}-\vec{r}\,'|}+\frac{1}{|\vec{z}-\vec{y}|}\Big]. \tag{1.5.16}$$

Again the N_c factors have canceled and thus the amplitude of the meson-baryon scattering also has a smooth large-N_c limit. This is consistent with the above consideration of the relevant Feynman diagrams.

1.5.3 Baryons as Solitons

In the previous subsection, we have seen that for large N_c QCD is regarded as a weakly coupled mesons field theory. It is therefore illuminating to find the behavior of the effective coupling

constant which defines these interactions. The results from the scattering processes defines an effective coupling constant, g_{eff}. For the case of two meson scattering the effective coupling upon using equation (1.5.4) gives

$$g_{\text{eff}} = \Gamma^2 \propto \frac{1}{N_c}. \tag{1.5.17}$$

In summary our results shows that

- the baryon mass, M_B can be written as $\dfrac{1}{g_{\text{eff}}}$
- and the amplitude of the meson-baryon scattering as well as baryon radii are $\mathcal{O}(g^0_{\text{eff}})$.

The above features leads to the conjecture[10] that baryons emerge as soliton solutions in the limit of large N_c.

In what follows we verify the above properties for a typical example of the kink soliton in the ϕ^4 field theory in one space (x) and one time (t) dimension. The dynamics of this model is governed by the Lagrangian density

$$\mathcal{L}_4 = \frac{1}{2}\left[(\partial_t\phi)^2 - (\partial_x\phi)^2\right] - \frac{\lambda}{4}\left(\phi^2 - \frac{m^2}{\lambda}\right)^2, \tag{1.5.18}$$

with a fourth order self-interaction potential. Here λ is identify as the effective coupling constant with $\lambda \sim \Gamma^{(4)}$ and m is a real constant. The classical equation of motion reveals that the above Lagrangian has two degenerate stable vacuum solutions $\phi_{\text{vac}} = \pm\dfrac{m}{\sqrt{\lambda}}$. Furthermore there are stationary solutions[3]

$$\phi_\pm(x) = \pm\frac{m}{\sqrt{\lambda}}\tanh\left(\frac{m}{\sqrt{2}}x\right) \tag{1.5.19}$$

that connect these vacua. Thus, as x asymptotically goes to $\pm\infty$, ϕ approaches any of the two vacua. The positive profile function is called the kink soliton and the negative profile as the anti-kink soliton. These solutions are shown in Figure 1.8.

In the next step, we seek to find if the total classical energy configuration of this Lagrangian is finite. Classically, for static configurations we obtain the energy function as

$$E[\phi] = -\int_{-\infty}^{\infty} \mathrm{d}x\, \mathcal{L} = \int_{-\infty}^{\infty} \mathrm{d}x \left\{\frac{1}{2}(\partial_x\phi_+)^2 + \frac{\lambda}{4}\left(\phi_+^2 - \frac{m^2}{\lambda}\right)^2\right\} = \frac{2\sqrt{2}}{3}\frac{m^3}{\lambda} = \mathcal{O}\left(\frac{1}{g_{\text{eff}}}\right). \tag{1.5.20}$$

This satisfy the first property of soliton solutions. Its radii is given by the expectation value $\langle x^2\rangle$ with respect to the energy density

$$\langle x^2\rangle = \frac{1}{E}\int_{-\infty}^{\infty} \mathrm{d}x\, x^2 \left\{\frac{1}{2}(\partial_x\phi_+)^2 + \frac{\lambda}{4}\left(\phi_+^2 - \frac{m^2}{\lambda}\right)^2\right\} = -\frac{1}{m^2}\left(1 - \frac{\pi^2}{6}\right) = \mathcal{O}(g^0_{\text{eff}}). \tag{1.5.21}$$

Finally in analogy to the meson-baryon scattering we introduce time-dependent fluctuations modes around the kink solutions, $\phi(x,t) = \phi_+(x) + \eta(x,t)$. Here the fluctuations described the

[3] A moving kink-antikink solutions are obtained via Lorentz boosts.

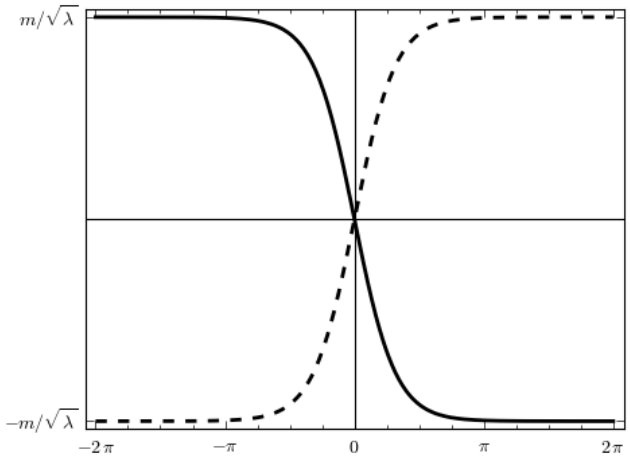

Figure 1.8: The kink (dash line) and anti-kink (solid line) solutions of the ϕ^4 soliton model.

meson wave-function in the background of the kink. For linear terms of these fluctuations, the equation of motion gives

$$\begin{aligned} 0 &= \frac{\partial^2\eta(x,t)}{\partial t^2} - \frac{\partial^2\eta(x,t)}{\partial x^2} - m^2 + 3\lambda\phi_+^2(x)\eta(x,t) \\ &= \frac{\partial^2\eta(x,t)}{\partial t^2} - \frac{\partial^2\eta(x,t)}{\partial x^2} - m^2 + 3m^2\tanh\left(\frac{m}{\sqrt{2}}x\right)\eta(x,t), \end{aligned} \tag{1.5.22}$$

which is the kink analog to equation (1.5.16). Clearly there is no dependence on the effective coupling constant. Hence the scattering data extracted from this model are $\mathcal{O}(g_{\text{eff}}^0)$. In conclusion the ϕ^4 soliton model meet the features of baryons in the large-N_c limit.

1.6 Deep Inelastic Scattering (DIS)

In this section we discuss the inelastic scattering of electrons from a nucleon at high energy and large momentum transfer. The scattering process is given as

$$e(k) + N(p) \to e(k') + X(p_n) \tag{1.6.1}$$

where e is the electron, N the nucleon and X is the system of hadrons produced in the scattering processes. The arguments denotes the respective momenta; p_n indicates that X is a configuration with n hadrons. The process proceeds via one photon exchange shown in the Feynman diagram of Figure 1.9. In the experiment only the momentum k' of the final electron is observed[4]. Of course, the initial kinematic variables are all known.

The Lorentz invariant kinematical variables for the scattering process are defined by

$$s = (p+k)^2, \quad q^2 = (k-k')^2, \quad W^2 = (p+q)^2. \tag{1.6.2}$$

Here s denotes the total energy squared of the electron-nucleon system, q^2 is the momentum squared transferred by the virtual photon to the hadrons and W^2 is the mass squared of the final hadron system. In the nucleon rest frame $p = (M, 0, 0, 0)$ where M is the mass of the

[4]Experiments of this nature are called inclusive experiments.

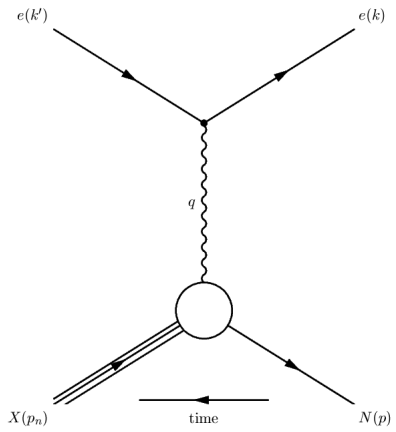

Figure 1.9: Feynman diagram for deep inelastic processes in the one-proton approximation.

proton, $k_\mu = (E, \vec{k})$ and $k'_\mu = (E', \vec{k}')$. When neglecting the electron mass the kinematical variables become

$$\begin{aligned} s &= (2E + M)M \geq M^2 \\ q^2 &= -4EE' \sin^2 \frac{\theta}{2} \leq 0, \quad Q^2 = -q^2 \\ W^2 &= q^2 + M^2 + 2M(E - E') \geq M^2 \end{aligned} \tag{1.6.3}$$

where θ is the scattering angle of the electron. The last inequality arises from the fact that the unobserved X has at least one nucleon by baryon number conservation. (The case $X \equiv N$ and $W^2 = M^2$ is elastic scattering). Formally, the variable $\nu = \dfrac{p \cdot q}{M}$, is frequently used in place of W^2. In the nucleon rest frame, $\nu = E - E'$. Furthermore one defines the Bjorken variable

$$x = \frac{-q^2}{2M\nu} = \frac{Q^2}{2M\nu} \tag{1.6.4}$$

which is bounded by $0 \leq x \leq 1$. The upper bound represent elastic scattering.

The scattering amplitude for this process is given as

$$\langle eX|T|eN\rangle = e^2 \bar{u}_{\lambda'}(k')\gamma^\mu u_\lambda(k)\frac{1}{q^2}\langle n|J_\mu(0)|p, s\rangle \tag{1.6.5}$$

where λ', λ and s are the spins of final and initial electron, and that of nucleon respectively, $|p, s\rangle$ is the state of the nucleon, $|n\rangle$ is the state of final hadron system, and J_μ is the hadronic part of the electromagnetic current operator. Summing over all possible final states of the hadrons gives the inclusive cross-section [6, 12]

$$\frac{\mathrm{d}^2\sigma}{\mathrm{d}\Omega \mathrm{d}E'} = \frac{\alpha^2}{q^4}\left(\frac{E'}{E}\right) L^{\mu\nu}W_{\mu\nu}, \tag{1.6.6}$$

where $\alpha = \dfrac{e^2}{4\pi}$ is the fine structure constant, $L^{\mu\nu}$ and $W_{\mu\nu}$ are the leptonic and hadronic tensors respectively. The leptonic tensor is computed by standard techniques for Dirac spinors

$$L^{\mu\nu} = \frac{1}{4}\,\mathrm{tr}\left(\not{k}\gamma^\mu \not{k}'\gamma^\nu\right) = 2\left(k'^\mu k^\nu + k'^\nu k^\mu + \frac{q^2}{2}g^{\mu\nu}\right). \tag{1.6.7}$$

Since the hadronic state is not observed we sum over all possible configurations

$$W_{\mu\nu}(p,q) = \sum_{n,\vec{p}_n} \langle p,s|J_\mu(0)|n\rangle \langle n|J_\nu(0)|p,s\rangle (2\pi)^4 \delta^4(p_n - p - q) = \int \mathrm{d}^4\xi\, e^{\imath q\cdot\xi} \langle p,s|J_\mu(\xi)J_\nu(0)|p,s\rangle\,, \quad (1.6.8)$$

by translational invariance. The opposite order $\langle p,s|J_\nu(0)J_\mu(\xi)|p,s\rangle$ involves $\delta(p_n - p + q)$. In the lab frame this requires $p_n^0 = M - \nu \leq M$, which is impossible. Hence

$$W_{\mu\nu}(p,q) = \int \mathrm{d}^4\xi\, e^{\imath q\cdot\xi} \langle p,s|\left[J_\mu(\xi), J_\nu(0)\right]|p,s\rangle\,. \quad (1.6.9)$$

A similar calculation for the time ordered product yields ($\epsilon \to 0^+$)

$$T_{\mu\nu}(p,q) = \imath \int \mathrm{d}^4\xi\, e^{\imath q\cdot\xi} \langle p,s|T\left(J_\mu(\xi)J_\nu(0)\right)|p,s\rangle = (2\pi)^3 \sum_{n,\vec{p}_n} \left\{ \frac{\delta^3(\vec{p}_n - \vec{p} - \vec{q})}{p_n^0 - p^0 - q^0 - \imath\epsilon} \langle p,s|J_\mu(0)|n\rangle \langle n|J_\nu(0)|p,s\rangle \right.$$
$$\left. + \frac{\delta^3(\vec{p}_n - \vec{p} + \vec{q})}{p_n^0 - p^0 + q^0 - \imath\epsilon} \langle p,s|J_\nu(0)|n\rangle \langle n|J_\mu(0)|p,s\rangle \right\}. \quad (1.6.10)$$

Using Dirac formula $\dfrac{1}{x - \imath\epsilon} = \mathcal{P}\left(\dfrac{1}{x}\right) + \imath\pi\delta(x)$ the imaginary part of the first term in equation (1.6.10) yields equation (1.6.8), while the second term in equation (1.6.10) does not have an imaginary part by the kinematical argument used above to introduce the commutator. Hence we can write

$$W_{\mu\nu}(p,q) = \frac{1}{2\pi} \operatorname{Im} T_{\mu\nu}(p,q). \quad (1.6.11)$$

This relation will be important for later calculations because the matrix element of a time ordered product is accessible more conveniently in any path integral formulation of a quantum field theory. Physically $T_{\mu\nu}$ is the Compton scattering amplitude and $\operatorname{Im} T_{\mu\nu}$ is its absorptive part.

Current conservation, Lorentz covariance and parity invariance dictate the general decomposition of the hadronic tensor

$$W_{\mu\nu}(p,q) = MW_1(\nu,Q^2)\left(-g_{\mu\nu} + \frac{q_\mu q_\nu}{q^2}\right) + \frac{W_2(\nu,Q^2)}{M}\left(p_\mu - \frac{p\cdot q}{q^2}q_\mu\right)\left(p_\nu - \frac{p\cdot q}{q^2}q_\nu\right)$$
$$+ \imath\epsilon_{\mu\nu\lambda\sigma}q^\lambda \left\{ MG_1(\nu,Q^2)s^\sigma + \frac{G_2(\nu,Q^2)}{M}\left((p\cdot q)s^\sigma - (q\cdot s)p^\sigma\right)\right\}, \quad (1.6.12)$$

where $W_{1,2}$ and $G_{1,2}$ are the unpolarized and polarized form factors of the nucleon respectively. These functions depend only on the Lorentz invariants $Q^2 = -q^2$ and ν. In the case the inelastic scattering occurs off a spin-zero hadron the polarized form factors G_1 and G_2 are absent.

1.6.1 Bjorken Scaling

In what follows, we consider the symmetric part of the hadronic tensor

$$W^S_{\mu\nu} = MW_1(\nu,Q^2)\left(-g_{\mu\nu} + \frac{q_\mu q_\nu}{q^2}\right) + \frac{W_2(\nu,Q^2)}{M}\left(p_\mu - \frac{p\cdot q}{q^2}q_\mu\right)\left(p_\nu - \frac{p\cdot q}{q^2}q_\nu\right). \quad (1.6.13)$$

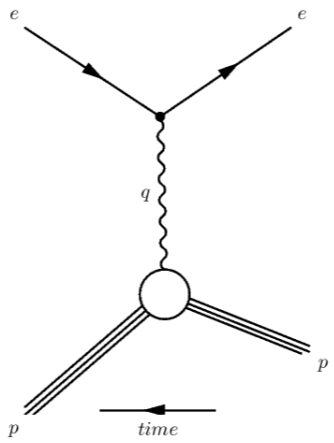

Figure 1.10: Feynman diagram for elastic electron-proton scattering.

Substituting this equation into (1.6.6) and using (1.6.7) in the nucleon rest frame gives

$$\frac{\mathrm{d}^2\sigma}{\mathrm{d}\Omega \mathrm{d}E'} = \frac{\alpha^2 \cos^2\frac{\theta}{2}}{4E^2 \sin^4\frac{\theta}{2}} \left[2W_1 \tan^2\frac{\theta}{2} + W_2\right]. \tag{1.6.14}$$

Thus, the form factors carry all the information on measurement of the inclusive cross-section $eN \to eX$.

Now, we consider the target nucleon (N) to be a proton (p) and assume it to be composed of point-like, spin-$\frac{1}{2}$ particles (quarks) normally referred to as partons. At small wavelengths (large Q^2) this point-charge proton behaves like a free Dirac particle. Contrasting this bahavior with that for the elastic electron-proton scattering $ep \to ep$ Figure 1.10, one would expect the differential cross-section for the point-like proton to be that of the electron-muon ($e\mu \to e\mu$) cross-section, which in the muon rest (laboratory) frame is

$$\left(\frac{\mathrm{d}\sigma}{\mathrm{d}\Omega}\right)_{e\mu\to e\mu} = \frac{\alpha^2 \cos^2\frac{\theta}{2}}{4E^2 \sin^4\frac{\theta}{2}} \left[\frac{Q^2}{2M_\mu^2} \tan^2\frac{\theta}{2} + 1\right] \frac{E'}{E}, \tag{1.6.15}$$

where

$$\frac{E'}{E} = \frac{1}{1 + \frac{2E}{M_\mu} \sin^2\frac{\theta}{2}}. \tag{1.6.16}$$

It turns out, however, that the differential cross-section resembles that of an extended particle given by the Rosenbluth formula

$$\frac{\mathrm{d}\sigma^{\text{elastic}}}{\mathrm{d}\Omega} = \frac{\alpha^2 \cos^2\frac{\theta}{2}}{4E^2 \sin^4\frac{\theta}{2}} \left[G_M^2 \frac{Q^2}{2M^2} \tan^2\frac{\theta}{2} + \frac{G_E^2 + G_M^2 \frac{Q^2}{4M^2}}{1 + \frac{Q^2}{4M^2}}\right] \frac{E'}{E} \tag{1.6.17}$$

where

$$G_E = F_1 + 2M_\mu \kappa_p F_2 \quad \text{and} \quad G_M = F_1 - \frac{\kappa_p Q^2}{4M_\mu^2} F_2 \tag{1.6.18}$$

are the electric and magnetic form factors. The Lorentz invariant form factors $F_i = F_i(Q^2)$ are introduced as modifications of the proton matrix element of the electromagnetic current to

model the structure of the proton

$$\langle p|J_\mu(0)|p\rangle = \bar{u}(p')\left[\gamma_\mu F_1 + \imath\sigma_{\mu\nu}q^\nu \frac{\kappa_p}{2M_N}F_2\right]u(p). \tag{1.6.19}$$

Here u is the free Dirac spinor for the nucleon and κ_p is the magnetic moment of the proton with $\sigma_{\mu\nu} = \frac{\imath}{2}[\gamma_\mu, \gamma_\nu]$. Empirically these form factors are well approximated by the so-called (double) dipole formula

$$\frac{G_M}{\kappa_p} = G_E = \left(1 + \frac{Q^2}{0.7(\text{GeV})^2}\right)^{-2}, \tag{1.6.20}$$

where $\kappa_\text{p} = 2.79$. This implies that at large Q^2, the scattering rate of equation (1.6.17) is suppressed at large angles.

Note that we also can take the elastic approximation for the hadronic tensor by restricting the sum in (1.6.8) to $n =$ proton. Obviously this involves the square of the current matrix element, (1.6.19). Furthermore using

$$\begin{aligned}\delta\left(E'_N - M - E + E'\right) &= \delta\left(E'_N - M - \nu\right) = 2M\delta\left(2M' - 2ME'_N + 2M\nu\right), \\ &= 2M\delta\left(q^2 + 2M\nu\right),\end{aligned} \tag{1.6.21}$$

the comparison with equation (1.6.17) yields

$$W_1^{el} = -\delta\left(2M\nu - Q^2\right)\frac{Q^2}{2M}G_M^2(Q^2) \tag{1.6.22}$$

$$W_2^{el} = \delta\left(2M\nu - Q^2\right)\frac{2M}{\left(1 + \frac{Q^2}{4M^2}\right)}\left[G_E^2(Q^2) + \frac{Q^2}{4M^2}G_M^2(Q^2)\right]. \tag{1.6.23}$$

The particular case of a point-like nucleon yields

$$2W_1^{\text{point}} = \frac{Q^2}{2M}\delta\left(\nu - \frac{Q^2}{2M}\right) = \frac{Q^2}{2M\nu}\delta\left(1 - \frac{Q^2}{2M\nu}\right), \tag{1.6.24}$$

$$W_2^{\text{point}} = 2M\delta\left(\nu - \frac{Q^2}{2M}\right) = \frac{2M}{\nu}\delta\left(1 - \frac{Q^2}{2M\nu}\right). \tag{1.6.25}$$

An intuitive picture is that, at least at large Q^2, we can view the inelastic electron-proton scattering as an elastic system where the 'free' quarks within the proton are bombarded with electrons. Gluons are not affected because they do not have electric charge. Then, the above equations reveal that the form factor depend only on the variable

$$x = \frac{Q^2}{2M\nu} \quad \text{satisfying} \quad 0 \leq x \leq 1. \tag{1.6.26}$$

In that case the form factors are called structure functions. This is the well known approximate scaling law (Bjorken scaling) which states that, the structure functions are constant at large Q^2 and ν with x held fixed.

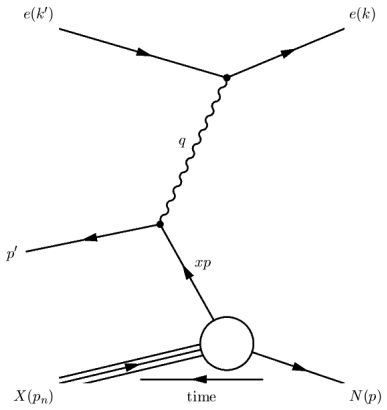

Figure 1.11: The incoherence of electron scattering off partons.

1.6.2 The Parton Model

We have seen that Bjorken scaling is attributed to the point-like structures in elastic electron-proton scattering. In this section we seek to answer whether we can apply such scaling behavior in the deep inelastic scattering (DIS) of electrons to protons. We assume the proton to be made up of partons. Because in the DIS regime Q^2 and ν are large, the parton mass and its momentum are negligible and the partons are hypothesized to carry a fraction of the original hadron momentum

$$P = xp \quad \text{with} \quad 0 \leq x \leq 1. \tag{1.6.27}$$

Further, we assume the partons to be evenly distributed in the proton and denote $f(x)$ as the probability that each parton carries a fraction x of the proton momentum distribution satisfying

$$\int_0^1 \mathrm{d}x\, f(x) = 1. \tag{1.6.28}$$

Viewing this inelastic process as incoherent scattering off partons inside the protons as shown in Figure 1.11 the structure functions become[6]

$$MW_1 = \sum_{i=1} e_i^2 f_i(x) \equiv F_1(x), \tag{1.6.29}$$

$$\nu W_2 = 2\sum_{i=1} e_i^2 x f_i(x) \equiv F_2(x), \tag{1.6.30}$$

where $\sum_i e_i^2$ is the total proton charge. Obviously these equations satisfy the so-called Callan-Gross relation

$$2xF_1(x) = F_2(x). \tag{1.6.31}$$

It is important to stress that this relation emerges from the (point-like version of) the current, equation (1.6.19). That is the charge partons are Dirac particles with spin-$\frac{1}{2}$.

Similar analysis can be carried out for the antisymmetric part of the hadronic tensor. Let $\delta f_i(x)$ be the difference of distributions with opposite spin orientation. Then

$$M^2\nu G_1(x) = \sum e_1^2 \delta f_1(x) =: \mathsf{g}_1(x). \tag{1.6.32}$$

Unfortunately the second polarized structure function

$$M\nu G_2(x) =: \mathrm{g}_2(x) \tag{1.6.33}$$

does not have a simple parton interpretation [13].

Hence in the Bjorken limit (for x fixed and Q^2 large) the structure functions measure the momentum and spin distributions of the parton in the target nucleon and the hadronic tensor of (1.6.12) becomes

$$\begin{aligned} W_{\mu\nu}(p,q) = F_1(x)\left(-g_{\mu\nu}+\frac{q_\mu q_\nu}{q^2}\right)+\frac{F_2(x)}{p\cdot q}\left(p_\mu-\frac{p\cdot q}{q^2}q_\mu\right)\left(p_\nu-\frac{p\cdot q}{q^2}q_\nu\right) \\ +\imath\epsilon_{\mu\nu\lambda\sigma}\frac{q^\lambda M}{p\cdot q}\left\{\mathrm{g}_1(x)s^\sigma+\mathrm{g}_2(x)\left(s^\sigma-\frac{q\cdot s}{q\cdot p}p^\sigma\right)\right\}. \end{aligned} \tag{1.6.34}$$

1.7 Summary of Introduction and Outline

In this introduction we have reviewed essential properties of QCD at low energies, in particular chiral symmetry and its dynamical breaking. In the next chapter we will discuss the Nambu-Jona-Lasinio model [14] that effectively describes that phenomenon. We have also explained Witten's argument that baryons emerge as solitons in an effective meson theory for QCD. We will get to that point in chapter 3 and in particular in chapter 4 where we discuss the soliton solution of the NJL model. In this introduction we have also discussed the physics relevant for structure functions. In chapter 5 we explain how they are calculated within the NJL model. In chapters 6 and 7 we present the numerical results of that formalism. In chapter 8 we discuss the DGLAP evolution equations that model perturbative QCD effects and compare the resulting solutions from it to experimental data. We summarize and conclude in chapter 9. We have recorded some lengthy formulas in appendices.

Chapter 2

Bosonization of the NJL Model

In this chapter we discuss the NJL model as an effective, chirally invariant theory with two light flavor (up and down) quarks. In section 2.2 we bosonize the NJL model by using the functional integral procedure. The solutions of this effective bosonized theory using mean field approximation posses an ultraviolet divergence. We analyze this divergence by introducing the Pauli-Villar's regularization scheme. In section 2.3 we show that the chiral symmetry of this model is spontaneously broken which subsequently leads to the generation of dynamical quark mass. In particular there is an emergence of Goldstone bosons in the breakdown of the chiral symmetry. We then discuss the properties of this Goldstone bosons by deriving their propagators, masses and their decay constant which will be needed in fixing the parameters of this model.

2.1 The NJL Model

The Nambu-Jona-Lasinio (NJL) model was first introduced in Ref.[14] to study the dynamical breaking of chiral symmetry. At that time nucleons were considered as the elementary fermions. Nowadays they are replaced by quarks. Here we consider the simplest $SU(2)$ version (thus we limit ourselves to the up (u) and down (d) quark flavors)

$$\mathcal{L}_{NJL}(q) = \bar{q}\left(\imath\partial\!\!\!/ - m^0\right) q + \frac{G}{2}\left[(\bar{q}q)^2 + (\bar{q}\vec{\tau}\imath\gamma_5 q)^2\right], \tag{2.1.1}$$

this Lagrangian contains a local four-fermion (quark) interaction coupled chirally symmetric through scalar and pseudoscalar interactions. The free and interaction quark bilinear parts are respectively given as:

$$\mathcal{L}_{free}(q) = \bar{q}\left(\imath\partial\!\!\!/ - m^0\right) q, \tag{2.1.2}$$

$$\mathcal{L}_{int}(q) = \frac{G}{2}\left[(\bar{q}q)^2 + (\bar{q}\vec{\tau}\imath\gamma_5 q)^2\right]. \tag{2.1.3}$$

The interaction part, $\mathcal{L}_{int}$, induces ultraviolet divergences that cannot be renormalized and thus require regularization. Here $q = q(x)$ denotes a quark field of flavor u and d with $N_c = 3$ colors

and

$$m^0 = \text{diag}\left(m_u^0, m_d^0\right) \tag{2.1.4}$$

represents the current quark mass. We will neglect isospin breaking by setting $m_u^0 = m_d^0 = m^0$ in our computations. The components of the vector $\vec{\tau}$, are the usual Pauli matrices which act on the $SU(2)$ isospin degrees of freedom and G is a yet undetermined coupling constant with dimension $[\text{mass}]^{-2}$.

This model can be motivated from QCD by linearizing the Yang-Mills Lagrangian and integrating out the Abelian field strength tensor $F^a_{\mu\nu}$ (1.1.4) [15]. This yields a color current-current interaction, which can be rearranged by Fierz-transformation into a color singlet meson and a diquark correlation. The later is suppressed by a relative factor $\frac{1}{N_c}$. The model is finally obtained by omitting these diquark correlations. The above yields $G \propto g^2_{QCD}$ which via equation (1.5.1) implies that G is of order $\frac{1}{N_c}$. This will be reflected later when we adjust G to pion properties.

In the following we will analyze the global symmetries of the NJL model. It is straightforward to verify that

- The Lagrangian (2.1.1) is symmetric under the global $U(1)$ transformation
$$q(x) \to \exp(\imath\theta) q(x), \tag{2.1.5}$$
where θ is a real constant.
- Assuming isospin symmetry, this Lagrangian is invariant under the global isospin rotation
$$q(x) \to \exp\left(\imath \frac{1}{2}\vec{\epsilon}\cdot\vec{\tau}\right) q(x), \tag{2.1.6}$$
where $\vec{\epsilon}$ is a real constant vector that characterizes the transformation.
- In addition for $m^0 = 0$ the Lagrangian is invariant under the global axial-chiral rotation
$$q(x) \to \exp\left(\imath \frac{1}{2}\gamma_5\vec{\epsilon}'\cdot\vec{\tau}\right) q(x). \tag{2.1.7}$$
- There is also a symmetry
$$q(x) \to \exp\left(\imath\epsilon\frac{\gamma_5}{2}\right) q(x) \tag{2.1.8}$$
on the classical level. Once photon fields are added by minimal substitutions this symmetry is broken at the one-loop quantum level. Of course this is the famous axial anomaly [16, 17].

The properties of above transformations generate the following Noether currents:

$$\begin{aligned} B_\mu &= \bar{q}\gamma_\mu q, && \text{(baryon current)} \\ \vec{V}_\mu &= \bar{q}\gamma_\mu\frac{\vec{\tau}}{2}q, && \text{(vector current)} \\ \vec{A}_\mu &= \bar{q}\gamma_\mu\gamma_5\frac{\vec{\tau}}{2}q. && \text{(axial current)} \end{aligned} \tag{2.1.9}$$

with the corresponding divergences

$$\begin{aligned}\partial_\mu B^\mu &= 0,\\ \partial_\mu \vec{V}^\mu &= \imath\bar{q}\left[m^0, \frac{\vec{\tau}}{2}\right] q,\\ \partial_\mu \vec{A}^\mu &= \imath\bar{q}\gamma_5\left\{m^0, \frac{\vec{\tau}}{2}\right\} q.\end{aligned} \tag{2.1.10}$$

Here the commutator and anti-commutator of the isospin matrix act on the flavor index of the quark fields.

We decompose the quark fields in right-and left- handed components, i.e,

$$q_R = P_R q, \quad q_L = P_L q, \quad \text{with} \quad q = q_R + q_L, \tag{2.1.11}$$

where

$$P_{R,L} = \frac{1}{2}\left(1 \pm \gamma_5\right) \tag{2.1.12}$$

are the corresponding chiral projections[1]. It is then illuminating to write the isospin transformations infinitesimally

$$\begin{aligned} q &\to \left(1 + \imath\vec{\epsilon}\cdot\vec{\tau} + \imath\vec{\epsilon}'\cdot\vec{\tau}\gamma_5\right) q + \cdots\\ &\to \left(1 + \imath(\vec{\epsilon}+\vec{\epsilon}')\cdot\vec{\tau}P_R + \imath(\vec{\epsilon}-\vec{\epsilon}')\cdot\vec{\tau}P_L\right) q + \cdots\end{aligned} \tag{2.1.13}$$

Hence

$$q_L \to \left(1 + \imath(\vec{\epsilon}+\vec{\epsilon}')\cdot\vec{\tau}\right) q_L + \cdots \tag{2.1.14}$$

and

$$q_R \to \left(1 + \imath(\vec{\epsilon}-\vec{\epsilon}')\cdot\vec{\tau}\right) q_R + \cdots \tag{2.1.15}$$

Thus, the NJL Lagrangian (2.1.1) exhibits a

$$SU_L(2) \otimes SU_R(2) \otimes U(1) \tag{2.1.16}$$

chiral symmetry in the limit $m^0 \to 0$, which is, of course, the same as in QCD, of section 1.3.

To explain the physical significant of the chiral symmetry, we consider free massless quarks $q(x)$. These fields satisfy the Dirac equation

$$\not{p}q(x) = 0, \quad \text{where} \quad \not{p} = \gamma_\mu p^\mu = \gamma_0 E - \vec{\gamma}\cdot\vec{p}, \tag{2.1.17}$$

with $E = |\vec{p}| = p$ since the quark is massless. Using the definition of γ-matrices (see Appendix A.2)

$$\vec{\gamma} = \beta\vec{\alpha} \quad \text{with} \quad \vec{\alpha} = \vec{\sigma}\otimes\gamma_5, \tag{2.1.18}$$

[1]Using the relation $\{\gamma_\mu, \gamma_5\} = 0$, their respective conjugates becomes : $\bar{q}_L = q_L^\dagger\gamma^0 = \bar{q}P_R$ and $\bar{q}_R = q_R^\dagger\gamma^0 = \bar{q}P_L$.

we can write (2.1.17) as

$$(p - \vec{\sigma}\cdot\vec{p}\gamma_5)\, q(x) = 0. \tag{2.1.19}$$

Now, separating right-and left-handed fields in equation (2.1.19) gives

$$\frac{\vec{\sigma}\cdot\vec{p}}{p} q_R(x) = q_R(x) \quad \text{and} \quad \frac{\vec{\sigma}\cdot\vec{p}}{p} q_L(x) = -q_L(x). \tag{2.1.20}$$

Since $\dfrac{\vec{\sigma}\cdot\vec{p}}{p}$ is the helicity operator this shows that the quarks $q_R(x)$ and $q_L(x)$ are eigenstates of this helicity with eigenvalues ± 1. Furthermore, for $m^0 \neq 0$ the mass term

$$\mathcal{L}_{mass} = -\bar{q} m^0 q = -\left(\bar{q}_R m^0 q_L + \bar{q}_L m^0 q_R\right) \tag{2.1.21}$$

couples left-to right-handed fields and vice versa. This then breaks the chiral symmetry explicitly. However, since $m^0 \ll \Lambda_{QCD}$, chiral symmetry can be considered as a good approximation, at least within the up - down flavor subspace.

2.2 Auxillary Meson Fields

The idea of bosonization is to map NJL quark model onto an effective meson theory. This will replace the four quark interaction Lagrangian by terms quadratic in quark bilinears. The formal treatment has thoroughly been discussed in Refs.[18–21]. Here we will give an overview. We write the interaction part of the NJL Lagrangian (2.1.3) in a more compact form as

$$\mathcal{L}_{int} = 2G\left(\bar{q}\Lambda_\alpha q\right)^2, \tag{2.2.1}$$

where

$$\Lambda_\alpha = \mathbf{1}_c \otimes \left(\frac{\vec{\tau}}{2}\right)_f \otimes \Gamma_\alpha, \qquad \Gamma_\alpha \in \{1, \imath\gamma_5\} \tag{2.2.2}$$

is the tensor product of color, flavor and Dirac matrices. For convenience, we restrained from making the (axial) vector interaction explicit. We introduce auxiliary fields $\phi = \phi_\alpha \Lambda_\alpha$ (which is a single valued matrix of color singlet quark bilinear (mesons) $\bar{q}q$) by completion of squares

$$\frac{1}{8G}\phi_\alpha^2 + \phi_\alpha \bar{q}\Lambda_\alpha q = \frac{1}{8G}\left(\phi_\alpha + 4G\bar{q}\Lambda_\alpha q\right)^2 - 2G\left(\bar{q}\Lambda_\alpha q\right)^2, \tag{2.2.3}$$

and perform a Gaussian integral over the auxiliary field ϕ

$$\exp\left(-\imath 2G\int \mathrm{d}^4x\, \left(\bar{q}\Lambda_\alpha q\right)^2\right) = \int \mathcal{D}\phi \exp\left(-\frac{\imath}{8G}\int \mathrm{d}^4x\, \phi_\alpha^2 - \imath\int \mathrm{d}^4x\, \phi_\alpha \bar{q}\Lambda_\alpha q\right), \tag{2.2.4}$$

and the shift $\phi \to \phi + m^0$, gives the generating functional of the NJL Lagrangian as

$$\begin{aligned} Z_{NJL} &= \int \mathcal{D}q\mathcal{D}\bar{q} \exp\left(\imath\int \mathrm{d}^4x\, \mathcal{L}_{NJL}\right) \\ &= \int \mathcal{D}\phi \exp\left(-\frac{\imath}{8G}\int \mathrm{d}^4x\ \mathrm{Tr}\left[\phi - m^0\right]^2\right) \int \mathcal{D}q\mathcal{D}\bar{q} \exp\left(\imath\int \mathrm{d}^4x\, \bar{q}\left(\imath\partial\!\!\!/ - \phi\right) q\right), \end{aligned} \tag{2.2.5}$$

where $\mathcal{D}q$, $\mathcal{D}\bar{q}$ and $\mathcal{D}\phi$ are the functional measures of the quark, antiquark and the auxiliary field respectively. Furthermore Tr denotes the trace over flavor and Dirac indices. The bilinear term (in the quark fields) of this generating functional is interpreted as the quantum transition amplitude of a non-interacting quark system in an external field $\phi = \phi_\alpha \Lambda_\alpha$ and is the same as

$$\lim_{T\to\infty} \left\langle 0 \middle| \exp\left(-\imath \int \mathrm{d}^3x\, q^\dagger h q T\right) \middle| 0 \right\rangle . \tag{2.2.6}$$

Here T denotes a large Euclidean time interval. Also, the integral $\int \mathrm{d}^3x q^\dagger h q$ contains a one-particle Dirac Hamiltonian in the second quantized form. In Minkowski space h is given by

$$h = \vec{\alpha}\cdot\vec{p} + \beta\phi \tag{2.2.7}$$

and is extracted from the relation

$$\imath\partial\!\!\!/ - \phi = \beta\left(\imath\partial_t - h\right), \tag{2.2.8}$$

where $\beta = \gamma_0$ and $\vec{\alpha} = \beta\vec{\gamma}$ are the Dirac matrices.

Without loss of generality, the generic meson field ϕ is decomposed into irreducible Lorentz components

$$\phi = S + \imath\gamma_5 P \tag{2.2.9}$$

where S and P are scalar and pseudoscalar fields, respectively. These are hermitian matrices in flavor space, i.e.

$$S = S_0\mathbf{1} + \frac{1}{2}\vec{S}\cdot\vec{\tau} \quad \text{and} \quad P = P_0\mathbf{1} + \frac{1}{2}\vec{P}\cdot\vec{\tau}. \tag{2.2.10}$$

For convenience we introduce a short-hand notation for the generic field ϕ by defining the complex fields $M = S + \imath P$ and $M^\dagger = S - \imath P$ with

$$\phi = \frac{1}{2}(M + M^\dagger) + \frac{\gamma_5}{2}(M - M^\dagger) = MP_R + M^\dagger P_L. \tag{2.2.11}$$

In functional integral theorem, the quark fields (q and $\bar{q}$) are anticommuting Grassmann varibles [22]: $\{q,\bar{q}\} = \{q,q\} = \{\bar{q},\bar{q}\} = 0$. Employing the standard formula for path integrals over Grassmann fields

$$\int \Pi_j \left(\imath \mathrm{d}\bar{q}_j \mathrm{d}q_j\right) \exp(\imath \bar{q}_j A_{jk} q_k) = \mathrm{Det}(A) \tag{2.2.12}$$

the bilinear term (in the quark fields) of the generating functional can be integrated out formally. This yields the determinant of the Dirac operator. Using equation (2.2.11) and the relation

$$\mathrm{Det}(A) = \exp \mathrm{Tr}\log(A), \tag{2.2.13}$$

the generating function becomes

$$\begin{aligned} Z_{NJL} &= \int \mathcal{D}\phi \exp(\imath\mathcal{A}[M,M^\dagger]) \quad \text{with} \\ \mathcal{A}[M,M^\dagger] &= -\frac{1}{4G}\int \mathrm{d}^4x\ \mathrm{tr}\left[MM^\dagger - m^0(M+M^\dagger)\right] - \imath N_c\,\mathrm{Tr}_\Lambda \log \imath D, \end{aligned} \tag{2.2.14}$$

as the effective action. Here, the trace tr, is over flavor space. The functional trace is defined as $\mathrm{Tr}_\Lambda := \int_\Lambda \mathrm{d}^4x\ \mathrm{Tr}$, (understood as regularized trace over a four dimensional space). As mentioned, the path integral was computed formally, because the resulting integral is ultraviolet divergent and hence requires regularization. This is indicated by the cut-off Λ in the subscript. The model itself is not renormalizable, hence the cut-off will (later on) acquire a physical meaning. A major requirement on the regularization prescription is the compliance with the symmetries of the model. In this project we will adopt the Pauli-Villars subtraction scheme [23], which will be explained later in the section. The quarks carry color degrees of freedom and this induces the factor N_c, as a multiplication to the trace, as the original NJL model had no color interaction.

This action is a non-linear, even non-polynomial function of the meson field, with the non-local term $\mathrm{Tr}_\Lambda \log(\imath D)$, where

$$\imath D = \imath\partial\!\!\!/ - \left(MP_R + M^\dagger P_L\right). \tag{2.2.15}$$

Essentially we need to find the eigenvalues of this operator which describe the motion of quarks in the background of the meson fields ϕ. In the particular case that ϕ is static, $\mathrm{Tr}_\Lambda \log \imath D$ is evaluated as the regularized sum of the eigenvalues of h, defined in equation (2.2.7), after summing the Matsubara frequencies.

Furthermore, the quantum properties of this action are equivalent to the underlying quantum structures of the NJL model. The one fermion-loop quantum contributions are fully contained in the eigenvalues of $\imath D$. Treating the mesons fields classically represents the one-loop approximation to the NJL model. Because of this, the effective action (2.2.14) with classical meson fields is called semi-bosonized NJL model.

To maintain the chiral anomaly in Minkowski space, we write the additive contribution to the effective action into a γ_5- odd (abnormal pseudoparity) and γ_5- even (normal pseudoparity) parts [24–26]. Formally, only the latter requires regularization and we regularize it by means of Pauli-Villars scheme explained below. To do this we introduce the operator

$$\imath D_5 = -\imath\partial\!\!\!/ - (S - \imath\gamma_5 P) = -\imath\partial\!\!\!/ - \left(MP_L + M^\dagger P_R\right). \tag{2.2.16}$$

This operator is obtained from $\imath D$ by first performing a Wick rotation ($\partial_t \to \imath\partial_t$, $\beta \to \imath\beta$, $\partial^i \to \partial_i$ and $\gamma^i \to -\gamma^i$) yielding $\imath D_E$. Subsequently $(\imath D_E)^\dagger$ is rotated back to Minkowski space. Without regularization the operator, D_5, is irrelevant. The effective action of the bosonized NJL model then becomes[24, 27]

$$\mathcal{A}[M, M^\dagger] = \mathcal{A}_\mathrm{R} + \mathcal{A}_\mathrm{I} + \mathcal{A}_m, \tag{2.2.17}$$

with

$$\mathcal{A}_{\mathrm{R}} = -\imath\frac{N_c}{2}\sum_{i=0}^{2} c_i \,\mathrm{Tr}\log\left[-DD_5 + \Lambda_i^2 - \imath\epsilon\right], \tag{2.2.18}$$

$$\mathcal{A}_{\mathrm{I}} = -\imath\frac{N_c}{2}\,\mathrm{Tr}\log\left[-D(D_5)^{-1} - \imath\epsilon\right], \tag{2.2.19}$$

$$\mathcal{A}_m = \frac{1}{4G}\int \mathrm{d}^4x \;\mathrm{tr}\left[m^0(M+M^\dagger) - MM^\dagger\right]. \tag{2.2.20}$$

In equation (2.2.18), we finally made the Pauli-Villars regularization scheme explicit. As noted above only the γ_5-even piece (real part)-$\mathcal{A}_{\mathrm{R}}$ of the action is regularized because it is ultraviolet divergent when restricted to the Feynman boundary conditions, while A_{I} remains finite. One could choose to also regularize A_{I}. This however, may be in conflict with the $U_A(1)$ anomaly[28]. The c_i's are coefficients chosen to make the action finite and the Λ_i's are the Pauli-Villars regulators.

To this end, two subtractions are performed in order to make the action finite with

$$c_0 = 1, \quad \Lambda_0 = 0, \quad \sum_{i=0}^{2} c_i = 0 \quad \text{and} \quad \sum_{i=0}^{2} c_i\Lambda_i^2 = 0. \tag{2.2.21}$$

Moreover, we choose the limits $\Lambda_1 = \Lambda_2 \to \Lambda$. This enables one to eliminate the coefficients c_i by using the identity (see Appendix B.1) [29]

$$\lim_{\Lambda_1\to\Lambda_2\equiv\Lambda}\sum_{i=1}^{2} c_i g(\Lambda_i^2) = g(0) - g(\Lambda^2) + \Lambda^2\frac{\partial g(\Lambda^2)}{\partial\Lambda^2}. \tag{2.2.22}$$

2.3 Spontaneous Breaking of Chiral Symmetry

As discussed in chapter 1 (section 1.3) dynamical breaking of chiral symmetry is an important empirical feature. We consider the mean field approximation of the NJL Lagrangian (2.1.1). This requires to linearize the interaction term (2.2.1) of the NJL model by replacing ϕ_α with $m^0 + 4\langle\bar{q}\Lambda_\alpha q\rangle$, more care about the role of the shift $\phi \to \phi + m^0$ is needed when defining/calculating the constituent quark mass, and its relation to $\langle\bar{q}q\rangle$. Here $\langle\bar{q}\Lambda_\alpha q\rangle$ is the vacuum expectation value (VEV) with Λ_α given in equation (2.2.2). For a Lorentz covariant, isospin invariant and parity conserving vacuum, the scalar quark pair condensate $\langle\bar{q}q\rangle$ is the only non-zero VEV which is related to the scalar density by $\bar{q}q = q^\dagger\beta q$. Since $\Lambda_0 = \frac{1}{2}\mathbf{1}$ (see equation (2.2.2)) this yields the mean field Lagrangian [21]

$$\mathcal{L}^{MFA} = \bar{q}\left(\imath\partial\!\!\!/ - \left[m^0 - 2G\langle\bar{q}q\rangle\right]\right)q, \tag{2.3.1}$$

which defines the dynamical or constituent quark mass via the so-called gap equation

$$m = m^0 - 2G\langle\bar{q}q\rangle, \tag{2.3.2}$$

and the corresponding Dirac equation for the quark field $q(x)$ reads

$$\left(\imath\partial\!\!\!/ - \left[m^0 - 2G\langle\bar{q}q\rangle\right]\right)q(x) = 0. \tag{2.3.3}$$

Figure 2.1: Graphical representation of the gap equation (2.3.2). The current quark mass m^0 is represented by the straight line.

For a Lorentz covariant, isospin invariant and parity conserving vacuum one can identify the quark condensate with the vacuum expectation value (VEV) of the scalar field from the above equation with

$$S = \langle S \rangle = -2G\langle \bar{q}q \rangle \quad \text{and} \quad P = \langle P \rangle = 0. \tag{2.3.4}$$

Formally this is found by varying the regularized effective action with respect to the scalar field

$$\frac{\partial \mathcal{A}[M, M^\dagger]}{\partial S} = -\frac{1}{2G}(S - m^0) - 4\imath N_c S \sum_{i=0}^{2} c_i \int \frac{\mathrm{d}^4 k}{(2\pi)^4} \left[-k^2 + S^2 + \Lambda_i^2 - \imath\epsilon\right]^{-1} = 0, \tag{2.3.5}$$

leading to the explicit gap equation

$$S = m^0 - 8G\imath N_c S \sum_{i=0}^{2} c_i \int \frac{\mathrm{d}^4 k}{(2\pi)^4} \left[-k^2 + S^2 + \Lambda_i^2 - \imath\epsilon\right]^{-1}. \tag{2.3.6}$$

In the first line of equation (2.3.5) we have made use of the Fourier transformation into momentum space after expanding the operator $-DD_5 = \not{\partial}^2 + S^2 + P^2 + \left\{\not{\partial}, \gamma_5 P\right\}$. Lorentz covariance and isospin invariance induce

$$S = \langle S \rangle = m\mathbf{1}, \tag{2.3.7}$$

where $\mathbf{1}$ is 2×2 unity matrix with

$$\langle \bar{q}q \rangle = -4\imath N_c m \sum_{i=0}^{2} c_i \int \frac{\mathrm{d}^4 k}{(2\pi)^4} \left[-k^2 + m^2 + \Lambda_i^2 - \imath\epsilon\right]^{-1} = \frac{mN_c}{4\pi^2} \left[\Lambda^2 - m^2 \log\left(1 + \frac{\Lambda^2}{m^2}\right)\right]. \tag{2.3.8}$$

In the second line we have make use of the formula for single cut-off (2.2.22) (see Appendix B.2).

The non-zero value $S = m\mathbf{1}$ from (2.3.2) enters the one-particle Dirac Hamiltonian (2.2.7) in the same way as the current quark mass m^0 (and thus, acts as a mass for the quark flavors) and is usually interpreted as the constituent quark mass

$$m = \mathrm{diag}\left(m_u, m_d\right), \tag{2.3.9}$$

where m_u and m_d are the up and down constituent quark mass respectively. Even for $m^0 = 0$, $m \neq 0$ gives a non-zero quark mass $S = m\mathbf{1}$. This value of S in the vacuum sector signals the

dynamical breaking of chiral symmetry with the quark condensate as the corresponding order parameter. Furthermore, because we have restricted ourselves to the isospin limit, $m^0 := m_u^0 = m_d^0$, the up and down constituent quark masses and quark condensates are equal as well, with $m_u = m_d$ and $\langle \bar{u}u \rangle = \langle \bar{d}d \rangle$. In subsequent discussions we will always assume this limit.

2.4 Excitations of the Pseudoscalar Field and their Properties

The spontaneous breakdown of chiral symmetry by the quark condensate suggests the pseudoscalar mesons fields to be Goldstone bosons. In this regard the physical mesons (pions) emerge as low-lying collective quark-antiquark excitations of the translational invariant vacuum field configuration $S = m\mathbf{1}$ cf. equation (2.3.7). This is revealed by expanding the effective action (2.2.17) to quadratic power in the pion fluctuations of the pseudoscalar field, where the pion field is defined as

$$2\pi(x) = \vec{\pi} \cdot \vec{\tau}, \tag{2.4.1}$$

and extracting the Bethe-Salpeter equation[2] from it.

Now, since in the vacuum sector, the VEV of the pseudoscalar vanishes, we introduce the fluctuating pion field orthogonal to $\langle S \rangle \neq 0$ via the complex field

$$M = mU = m \exp\left(\frac{\imath g}{m} \vec{\pi} \cdot \vec{\tau}\right), \tag{2.4.2}$$

where U, m and g are the chiral field, the VEV of the scalar field and g is the Yukawa coupling constant, respectively. In what follows, we expand the effective action up to second order (small amplitude approximation) in the pseudoscalar meson field. Formally, the chiral field is expanded up to quadratic order

$$U = \exp\left(\frac{\imath g}{m} \vec{\pi} \cdot \vec{\tau}\right) = 1 + \imath \frac{g}{m} \vec{\pi} \cdot \vec{\tau} - \frac{g^2}{2m^2} \vec{\pi}^2 + \cdots\cdots \tag{2.4.3}$$

Linear terms in $\vec{\pi}$ do not emerge in $\mathcal{A}$ since $\operatorname{tr} \pi = \frac{1}{2} \vec{\pi} \cdot \operatorname{tr}(\vec{\tau}) = 0$.

Using equation (2.4.3) the mesonic action becomes

$$\mathcal{A}_m = \frac{1}{2G} \int \mathrm{d}^4 x \left(m^2 + 2mm^0 - \frac{m^0}{m} g^2 \vec{\pi}^2 \right) + \mathcal{O}(\vec{\pi}^3). \tag{2.4.4}$$

To this end, we perform the Fourier transformation of the fluctuating pion field and the bilinear mass term of the mesonic action, $\mathcal{A}_m$ is obtained to be [15, 19]

$$\mathcal{A}_m^2 = - \int \frac{\mathrm{d}^4 q}{(2\pi)^4} \vec{\pi}(q) \cdot \vec{\pi}(-q) \frac{g^2}{2G} \frac{m^0}{m}. \tag{2.4.5}$$

[2] In the present context this would be the inverse propagator for the pseudoscalar mesons.

For the non-local term of the effective action, we consider the regularized part $\mathcal{A}_{\mathrm{R}}$. It is therefore sufficient to consider

$$\begin{aligned} -DD_5 &= \partial^2 + \left[\imath\partial\!\!\!/, P_R M + P_L M^\dagger\right] + P_R M^\dagger M + P_L M M^\dagger, \\ &= \partial^2 + m^2 + g\gamma_5\left[\partial\!\!\!/, \vec{\pi}\cdot\vec{\tau}\right] + \frac{g^2}{2m}\left[\imath\partial\!\!\!/, \vec{\pi}^2\right]. \end{aligned} \tag{2.4.6}$$

Let

$$A_0 = \partial^2 + m^2, \quad A_1 = g\gamma_5\left[\partial\!\!\!/, \vec{\pi}\cdot\vec{\tau}\right], \quad A_2 = \frac{g^2}{2m}\left[\imath\partial\!\!\!/, \vec{\pi}^2\right]$$

then we have the regularized part of the effective action as

$$\begin{aligned} \mathcal{A}_{\mathrm{R}} &= -\imath\frac{N_c}{2}\sum_{i=0}^{2} c_i \operatorname{Tr}\log\left[A_0 + A_1 + A_2 + \Lambda_i^2 - \imath\epsilon\right] \\ &= -\imath\frac{N_c}{2}\sum_{i=0}^{2} c_i \operatorname{Tr}\log\left[A_0 + \Lambda_i^2 - \imath\epsilon\right] - \imath\frac{N_c}{2}\sum_{i=0}^{2} c_i \operatorname{Tr}\log\left[1 + \left(A_0 + \Lambda_i^2 - \imath\epsilon\right)^{-1}(A_1 + A_2)\right] \\ &= -\imath\frac{N_c}{2}\sum_{i=0}^{2} c_i \operatorname{Tr}\log\left[A_0 + \Lambda_i^2 - \imath\epsilon\right] - \imath\frac{N_c}{2}\sum_{i=0}^{2} c_i \operatorname{Tr}\left(A_0 + \Lambda_i^2 - \imath\epsilon\right)^{-1} A_1 \\ &\quad + \imath\frac{N_c}{4}\sum_{i=0}^{2} c_i \operatorname{Tr}\left(A_0 + \Lambda_i^2 - \imath\epsilon\right)^{-1} A_1 \left(A_0 + \Lambda_i^2 - \imath\epsilon\right)^{-1} A_1 + \mathcal{O}(\pi^3). \end{aligned} \tag{2.4.7}$$

At quadratic order in the pion field we first consider the second term of equation (2.4.7). Now, for a single Dirac matrix γ^μ (see Appendix A.2) we have $\operatorname{Tr}\gamma^\mu = 0$, hence this contribution is zero. Finally, due to the chiral invariance of $\mathrm{Det}(-DD_5)$ only derivatives of $\vec{\pi}$ occur in A_1. This gives

$$\mathcal{A}_{\mathrm{R}}^2 = \imath\frac{N_c}{4}\sum_{i=0}^{2} c_i \operatorname{Tr}\left[\partial^2 + m^2 + \Lambda_i^2 - \imath\epsilon\right]\left(g\gamma_5\partial\!\!\!/\vec{\pi}\cdot\vec{\tau}\right)\left[\partial^2 + m^2 + \Lambda_i^2 - \imath\epsilon\right]\left(g\gamma_5\partial\!\!\!/\vec{\pi}\cdot\vec{\tau}\right). \tag{2.4.8}$$

Taking the Fourier transformation to momentum space and employing the Feynman integral formalism gives

$$\begin{aligned} \mathcal{A}_{\mathrm{R}}^2 &= \imath\frac{N_c}{4}\sum_{i=0}^{2} c_i \int\frac{\mathrm{d}^4p}{(2\pi)^4}\int\frac{\mathrm{d}^4k}{(2\pi)^4}\ \operatorname{Tr}\left\langle p\right|\left[\partial^2 + m^2 + \Lambda_i^2 - \imath\epsilon\right]\left(g\gamma_5\partial\!\!\!/\vec{\pi}\cdot\vec{\tau}\right)\left|k\right\rangle \\ &\quad \times\left\langle k\right|\left[\partial^2 + m^2 + \Lambda_i^2 - \imath\epsilon\right]\left(g\gamma_5\partial\!\!\!/\vec{\pi}\cdot\vec{\tau}\right)\left|p\right\rangle, \\ &= \imath\frac{N_c}{4}\sum_{i=0}^{2} c_i \int_0^1 \mathrm{d}x\int\frac{\mathrm{d}^4q}{(2\pi)^4}\int\frac{\mathrm{d}^4k}{(2\pi)^4}\ \operatorname{Tr} g^2\gamma_5^2 q^\mu\gamma_\mu(-q_\mu)\gamma^\mu\vec{\pi}(q)\cdot\vec{\pi}(-q)\vec{\tau}^2 \\ &\quad \times\left[m^2 - k^2 - q^2x(1-x) + \Lambda_i^2 - \imath\epsilon\right]^{-2}, \\ &= -2\imath N_c g^2 q^2\sum_{i=0}^{2} c_i \int_0^1 \mathrm{d}x\int\frac{\mathrm{d}^4q}{(2\pi)^4}\int\frac{\mathrm{d}^4k}{(2\pi)^4}\,\vec{\pi}(q)\cdot\vec{\pi}(-q)\left[m^2 - k^2 - q^2x(1-x) + \Lambda_i^2 - \imath\epsilon\right]^{-2}. \end{aligned} \tag{2.4.9}$$

In the second line we have introduced $q = k - p$ and x as a Feynman parameter. The factor, $8 \times \frac{1}{4}$, results from the trace over Dirac and isospin matrices respectively.

Combining equations (2.4.5) and (2.4.9) we have

$$\mathcal{A}[M, M^\dagger] = g^2 \int \frac{\mathrm{d}^4 q}{(2\pi)^4}\, \vec{\pi}(q) \cdot \vec{\pi}(-q) D^{-1}(q^2) + \mathcal{O}(\vec{\pi}^4) \tag{2.4.10}$$

with

$$D^{-1}(q^2) = 2N_c q^2 \Pi(q^2) - \frac{1}{2G}\frac{m^0}{m} \tag{2.4.11}$$

as the inverse pion propagator, where

$$\begin{aligned}\Pi(q^2) &= -\imath \sum_{i=0}^{2} c_i \int \frac{\mathrm{d}^4 k}{(2\pi)^4} \int_0^1 \mathrm{d}x\, \frac{1}{\left[m^2 - k^2 - x(1-x)q^2 + \Lambda_i^2 - \imath\epsilon\right]^2}, \\ &= -\frac{1}{16\pi^2}\int_0^1 \mathrm{d}x \left\{ \frac{\Lambda^2}{m^2 - x(1-x)q^2 + \Lambda^2} - \log\left(\frac{m^2 - x(1-x)q^2 + \Lambda^2}{m^2 - x(1-x)q^2}\right)\right\},\end{aligned} \tag{2.4.12}$$

is the regularized polarization function. In the second line we have performed the Wick rotation and make use of the formula for single cut-off (2.2.22) (see Appendix B.3). The on-shell mass condition of the inverse pion propagator

$$D^{-1}(q^2 = m_\pi^2) = 0, \tag{2.4.13}$$

determines the physical meson mass from the implicit equation

$$m_\pi^2 = \frac{1}{2G}\frac{m^0}{m}\frac{1}{2N_c \Pi(m_\pi^2)}, \tag{2.4.14}$$

with m^0 and m being matrix elements defined in equations (2.1.4) and (2.3.9) respectively. The Yukawa coupling constant, g, is determined by demanding a unit residue of the propagator at the pole

$$\frac{1}{g^2} = 4N_c \frac{\mathrm{d}}{\mathrm{d}q^2}\left[q^2 \Pi(q^2)\right]\Big|_{q^2 = m_\pi^2}. \tag{2.4.15}$$

From equations (2.4.11), (2.4.12) and (2.4.14) we have the following:

- Pions become massless ($m_\pi = 0$) Goldstone bosons in the chiral limit $m^0 \to 0$.
- Carrying out a Taylor expansion of the polarization function $\Pi(q^2)$ for large Λ^2

$$\begin{aligned}\frac{\Lambda^2}{m^2 - q^2 x(1-x) + \Lambda^2} &\approx 1 + \frac{x(1-x)q^2 - m^2}{\Lambda^2} + \cdots \\ \log\left(m^2 - x(1-x)q^2 + \Lambda^2\right) &\approx \log\Lambda^2 + \frac{m^2 - x(1-x)q^2}{\Lambda^2} + \cdots\end{aligned}$$

  we have

$$\begin{aligned}\Pi(q^2) &= -\frac{1}{16\pi^2}\int_0^1 \mathrm{d}x \left\{ \left(1 - \frac{m^2 - x(1-x)q^2}{\Lambda^2}\right) - \left(\log(\Lambda^2) + \frac{m^2 - x(1-x)q^2}{\Lambda^2}\right) \right. \\ &\qquad \left. + \log\left(m^2 - x(1-x)q^2\right) + \cdots \right\}, \\ &\approx -\frac{1}{16\pi^2}\int_0^1 \mathrm{d}x \log\left(\frac{m^2 - x(1-x)q^2}{\Lambda^2}\right) + \mathcal{O}\left(\frac{1}{\Lambda^2}\right).\end{aligned} \tag{2.4.16}$$

For convenience we put the meson field in an on shell by setting $q^2 = m_\pi^2$, where m_π is the pion mass. We note that $x(1-x) < \frac{1}{4}$, hence for $m_\pi < 2m$, $\Pi(m_\pi^2)$ is real and we have Im $\Pi(m_\pi^2) = 0$.

Nevertheless, let us consider the case $m_\pi > 2m$ for the time being. Then the argument of the logarithm can be negative. Using the relation

$$\log(-A) = \log(A) + \imath\pi \tag{2.4.17}$$

we have for $m_\pi > 2m$

$$\text{Im } \Pi(m_\pi^2) = \frac{1}{16}\int_0^1 \mathrm{d}x\, \theta\left(m_\pi^2 x(1-x) - m^2\right) = \frac{1}{16\pi}\sqrt{1 - 4\frac{m^2}{m_\pi^2}}\theta(m_\pi - 2m), \tag{2.4.18}$$

where θ is the step size function. This yields the decay rate

$$\Gamma = \frac{1}{16\pi m_\pi}\sqrt{1 - 4\frac{m^2}{m_\pi^2}}\theta(m_\pi - 2m). \tag{2.4.19}$$

Hence, for $m_\pi > 2m$ the polarization function gets an imaginary part, describing the decay of mesons into quarks and antiquarks [3].

2.5 Fixing Parameters

The vector and axial-vector Noether currents that arises from the NJL model, i.e equation (2.1.9) induce the following hadron isotopic charges

$$Q^i(t) = \int \mathrm{d}^3x \left(q^\dagger(x)\frac{\tau^i}{2}q(x)\right) \quad \text{and} \quad Q_5^i(t) = \int \mathrm{d}^3x \left(q^\dagger(x)\gamma_5\frac{\tau^i}{2}q(x)\right) \quad \text{for} \quad i = 1,2,3, \tag{2.5.1}$$

where Q^i (Q_5^i) are even(odd) under the parity operation

$$PQ^i(t)P^{-1} = Q^i(t), \quad PQ_5^i(t)P^{-1} = -Q_5^i(t) \tag{2.5.2}$$

respectively. Furthermore, these operators satisfies the Gell-Mann relations

$$\left[Q^i, Q^j\right] = \imath\epsilon^{ijk}Q^k, \quad \left[Q^i, Q_5^j\right] = \imath\epsilon^{ijk}Q_5^k, \quad \left[Q_5^i, Q_5^j\right] = \imath\epsilon^{ijk}Q_5^k, \tag{2.5.3}$$

and serve as generators of the $SU_L(2) \otimes SU_R(2)$ algebra. Here ϵ^{ijk} is the totally antisymmetric tensor. Chiral combination of the vector and axial-vector charges

$$Q_R^i = \frac{1}{2}\left(Q^i + Q_5^i\right), \quad Q_L^i = \frac{1}{2}\left(Q^i - Q_5^i\right) \tag{2.5.4}$$

diagonalizes the current algebra in equation (2.5.3) to

$$\left[Q_L^i, Q_L^j\right] = \imath\epsilon^{ijk}Q_L^k, \quad \left[Q_R^i, Q_R^j\right] = \imath\epsilon^{ijk}Q_R^k, \quad \left[Q_L^i, Q_R^j\right] = 0. \tag{2.5.5}$$

[3] Thus the NJL model does not confine. However, the chiral symmetry breaking in this model and the emergence of pions as Goldstone bosons makes this model worthwhile to be considered.

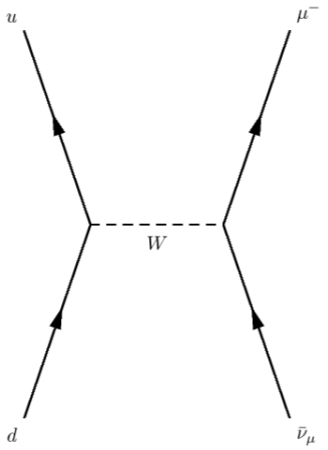

Figure 2.2: Feynman diagram for the pion decay.

Equation (2.5.5) means that $SU_L(2)$ algebra are generated by Q^i_L's charges while $SU_R(2)$ algebra are generated by Q^i_R's charges. In other words, left(right)-handed charges only interact with left(right)-handed charges.

Furthermore, we complement the pseudoscalar isospace components '$\vec{\pi}$' to that of the scalar (formally defined as the 'σ' field) to form a four-vector space. The rotational operators $Q^i(t)$ couples with the pseudoscalar components and leave the scalar component unaffected, whereas the axial-charge operators $Q^i_5(t)$ couples scalar to the pseudoscalar components and vice versa:

$$\begin{aligned} [Q^i(t), \pi^j] &= \imath\epsilon^{ijk}\pi^k, \qquad & [Q^i_5(t), \pi^j] &= -\imath\delta^{ij}\sigma \\ [Q^i(t), \sigma] &= 0, & [Q^i_5(t), \sigma] &= -\imath\pi^i. \end{aligned} \tag{2.5.6}$$

It follows from equations (2.5.2) and (2.5.6) that the scalar field (σ) creates a positive parity boson particles with isospin singlet, whereas the pions ($\vec{\pi}$) create isovector-pseudoscalar particles.

The spontaneous breakdown of chiral symmetry with non-vanishing quark condensate in section 2.3 is a manifestation of the Goldstone theorem and implies that the axial charges $Q^i_5(t)$ do not annihilate the vacuum $Q^i_5|0\rangle \neq 0$. Hence in the chiral limit $m^0 \to 0$ one expects that the axial current $\vec{A}_\mu$ (see equation (2.1.9)) couples the Goldstone bosons (pions) to the vacuum. To examine the physical consequences of this coupling we consider the weak pion decay:

$$\pi^-(q) \to \mu^-(p) + \bar{\nu}_\mu(p'), \tag{2.5.7}$$

with their interaction described by the Lagrangian (Fermi model)

$$\mathcal{L}_{eff} = -\frac{G_F}{\sqrt{2}} J^\dagger_\lambda(x) J^\lambda(x) + \text{h.c.} \tag{2.5.8}$$

Here G_F is the Fermi coupling constant, with the weak current being of the vector-minus-axial-vector $(V-A)$ structure.

In what follows, we decompose the weak current into its leptonic and hadronic parts:

$$J_\lambda(x) = J^l_\lambda(x) + J^h_\lambda(x). \tag{2.5.9}$$

We write the leptonic current in terms of its fields as

$$J^l_\lambda = \bar{\nu}_\mu \gamma_\lambda (1-\gamma_5)\mu \tag{2.5.10}$$

and that of the hadronic currents in terms of the quark fields as

$$J^h_\lambda = \bar{u}\gamma_\lambda(1-\gamma_5)\cos\theta_c d, \tag{2.5.11}$$

where θ_c is the Cabibbo angle. In the next step, we consider the pion decay amplitude, which in the approximation of vanishing Cabbibo angle is of the form [30]

$$T_\pi = \frac{G_F}{\sqrt{2}}\langle \pi^- | A_\lambda | 0\rangle l_\lambda, \tag{2.5.12}$$

with

$$l_\lambda = \bar{u}(p)\gamma_\lambda(1-\gamma_5)v(p'), \tag{2.5.13}$$

being the lepton part of the transition matrix element written in terms of the free Dirac spinors for the electron (u) and anti-neutrino (v). In the standard model this transition is described by the exchange of a W-boson as shown in Figure 2.2. At low energies the W propagator may well be approximated by its mass (inverse squared) leading to the Fermi model. Here because of isospin and Lorentz invariant only the axial current $A_\lambda = \bar{u}\gamma_\lambda\gamma_5 d$ contributes to the hadron matrix elements, i.e $\langle \pi^- | V_\lambda | 0\rangle = 0$, where $V_\lambda = \bar{u}\gamma_\lambda d$. By symmetry, the hadron matrix elements is parametrized to the form

$$\langle \pi^- | A_\lambda | 0\rangle = \imath F_\lambda e^{-\imath q\cdot x}. \tag{2.5.14}$$

where F_λ is a form factor. Now, since the pion is spinless, the only vector associated with it, out of which we might construct F_λ, is its momentum q_λ. Also, since the matrix element is Lorentz covariant we have F_λ as

$$F_\lambda = F(q^2)q_\lambda. \tag{2.5.15}$$

For on-shell pions, as in their weak decay, we have $f_\pi = F(m_\pi^2)$ which defines the pion decay constant. Therefore

$$\left\langle \pi^-(q) | A_\lambda(x) | 0 \right\rangle = \imath f_\pi q_\lambda e^{-\imath q\cdot x} \tag{2.5.16}$$

enters the decay amplitude T_π in equation (2.5.12). The observed decay width

$$T = \frac{1}{\Gamma\left(\pi^- \to \mu^- + \bar{\nu}_\mu\right)} = 2.6\times 10^{-8}\text{sec} \tag{2.5.17}$$

then yields $f_\pi = 93\,\text{MeV}$.

We find the axial current in the NJL model by introducing an external axial source into the effective action via

$$\imath D \to \imath D + \not{a}\gamma_5 \quad \text{and} \quad \imath D_5 \to \imath D_5 + \not{a}\gamma_5 \quad \text{where} \quad \not{a} = a^\mu_a \gamma_\mu \frac{\tau^a}{2}, \tag{2.5.18}$$

and identify the linear coupling to this source

$$A^b_\mu(x) = \frac{\delta}{\delta a^b_\mu(x)} \left\{ -\imath \frac{N_c}{2} \sum_{i=0}^{2} c_i \,\mathrm{Tr}\log\left[-DD_5 + \Lambda_i^2 - \imath\epsilon\right] \right\}\Big|_{a_\mu=0}. \tag{2.5.19}$$

Furthermore we are only interested in the one pion matrix element of A_μ. Hence it is sufficient to expand A_μ to linear order in the pion field (operator) $\pi_\mu(q)$. Using the identity (2.4.6) and taking the Fourier transformation to momentum space gives

$$\begin{aligned} A^b_\mu(x) &= -\imath \frac{N_c}{2} \sum_i c_i \int \frac{\mathrm{d}^4p}{(2\pi)^4} \int \frac{\mathrm{d}^4k}{(2\pi)^4} \int_0^1 \mathrm{Tr}\, \frac{\left(g\gamma_5 p_\mu \gamma^\mu \tau^b \pi^b(p)\right)\left(m\gamma_5\gamma_\mu\tau^b e^{-\imath p\cdot x}\right)}{\left[-k^2+m^2-x(1-x)p^2+\Lambda_i^2-\imath\epsilon\right]^2} + \mathcal{O}(\pi^2) \\ &\approx 4mgN_c \int \frac{\mathrm{d}^4p}{(2\pi)^4} \Pi(p^2) p_\mu \vec{\pi}^b(p) e^{-\imath p\cdot x}, \end{aligned} \tag{2.5.20}$$

where $\Pi(p^2)$ is the regularized polarization function cf. equation (2.4.12). The factor 4 results from the trace over the Dirac and isospin indices. Finally, the identity

$$\left\langle \pi^-(p)|\vec{\pi}^b(p')|0\right\rangle = 2E_p\delta^{ab}(2\pi)^3\delta^3(p-p')$$

gives the matrix elements as

$$\left\langle \pi^-(q)|A_\mu(x)|0\right\rangle = 4mgN_c\Pi(q^2)q_\mu e^{-\imath q\cdot x}. \tag{2.5.21}$$

Hence the NJL model predicts the pion decay constant

$$f_\pi = 4mgN_c\Pi(m_\pi^2). \tag{2.5.22}$$

In this project the model parameters m^0 and Λ will be determined by imposing the empirical values $m_\pi = 138\,\mathrm{MeV}$ and $f_\pi = 93\,\mathrm{MeV}$. In what follows, we eliminate the coupling constant G in favor of the constituent quark mass (see equation (2.3.9)), which in the chiral limit using equations (2.5.22) and (2.4.15) is written as $m = gf_\pi$ [31] . It is particularly important to recognize that the pion decay constant is proportional to $\sqrt{N_c}$ since $g \sim \frac{1}{\sqrt{N_c}}$, cf. equation (2.4.15). This is crucial when discussing the effective meson theory for QCD.

To round up this chapter, we note that using equations (2.3.2), (2.4.14) and (2.5.22) reproduce the Gell-Mann-Renner-Oakes relation

$$m_\pi^2 f_\pi^2 = \frac{m^0 m}{G} = 2m^0\langle\bar{q}q\rangle\frac{m}{m-m^0} \approx 2m^0\langle\bar{q}q\rangle. \tag{2.5.23}$$

Chapter 3

Soliton Model

In this chapter we reflect on the soliton picture for baryons. Using the chiral symmetry properties of the NJL model we construct the non-linear sigma model and discuss its properties. In particular we discuss the Skyrme soliton model, its solutions and topological properties.

3.1 The Non-Linear Sigma Model

Equations (2.5.3), (2.5.5) and (2.5.6) show that the chiral $SU_L(2) \otimes SU_R(2)$ symmetry is isomorphic to the four-dimensional group $SO(4)$ and the four-fields $(\sigma, \vec{\pi})$ transform as a vector under $SO(4)$. The corresponding invariant Lagrangian must only contain scalar products of the four-fields $(\sigma, \vec{\pi})$ and their derivatives [1]

$$\mathcal{L} = \frac{1}{2}\left[(\partial_\mu \sigma)^2 + (\partial_\mu \vec{\pi})^2\right] - V(\sigma^2 + \vec{\pi}^2), \tag{3.1.1}$$

this Lagrangian has its lowest energy when the four-fields $(\sigma, \vec{\pi})$ are stationary. Subsequently, this configuration minimize the potential $V(\sigma^2 + \vec{\pi}^2)$.

To get the stationary values (VEV), we choose, V, to be

$$V(\sigma^2 + \vec{\pi}^2) = \frac{\lambda}{4}\left[(\sigma^2 + \vec{\pi}^2)^2 - 2\frac{\mu^2}{\lambda}(\sigma^2 + \vec{\pi}^2)\right], \tag{3.1.2}$$

where λ and μ are the coupling constant and mass parameter respectively. This potential is minimized for $\mu > 0$ and

$$\sigma^2 + \vec{\pi}^2 = f_\pi^2, \tag{3.1.3}$$

where $f_\pi = \sqrt{\frac{\mu^2}{\lambda}}$. Thus, the VEV consists of infinitely many degenerate states. For large coupling $\lambda \gg 0$, the relation, equation (3.1.3) holds true also for space-time dependent configurations. This suggest to combine the four-fields $(\sigma, \vec{\pi})$ into one $SU(2)$ valued matrix

$$\frac{1}{f_\pi}(\vec{\sigma} + \vec{\pi} \cdot \vec{\tau}) = U(x) = \exp\left(\imath \vec{\tau} \cdot \hat{\phi}(x)\phi(x)\right) = \cos\phi + \imath \vec{\tau} \cdot \hat{\phi} \sin\phi \tag{3.1.4}$$

[1] A model of this type is usually called the σ model.

identified as the so-called chiral field. Here $\vec{\phi}(x)$ is the fundamental field with $\phi = |\vec{\phi}|$ and $\hat{\phi} = \dfrac{\vec{\phi}}{\phi}$. Equation (3.1.4) has three degrees of freedom. The isovector field $\vec{\phi}(x)$ can be connected to $\vec{\pi}$ and σ via

$$\sigma = f_\pi \cos\phi, \quad \vec{\pi} = f_\pi \hat{\phi} \sin\phi. \tag{3.1.5}$$

We note from the above equation,

$$UU^\dagger = U^\dagger U = (\sigma^2 + \vec{\pi}^2)\mathbf{1}, \tag{3.1.6}$$

with determinant

$$\det(U) = \sigma^2 + \vec{\pi}^2, \tag{3.1.7}$$

where $\mathbf{1}$ is the 2×2 unity matrix. On the level of the chiral field U the global transformations, equation (2.5.6) are parametrized by multiplications with constant matrices L and R

$$U(x) \to LU(x)R^\dagger. \tag{3.1.8}$$

In particular the infinitesimal transformation are obtained from linearizing

$$L = R = e^{\imath\vec{\epsilon}\cdot\vec{\tau}} \approx 1 + \imath\vec{\epsilon}\cdot\vec{\tau} \tag{3.1.9}$$

and

$$L = R^\dagger = e^{\imath\gamma_5\vec{\epsilon}\cdot\vec{\tau}} \approx 1 + \imath\gamma_5\vec{\epsilon}\cdot\vec{\tau} \tag{3.1.10}$$

for the vector and axial vector cases, respectively.

Empirically there is no indication that the vacuum has a preferred isospin direction. Hence the vacuum configuration is

$$\langle\vec{\pi}\rangle = 0 \quad \text{and} \quad \langle\sigma\rangle = f_\pi, \tag{3.1.11}$$

which corresponds to $\langle U\rangle = \mathbf{1}$. Expanding the potential, equation (3.1.2) does not produce a term quadratic in the $\vec{\pi}$-fluctuations around this vacuum. Hence the pions are indeed the Goldstone bosons of chiral symmetry (if $m_\pi = 0$). Furthermore, the constraint (3.1.3) implies that the potential V is a constant and hence can be omitted and the Lagrangian becomes

$$\mathcal{L}_{nl\sigma} = \frac{f_\pi^2}{4} \operatorname{tr}\left(\partial_\mu U \partial^\mu U^\dagger\right), \tag{3.1.12}$$

which is the so-called non-linear σ-model Lagrangian and is invariant under the $SU_L(2)\otimes SU_R(2)$ chiral symmetry. Here, tr is the trace over isospin indices.

3.2 The Skyrme Model Soliton

We have seen from section 1.5 that, QCD, the theory of the strong interaction, may be equivalent to an effective meson theory in which baryons are found as soliton solutions. The meson theory should, of course, contain the symmetries of QCD at low energies. Only the lightest mesons

need to be considered. The above non-linear σ-model Lagrangian serves as a good starting point with the chiral symmetry $SU_L(2) \otimes SU_R(2)$ in place. But the chiral symmetry has to be broken explicitly by a small mass term when describing physical pions. Hence we introduce the mass term

$$\mathcal{L}_m = \frac{m_\pi^2 f_\pi^2}{4} \operatorname{tr}\left[U + U^\dagger - 2\right]. \tag{3.2.1}$$

The total Lagrangian becomes

$$\mathcal{L} = \mathcal{L}_{nl\sigma} + \mathcal{L}_m, \tag{3.2.2}$$

with the static energy functional given as

$$E[U] = -\int \mathrm{d}^3 r\, \mathcal{L} = \int \mathrm{d}^3 r \left\{ \frac{f_\pi^2}{4} \operatorname{tr}\left(\vec{\nabla} U\right) \cdot \left(\vec{\nabla} U^\dagger\right) + \frac{m_\pi^2 f_\pi^2}{4} \operatorname{tr}\left[2 - U - U^\dagger\right] \right\}. \tag{3.2.3}$$

In what follows, we assume that the chiral field $U = \cos\phi + \imath\vec{\tau}\cdot\hat{\phi}\sin\phi$ maps the three dimensional coordinate space onto $SU(2)$ isospace. Since this target space is to be fully covered, the unit isovector $\hat{\phi}(\vec{x})$ must cover a unit two dimensional sphere S^2 in isospace. For the above condition to be valid, we adopt the so-called hedgehog ansatz [32]

$$\phi(\vec{x}) = \hat{x} \tag{3.2.4}$$

when $\hat{x}$ is the unit coordinate vector. Then the chiral field becomes

$$U(\vec{x}) = \exp(\imath\vec{\tau}\cdot\hat{x}\phi(\vec{x})) \tag{3.2.5}$$

for all t. We apply Derrick's theorem [33] to show that the functional does not have a stable solution. To this end, we introduce a new field with a scalar parameter $\eta > 0$ with

$$U_\eta = U(\eta\vec{x}). \tag{3.2.6}$$

We substitute the configuration (3.2.6) into the functional (3.2.3) and change the coordinate variable to

$$\vec{v} = \eta\vec{x}. \tag{3.2.7}$$

Then we have

$$E[U_\eta] = -\frac{1}{\eta^3}\int \mathrm{d}^3 v \left\{ \frac{\eta^2 f_\pi^2}{4} \operatorname{tr}\left(\partial_v U \partial^v U^\dagger\right) + \frac{m_\pi^2 f_\pi^2}{4} \operatorname{tr}\left[U + U^\dagger - 2\right] \right\} = \frac{1}{\eta} E_{nl\sigma}[U] + \frac{1}{\eta^3} E_m[U], \tag{3.2.8}$$

with $E_{nl\sigma}[U]$, $E_m[U] \geq 0$. If U were a minimum of the energy functional, $E[U_\eta]$ would be minimal for $\eta = 1$. We thus compute

$$\frac{\partial E[U_\eta]}{\partial \eta} = -\frac{1}{\eta^2} E_{nl\sigma}[U] - \frac{3}{\eta^4} E_m[U] \tag{3.2.9}$$

which only vanishes for $\eta \to \infty$ but not for $\eta = 1$. This clearly contradicts the above condition that a stable solution exist. In this case the minimal energy shrinks the configuration to zero

size. We note from the above argument that, a four derivative term, will scale as η and equation (3.2.9) will change to

$$\frac{\partial E[U_\eta]}{\partial \eta} = -\frac{1}{\eta^2} E_{nl\sigma}[U] - \frac{3}{\eta^4} E_m[U] + E_{Sk}[U], \tag{3.2.10}$$

thereby eventually stabilizing the energy configuration. The Lagrangian

$$\mathcal{L}_{Sk} = \frac{1}{32e^2} \operatorname{tr}\left(\left[U^\dagger \partial_\mu U, U^\dagger \partial_\nu U\right]\left[U^\dagger \partial^\mu U, U^\dagger \partial^\nu U\right]\right) \tag{3.2.11}$$

was suggested by Skyrne [34] as the four derivative term to stabilize the energy configuration. This commutator structure has the advantage that time derivatives only appear quadratically so that there is a unique relation between the field velocities and their conjugate momenta. Typically e is treated as a free parameter, though it can be related to the pion-pion scattering amplitude. This amplitude is then proportional to $\frac{1}{e^2 f_\pi^4}$. According to equation (1.5.4) the amplitude scales as $\frac{1}{N_c}$. As discussed at the end of chapter 2, $f_\pi \sim \sqrt{N_c}$; hence $e \sim \frac{1}{\sqrt{N_c}}$.

Combining equations (3.1.12), (3.2.1) and (3.2.11) gives the Skyrme model Lagrangian

$$\mathcal{L} = \mathcal{L}_{nl\sigma} + \mathcal{L}_m + \mathcal{L}_{Sk}. \tag{3.2.12}$$

For symmetry reasons, we choose $\phi(\vec{x}) = F(r)$, where $r = |\vec{x}|$ ($F(r)$ is often called the chiral angle) with

$$U(\vec{x}) = \exp\left(\imath \vec{\tau} \cdot \hat{x} F(r)\right). \tag{3.2.13}$$

For convenience we introducing the dimensionless quantities

$$r = |\vec{x}| e f_\pi \quad \text{and} \quad \mu_\pi = \frac{m_\pi}{e f_\pi}, \tag{3.2.14}$$

and the classical energy functional becomes

$$\begin{aligned} E_{cl}[F] &= -\int \mathrm{d}^3x \left[\mathcal{L}_{nl\sigma} + \mathcal{L}_m + \mathcal{L}_{Sk}\right], \\ &= \frac{2\pi f_\pi}{e} \int_0^\infty \mathrm{d}r \left\{ r^2 (\partial_r F)^2 + 2\sin^2 F + 2\mu_\pi^2 r^2 (1 - \cos F) + \sin^2 F \left(2(\partial_r F)^2 + \frac{\sin^2 F}{r^2}\right)\right\}. \end{aligned} \tag{3.2.15}$$

It is clear from the scaling behavior of e and f_π that this classical energy scales like $\mathcal{O}(N_c)$. Using variational principle we obtain the stationary condition

$$\frac{\partial^2 F}{\partial r^2} = \frac{\left\{\mu_\pi^2 r^2 \sin F + \sin 2F \left(1 + (\partial_r F)^2 + \frac{\sin^2 F}{r^2}\right)\right\}}{r^2 + 2\sin^2 F}. \tag{3.2.16}$$

We shall see later that solutions of this nature also arise with the NJL model. This stationary solutions are referred to as solitons, in the case of the Skyrme model is often called Skyrmions.

3.3 Topological Currents

In non-linear field theories, solitons are generally understood as classical, finite energy field solutions to the field equation. Finiteness of the energy requires the corresponding energy density to vanish at spatial infinity. From the above discussion finiteness of energy requires the chiral field to asymptotically approach a constant value at spatial infinity. As a consequence of the chiral symmetry we impose the boundary condition (for all t)

$$U(\vec{x}) \to \mathbf{1} \quad \text{as} \quad |\vec{x}| = r \to \infty. \tag{3.3.1}$$

Hence for any finite energy (considering the case for two flavors) the chiral field defines a mapping from the coordinate space $\mathbb{R}^3$ to the three-dimensional sphere S^3 (the group manifold of the isospin group $SU(2)$). However, the boundary condition (3.3.1) implies that all points of spatial infinity are identified, thus the coordinate space is compactified to the three-dimensional sphere S^3 and the soliton configuration is a mapping

$$U : S^3 \to S^3. \tag{3.3.2}$$

This then allows us to topologically classify the chiral field $U(\vec{x})$. Topologically different configuration are distinguished by the winding number $W \in \mathbb{Z}$ which in the $3+1$ dimensional case becomes

$$W[U] = \int \mathrm{d}^3 r \, B^0(r). \tag{3.3.3}$$

Here B^μ is the topological current density, which is explicitly given as [9]

$$B^\mu = \frac{1}{24\pi^2} \epsilon^{\mu\nu\sigma\rho} \operatorname{tr}\left[(U^\dagger \partial_\nu U)(U^\dagger \partial_\sigma U)(U^\dagger \partial_\rho U)\right], \tag{3.3.4}$$

where $\epsilon^{\mu\nu\sigma\rho}$ is the totally antisymmetric tensor with $\mu\nu\sigma\rho$ as the Lorentz indices. It can be verified that the topological current density becomes conserved, when the chiral field is continuously deformed in equal space and time. This is independent of the field equations. Hence B_μ is not a Noether current. Furthermore, in models like the semi-bosonized NJL model B_μ is the leading term of the gradient expansion of the baryon number current (typically a Noether current) [35]. The higher gradients do not contribute to integrals like equation (3.3.3). Hence the winding number can be identified with the baryon number. Substituting the chiral field (3.2.13) into equation (3.3.4), we have the winding number current to be

$$B_\mu = -\frac{1}{2\pi^2} (\partial_r F) \frac{\sin^2 F}{r^2} g_{\mu 0}. \tag{3.3.5}$$

From this the winding number becomes

$$W[U] = B = -\frac{2}{\pi} \int_0^\infty \mathrm{d}r \, (\partial_r F) \sin^2 F = \frac{1}{\pi} \left[F(0) - F(\infty)\right]. \tag{3.3.6}$$

To uphold the boundary condition (3.3.1), requires $F(r)$ to satisfy the following

$$F(r = \infty) = 0, \quad \text{and} \quad F(r = 0) = n\pi, \quad n \in \mathbb{Z}. \tag{3.3.7}$$

Then we have

$$W[U] = B = n \tag{3.3.8}$$

identified as the baryon number. From equation (3.3.2), it is obvious that B counts the number of times the image of $U(\vec{r})$ is wound around the three dimensional unit sphere S^3 as the chiral angle $F(r)$ goes around its domain (S^3).

3.4 The Hedgehog Field

An interesting feature of the chiral field $U(x)$ is that, for a non-zero topological current, the interacting pions around the vacuum carry the baryon number current 'B_μ'. For $U \neq 1$ the isospin transformation

$$U \to AUA^{-1} \tag{3.4.1}$$

with constant $A \in SU(2)$ is a symmetry of the model. For equation (3.2.13), the so-called hedgehog configuration the transformation amounts to

$$U_H \to \exp\left(\imath A\vec{\tau} \cdot \hat{x} A^\dagger F(r)\right), \tag{3.4.2}$$

which can be expressed via the adjoint representation $D_{ij} = \frac{1}{2}\operatorname{tr}\left(\tau_i A \tau_j A^\dagger\right)$

$$U_H \to \exp\left(\imath\tau_i (D_{ij}\hat{x}_j) F(r)\right). \tag{3.4.3}$$

Since the adjoint representation also describes $SO(3)$ transformations, i.e D is an orthogonal matrix, we establish that iso - and coordinate rotations are equivalent for the hedgehog configuration. This will be important when quantizing the fluctuations about the soliton.

In terms of the pseudoscalar and scalar fields we have

$$\frac{1}{f_\sigma}\sigma = \sin F(r), \quad \frac{1}{f_\pi}\vec{\pi} = \hat{x}\cos F(r) \tag{3.4.4}$$

showing that at each point $\vec{x}$ in the unit sphere S^3 in isospace, the pion field points in a radial direction with respect to the reference point (spatial origin $\vec{r} = 0$) of the pions. In other words, the direction of the pions are not distinguished from each other in isospace.

Chapter 4

Self Consistent Soliton

Here we discuss the emergence of solitons as self-consistent solution within the regularized NJL model. We give a brief sketch of the Dirac spectrum of these solutions in section 4.2. In this regime the chiral field 'U' binds a discrete valence level and the baryon state corresponds to the Hartree Fock picture with the quarks occupying all negative Dirac sea levels. In the next step, we quantize the soliton solutions. To this end we introduce collective coordinates for the rotational zero modes and discuss their moment of inertia as well as the quantized soliton energy. Here we follow Refs. [19, 20, 24].

4.1 The Soliton Energy

In this section we construct the soliton and investigate its energy for the NJL model in the $B = 1$ regime by adopting the self-consistent procedure. We consider the non-local part of the effective action (2.2.14), i.e. $-\imath N_c \operatorname{Tr}_\Lambda \log \imath D$ and evaluate it in the presence of equation (3.2.13). Here

$$\imath D = \left(\imath \partial\!\!\!/ - (M P_R + M^\dagger P_L)\right) = \beta \left(\imath \partial_t - h\right), \quad \beta = \gamma^0, \tag{4.1.1}$$

introduces the one-particle Hermitian Dirac Hamiltonian, h, which in the presence of the hedgehog configuration becomes

$$h = -\imath \beta \vec{\gamma} \cdot \vec{\partial} + \beta m \left\{U(\vec{r})\right\}^{\gamma_5} \quad \text{with} \quad \left\{U(\vec{r})\right\}^{\gamma_5} = \exp\left(\imath \gamma_5 \vec{\tau} \cdot \hat{r} F(r)\right) = P_R U + P_L U^\dagger. \tag{4.1.2}$$

In the vacuum sector, $\langle U(\vec{r}) \rangle = 1$, and the corresponding Dirac Hamiltonian is

$$h^0 = -\imath \beta \vec{\gamma} \cdot \vec{\partial} + \beta m. \tag{4.1.3}$$

It is therefore necessary to consider effects in the vacuum sector in the computation of the total soliton energies.

We note that

$$\operatorname{Det}\left(\imath D\right) = \operatorname{Det} \beta \operatorname{Det}\left(\imath \partial_t - h\right) = \operatorname{Det}\left(\imath \partial_t - h\right) \tag{4.1.4}$$

since $\mathrm{Det}\,\beta = 1$. Thus, this determinant is determined by the eigenvalues of $\imath\partial_t - h$. For static fields, h and $\imath\partial_t$ commute with each other. Hence, the eigenvalues of equation (4.1.1) are given by the independent eigenvalues of h and $\imath\partial_t$. Formally the (anti-)quark fields (which are fermions in Euclidean space) assume anti-periodic boundary conditions

$$q(t+T,\vec{x}) = -q(T,\vec{x}) \tag{4.1.5}$$

on the time interval T and the eigenvalues of $\imath\partial_t$ take the form

$$\Omega_n = \frac{(2n+1)\pi}{T}, \quad n = 0, \pm 1, \pm 2, \ldots \tag{4.1.6}$$

The value Ω_n is the so-called Matsubara frequencies. Furthermore, the eigenvalues of the Hamiltonian are discretized by imposing spatial boundary conditions to be discussed later. Then

$$h\Psi_\alpha = \epsilon_\alpha \Psi_\alpha \tag{4.1.7}$$

yields eigenfunctions Ψ_α and real energy eigenvalues ϵ_α[1]. In the vacuum sector, the eigenvalue problem for the Hamiltonian is written as

$$h^0\Psi^0_\alpha = \epsilon^{(0)}_\alpha \Psi^0_\alpha, \tag{4.1.8}$$

where ϵ^0_α and Ψ^0_α are the corresponding eigenvalues and eigenfunctions. The (anti-)quark determinant of (4.1.4) then formally (i.e without regularization) reduces to a product of the respective eigenvalues of h and $\imath\partial_t$ [36, 37]

$$\mathrm{Det}(\imath D) = \prod_\alpha \prod_n (\Omega_n - \epsilon_\alpha) = \mathcal{C} \prod_\alpha \prod_{\Omega_n > 0} \left(1 - \left(\frac{\epsilon_\alpha}{\Omega_n}\right)^2\right). \tag{4.1.9}$$

The information about static meson field is only contained in the eigenvalues ϵ_α, while the frequencies Ω_n do not depend on the dynamical properties. Hence the constant

$$\mathcal{C} = \prod_\alpha \prod_{n \geq 0} \left(-\Omega_n^2\right) \tag{4.1.10}$$

may be absorbed into the normalization of the determinant. From the infinite product representations of trigonometrical functions we have

$$\begin{aligned} \prod_{n=0}^{\infty} \left(1 - \left[\frac{\epsilon_\alpha T}{(2n+1)\pi}\right]^2\right) &= \prod_\alpha \cos\left(\frac{\epsilon_\alpha T}{2}\right) = \prod_\alpha \left[1 + \exp\left(-\imath|\epsilon_\alpha|T\right)\right] \left[\exp\left(\frac{\imath}{2}\sum_\alpha |\epsilon_\alpha| T\right)\right], \\ &= \sum_{\{\eta_\alpha\}} \exp\left[-\imath \sum_\alpha \eta_\alpha |\epsilon_\alpha| T\right] \left[\exp\left(\frac{\imath}{2}\sum_\alpha |\epsilon_\alpha| T\right)\right], \end{aligned} \tag{4.1.11}$$

where the sum $\sum_{\{\eta_\alpha\}}$ goes over all possible sets of (anti-)quark occupation numbers $\eta_\alpha = 0, 1$.

[1] Here the eigenfunctions and the eigenvalues parametrically depend on the chiral angle $F(r)$.

Then the (anti-)quark determinant can be factorized as

$$\mathrm{Det}\,(\imath D) = \mathcal{C}\sum_{\{\eta_\alpha\}} \exp\left[\imath\mathcal{A}_{\mathrm{v}}^{\{\eta_\alpha\}}\right]\exp\left[\imath\mathcal{A}_{\mathrm{s}}\right]. \tag{4.1.12}$$

This determinant provides a natural decomposition into vacuum

$$\mathcal{A}_{\mathrm{s}} = T\frac{N_c}{2}\sum_\alpha |\epsilon_\alpha| \tag{4.1.13}$$

and valence (anti-)quark

$$\mathcal{A}_{\mathrm{v}}^{\{\eta_\alpha\}} = -TN_c\sum_\alpha \eta_\alpha|\epsilon_\alpha| \tag{4.1.14}$$

contributions. It can be verified from the above equations, that in the limit of a large Euclidean time interval $T\to\infty$ only the vacuum state contribute to the functional integral as only the term with all $\eta_\alpha = 0$ survives. The color index N_c has been introduced as a multiplication factor since there is no explicit color interaction.

Furthermore, the above considerations yield the energy

$$E_{\eta_\alpha} = \sum_\alpha\left(-\frac{1}{2}|\epsilon_\alpha| + \eta_\alpha|\epsilon_\alpha|\right). \tag{4.1.15}$$

The vacuum of this system is obtained, when all $\eta_\alpha = 0$, with the filled Dirac sea of energy

$$E_{\mathrm{s}} = -\frac{1}{2}\sum_\alpha |\epsilon_\alpha|. \tag{4.1.16}$$

However, in the presence of hedgehog configuration (3.4.2) the vacuum energy E_{s} always diverges as it is given by the infinite sum of the energy eigenvalues ϵ_α and thus requires regularization, discussed below. The excited (valence) system is obtained, for some $\{\eta_\alpha\}$. Its energy contribution is extracted from the valence action as

$$E_{\mathrm{v}}^{\{\eta_\alpha\}} = \sum_\alpha \eta_\alpha|\epsilon_\alpha|. \tag{4.1.17}$$

To specify $\{\eta_\alpha\}$ we relate it to the baryon number. We start from the baryon number current

$$j^\mu(x) = \frac{1}{N_c}\langle\bar{q}(x)\gamma^\mu q(x)\rangle = \frac{1}{N_c}\frac{\imath\delta}{\delta v_\mu(x)}\log\mathrm{Det}\,(\imath D - \not{v})\Big|_{v_\mu(x)=0}, \tag{4.1.18}$$

as a single quark carries baryon number $\frac{1}{N_c}$. Applying the functional derivative onto equation (4.1.12) we can write the baryon current as

$$j^\mu(x) = \sum_{\{\eta_\alpha\}} j^\mu_{\{\eta_\alpha\}}(x) = j^\mu_{\mathrm{v}}(x) + j^\mu_{\mathrm{s}}(x) \tag{4.1.19}$$

where $j^\mu_{\mathrm{s}}(x)$ and $j^\mu_{\mathrm{v}}(x)$ are the vacuum and the valence (anti-)quark contributions. To derive explicit expressions for these currents we write the energy eigenvalues as

$$\epsilon_\alpha = -\int \mathrm{d}^3r\,\Psi^\dagger_\alpha(x)\left(\imath\partial_t - h - \beta\not{v}\right)\Psi_\alpha(x), \tag{4.1.20}$$

where $\Psi_\alpha(x)$ is the eigenfunction and treat $v_\mu(x)$ as a perturbation in the eigenvalue problem $(h+\beta\not{\psi})\,\Psi_\alpha(x)=\epsilon_\alpha\Psi_\alpha(x)$. This gives

$$\left.\frac{\delta\epsilon_\alpha}{\delta v_\mu(x)}\right|_{v_\mu(x)=0}=\Psi^\dagger_\alpha(x)\beta\gamma^\mu\Psi_\alpha(x), \tag{4.1.21}$$

hence from equations (4.1.13) and (4.1.14) we have the baryon number current as [36]

$$\begin{aligned} j^\mu_{\rm s}(x)&=-\frac{1}{2}\sum_\alpha \mathrm{sign}(\epsilon_\alpha)\bar\Psi_\alpha(x)\gamma^\mu\Psi_\alpha(x),\\ j^\mu_{\rm v}(x)&=\sum_\alpha \eta_\alpha\mathrm{sign}(\epsilon_\alpha)\bar\Psi_\alpha(x)\gamma^\mu\Psi_\alpha(x). \end{aligned} \tag{4.1.22}$$

Assuming the proper normalization condition of the eigenfunctions

$$\int \mathrm{d}^3r\;\Psi^\dagger_\alpha(x)\Psi_\beta(x)=\delta_{\alpha\beta}$$

we obtain the baryon number

$$B\left(\{\eta_\alpha\}\right)=\int \mathrm{d}^3x\,j^0(x)=\sum_\alpha\left(\eta_\alpha-\frac{1}{2}\right)\mathrm{sign}(\epsilon_\alpha). \tag{4.1.23}$$

For a prescribed baryon number we choose the η_α to minimize E_{η_α} and to match the right hand side of equation (4.1.15). Unless degenerate ϵ_α are involved, this determines η_α uniquely.

Finally, we compute the vacuum contribution $E_{\rm s}$ from the regularized bosonized action (2.2.14). In this case we also require the operator $\imath D_5$ to introduce a one-particle Dirac Hamiltonian. In the presence of hedgehog configuration it becomes

$$\imath D_5=\left(-\imath\partial_t-h\right)\beta. \tag{4.1.24}$$

Like before the determinant of this operator becomes $\mathrm{Det}(\imath D_5)=\mathrm{Det}\left(-\imath\partial_t-h\right)$. Since h is time independent we have

$$-DD_5=\beta\left(\partial_t^2+h^2\right)\beta \tag{4.1.25}$$

and $\mathcal{A}_{\rm R}$ from equation (2.2.18) becomes

$$\mathcal{A}_{\rm R}=-\imath\frac{N_c}{2}\sum_{i=0}^{2}c_i\sum_{\alpha,n}\left(\log\left[-\Omega_n^2+\epsilon_\alpha^2+\Lambda_i^2-\imath\epsilon\right]-\log\left[-\Omega_n^2+\epsilon_\alpha^{(0)\,2}+\Lambda_i^2-\imath\epsilon\right]\right). \tag{4.1.26}$$

The Matsubara frequencies become continuous when $T\to\infty$, so that

$$\sum_n f(\Omega_n)\to T\int\frac{\mathrm{d}z}{2\pi}\,f(z) \tag{4.1.27}$$

and thus

$$\mathcal{A}_{\rm R}=-\imath T\frac{N_c}{2}\sum_{i=0}^{2}c_i\sum_\alpha\int\frac{\mathrm{d}z}{2\pi}\left(\log\left[-z^2+\epsilon_\alpha^2+\Lambda_i^2-\imath\epsilon\right]-\log\left[-z^2+\epsilon_\alpha^{(0)\,2}+\Lambda_i^2-\imath\epsilon\right]\right). \tag{4.1.28}$$

We note that the integral is defined only for the principal value ($\mathcal{P}$) prescription. The '$\imath\epsilon$' induces the Wick rotation with $z \to \imath z$. Considering the first term and noting that the terms with odd of the powers of z vanish under the principal value prescription for the z integration, gives

$$\mathcal{P}\int_{-\infty}^{\infty}\frac{\mathrm{d}z}{2\pi}\,\log\left[-z^2+\epsilon_\alpha^2+\Lambda_i^2-\imath\epsilon\right]\xrightarrow[\text{rotation}]{\text{Wick}}\frac{-\imath}{\pi}\int_{-\infty}^{\infty}\mathrm{d}z\,\frac{z^2}{z^2+\epsilon_\alpha^2+\Lambda_i^2}$$
$$=\frac{\imath}{\pi}\int_{-\infty}^{\infty}\mathrm{d}z\,\left[-1+\frac{\epsilon_\alpha^2+\Lambda_i^2}{z^2+(\epsilon_\alpha^2+\Lambda_i^2)}\right]. \tag{4.1.29}$$

The first term of this result would cause a quartic divergence in A_s but cancels out from similar contribution from the second part with $\epsilon_\alpha^{(0)}$. The remaining term is computed by using the residue theorem for Cauchy's integrals and we find

$$\mathcal{A}_\mathrm{R}=T\frac{N_c}{2}\sum_{i=0}^{2}c_i\sum_\alpha\left\{\sqrt{\epsilon_\alpha^2+\Lambda_i^2}-\sqrt{\epsilon_\alpha^{(0)\,2}+\Lambda_i^2}\right\}. \tag{4.1.30}$$

This gives the vacuum contribution of the energy as

$$E_\mathrm{s}=-\frac{N_c}{2}\sum_{i=0}^{2}c_i\sum_\alpha\left\{\sqrt{\epsilon_\alpha^2+\Lambda_i^2}-\sqrt{\epsilon_\alpha^{(0)\,2}+\Lambda_i^2}\right\}. \tag{4.1.31}$$

Collecting pieces and using again equation (2.2.22), we have the regularized total energy as

$$E[F(r)]=N_c\sum_\alpha\eta_\alpha|\epsilon_\alpha|-\frac{N_c}{2}\sum_\alpha\left\{\left[|\epsilon_\alpha|-\sqrt{\epsilon_\alpha^2+\Lambda^2}+\frac{1}{2}\frac{\Lambda^2}{\sqrt{\epsilon_\alpha^2+\Lambda^2}}\right]\right.$$
$$\left.-\left[|\epsilon_\alpha^{(0)}|-\sqrt{\epsilon_\alpha^{(0)\,2}+\Lambda^2}+\frac{1}{2}\frac{\Lambda^2}{\sqrt{\epsilon_\alpha^{(0)\,2}+\Lambda^2}}\right]\right\}+E_m, \tag{4.1.32}$$

where E_m is the contribution from local part of the effective action. Subtracting the energy functional associated with the trivial meson field and using equations (2.4.14) and (2.5.22) gives

$$E_m=-\frac{mm_0}{4G}\int\mathrm{d}^3r\;\mathrm{tr}\left[U+U^\dagger-2\right]=m_\pi^2f_\pi^2\int\mathrm{d}^3r\;(1-\cos F(r))\,. \tag{4.1.33}$$

In a last step we have to determine the $\{\eta_\alpha\}$. For $B=1$ the soliton has $F(0)=\pi$ (or $-\pi$, depending on conventions). As will be discussed below, such a configuration strongly binds a single Dirac level, the so-called valence quark level, with energy eigenvalues ϵ_v. To minimize E, only this level may be occupied, i.e $\eta_\alpha\equiv 0$ for $\alpha\neq\mathrm{v}$. If the profile function $F(r)$ is wide, ϵ_v turns negative. In view of equation (4.1.23) with $B=1$ we thus have

$$\eta_\mathrm{v}=\frac{1}{2}\left[1+\mathrm{sign}(\epsilon_\mathrm{v})\right]. \tag{4.1.34}$$

The total energy becomes

$$E[F(r)]=\frac{N_c}{2}\left[1+\mathrm{sign}(\epsilon_\mathrm{v})\right]\epsilon_\mathrm{v}-\frac{N_c}{2}\sum_\alpha\left\{\left[|\epsilon_\alpha|-\sqrt{\epsilon_\alpha^2+\Lambda^2}+\frac{1}{2}\frac{\Lambda^2}{\sqrt{\epsilon_\alpha^2+\Lambda^2}}\right]\right.$$
$$\left.-\left[|\epsilon_\alpha^{(0)}|-\sqrt{\epsilon_\alpha^{(0)\,2}+\Lambda^2}+\frac{1}{2}\frac{\Lambda^2}{\sqrt{\epsilon_\alpha^{(0)\,2}+\Lambda^2}}\right]\right\}+m_\pi^2f_\pi^2\int\mathrm{d}^3r\;(1-\cos F(r))\,. \tag{4.1.35}$$

Clearly the total energy is of order N_c as speculated for the total mass of a soliton in an effective field theory.

4.2 Energy Spectrum of the Dirac Hamiltonian

In this section we discuss the Dirac spectrum relevant to the total energy (4.1.35). First note that the hedgehog field configuration (3.4.2) does not preserve spin and isospin symmetries as

$$\left[h, \vec{J}\right] \neq 0 \quad \text{and} \quad \left[h, \frac{\vec{\tau}}{2}\right] \neq 0 \tag{4.2.1}$$

but rather

$$\left[h, \vec{J} + \frac{\vec{\tau}}{2}\right] = 0 \tag{4.2.2}$$

is a conserved quantity. We call

$$\vec{G} = \vec{J} + \frac{\vec{\tau}}{2} = \vec{L} + \frac{\vec{\sigma}}{2} + \frac{\vec{\tau}}{2} \tag{4.2.3}$$

the grand spin [19, 38]. Here $\vec{\sigma}$ and $\vec{\tau}$ are the spin and isospin Pauli matrices respectively. Since h preserves $\vec{G}$, the eigenstates of the Hamiltonian, h, are also eigenstates of $\vec{G}$. The quantum numbers of $\vec{G}$ are given as $\vec{G}^2 = G(G+1)$ and $G_3 = M$ (see Appendix C) and its eigenfunctions are the generalized spherical harmonics

$$[\mathcal{Y}_{LJGM}(\hat{r})]_{si} = \sum_{m,s_3,i_3,J_3} C^{GM}_{JJ_3,\frac{1}{2}i_3} C^{JJ_3}_{Lm,\frac{1}{2}s_3} Y_{Lm}(\hat{r}) \chi_s(s_3) \chi_i(i_3) \tag{4.2.4}$$

where $C^{GM}_{JJ_3,\frac{1}{2}i_3}$ and $C^{JJ_3}_{Lm,\frac{1}{2}s_3}$ are $SU(2)$ Clebsch-Gordon coefficients. The χ_s and χ_i are two components spinors in spin and isospin spaces, respectively, while Y_{Lm} denotes spherical harmonic functions.

To construct a four-component Dirac spinor, $\mu = 1, \cdots, 4$, we combine two Weyl spinors $[\mathcal{Y}_{\dots}(\hat{r})]_{si}$ with $\mu = s$ and $[\mathcal{Y}_{\dots}(\hat{r})]_{s'i}$ with $\mu = s' + 2$, by taking into account of the angular dependence and parity of the corresponding Dirac structures of the meson fields[2] ϕ (2.2.9). Thus, the eigenfunction of h carry good parity with eigenstates of the parity. We write the corresponding wavefunctions as (see Appendix C)

$$\Psi^{(G,+)}_\alpha(\vec{x}) = \begin{pmatrix} \imath g^{(G,+;1)}_\alpha(r) \mathcal{Y}_{GG+\frac{1}{2}GM}(\hat{x}) \\ f^{(G,+;1)}_\alpha(r) \mathcal{Y}_{G+1G+\frac{1}{2}GM}(\hat{x}) \end{pmatrix} + \begin{pmatrix} \imath g^{(G,+;2)}_\alpha(r) \mathcal{Y}_{GG-\frac{1}{2}GM}(\hat{x}) \\ -f^{(G,+;2)}_\alpha(r) \mathcal{Y}_{G-1G-\frac{1}{2}GM}(\hat{x}) \end{pmatrix} \tag{4.2.5}$$

$$\Psi^{(G,-)}_\alpha(\vec{x}) = \begin{pmatrix} \imath g^{(G,-;1)}_\alpha(r) \mathcal{Y}_{G+1G+\frac{1}{2}GM}(\hat{x}) \\ -f^{(G,-;1)}_\alpha(r) \mathcal{Y}_{GG+\frac{1}{2}GM}(\hat{x}) \end{pmatrix} + \begin{pmatrix} \imath g^{(G,-;2)}_\alpha(r) \mathcal{Y}_{G-1G-\frac{1}{2}GM}(\hat{x}) \\ f^{(G,-;2)}_\alpha(r) \mathcal{Y}_{GG-\frac{1}{2}GM}(\hat{x}) \end{pmatrix}, \tag{4.2.6}$$

where $r = |\vec{x}|$. Here, the intrinsic parity $\prod_{\text{intr}} = \pm 1$ is labeled by the second superscripts; and are defined by the parity eigenvalue as $\Pi = (-)^G \times \Pi_{\text{intr}}$. Also $g^{(G,\pm;i)}_\alpha$ and $f^{(G,\pm;i)}_\alpha (i = 1, 2)$ are radial functions. The index α refers to the energy eigenstate. It is discretized by demanding that there is no flux outside a ball with radius D much larger than the soliton extension. This

[2] The choice of the angular dependence must be compatible with the parity of the Dirac structures of the meson fields.

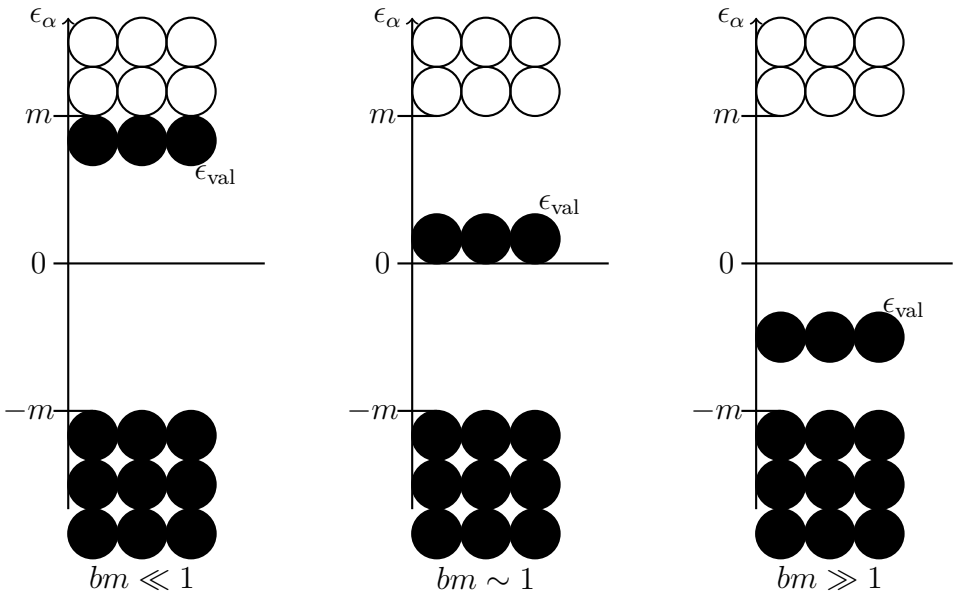

Figure 4.1: Visualization of the Dirac spectrum in the $G = 0$ channel for $N_c = 3$. In accordance to Dirac-hole theory, each circle represents a state (energy levels), levels shown with open circles are unoccupied whereas the levels shown with black circles are occupied. Also indicated here are the excited states with $|\epsilon_\alpha| \geq m$. Furthermore, the ϵ_{val} is the energy eigenvalue of the bound valence quark level.

is the case when one of the two radial functions vanishes at $r = D$ (requiring both to vanish over-constrains the system). There are various possibilities[19]. We choose to set to zero the components that have $L = G$ (at $r = D$) so that the matrix elements of $\vec{\tau}$ are diagonal in the free case. That is $g_\alpha^{(G,+;i)}(D) = 0$ and $f_\alpha^{(G,-;i)}(D) = 0$.

In what follows, we picture the Dirac spectrum of h by assuming the profile function $F(r)$ c.f equation (3.4.2) to be characterized by a single length scale, $b \ll D$. We consider the spectrum of the eigenspinor $\Psi_\alpha^{(0,+)}$, as the quarks becomes strongly bounded for $G = 0$. The only explicit parameter in the Dirac Hamiltonian is the constituent quark mass m. Hence we distinguish three different regions defined by the dimensionless combination bm. Their spectrum is depicted in Figure 4.1.

In the $bm \ll 1$ regime, the background weakly interacts with the quarks. The quarks at this level are weakly bound with positive energy and almost no polarization effect. Furthermore, in $bm \sim 1$ regime, the quarks are moderately bound as the interactions between the meson background and the quarks becomes strong. Though there is significant binding, summing the vacuum baryon number over positive and negative eigenvalues results in $B_{\text{s}} = 0$ as the energy eigenvalue of the valence quark is positive. Like the analyzes in previous section, this implies that the configurations $bm \ll 1$ and $bm \sim 1$ acquire unit baryon number by setting $\eta_{\text{v}} = 1$. For the case of the $bm \gg 1$ regime, the valence level enters the Dirac sea. In this case the valence quarks are so strongly bound that the energy eigenvalue becomes negative. Also the vacuum baryon number becomes $B_{\text{s}} = 1$ all occupation numbers must be set to zero, i.e $\eta_\alpha = 0$. In this regime, the vacuum becomes strongly polarized by the background in such a way that the

quarks acquires a baryonic charge. This actually corresponds to the Skyrme limit [39].

In conclusion, for a strong pion field in the $B = 1$ sector, only one bound valence state level exists. As the spatial size of the pion field increases, this level moves from the upper Dirac to the lower Dirac continuum as indicated in Figure 4.1.

4.3 The Static Chiral Soliton

The soliton solution is obtained as the profile function $F(r)$ by extremizing the static energy

$$\frac{\delta E[F(r)]}{\delta F(r)} = \sum_{\alpha} \frac{\partial E_{\rm s}}{\partial \epsilon_\alpha} \frac{\delta \epsilon_\alpha}{\delta F(r)} + \frac{\partial E_{\rm v}}{\partial \epsilon_{\rm v}} \frac{\delta \epsilon_{\rm v}}{\delta F(r)} + \frac{\delta E_m}{\delta F(r)} = 0. \tag{4.3.1}$$

From equations (4.1.2) and (4.1.20) we have

$$\frac{\delta \epsilon_\alpha[F(r)]}{\delta F(r)} = m \int \mathrm{d}\Omega\, \Psi_\alpha^\dagger(\vec{x}) \beta \left[-\sin F(r) + \imath \gamma_5 \vec{\tau} \cdot \hat{x} \cos F(r) \right] \Psi_\alpha(\vec{x}), \tag{4.3.2}$$

where $\int \mathrm{d}\Omega$ is the solid angle integral. Similar results also hold for functional derivative of $\epsilon_{\rm v}$ with respect to $F(r)$. Then the equation of motion for the profile function $F(r)$ becomes [40–42]

$$\cos F(r)\, \mathrm{tr} \int \mathrm{d}\Omega\, \rho(\vec{x},\vec{x}) \imath \gamma_5 \vec{\tau} \cdot \hat{x} = \sin F(r) \left\{ \mathrm{tr} \int \mathrm{d}\Omega\, \rho(\vec{x},\vec{x}) - \frac{m_\pi^2 f_\pi^2}{m N_c} \right\}, \tag{4.3.3}$$

where the traces are over flavor and Dirac indices only and $\rho(\vec{x},\vec{y})$ is the regularised density matrix. It is convenient to decompose it into vacuum and valence (anti-) quark parts:

$$\begin{aligned}
\rho(\vec{x},\vec{y}) &= \rho_{\rm s}(\vec{x},\vec{y}) + \rho_{\rm v}(\vec{x},\vec{y}), \\
\rho_{\rm s}(\vec{x},\vec{y}) &= -\frac{1}{2} \sum_{i=0}^{2} c_i \sum_{\alpha} \Psi_\alpha(\vec{x}) \frac{\epsilon_\alpha}{\sqrt{\epsilon_\alpha^2 + \Lambda_i^2}} \bar{\Psi}_\alpha(\vec{y}), \\
\rho_{\rm v}(\vec{x},\vec{y}) &= \frac{1}{2} \left[1 + \mathrm{sign}(\epsilon_{\rm v}) \right] \Psi_{\rm v}(\vec{x}) \bar{\Psi}_{\rm v}(\vec{y}).
\end{aligned} \tag{4.3.4}$$

In the literature [40–42] the soliton profile of the equation of motion is solved by the Hartree iteration: first a profile function $F(r)$ for the hedgehog configuration is guessed in such a way that it satisfies the boundary conditions (3.3.7). In what follows, the equation of motion (4.3.1) is employed to iterate the profile function $F(r)$. The numerical approach starts with reading all initial parameters from standard input. The profile function is then used to compute the eigenvalues ϵ_α and associated eigenfunctions Ψ_α of the Hamiltonian h by diagonalizing the Hamiltonian using a Jacobi routine in a large but finite volume (spherical cavity of radius $r = D$). The computed eigenvalues and eigenvectors are stored in an unformatted file, which we will later use when computing the structure functions. It must be emphasized that the quantity D has no physical meaning as it does not depend on the dynamical variable m and the single cutoff Λ. In our numerical calculations we have taken the radius of the spherical cavity to be $D = 10\,\mathrm{fm}$. Also, we impose a numerical momentum cut-off $k_{\max}$ several times

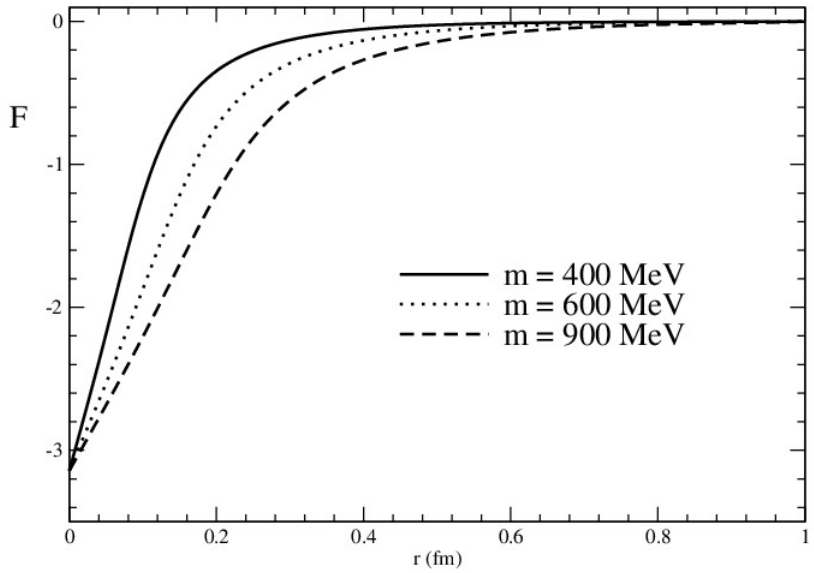

Figure 4.2: Solutions of the soliton profile function $F(r)$ for various values of the constituent quark masses. Shown here as a function of the radial coordinate r.

the Pauli-Villars cut-off Λ. Since discretization requires roots of spherical Bessel functions (see Appendix C) below $Dk_{\max}$, this induces also a grand spin cut-off, typical around $G_{\max} \approx 100$. Of course we have ensured stability against changes of the numerical parameters once D and $k_{\max}$ are taken large enough.

The eigenvalues and eigenfunctions are then used to update the profile function via equation (4.3.3). This subsequently serves as a new input profile function for the Hamiltonian. This procedure is repeated until convergence is reached and the final configuration is adopted as the soliton solution. We achieve this convergence after performing $15-20$ iterations. Self-consistent solutions were numerically obtained for $m \geq 325\,\text{MeV}$ [40]. Stable solutions must have $E < 3m$. We see from Table 4.1 that it requires a constituent quark mass slightly above 400 MeV. Also, the total energy varies only moderately with m.

In Figure 4.2, we present solutions for the profile function $F(r)$ for various values of the constituent quark mass m, as it is the only adjustable parameter in the model once the pion decay constant and the pion mass are fixed to their experimental values: $f_\pi = 93\,\text{MeV}$ and $m_\pi = 135\,\text{MeV}$. We observe that the profile function $F(r)$ spreads as m increases. Furthermore, for constituent masses less than 816 MeV the system has the valence level explicitly occupied. But for $m > 816\,\text{MeV}$ the valence quarks must not be explicitly occupied to generate baryon number ($\eta_{\text{v}} = 0$) as the Dirac sea becomes so strongly polarized that it carries the baryon number by itself and hence the valence level does not contribute to the total soliton mass of the system. In this regime the soliton becomes tightly bounded. This is also reflected

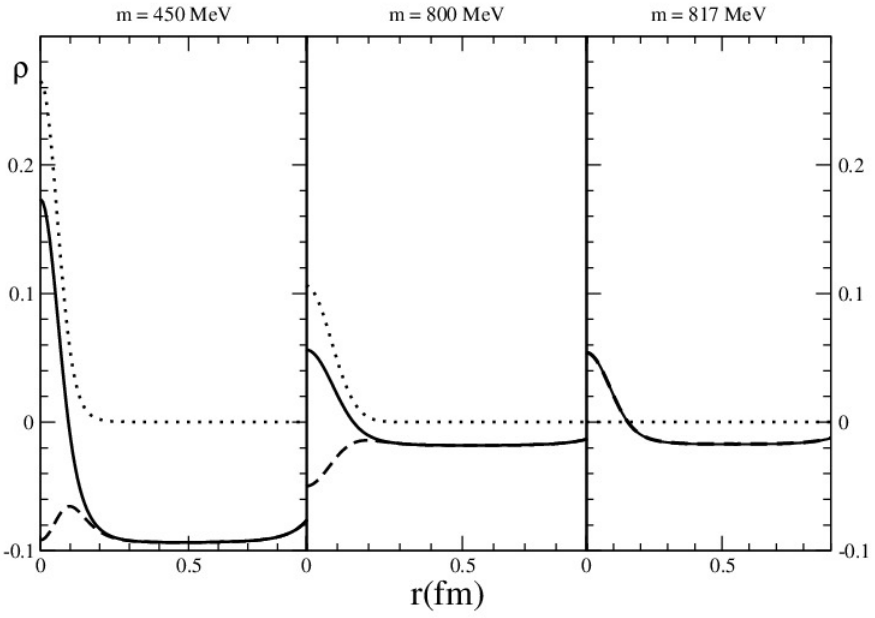

Figure 4.3: The scalar density distribution $\int \mathrm{d}\Omega\, \rho(\vec{x})$ in the $B = 1$ sector self-consistent solutions for $m = 400\,\mathrm{MeV}, 800\,\mathrm{MeV}$ and $817\,\mathrm{MeV}$. The straight line represent the total density distribution, while the dashed and dotted lines represent the vacuum and valence quark distributions respectively. For the case of $m = 817\,\mathrm{MeV}$ the vacuum density equals that of the total energy as the valence contribution becomes zero.

m	350	400	450	500	600	700	800
E_{tot}	1279	1286	1278	1263	1223	1176	1127
E_{v}	793	665	575	492	333	177	23
E_{s}	458	590	672	741	863	975	1084
E_m	27	30	31	29	26	23	20

Table 4.1: The soliton mass E_{tot}, the valence energy E_{v}, the vacuum energy E_{s} and the meson field energy E_m (all data in Mev) that defines (4.1.35) as functions of the constituent quark mass m.

in the baryon density, equation (4.3.4) that is shown in Figure 4.3.

4.4 Collective Prescription to the $SU(2)$ Chiral Soliton

So far we have discussed the chiral soliton solution in the $B = 1$ sector that arises from extremizing the static energy. However, since these solutions have zero grand spin they come as linear combinations of eigenstates with $|\vec{J}| = |\vec{I}|$ where $\vec{J}$ and $\vec{I}$ are angular momentum and isospin operators. To generate states with good spin and isospin quantum numbers, we perform time-dependent rotations in isospace and quantize them canonically. Due to the grand spin symmetry of the hedgehog field configuration (3.4.2) they also parametrize spatial rotations. These rotations are zero modes of the hedgehog configurations. We thus approximate the time

dependent field configuration as

$$U(t,\vec{x}) = A(t)U(\vec{x})A^{\dagger}(t). \tag{4.4.1}$$

Here $A(t)$ is an $SU(2)$ time-dependent collective coordinate matrix which parametrizes the isospin orientation of the soliton and $U(\vec{x})$ is the static hedgehog configuration, equation (3.2.13). According to the discussion of section 3.4 the hedgehog structure yields the identity

$$\left(\vec{x}\times\vec{\nabla}\right)_l U = -\imath\frac{1}{2}\left[U,\tau_j\right]D_{jl} \tag{4.4.2}$$

which corresponds to

$$\vec{J} = -\vec{I}D. \tag{4.4.3}$$

Thus the quantized soliton spin $\vec{J}$ coincides with the collective isospin $\vec{I}$ up to a rotation. This relation implies that the respective absolute values of the spin and isospin must always be equal

$$|\vec{J}| = |\vec{I}|. \tag{4.4.4}$$

We consider the effective action (2.2.14) in the presence of the isorotating hedgehog field: The mesonic part is time independent and does not depend on the collective coordinate $A(t)$. This is not the case for the non-local part of the action. We follow the discussion of [36] by eliminating the collective coordinate $A(t)$ from the pseudoscalar field by transforming the fermion field to the flavor rotating system

$$q \to q' = Aq. \tag{4.4.5}$$

Under this transformation the Dirac operators become

$$\begin{aligned}&\bar{q}\imath Dq = \bar{q}'\imath D'q' \quad \text{and} \quad \bar{q}\imath D_5 q = \bar{q}'\imath D_5' q' \quad \text{with}\\ &\imath D' = A\beta\left(\imath\partial_t - \frac{1}{2}\vec{\Omega}\cdot\vec{\tau} - h\right)A^{\dagger} \quad \text{and} \quad \imath D_5' = A\left(-\imath\partial_t + \frac{1}{2}\vec{\Omega}\cdot\vec{\tau} - h\right)\beta A^{\dagger},\end{aligned} \tag{4.4.6}$$

which introduces the angular velocity vector $\vec{\Omega}$ via

$$A^{\dagger}(t)\dot{A}(t) = \frac{\imath}{2}\vec{\Omega}\cdot\vec{\tau} \tag{4.4.7}$$

and the intrinsic Dirac Hamiltonians are

$$h' = h + \frac{1}{2}\vec{\Omega}\cdot\vec{\tau} \quad \text{and} \quad h_5' = h - \frac{1}{2}\vec{\Omega}\cdot\vec{\tau} \tag{4.4.8}$$

for the Dirac operators $\imath D'$ and $\imath D_5'$ respectively. The exact eigenvalues for the Hamiltonians are unknown in this case and we perform a perturbation expansion. The collective rotation is assumed to be adiabatic so that only the leading contribution in $\vec{\Omega}$ must be retained. To this end, we compute the fermion determinant of these operators following analogous calculation from section 4.1. This again separates into vacuum and valence (anti-) quark parts. Due to

isospin symmetry only even powers of $\vec{\Omega}$ will contribute. We obtain the valence contribution part as

$$\mathcal{A}_{\rm v}^{\{\eta_\alpha\}} = -N_c T E_{\rm v} + \frac{T}{2}\sum_{i,j}^{3} F_{ij}^{\rm v}\Omega_i\Omega_j + \mathcal{O}(\vec{\Omega}^4). \tag{4.4.9}$$

Here $F_{ij}^{\rm v}$ denotes the valence quark contribution to the moment of inertia [36, 43] obtained in standard time independent perturbation theory

$$F_{ij}^{\rm v} = -\frac{N_c}{2}\sum_{\beta\neq{\rm v}}\eta_{\rm v}\frac{\langle {\rm v}|\tau_i|\beta\rangle\langle\beta|\tau_j|{\rm v}\rangle}{\epsilon_{\rm v}-\epsilon_\beta}. \tag{4.4.10}$$

Here $|{\rm v}\rangle$ represents the occupied valence quark level in the static solutions while β runs over positive and negative energy levels.

Next we consider the vacuum contribution to the moment of inertia by extracting it from the real part of the effective action in the presence of the adiabatic perturbation $\vec{\Omega}$,

$$\mathcal{A}_{\rm R} = -\imath\frac{N_c}{2}T\sum_{i=0}^{2}c_i\int\frac{{\rm d}z}{2\pi}\,{\rm Tr}\log\Big[\left(-z^2+h^2+\Lambda_i^2-\imath\epsilon\right)+z\vec{\Omega}\cdot\vec{\tau}+\frac{1}{2}\left[\vec{\Omega}\cdot\vec{\tau},h\right]-\frac{1}{4}\left(\vec{\Omega}\cdot\vec{\tau}\right)^2\Big]. \tag{4.4.11}$$

Let

$$B_0 = -z^2+h^2+\Lambda_i^2-\imath\epsilon,\quad B_1 = z\vec{\Omega}\cdot\vec{\tau},\quad B_2 = \frac{1}{2}\left[\vec{\Omega}\cdot\vec{\tau},h\right],\quad B_3 = -\frac{1}{4}(\vec{\Omega}\cdot\vec{\tau})^2. \tag{4.4.12}$$

The expansion of $\mathcal{A}_R$ up to quadratic order in $\vec{\Omega}$ gives

$$\begin{aligned}\mathcal{A}_R &= -\imath\frac{N_c}{2}T\sum_{i=0}^{2}c_i\int\frac{{\rm d}z}{2\pi}\,{\rm Tr}\log\left[B_0+B_1+B_2+B_3\right]\\ &= -\imath\frac{N_c}{2}T\sum_{i=0}^{2}c_i\int\frac{{\rm d}z}{2\pi}\,{\rm Tr}\log B_0 - \imath\frac{N_c}{2}T\sum_{i=0}^{2}c_i\int\frac{{\rm d}z}{2\pi}\,{\rm Tr}\,B_0^{-1}\left[B_1+B_2\right]\\ &\quad+\imath\frac{N_c}{2}T\sum_{i=0}^{2}c_i\int\frac{{\rm d}z}{2\pi}\,{\rm Tr}\,B_0^{-1}\left[B_1+B_2\right]B_0^{-1}\left[B_1+B_2\right]+\mathcal{O}(\vec{\Omega}^4).\end{aligned} \tag{4.4.13}$$

In the second line of equation (4.4.13), the odd terms in z (second term) vanish under the integral with respect to z. Evaluating the traces in the eigenbasis of h (4.1.7) we have the vacuum contribution upto quadratic order in $\vec{\Omega}$, in the isospin limit as

$$\mathcal{A}_{\rm R} = -TE_{\rm s} + \frac{T}{2}F_{ij}^{\rm s}\Omega_i\Omega_j + \mathcal{O}(\vec{\Omega}^4), \tag{4.4.14}$$

with the moment of inertia functional

$$F_{ij}^{\rm s} = \imath\frac{N_c}{2}\sum_{\alpha\neq\beta}\sum_{i=0}^{2}c_i\int\frac{{\rm d}z}{2\pi}\,\frac{\left(z^2+\epsilon_\alpha\epsilon_\beta+\Lambda_i^2\right)\langle\alpha|\tau_i|\beta\rangle\langle\beta|\tau_j|\alpha\rangle}{\left[-z^2+\epsilon_\alpha^2+\Lambda_i^2-\imath\epsilon\right]\left[-z^2+\epsilon_\beta^2+\Lambda_i^2-\imath\epsilon\right]}. \tag{4.4.15}$$

The '$\imath\epsilon$' prescription requires to perform the Wick rotation $z\to\imath z$. Using the residue theorem for Cauchy's integrals we have

$$\begin{aligned}F_{ij}^{\rm s} &\xrightarrow[\text{rotation}]{\text{Wick}} \frac{N_c}{2}\sum_{\alpha\neq\beta}\sum_{i=0}^{2}c_i\int\frac{{\rm d}z}{2\pi}\,\frac{\left(-z^2+\epsilon_\alpha\epsilon_\beta+\Lambda_i^2\right)\langle\alpha|\tau_i|\beta\rangle\langle\beta|\tau_j|\alpha\rangle}{\left[z^2+\epsilon_\alpha^2+\Lambda_i^2\right]\left[z^2+\epsilon_\beta^2+\Lambda_i^2\right]},\\ &= \frac{N_c}{2}\sum_{\alpha\neq\beta}\sum_{i=0}^{2}c_i\left\{\frac{\sqrt{\epsilon_\alpha^2+\Lambda_i^2}-\sqrt{\epsilon_\beta^2+\Lambda_i^2}}{2\left(\epsilon_\alpha^2-\epsilon_\beta^2\right)}+\frac{\epsilon_\alpha\epsilon_\beta+\Lambda_i^2}{2\left(\epsilon_\alpha^2-\epsilon_\beta^2\right)}\frac{\sqrt{\epsilon_\beta^2+\Lambda_i^2}-\sqrt{\epsilon_\alpha^2+\Lambda_i^2}}{\sqrt{\epsilon_\alpha^2+\Lambda_i^2}\sqrt{\epsilon_\beta^2+\Lambda_i^2}}\right\}\langle\alpha|\tau_i|\beta\rangle\langle\beta|\tau_j|\alpha\rangle.\end{aligned} \tag{4.4.16}$$

m	$\alpha_{\rm v}^2[F(r)]$	$\alpha_{\rm s}^2[F(r)]$	$\alpha^2[F(r)]$
350	8.049	1.054	9.103
400	4.708	1.173	5.881
450	3.548	1.192	4.740
500	2.869	1.181	4.049
600	2.070	1.106	3.176
700	1.604	0.996	2.600
800	1.296	0.874	2.170

Table 4.2: The valence $\alpha_{\rm v}^2$, the vacuum $\alpha_{\rm s}^2$ and the total α^2 contribution to the moment of inertia given in GeV^{-1} for various values of the constituent quark masses m.

Finally using the formula for single cut-off (see Appendix B.1) we obtain

$$\begin{aligned} F_{ij}^{\rm s} = & \frac{N_c}{4}\sum_{\alpha\neq\beta}\frac{\langle\alpha|\tau_i|\beta\rangle\langle\beta|\tau_j|\alpha\rangle}{\left(\epsilon_\alpha^2-\epsilon_\beta^2\right)} \\ & \times\left(\left\{\left[|\epsilon_\alpha|-\sqrt{\epsilon_\alpha^2+\Lambda^2}+\frac{1}{2}\frac{\Lambda^2}{\sqrt{\epsilon_\alpha^2+\Lambda^2}}\right]-\left[|\epsilon_\beta|-\sqrt{\epsilon_\beta^2+\Lambda^2}+\frac{1}{2}\frac{\Lambda^2}{\sqrt{\epsilon_\beta^2+\Lambda^2}}\right]\right\}\right. \\ & +\epsilon_\alpha\epsilon_\beta\left\{\frac{|\epsilon_\beta|-|\epsilon_\alpha|}{|\epsilon_\alpha||\epsilon_\beta|}-\frac{\sqrt{\epsilon_\beta^2+\Lambda^2}-\sqrt{\epsilon_\alpha^2+\Lambda^2}}{\sqrt{\epsilon_\alpha^2+\Lambda^2}\sqrt{\epsilon_\beta^2+\Lambda^2}}\right\}-\left(\epsilon_\alpha\epsilon_\beta+\Lambda^2\right)\frac{\Lambda^2}{2}\left.\frac{\sqrt[3]{\epsilon_\beta^2+\Lambda^2}-\sqrt[3]{\epsilon_\alpha^2+\Lambda^2}}{\sqrt[3]{\epsilon_\beta^2+\Lambda^2}\sqrt[3]{\epsilon_\alpha^2+\Lambda^2}}\right). \end{aligned} \tag{4.4.17}$$

From equations (4.4.9) and (4.4.14), we have the energy functional upto quadratic order in $\vec{\Omega}$ (as a result of perturbation expansion in $\vec{\Omega}$) as

$$E[U(t,\vec{x})] = -E[F(r)] + \frac{1}{2}\Omega_i F_{ij}[F(r)]\Omega_j + \cdots \tag{4.4.18}$$

where $F_{ij}[F(r)]$ is the moment of inertia functional given as

$$F_{ij}[F(r)] = \left.\frac{\partial^2\mathcal{A}}{\partial\Omega_i\partial\Omega_j}\right|_{\vec{\Omega}=0} = \delta_{ij}\alpha^2[F(r)] = F_{ij}^{\rm s}[F(r)] + F_{ij}^{\rm v}[F(r)], \tag{4.4.19}$$

which is diagonal since no direction in isospace is distinguished. It must be emphasized that, like the soliton energy, the moment of inertia functional is of order N_c. Replacing $\langle\alpha|\tau_i|\beta\rangle\langle\beta|\tau_j|\alpha\rangle$ by $|\langle\alpha|\tau_3|\beta\rangle|^2$ in equations (4.4.10) and (4.4.17) yields the valence ($\alpha_{\rm v}^2$) and vacuum ($\alpha_{\rm s}^2$) parts, respectively. Table 4.2 shows the results for the moment of inertia $\alpha^2[F(r)]$ for various values of the constituent mass (m). One observes from this table that, as the valence quark contribution $\alpha_{\rm v}^2[F(r)]$ decreases, the vacuum contribution $\alpha_{\rm s}^2[F(r)]$ varies moderately with m. This is as a result of the vacuum being moderately polarized. Also, the total moment of inertia decreases with m.

Using the Fierz identity

$$(\tau_a)_{ij}(\tau_a)_{kl} = 2\delta_{il}\delta_{jk} - \delta_{ij}\delta_{kl} \tag{4.4.20}$$

yields

$$\dot{D}_{ij}D_{kj} = -\frac{1}{2}\epsilon_{ikl}\Omega_l. \tag{4.4.21}$$

so that

$$\begin{aligned}\dot{U}(t,\vec{r}) &= \imath\tau_i \dot{D}_{ij}\hat{r}_j \sin F(r) = -\frac{\imath}{2}\Omega_l \epsilon_{ikl}\tau_k D_{ij}\hat{r}_j \sin F(r), \\ &= -\imath\frac{1}{2}\Omega_l \left[\tau_l, U\right]. \end{aligned} \tag{4.4.22}$$

From this relation the spin is obtained by the Noether charge

$$\vec{J} = \int \mathrm{d}^3 r \ \mathrm{tr}\left\{\frac{\partial L}{\partial \dot{U}}\frac{\partial \dot{U}}{\partial \vec{\Omega}} + \frac{\partial L}{\partial \dot{U}^\dagger}\frac{\partial \dot{U}^\dagger}{\partial \vec{\Omega}}\right\} = \frac{\partial L}{\partial \vec{\Omega}} = \alpha^2 \vec{\Omega} \tag{4.4.23}$$

and the Hamiltonian operator becomes

$$H = \vec{J}\cdot\frac{\partial L}{\partial \vec{\Omega}} - L = E + \frac{1}{2\alpha^2}\vec{J}^2. \tag{4.4.24}$$

We thus see that the collective coordinate quantization is that of an $SU(2)$ rigid top. This formulation is standard[44]. The eigenfunction can be written as Wigner-D functions of Euler angles representing $A(t)$. Then the eigenvalue equations are

$$\vec{J}^2 D^{J=I}_{m,m'}(A) = \vec{I}^2 D^{J=I}_{m,m'}(A) = J(J+1)D^{J=I}_{m,m'}(A) \tag{4.4.25}$$

$$J_3 D^{J=I}_{m,m'}(A) = -m' D^{J=I}_{m,m'}(A) \quad \text{and} \quad I_3 D^{J=I}_{m,m'}(A) = m' D^{J=I}_{m,m'}(A). \tag{4.4.26}$$

Furthermore, from equation (4.4.3) we have[45]

$$\langle N|D_{ij}|N\rangle = -\frac{4}{3}\langle N|I_i J_j|N\rangle, \tag{4.4.27}$$

where $|N\rangle$ is the nucleon state with $I = J = \frac{1}{2}$.

Chapter 5

Nucleon Structure Functions in the NJL model

Nucleon structure functions within the NJL soliton model have been studied in the past four decades. The authors Refs [46, 47] investigated the polarized and unpolarized structure functions of the nucleon within the valence quark approximation. This avoids the problem of regularizing the structure functions and should be reliable as $x \sim 1$ and is with structure function sum rules as they only probe the valence quark content. However, for $x \to 0$ the important sea contribution is not included.

In attempt to include vacuum polarization effects an ad hoc subtraction scheme was considered Refs[48, 49]. Those calculations were restricted to the isosinglet unpolarized and the isovector longitudinal polarized structure functions. This only yields the leading $\frac{1}{N_c}$ contributions and does not distinguish between proton and neutrons. More recent studies implement subleading $\frac{1}{N_c}$ contributions but still with an ad hoc regularization [50, 51].

To consistently incorporate the vacuum polarization effects within the bosonized NJL model, we will adopt the Pauli-Villars subtraction regularization scheme and take the Compton tensor as starting point of the calculation. The optical theorem relates the hadronic tensor to the imaginary part of the virtual Compton scattering amplitude, see also equation (1.6.11),

$$W_{\mu\nu}(p,q) = \frac{1}{2\pi} \operatorname{Im}\left[T_{\mu\nu}(p,q)\right]. \tag{5.0.1}$$

The Compton tensor itself is given as the matrix element of a time-ordered product of the hadronic currents

$$T_{\mu\nu}(p,q) = \int \mathrm{d}^3\xi e^{\imath q\cdot\xi} \left\langle p,s\right| T\left(J_\mu(\xi)J_\nu(0)\right)\left|p,s\right\rangle \tag{5.0.2}$$

rather than their commutator. This has the advantage that the time-ordered product is obtained from the regularized action of the NJL model (discussed in the preceding chapter) as

$$T\left(J_\mu(\xi)J_\nu(0)\right) = \frac{\delta^2}{\delta v_\mu(\xi)\delta v_\nu(0)} \operatorname{Tr}_\Lambda \log\left[\imath\partial\!\!\!/ - (MP_R + M^\dagger P_L) + \mathcal{Q}\not{v}\right]\Big|_{v_\mu=0}. \tag{5.0.3}$$

Once the Compton tensor has been obtained, Cutkosky's rules will relate that result to the hadronic tensor and thus provide the structure functions. Some formal analysis of this approach has already been carried out in reference [24].

In this project we will undertake the cumbersome task of their numerical evaluation. This will provide important predictions for the $x \to 0$ behavior of the structure functions. Since the model is designed to mimic QCD at low energies, the DGLAP evolution program will have to be applied to these numerical results before comparing with data.

This chapter serves to formally derive expressions for the consistently regularized structure functions in the NJL (soliton) model. To set up the calculations we first consider pion structure functions.

5.1 The Pion Structure Function and Bjorken Scaling

Here, we want to first discuss DIS for the pion in the NJL model. Eventually this will suggest useful simplifications for the calculation of nucleon structure function in the same model. To proceed with the discussions, we write the current operator in equation (1.6.9) as

$$J_\mu = \bar{q}(\xi)\mathcal{Q}\gamma_\mu q(\xi), \tag{5.1.1}$$

where $\mathcal{Q}$ is the flavor quark charge matrix. This will serve as a framework in computing the DIS properties of both the pion and the nucleon. It is one of the symmetry currents in chiral models that have an immediate connection to QCD.

To compute the virtual Compton scattering amplitude, we need to construct the time ordered product of two current operators, which by definition is straightforwardly obtained by path integral quantization. To do so, we introduce an external photon-like vector source in the effective action with

$$\imath D \to \imath D + \mathcal{Q}\not{v} \quad \text{and} \quad \imath D_5 \to \imath D_5 - \mathcal{Q}\not{v},$$

then the time-ordered product of the current-current product, whose matrix element is the Compton amplitude c.f equation (5.0.2) becomes

$$T\left(J_\mu(\xi)J_\nu(0)\right) = -\imath N_c \frac{\delta^2}{\delta v_\mu(\xi)\delta v_\nu(0)} \operatorname{Tr}_\Lambda \log\left[\imath\not{\partial} - (MP_R + M^\dagger P_L) + \mathcal{Q}\not{v}\right]\Big|_{v_\mu=0}. \tag{5.1.2}$$

When evaluating this time-ordered product from the regularized action isospin violating dimension -five operators emerge due to the separation of $\imath D$ and $\imath D_5$. Fortunately isospin violating pieces cancel when expanding the regularized part of the effective action in the photon field v_μ to quadratic order [24]. This cancellation is a feature of Bjorken limit: the quark propagator with infinitely large photon momentum (Q^2) should be approximated by the one of the non-interacting (massless) fermions. In this regime contributions of the form $\dfrac{\Lambda^2}{Q^2}$ drop out. Thus,

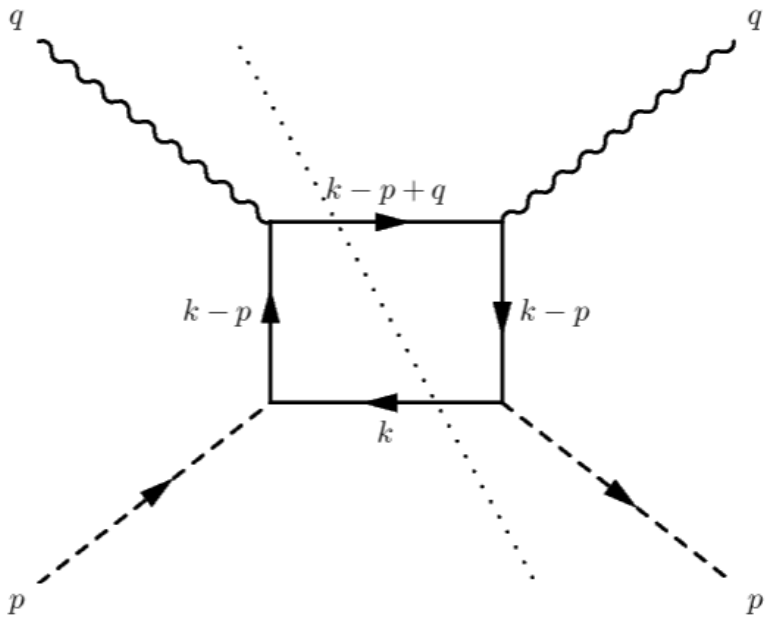

Figure 5.1: Graphical representation of the handbag diagram. This contribute to the imaginary part of the forward amplitude for the scattering of a virtual photon by the pion.

there will be no effect of the Pauli-Villar's regulators in this propagator. Hence we may take

$$\mathcal{A}^{2,v}_{\Lambda,\mathrm{R}} = -\imath\frac{N_c}{4}\sum_{i=0}^{2} c_i \,\mathrm{Tr}\left\{\left(-DD_5+\Lambda_i^2\right)^{-1}\left[\mathcal{Q}^2\not{v}(\not{\partial})^{-1}\not{v}D_5 - D\left(\not{v}(\not{\partial})^{-1}\not{v}\right)_5\mathcal{Q}^2\right]\right\} \tag{5.1.3}$$

as starting point for the expansion. To explore off-shell pion Compton scattering $\gamma^*\pi \to \gamma^*\pi$ we write

$$\imath D = \imath\not{\partial} + m + \imath g\gamma_5\vec{\pi}\cdot\vec{\tau} \quad \text{and} \quad \imath D_5 = -\imath\not{\partial} + m - \imath g\gamma_5\vec{\pi}\cdot\vec{\tau}$$

and also expand to $\mathcal{O}(\vec{\pi}^2)$. The expression that multiplies $\vec{\pi}^2 v_\mu v_\nu$ is identified as the Compton amplitude [24, 52]

$$T^{\mu\nu} = \sum_{i=0}^{2} c_i\Bigg\{(4N_c g^2)\frac{5}{9}\int\frac{\mathrm{d}^4k}{(2\pi)^4}\frac{\mathrm{tr}(\not{k}-\not{p}+\not{q}+m)\gamma^\mu(\not{k}-\not{p}+m)}{(-(k-p+q)^2+m^2+\Lambda_i^2-\imath\epsilon)\left[-(k-p)^2+m^2+\Lambda_i^2-\imath\epsilon\right]^2} \times\frac{\gamma^5(\not{k}+m)\gamma^5(\not{k}-\not{p}+m)\gamma^\nu}{(-k^2+m^2+\Lambda_i^2-\imath\epsilon)}\Bigg\}.$$

Here the constant term $(4N_c g^2)\frac{5}{9}$ results from the trace of the photon and pion vertices respectively: $\mathrm{tr}(\tau_a\tau_a\mathcal{Q}\mathcal{Q}) = \frac{10}{9}$ and $\mathrm{tr}(\tau_b\tau_b gg) = 2g^2\delta_{ab}$. The momenta q_μ and p_μ are those of the external photon and pion, respectively, while k_μ is the momentum of the looping quark. Figure 5.1 shows the Feynman diagram representation of $T^{\mu\nu}$. Obviously this is the standard handbag diagram[52]. We want to extract the imaginary (or absorptive) part in the Bjorken limit. According to Cutkosky's rules we obtain the imaginary part by replacing the propagators

with the indicated cut in Figure 5.1 by their pole terms

$$\frac{1}{(-k^2+m^2+\Lambda_i^2-\imath\epsilon)} \to -2\pi\imath\delta\left(k^2-m^2-\Lambda_i^2\right)$$
$$\frac{1}{(-(k\pm q-p)^2+m^2+\Lambda_i^2-\imath\epsilon)} \to 2\pi\imath\delta\left((k\pm q-p)^2-m^2-\Lambda_i^2\right)$$

Introducing light cone coordinates $q^{\pm}=\frac{1}{\sqrt{2}}\left(q^0\pm q^3\right)=\frac{1}{\sqrt{2}}\left(q_0\mp q_3\right)$ etc the Bjorken limit reads $q^-\to\infty$ and $q^+\to xp^+=xM$ where Bjorken x is defined in equation (1.6.4). To leading order in $\frac{1}{q^-}$ we write

$$\delta\left((k\pm q-p)^2-m^2-\Lambda_i^2\right)\sim\frac{1}{2q^-}\delta\left(k^+-p^+\pm q^+\right). \tag{5.1.4}$$

This gives the hadronic tensor

$$W^{\mu\nu}=\operatorname{Im}T^{\mu\nu}=(2N_cg^2)\frac{5}{9}\sum_{i=0}^{2}c_i\int\frac{\mathrm{d}^4k}{(2\pi)^4}\frac{\operatorname{tr}(-\not{k}+m)(\not{k}-\not{p}+m)\gamma^\mu\gamma^\rho q_\rho\gamma^\nu(\not{k}-\not{p}+m)}{(-k^2+m^2+\Lambda_i^2-\imath\epsilon)_{\mathrm{p}}\left[-(k-p)^2+m^2+\Lambda_i^2-\imath\epsilon\right]^2}$$
$$\times\frac{\delta(k^+-p^++q^+)}{q^-}.$$

Here the subscript 'p' denote 'pole' contribution. Again, in the Bjorken limit, $\gamma^\rho q_\rho\sim\gamma^+q^-$. We evaluate the Dirac trace from the identity

$$\gamma^\mu\gamma^\rho\gamma^\nu=S^{\mu\rho\nu\sigma}\gamma_\sigma-\imath\epsilon^{\mu\rho\nu\sigma}\gamma_\sigma\gamma_5, \tag{5.1.5}$$

where

$$S^{\mu\rho\nu\sigma}=g^{\mu\rho}g^{\nu\sigma}+g^{\mu\sigma}g^{\rho\nu}-g^{\mu\nu}g^{\rho\sigma} \tag{5.1.6}$$

and $\epsilon^{\mu\rho\nu\sigma}$ is the total anti-symmetric Levi-Civita tensor in four dimensions. The resulting tensor is then calculated using $\mu=\nu=i$ with $i=1,2$ as the transverse direction. This gives

$$S^{i+i\sigma}=g^{i+}g^{i\sigma}+g^{i\sigma}g^{i+}-g^{ii}g^{+\sigma}.$$

Noting that, the non-vanishing elements of the metric tensor of the light-cone coordinates are:

$$g^{+-}=g^{-+}=1,\quad\text{and}\quad g^{11}=g^{22}=-1, \tag{5.1.7}$$

implies $g^{i+}g^{i\sigma}=g^{i\sigma}g^{i+}=0$ with $\sigma=-$. Then $S^{i+i-}=1$ and

$$\sum_{i=1}^{2}W^{ii}=(2N_cg^2)\frac{5}{9}\sum_{i=0}^{2}c_i\int\frac{\mathrm{d}^4k}{(2\pi)^4}\frac{\delta(k^+-p^++q^+)\operatorname{tr}(-\not{k}+m)(\not{k}-\not{p}+m)\gamma^+(\not{k}-\not{p}+m)}{(-k^2+m^2+\Lambda_i^2-\imath\epsilon)_{\mathrm{p}}\left[-(k-p)^2+m^2+\Lambda_i^2-\imath\epsilon\right]^2}.$$

Substituting the pole term, two of the momentum integrals can be trivially evaluated; leaving the integration over transverse momenta.

On the other side, pion DIS is described by a single form factor

$$W_{\mu\nu}=G(x,Q^2)\left[-g_{\mu\nu}+\frac{q_\mu q_\nu}{q^2}-\frac{1}{q^2}\left(p_\mu-\frac{q_\mu}{2x}\right)\left(p_\nu-\frac{q_\nu}{2x}\right)\right] \tag{5.1.8}$$

which becomes a structure function in the Bjoken limit[1]

$$F(x) = \lim_{\substack{Q^2\to\infty \\ x \text{ fixed}}} G(x, Q^2). \tag{5.1.9}$$

Comparison with the NJL model calculation yields[52]

$$\begin{aligned} F(x) &= (2N_c g^2)\frac{5}{9}\sum_{i=0}^{2} c_i \int \frac{\mathrm{d}^2 k_\perp}{(2\pi)^3} \frac{\vec{k}_\perp^2 + m^2 + \Lambda_i^2}{\left[m^2 + \vec{k}_\perp^2 + \Lambda_i^2 - x(1-x)m_\pi^2\right]^2}, \\ &= (2N_c g^2)\frac{5}{9}\sum_{i=0}^{2} c_i \int \frac{\mathrm{d}^2 k_\perp}{(2\pi)^3} \left\{ \frac{1}{m^2 + \vec{k}_\perp^2 + \Lambda_i^2 - x(1-x)m_\pi^2} + \frac{m_\pi^2 x(1-x)}{\left[m^2 + \vec{k}_\perp^2 + \Lambda_i^2 - x(1-x)m_\pi^2\right]^2} \right\}. \end{aligned} \tag{5.1.10}$$

In the next step, we write the polarization function Eq (2.4.12) as a Feynman parameter integral

$$\Pi(q^2) = \int_0^1 \mathrm{d}x\, \Pi(q^2, x), \tag{5.1.11}$$

where

$$\Pi(q^2, x) = -\imath \sum_{i=0}^{2} c_i \int \frac{\mathrm{d}^4 k}{(2\pi)^4} \frac{1}{\left[m^2 - k^2 - x(1-x)q^2 + \Lambda_i^2 - \imath\epsilon\right]^2}. \tag{5.1.12}$$

Using the identity(regularization implied) [53, 54]

$$\begin{aligned} -\imath \int \frac{\mathrm{d}^4 k}{(2\pi)^4} \frac{1}{\left[-k^2 + \mu^2 - \imath\epsilon\right]^2} &= -\imath \int \frac{\mathrm{d}^2 k_\perp}{(2\pi)^2} \int \frac{\mathrm{d}^2 k_\parallel}{(2\pi)^2} \frac{1}{\left[-k_\parallel^2 + k_\perp^2 + \mu^2 - \imath\epsilon\right]^2} \\ &= (-\imath)\imath \frac{1}{(4\pi)^{\frac{2}{2}}} \frac{\Gamma(2-1)}{\Gamma(2)} \int \frac{\mathrm{d}^2 k_\perp}{(2\pi)^2} \left(\frac{1}{k_\perp^2 + \mu^2}\right)^{2-1} = \frac{1}{2} \int \frac{\mathrm{d}^2 k_\perp}{(2\pi)^3} \frac{1}{k_\perp^2 + \mu^2}, \end{aligned} \tag{5.1.13}$$

gives

$$\Pi(q^2, x) = \frac{1}{2}\sum_{i=0}^{2} c_i \int \frac{\mathrm{d}^2 k_\perp}{(2\pi)^3} \frac{1}{m^2 + \vec{k}_\perp^2 + \Lambda_i^2 - x(1-x)q^2}. \tag{5.1.14}$$

Comparing this expression with our result for the structure function in Eq (5.1.10) we obtain the compact expression

$$F(x) = \frac{5}{9}(4N_c g^2)\left\{\Pi(q^2, x) + q^2 \Pi'(q^2, x)\right\}\Big|_{q^2 = m_\pi^2} = \frac{5}{9}(4N_c g^2)\frac{\mathrm{d}}{\mathrm{d}q^2}\left[q^2 \Pi(q^2, x)\right]\Big|_{q^2 = m_\pi^2}, \tag{5.1.15}$$

where the prime denote differentiation with respect to q^2. There are two important observations. First, comparison with Eq (2.4.15) shows that

$$\int_0^1 \mathrm{d}x\, F(x) = \frac{5}{9} = \sum_i e_i^2, \tag{5.1.16}$$

the structure function is normalized to summed square of the constituent charges. Second, in the chiral limit ($m_\pi = 0$), $F(x) = \frac{5}{9}$ for $0 \le x \le 1$ and zero otherwise.

[1] Notation not to be confused with the chiral angle.

5.2 Nucleon Structure Functions

Having understood DIS of pions in the NJL model, we next consider DIS of nucleon. This is described by four structure functions, cf. equations (1.6.12) and (1.6.34): The unpolarized structure functions $F_1(x)$ and $F_2(x)$ which do not depend on the nucleon spin and the polarized structure functions $\mathrm{g}_1(x)$ and $\mathrm{g}_2(x)$ that multiply the allowed Lorentz structures sensitive to the nucleon spin.

Applying the Bjorken limit to the unregularized part of the effective action and taking into account that the quark propagator with the infinite photon momentum should be taken to be free and massless requires to differentiate

$$\begin{aligned}\mathcal{A}^{(2,v)}_{\Lambda} = \frac{N_c}{4\imath}\sum_{i=0}^{2} c_i \,\mathrm{Tr}\left\{\left(-DD_5+\Lambda_i^2\right)^{-1}\left[\mathcal{Q}^2\not{v}(\not{\partial})^{-1}\not{v}D_5 - D\left(\not{v}(\not{\partial})^{-1}\not{v}\right)_5\mathcal{Q}^2\right]\right\}\\ + \frac{N_c}{4\imath}\,\mathrm{Tr}\left\{(-DD_5)^{-1}\left[\mathcal{Q}^2\not{v}(\not{\partial})^{-1}\not{v}D_5 + D\left(\not{v}(\not{\partial})^{-1}\not{v}\right)_5\mathcal{Q}^2\right]\right\},\end{aligned} \tag{5.2.1}$$

with respect to the photon field v_μ as in equation (5.0.3). Here $\imath D$ and $\imath D_5$ are those of equations (2.2.15) and (2.2.16) i.e with $v_\mu = 0$. The subscript "5" in equation (5.2.1) defines

$$\left(\gamma^\mu\gamma^\rho\gamma^\nu\right)_5 = S^{\mu\rho\nu\sigma}\gamma_\sigma + \imath\epsilon^{\mu\rho\nu\sigma}\gamma_\sigma\gamma_5. \tag{5.2.2}$$

The unconventional sign of the ϵ-term is required because axial sources appear with opposite signs in $\imath D$ and $\imath D_5$. Consistency of regularization requires its implementation [24]; these terms obviously cancel in the unregularized formulation with $\Lambda_i^2 = 0$.

So far we have considered the rotational zero modes (equation (4.4.1)) associated with the static configuration. The only large amplitude fluctuation of the static configuration left to be considered is the translational zero mode. Its quantization generates the linear momentum $\vec{p}$ of the nucleon. We introduce this mode by shifting the center of the nucleon coordinates in the Compton amplitude and averaging

$$\begin{aligned}T_{\mu\nu} &= 2\imath M\int \mathrm{d}^4\xi \int \mathrm{d}^3R\, e^{\imath q\cdot\xi}\langle p,s|T\left(J_\mu(\xi-\vec{R})J_\nu(-\vec{R})\right)|p,s\rangle\\ &= 2\imath M\int \mathrm{d}^4\xi_1 \int \mathrm{d}^3\xi_2\, e^{\imath q\cdot(\xi_1-\xi_2)}\langle s|T\left(J_\mu(\xi_1)J_\nu(\xi_2)\right)|s\rangle,\end{aligned} \tag{5.2.3}$$

where $\vec{R}$ is the collective coordinate that describes the position of the nucleon [55]. The coordinate ξ_2 is treated as a four-vector keeping in mind that $\xi_2^0 = 0$. The factors $2M$ arise from the normalization of the eigenstates of the momentum $\vec{p}$ that is conjugate to $\vec{R}$. The momentum $\vec{p}$ of the nucleon is introduced by the plane-wave function

$$\langle\vec{R}|\vec{p}\rangle = \sqrt{2E}\exp(\imath\vec{R}\cdot\vec{p}) \quad \text{with the nucleon energy} \quad E=\sqrt{p^2+M^2}. \tag{5.2.4}$$

To compute the time-ordered product of the action (5.2.1) few remarks follow:

- The functional trace of the operators in the square brackets that appear in the action functional $\mathcal{A}^{2,v}_{\Lambda}$ is computed by using the plane-wave basis (5.2.4). The matrix elements of the operators in equations (2.2.15) and (2.2.16) are evaluated by using the eigenfunctions Ψ_α of the Dirac Hamiltonian (4.1.2).

- In the next step, the action is expanded up to linear order in the angular velocities $\vec{\Omega}$ c.f (4.4.7) (Note that the angular velocity $\vec{\Omega}$ is of order $\frac{1}{N_c}$). This is done by expanding the nonlocal object $A^\dagger(\xi_1^0)\mathcal{Q}^2A(\xi_2^0)$ which arises by rotating the charge matrix

$$\mathcal{Q}^2 \to A^\dagger(\xi_1^0)\mathcal{Q}^2A(\xi_2^0), \tag{5.2.5}$$

where $\xi_1^0 = t$ and $\xi_2^0 = 0$ are the time coordinates. The expansion can be done around ξ_2^0 or ξ_1^0 yielding [50, 56–58]

$$A^\dagger(\xi_1^0)\mathcal{Q}^2A(\xi_2^0) = A^\dagger(\xi_2^0)\mathcal{Q}^2A(\xi_2^0) + (\xi_1^0 - \xi_2^0)A^\dagger(\xi_2^0)\mathcal{Q}^2\dot{A}(\xi_2^0) + \cdots \tag{5.2.6}$$

or

$$A^\dagger(\xi_1^0)\mathcal{Q}^2A(\xi_2^0) = A^\dagger(\xi_1^0)\mathcal{Q}^2A(\xi_1^0) - (\xi_1^0 - \xi_2^0)\dot{A}^\dagger(\xi_1^0)\mathcal{Q}^2A(\xi_1^0) + \cdots \tag{5.2.7}$$

Since both expansions give the same results for the rotational correction to the matrix element at the leading order of $\frac{1}{N_c}$ [57], we replace the above expansions by their symmetric form:

$$\begin{aligned} A^\dagger(\xi_1^0)\mathcal{Q}^2A(\xi_2^0) &\to A^\dagger\mathcal{Q}^2A + \frac{1}{2}(\xi_1^0 - \xi_2^0)\left[A^\dagger\mathcal{Q}^2AA^\dagger\dot{A} - \dot{A}^\dagger AA^\dagger\mathcal{Q}^2A\right], \\ &= A^\dagger\mathcal{Q}^2A + \frac{\imath}{4}t\left[A^\dagger\mathcal{Q}^2A\vec{\Omega}\cdot\vec{\tau} + \vec{\Omega}\cdot\vec{\tau}A^\dagger\mathcal{Q}^2A\right], \\ &= \mathcal{Q}_A^2 + \frac{\imath}{4}t\left\{\vec{\Omega}\cdot\vec{\tau}, \mathcal{Q}_A^2\right\}, \end{aligned} \tag{5.2.8}$$

where

$$\mathcal{Q}_A^2 = A^\dagger(\xi_1^0)\mathcal{Q}^2A(\xi_2^0) \tag{5.2.9}$$

denotes the collectively rotated charge matrix at a distinct time. Thus the rotational correction associated with the nonlocal operator $A^\dagger(\xi_1^0)\mathcal{Q}^2A(\xi_2^0)$ is proportional to the angular velocity, cf. equation (4.4.7). In the computation of the nucleon structure function, we will make use of the identity

$$A^\dagger(\xi_1^0)\tau_iA(\xi_2^0) = \frac{1}{2}\,\mathrm{Tr}\left(A^\dagger(\xi_1^0)\tau_iA(\xi_2^0)\tau_j\right)\tau_j, \tag{5.2.10}$$

whenever the rotated quark charge matrix contains an isospin factor. Now, considering the time evolution of the collective coordinate $A(t)$, one can write [56]

$$A^\dagger(\xi_1^0) = \exp\left(-\imath\left(\xi_1^0 - \xi_2^0\right)\frac{\vec{J}}{\alpha^2}\right)A(\xi_2^0)\exp\left(\imath\left(\xi_1^0 - \xi_2^0\right)\frac{\vec{J}}{\alpha^2}\right)\vec{\tau}, \tag{5.2.11}$$

where $\vec{J}$ is the spin operator, cf. equation (4.4.23) and α^2 is the moment of inertia cf. equation (4.4.19). But the moment of inertia is of order N_c, therefore an expansion around $\xi_1^0 \approx \xi_2^0$

$$\frac{1}{2}\,\mathrm{Tr}\left(A^\dagger(\xi_1^0)\tau_i A(\xi_2^0)\tau_j\right) = D_{ij} + \mathcal{O}\left(\frac{1}{N_c}\right). \tag{5.2.12}$$

Thus we can write the quantity $\frac{1}{2}\,\mathrm{Tr}\left(A^\dagger(\xi_1^0)\tau_i A(\xi_2^0)\tau_j\right)$ in terms of the adjoint representation. Furthermore, taking traces of the time-dependent collective coordinate matrix $A(t)$ in the plane wave basis gives

$$\left\langle t, \vec{\xi}\middle| A(t) \middle|\omega, \alpha\right\rangle = A(t)e^{-\imath\omega t}\Psi_\alpha(\vec{\xi}). \tag{5.2.13}$$

- Furthermore, the matrix elements of the operators in equations (2.2.15) and (2.2.16) are also expanded up to linear order in $\vec{\Omega}$

$$\langle\omega,\alpha|\left(-DD_5+\Lambda_i^2\right)^{-1}|\omega,\beta\rangle = \frac{\delta_{\alpha\beta}}{\omega^2-\epsilon_\alpha^2-\Lambda_i^2} - \frac{\left[\omega+(\epsilon_\alpha-\epsilon_\beta)\right]\langle\alpha|\vec{\tau}\cdot\vec{\Omega}|\beta\rangle}{\left[\omega^2-\epsilon_\alpha^2-\Lambda_i^2\right]\left[\omega^2-\epsilon_\beta^2-\Lambda_i^2\right]} + \mathcal{O}(\vec{\Omega}^2). \tag{5.2.14}$$

Using these remarks, up to linear order in $\vec{\Omega}$ the action becomes

$$\begin{aligned}
\mathcal{A}_\Lambda^{(2,v)} = &-\imath\frac{N_c}{4}\int\frac{\mathrm{d}\omega}{2\pi}\sum_\alpha \\
&\times\Bigg\{\langle\omega,\alpha|\mathcal{Q}_A^2\gamma^0\not{\psi}(\imath\not{\partial})^{-1}\not{\psi}|\omega,\alpha\rangle f_\alpha^+(\omega) + \frac{\imath}{4}\langle\omega,\alpha|\gamma^0\not{\psi}\,(\imath\not{\partial})^{-1}\not{\psi}\hat{t}\left\{\vec{\Omega}\cdot\vec{\tau},\mathcal{Q}_A^2\right\}|\omega,\alpha\rangle f_\alpha^+(\omega) \\
&+\langle\omega,\alpha|\mathcal{Q}_A^2\left[\not{\psi}(\imath\not{\partial})^{-1}\not{\psi}\right]_5\gamma^0|\omega,\alpha\rangle f_\alpha^-(\omega) + \frac{\imath}{4}\langle\omega,\alpha|\left[\not{\psi}\,(\imath\not{\partial})^{-1}\not{\psi}\hat{t}\left\{\vec{\Omega}\cdot\vec{\tau},\mathcal{Q}_A^2\right\}\right]_5\gamma^0|\omega,\alpha\rangle f_\alpha^-(\omega) \\
&+\sum_\beta\langle\alpha|\vec{\Omega}\cdot\vec{\tau}|\beta\rangle\left[\langle\omega,\beta|\mathcal{Q}_A^2\gamma^0\not{\psi}\,(\imath\not{\partial})^{-1}\not{\psi}|\omega,\alpha\rangle g_{\alpha\beta}^+(\omega) + \langle\omega,\beta|\mathcal{Q}_A^2\left[\not{\psi}\,(\imath\not{\partial})^{-1}\not{\psi}\right]_5\gamma^0|\omega,\alpha\rangle g_{\alpha\beta}^-(\omega)\right]\Bigg\}.
\end{aligned} \tag{5.2.15}$$

Here the frequency integral results from summing over the eigenvalues of $\imath\partial_t$ contained in the operators $\imath D$ and $\imath D_5$. Also, the Dirac matrix γ^0 results from the definition of the operators $\imath D$ and $\imath D_5$. Furthermore, $f_\alpha^\pm$ and $g_{\alpha\beta}^\pm$ are spectral functions that result from expansions as in equation (5.2.14). They are given as

$$f_\alpha^\pm = \sum_{i=0}^{2} c_i\frac{\omega\pm\epsilon_\alpha}{\omega^2-\epsilon_\alpha^2-\Lambda_i^2+\imath\epsilon} \pm \frac{\omega\pm\epsilon_\alpha}{\omega^2-\epsilon_\alpha^2+\imath\epsilon}, \tag{5.2.16}$$

and

$$g_{\alpha\beta}^\pm = \sum_{i=0}^{2} c_i\frac{(\omega\pm\epsilon_\alpha)(\omega\pm\epsilon_\beta)+\Lambda_i^2}{(\omega^2-\epsilon_\alpha^2-\Lambda_i^2+\imath\epsilon)\left(\omega^2-\epsilon_\beta^2-\Lambda_i^2+\imath\epsilon\right)} \pm \frac{(\omega\pm\epsilon_\alpha)(\omega\pm\epsilon_\beta)}{(\omega^2-\epsilon_\alpha^2+\imath\epsilon)\left(\omega^2-\epsilon_\beta^2+\imath\epsilon\right)}, \tag{5.2.17}$$

respectively. In equation (5.2.15), the contributions involving $f_\alpha^\pm$ are the leading terms of the $\frac{1}{N_c}$ counting, while the $g_{\alpha\beta}^\pm$ are subleading. Taking the functional derivative of $\mathcal{A}_\Lambda^{(2,v)}$ as in

equation (5.0.3) gives the Compton amplitude in the leading and subleading order of $\frac{1}{N_c}$

$$
\begin{aligned}
T_{\mu\nu}(q) = -M_N \frac{N_c}{2} \int \frac{\mathrm{d}\omega}{2\pi} \sum_\alpha \int \mathrm{d}t \int \mathrm{d}^3\xi_1 \int \mathrm{d}^3\xi_2 \int \frac{\mathrm{d}^4k}{(2\pi)^4}\, e^{\imath(q_0+k_0)t} e^{-\imath(\vec{q}+\vec{k})\cdot(\vec{\xi}_1-\vec{\xi}_2)} \\
\times \frac{1}{k^2+\imath\epsilon} \langle N| \Big\{ \Big[\Psi^\dagger_\alpha(\vec{\xi}_1)\gamma^0 \mathcal{Q}_A^2 \gamma_\mu \not{k} \gamma_\nu \Psi_\alpha(\vec{\xi}_2) e^{\imath\omega t} - \Psi^\dagger_\alpha(\vec{\xi}_2)\gamma^0 \mathcal{Q}_A^2 \gamma_\nu \not{k} \gamma_\mu \Psi_\alpha(\vec{\xi}_1) e^{-\imath\omega t} \Big] f^+_\alpha \\
+ \Big[\Psi^\dagger_\alpha(\vec{\xi}_1) \mathcal{Q}_A^2 (\gamma_\mu \not{k} \gamma_\nu)_5 \gamma^0 \Psi_\alpha(\vec{\xi}_2) e^{\imath\omega t} - \Psi^\dagger_\alpha(\vec{\xi}_2) \mathcal{Q}_A^2 (\gamma_\nu \not{k} \gamma_\mu)_5 \gamma^0 \Psi_\alpha(\vec{\xi}_1) e^{-\imath\omega t} \Big] f^-_\alpha \\
+ \frac{\imath}{4} \Big[\Psi^\dagger_\alpha(\vec{\xi}_1)\gamma^0 \vec{\Omega}\cdot\vec{\tau} \mathcal{Q}_A^2 \hat{t} \gamma_\mu \not{k} \gamma_\nu \Psi_\alpha(\vec{\xi}_2) e^{\imath\omega t} + \Psi^\dagger_\alpha(\vec{\xi}_2)\gamma^0 \hat{t} \mathcal{Q}_A^2 \vec{\Omega}\cdot\vec{\tau} \gamma_\nu \not{k} \gamma_\mu \Psi_\alpha(\vec{\xi}_1) e^{-\imath\omega t} \Big] f^+_\alpha \\
+ \frac{\imath}{4} \Big[\Psi^\dagger_\alpha(\vec{\xi}_1) \vec{\Omega}\cdot\vec{\tau} \mathcal{Q}_A^2 \hat{t}\, (\gamma_\mu \not{k} \gamma_\nu)_5\, \gamma^0 \Psi_\alpha(\vec{\xi}_2) e^{\imath\omega t} + \Psi^\dagger_\alpha(\vec{\xi}_2) \hat{t} \mathcal{Q}_A^2 \vec{\Omega}\cdot\vec{\tau}\, (\gamma_\nu \not{k} \gamma_\mu)_5\, \gamma^0 \Psi_\alpha(\vec{\xi}_1) e^{-\imath\omega t} \Big] f^-_\alpha \\
+ \sum_\beta \langle \alpha | \vec{\Omega}\cdot\vec{\tau} | \beta \rangle \Big(\Big[\Psi^\dagger_\beta(\vec{\xi}_1)\gamma^0 \mathcal{Q}_A^2 \gamma_\mu \not{k} \gamma_\nu \Psi_\alpha(\vec{\xi}_2) e^{\imath\omega t} - \Psi^\dagger_\beta(\vec{\xi}_2)\gamma^0 \mathcal{Q}_A^2 \gamma_\nu \not{k} \gamma_\mu \Psi_\alpha(\vec{\xi}_1) e^{-\imath\omega t} \Big] g^+_{\alpha\beta} \\
+ \Big[\Psi^\dagger_\beta(\vec{\xi}_1) \mathcal{Q}_A^2 (\gamma_\mu \not{k} \gamma_\nu)_5 \gamma^0 \Psi_\alpha(\vec{\xi}_2) e^{\imath\omega t} - \Psi^\dagger_\beta(\vec{\xi}_2) \mathcal{Q}_A^2 (\gamma_\nu \not{k} \gamma_\mu)_5 \gamma^0 \Psi_\alpha(\vec{\xi}_1) e^{-\imath\omega t} \Big] g^-_{\alpha\beta} \Big) \Big\} |N\rangle, \qquad (5.2.18)
\end{aligned}
$$

with the time coordinate $t = \xi_1^0$. Here the Dirac matrix γ^0 does not always combine to the spinor $\bar{\Psi}_\alpha$, because of the γ_5 prescription (5.2.2). We define the Fourier transform of the quark wave-function with

$$
\tilde{\Psi}_\alpha(\vec{p}) = \int \frac{\mathrm{d}^3x}{4\pi}\, \Psi_\alpha(\vec{x}) e^{\imath\vec{x}\cdot\vec{p}}. \qquad (5.2.19)
$$

Employing a full Fourier transform differs from the approaches of Refs [56, 57] who used the expansion from diagonalizing the Dirac Hamiltonian, Eq (4.1.7). This resulted in discontinuities of the numerically computed structure functions and required a smoothening procedure.

We perform the spatial integrals and identify the imaginary part of the Compton amplitude as the hadronic tensor by restricting the spectral integral to those values of ω which cause the denominators of the spectral functions (5.2.16) to vanish

$$
\frac{1}{\omega^2 - \epsilon_\alpha^2 - \Lambda_i^2 + \imath\epsilon} \to -\imath\pi\delta\left(\omega^2 - \epsilon_\alpha^2 - \Lambda_i^2\right), \qquad (5.2.20)
$$

etc. We mark this prescription by the subscript "pole(p)" on the affected spectral functions $f^\pm_\alpha$ and $g^\pm_{\alpha\beta}$ from equations (5.2.16) and (5.2.17). The leading order contributions becomes

$$
\begin{aligned}
W^{(\Omega_0)}_{\mu\nu}(q) = -\imath M_N \frac{N_c}{4} (4\pi)^2 \int \frac{\mathrm{d}\omega}{2\pi} \sum_\alpha \int \frac{\mathrm{d}^3k}{(2\pi)^2} \frac{1}{2|\vec{k}|} \\
\times \langle N| \Big\{ \Big[\tilde{\Psi}^\dagger_\alpha(\vec{q}+\vec{k})\gamma^0 \mathcal{Q}_A^2 \gamma_\mu \not{k} \gamma_\nu \tilde{\Psi}_\alpha(\vec{q}+\vec{k})\, \delta\left(|\vec{k}| - q_0 - \omega\right) \\
- \tilde{\Psi}^\dagger_\alpha(-\vec{q}-\vec{k}) \mathcal{Q}_A^2 \gamma_\nu \not{k} \gamma_\mu \gamma^0 \tilde{\Psi}_\alpha(-\vec{q}-\vec{k})\, \delta\left(|\vec{k}| - q_0 + \omega\right) \Big] f^+_\alpha(\omega)\Big|_{\mathrm{p}} \\
+ \Big[\tilde{\Psi}^\dagger_\alpha(\vec{q}+\vec{k})\gamma^0 \mathcal{Q}_A^2\, (\gamma_\mu \not{k} \gamma_\nu)_5\, \tilde{\Psi}_\alpha(\vec{q}+\vec{k})\, \delta\left(|\vec{k}| - q_0 - \omega\right) \\
- \tilde{\Psi}^\dagger_\alpha(-\vec{q}-\vec{k}) \mathcal{Q}_A^2\, (\gamma_\nu \not{k} \gamma_\mu)_5\, \gamma^0 \tilde{\Psi}_\alpha(-\vec{q}-\vec{k})\, \delta\left(|\vec{k}| - q_0 + \omega\right) \Big] f^-_\alpha(\omega)\Big|_{\mathrm{p}} \Big\} |N\rangle. \qquad (5.2.21)
\end{aligned}
$$

and the contribution linear in the angular velocity reads

$$
\begin{aligned}
W^{(\Omega_1)}_{\mu\nu}(q) = -\imath M_N \frac{N_c}{4}(4\pi)^2 \int \frac{\mathrm{d}\omega}{2\pi} \sum_\alpha \int \frac{\mathrm{d}^3k}{(2\pi)^2} \frac{1}{2|\vec{k}|} \\
\times \langle N| \Big\{ -\frac{\imath}{4} \Big[\tilde{\Psi}^\dagger_\alpha(\vec{q}+\vec{k}) \gamma^0 \vec{\Omega}\cdot\vec{\tau} \mathcal{Q}_A^2 \hat{t} \gamma_\mu \not{k} \gamma_\nu \tilde{\Psi}_\alpha(\vec{q}+\vec{k})\, \delta\left(|\vec{k}| - q_0 - \omega\right) \\
+ \tilde{\Psi}^\dagger_\alpha(-\vec{q}-\vec{k}) \hat{t} \mathcal{Q}_A^2 \vec{\Omega}\cdot\vec{\tau} \gamma_\nu \not{k} \gamma_\mu \gamma^0 \tilde{\Psi}_\alpha(-\vec{q}-\vec{k})\, \delta\left(|\vec{k}| - q_0 + \omega\right) \Big]\, f^+_\alpha(\omega) \Big|_{\mathrm{p}} \\
- \frac{\imath}{4} \Big[\tilde{\Psi}^\dagger_\alpha(\vec{q}+\vec{k}) \gamma^0 \vec{\Omega}\cdot\vec{\tau} \mathcal{Q}_A^2 \hat{t} \left(\gamma_\mu \not{k} \gamma_\nu\right)_5 \tilde{\Psi}_\alpha(\vec{q}+\vec{k})\, \delta\left(|\vec{k}| - q_0 - \omega\right) \\
+ \tilde{\Psi}^\dagger_\alpha(-\vec{q}-\vec{k}) \hat{t} \mathcal{Q}_A^2 \vec{\Omega}\cdot\vec{\tau} \left(\gamma_\nu \not{k} \gamma_\mu\right)_5 \gamma^0 \tilde{\Psi}_\alpha(-\vec{q}-\vec{k})\, \delta\left(|\vec{k}| - q_0 + \omega\right) \Big]\, f^-_\alpha(\omega) \Big|_{\mathrm{p}} \\
+ \sum_\beta \langle \alpha | \vec{\Omega}\cdot\vec{\tau} | \beta \rangle \Big(\Big[\tilde{\Psi}^\dagger_\beta(\vec{q}+\vec{k}) \gamma^0 \mathcal{Q}_A^2 \gamma_\mu \not{k} \gamma_\nu \tilde{\Psi}_\alpha(\vec{q}+\vec{k})\, \delta\left(|\vec{k}| - q_0 - \omega\right) \\
- \tilde{\Psi}^\dagger_\beta(-\vec{q}-\vec{k}) \mathcal{Q}_A^2 \gamma_\nu \not{k} \gamma_\mu \gamma^0 \tilde{\Psi}_\alpha(-\vec{q}-\vec{k})\, \delta\left(|\vec{k}| - q_0 + \omega\right) \Big]\, g^+_{\alpha\beta}(\omega) \Big|_{\mathrm{p}} \\
+ \Big[\tilde{\Psi}^\dagger_\beta(\vec{q}+\vec{k}) \gamma^0 \mathcal{Q}_A^2 \left(\gamma_\mu \not{k} \gamma_\nu\right)_5 \tilde{\Psi}_\alpha(\vec{q}+\vec{k})\, \delta\left(|\vec{k}| - q_0 - \omega\right) \\
- \tilde{\Psi}^\dagger_\beta(-\vec{q}-\vec{k}) \mathcal{Q}_A^2 \left(\gamma_\nu \not{k} \gamma_\mu\right)_5 \gamma^0 \tilde{\Psi}_\alpha(-\vec{q}-\vec{k})\, \delta\left(|\vec{k}| - q_0 + \omega\right) \Big]\, g^-_{\alpha\beta}(\omega) \Big|_{\mathrm{p}} \Big) \Big\} |N\rangle. \qquad (5.2.22)
\end{aligned}
$$

It must be emphasized that the pole contribution of the spectral functions occur in positive and negative pairs as such there is no clear distinction between the quark and anti-quark contributions to the hadronic tensor. Since the structure functions do or not depend on the nucleon spin we define the nucleon state as $|N, \vec{s}\,\rangle$, where $\vec{s}$ is an unspecified polarization of N. For convenience we choose the coordinate frame in such a way that the photon moves along the positive $\hat{e}_3$ direction, i.e $\vec{q} = |\vec{q}|\hat{e}_3$. This then allows us to introduce the Bjorken scaling variable

$$
q_0 = q_3 - Mx \qquad (5.2.23)
$$

in the Bjorken limit $|\vec{q}| \to \infty$. In what follows the integration variable $\vec{k}$ is changed to $\vec{p} = \vec{q} + \vec{k}$ and

$$
\int \mathrm{d}^3k = \int p^2 \mathrm{d}p \int \Omega_p, \quad p = |\vec{p}|, \qquad (5.2.24)
$$

where $\int \Omega_p$ is the solid angle integral. The wave function have their dominant support in the regime $|\vec{p}| \leq M$. Hence non-zero integrals require $\hat{k} = -\hat{q} = -\hat{e}_3$ [59, 60]. Then

$$
|\vec{k}| - q_0 - \omega \approx |q_3 - p_3| - q_0 - \omega \approx -(p_3 - Mx + \omega) \qquad (5.2.25)
$$

leading to

$$
\begin{aligned}
W^{(\Omega_0)}_{\mu\nu}(q) = -\imath M \frac{N_c}{4} \int \frac{\mathrm{d}\omega}{2\pi} \sum_\alpha \int \mathrm{d}^3p \\
\times \langle N, \vec{s}\,| \Big\{ \Big[\tilde{\Psi}^\dagger_\alpha(\vec{p}) \mathcal{Q}_A^2 \gamma^0 \gamma_\mu \not{p} \gamma_\nu \tilde{\Psi}_\alpha(\vec{p})\, f^+_\alpha(\omega) \Big|_{\mathrm{p}} \\
+ \tilde{\Psi}^\dagger_\alpha(\vec{p}) \mathcal{Q}_A^2 \gamma^0 (\gamma_\mu \not{p} \gamma_\nu)_5 \tilde{\Psi}_\alpha(\vec{p})\, f^-_\alpha(\omega)\big|_{\mathrm{p}} \Big] \delta\left(p_3 - Mx + \omega\right) \\
- \Big[\tilde{\Psi}^\dagger_\alpha(-\vec{p}) \mathcal{Q}_A^2 \gamma_\nu \not{p} \gamma_\mu \gamma^0 \tilde{\Psi}_\alpha(-\vec{p})\, f^+_\alpha(\omega) \Big|_{\mathrm{p}} \\
+ \tilde{\Psi}^\dagger_\alpha(-\vec{p}) \mathcal{Q}_A^2 (\gamma_\nu \not{p} \gamma_\mu)_5 \gamma^0 \tilde{\Psi}_\alpha(-\vec{p})\, f^-_\alpha(\omega)\big|_{\mathrm{p}} \Big] \delta\left(p_3 - Mx - \omega\right) \Big\} |N, \vec{s}\,\rangle. \qquad (5.2.26)
\end{aligned}
$$

For the cranking correction contribution, we express the coordinate time operator as a derivative with respect to the quark energy (q^0), which upon using the chain rule can be written in terms of the Bjorken variable as

$$\hat{t} \longrightarrow \frac{\partial x}{\partial q^0}\frac{\partial}{\partial x} = -\frac{1}{M}\frac{\partial}{\partial x}. \tag{5.2.27}$$

We write the δ-function as

$$\delta\left(p_3 - Mx + \omega\right) = \int \frac{\mathrm{d}\lambda}{2\pi} e^{\imath\lambda(p_3 - Mx + \omega)} \tag{5.2.28}$$

etc. Then the factor t is replaced by $\imath\lambda$. We then obtain the subleading contribution

$$\begin{aligned}
W^{(\Omega_1)}_{\mu\nu}(q) = -\imath M\frac{N_c}{4}\int\frac{\mathrm{d}\omega}{2\pi}\sum_\alpha\int\mathrm{d}^3p\int\frac{\mathrm{d}\lambda}{2\pi}\\
\times\langle N,\vec{s}\,|\Big\{\frac{\imath\lambda}{4}\Big[\tilde{\Psi}^\dagger_\alpha(\vec{p})\gamma^0\vec{\Omega}\cdot\vec{\tau}\mathcal{Q}_A^2\gamma_\mu\not{n}\gamma_\nu\tilde{\Psi}_\alpha(\vec{p})\ f^+_\alpha(\omega)\Big|_{\mathrm{p}}\\
+\tilde{\Psi}^\dagger_\alpha(\vec{p})\gamma^0\vec{\Omega}\cdot\vec{\tau}\mathcal{Q}_A^2(\gamma_\mu\not{n}\gamma_\nu)_5\tilde{\Psi}_\alpha(\vec{p})\ f^-_\alpha(\omega)\big|_{\mathrm{p}}\Big]e^{\imath\lambda(p_3-Mx+\omega)}\\
+\frac{\imath\lambda}{4}\Big[\tilde{\Psi}^\dagger_\alpha(-\vec{p})\mathcal{Q}_A^2\vec{\Omega}\cdot\vec{\tau}\gamma_\nu\not{n}\gamma_\mu\gamma^0\tilde{\Psi}_\alpha(-\vec{p})\ f^+_\alpha(\omega)\Big|_{\mathrm{p}}\\
+\tilde{\Psi}^\dagger_\alpha(-\vec{p})\mathcal{Q}_A^2\vec{\Omega}\cdot\vec{\tau}(\gamma_\nu\not{n}\gamma_\mu)_5\gamma^0\tilde{\Psi}_\alpha(-\vec{p})\ f^-_\alpha(\omega)\big|_{\mathrm{p}}\Big]e^{\imath\lambda(p_3-Mx-\omega)}\\
+\sum_\beta\langle\alpha|\vec{\Omega}\cdot\vec{\tau}|\beta\rangle\Big(\Big[\tilde{\Psi}^\dagger_\beta(\vec{p})\mathcal{Q}_A^2\gamma^0\gamma_\mu\not{n}\gamma_\nu\tilde{\Psi}_\alpha(\vec{p})\ g^+_{\alpha\beta}(\omega)\Big|_{\mathrm{p}}\\
+\tilde{\Psi}^\dagger_\beta(\vec{p})\mathcal{Q}_A^2\gamma^0(\gamma_\mu\not{n}\gamma_\nu)_5\tilde{\Psi}_\alpha(\vec{p})\ g^-_{\alpha\beta}(\omega)\Big|_{\mathrm{p}}\Big]e^{\imath\lambda(p_3-Mx+\omega)}\\
-\Big[\tilde{\Psi}^\dagger_\beta(-\vec{p})\mathcal{Q}_A^2\gamma_\nu\not{n}\gamma_\mu\gamma^0\tilde{\Psi}_\alpha(-\vec{p})\ g^+_{\alpha\beta}(\omega)\Big|_{\mathrm{p}}\\
+\tilde{\Psi}^\dagger_\beta(-\vec{p})\mathcal{Q}_A^2(\gamma_\nu\not{n}\gamma_\mu)_5\gamma^0\tilde{\Psi}_\alpha(-\vec{p})\ g^-_{\alpha\beta}(\omega)\Big|_{\mathrm{p}}\Big]e^{\imath\lambda(p_3-Mx-\omega)}\Big)\Big\}|N,\vec{s}\,\rangle,
\end{aligned} \tag{5.2.29}$$

where $n^\mu = (1,0,0,1)^\mu$ is the light-cone vector. Since the quark eigenstates possesses positive parity we have

$$\tilde{\Psi}_\alpha(-\vec{p}) = (-1)^{G_\alpha}\tilde{\Psi}_\alpha(\vec{p}). \tag{5.2.30}$$

Taking the Fourier transform back to coordinate space with

$$\Psi_\alpha(\vec{x}) = \int\frac{\mathrm{d}^3p}{2\pi^2}\tilde{\Psi}_\alpha(\vec{p})e^{-\imath\vec{p}\cdot\vec{x}}, \tag{5.2.31}$$

the leading order contribution to the hadronic tensor is [24]

$$\begin{aligned}
W^{(\Omega_0)}_{\mu\nu}(q) = -\imath\frac{MN_c\pi}{8}\int\frac{\mathrm{d}\omega}{2\pi}\sum_\alpha\int\mathrm{d}^3\xi\int\frac{\mathrm{d}\lambda}{2\pi}\,e^{\imath Mx\lambda}\\
\times\langle N,\vec{s}\,|\Big\{\Big[\bar{\Psi}_\alpha(\vec{\xi})\mathcal{Q}_A^2\gamma_\mu\not{n}\gamma_\nu\Psi_\alpha(\vec{\xi}+\lambda\hat{e}_3)e^{-\imath\lambda\omega}\\
-\bar{\Psi}_\alpha(\vec{\xi})\mathcal{Q}_A^2\gamma_\nu\not{n}\gamma_\mu\Psi_\alpha(\vec{\xi}-\lambda\hat{e}_3)e^{\imath\lambda\omega}\Big]\ f^+_\alpha(\omega)\Big|_{\mathrm{p}}\\
+\Big[\bar{\Psi}_\alpha(\vec{\xi})\mathcal{Q}_A^2\,(\gamma_\mu\not{n}\gamma_\nu)_5\,\Psi_\alpha(\vec{\xi}-\lambda\hat{e}_3)e^{-\imath\lambda\omega}\\
-\bar{\Psi}_\alpha(\vec{\xi})\mathcal{Q}_A^2\,(\gamma_\nu\not{n}\gamma_\mu)_5\,\Psi_\alpha(\vec{\xi}+\lambda\hat{e}_3)e^{\imath\lambda\omega}\Big]\ f^-_\alpha(\omega)\big|_{\mathrm{p}}\Big\}|N,\vec{s}\,\rangle,
\end{aligned} \tag{5.2.32}$$

while the subleading contribution is

$$
\begin{aligned}
W_{\mu\nu}^{(\Omega_1)}(q) = -\imath\frac{MN_c\pi}{8}\int\frac{\mathrm{d}\omega}{2\pi}\sum_\alpha\int\mathrm{d}^3\xi\int\frac{\mathrm{d}\lambda}{2\pi}\,e^{\imath Mx\lambda}\\
\times\langle N,\vec{s}\,|\Big\{\frac{\imath\lambda}{4}\Big[\bar{\Psi}_\alpha(\vec{\xi})\vec{\Omega}\cdot\vec{\tau}\mathcal{Q}_A^2\gamma_\mu\not{n}\gamma_\nu\Psi_\alpha(\vec{\xi}+\lambda\hat{e}_3)e^{-\imath\lambda\omega}\\
+\bar{\Psi}_\alpha(\vec{\xi})\mathcal{Q}_A^2\vec{\Omega}\cdot\vec{\tau}\gamma_\nu\not{n}\gamma_\mu\Psi_\alpha(\vec{\xi}-\lambda\hat{e}_3)e^{\imath\lambda\omega}\Big]\,f_\alpha^+(\omega)\Big|_{\mathrm{p}}\\
+\frac{\imath\lambda}{4}\Big[\bar{\Psi}_\alpha(\vec{\xi})\vec{\Omega}\cdot\vec{\tau}\mathcal{Q}_A^2\left(\gamma_\mu\not{n}\gamma_\nu\right)_5\Psi_\alpha(\vec{\xi}-\lambda\hat{e}_3)e^{-\imath\lambda\omega}\\
+\bar{\Psi}_\alpha(\vec{\xi})\mathcal{Q}_A^2\vec{\Omega}\cdot\vec{\tau}\left(\gamma_\nu\not{n}\gamma_\mu\right)_5\Psi_\alpha(\vec{\xi}+\lambda\hat{e}_3)e^{\imath\lambda\omega}\Big]\,f_\alpha^-(\omega)\big|_{\mathrm{p}}\\
+\sum_\beta\langle\alpha|\vec{\Omega}\cdot\vec{\tau}|\beta\rangle\Big(\Big[\bar{\Psi}_\beta(\vec{\xi})\mathcal{Q}_A^2\gamma_\mu\not{n}\gamma_\nu\Psi_\alpha(\vec{\xi}+\lambda\hat{e}_3)e^{-\imath\lambda\omega}\\
-\bar{\Psi}_\beta(\vec{\xi})\mathcal{Q}_A^2\gamma_\nu\not{n}\gamma_\mu\Psi_\alpha(\vec{\xi}-\lambda\hat{e}_3)e^{\imath\lambda\omega}\Big]\,g_{\alpha\beta}^+(\omega)\Big|_{\mathrm{p}}\\
+\Big[\bar{\Psi}_\beta(\vec{\xi})\mathcal{Q}_A^2\left(\gamma_\mu\not{n}\gamma_\nu\right)_5\Psi_\alpha(\vec{\xi}-\lambda\hat{e}_3)e^{-\imath\lambda\omega}\\
-\bar{\Psi}_\beta(\vec{\xi})\mathcal{Q}_A^2\left(\gamma_\nu\not{n}\gamma_\mu\right)_5\Psi_\alpha(\vec{\xi}+\lambda\hat{e}_3)e^{\imath\lambda\omega}\Big]\,g_{\alpha\beta}^-(\omega)\Big|_{\mathrm{p}}\Big)\Big\}|N,\vec{s}\,\rangle. \qquad (5.2.33)
\end{aligned}
$$

This is similar to the decomposition into quark and anti-quark distributions as in the case of the parton model with additional contributions coming from the dispersion relation associated with the Pauli-Villars regularization scheme which also contains the regulators, Λ_i.

Using the 'γ_5' description (i.e equations (5.1.5), (5.1.6), (5.2.2)), we have the symmetric part of the leading order of the hadronic tensor as

$$
\begin{aligned}
S_{\mu\nu}^{(\Omega_0)}(q) = -\imath MN_c\frac{\pi}{4}S_{\mu\rho\nu\sigma}n^\rho\int\frac{\mathrm{d}\omega}{2\pi}\sum_\alpha\int\mathrm{d}^3\xi\int\frac{\mathrm{d}\lambda}{2\pi}\,e^{\imath Mx\lambda}\left(\sum_{i=0}^{2}c_i\frac{\omega+\epsilon_\alpha}{\omega^2-\epsilon_\alpha^2-\Lambda_i^2+\imath\epsilon}\right)_{\mathrm{p}}\\
\times\langle N,\vec{s}\,|\bar{\Psi}_\alpha(\vec{\xi})\mathcal{Q}_A^2\gamma^\sigma\Psi_\alpha(\vec{\xi}+\lambda\hat{e}_3)e^{-\imath\omega\lambda}-\bar{\Psi}_\alpha(\vec{\xi})\mathcal{Q}_A^2\gamma^\sigma\Psi_\alpha(\vec{\xi}-\lambda\hat{e}_3)e^{\imath\omega\lambda}|N,\vec{s}\,\rangle, \qquad (5.2.34)
\end{aligned}
$$

and the antisymmetric part as

$$
\begin{aligned}
A_{\mu\nu}^{(\Omega_0)}(q) = -MN_c\frac{\pi}{4}\epsilon_{\mu\rho\nu\sigma}n^\rho\int\frac{\mathrm{d}\omega}{2\pi}\sum_\alpha\int\mathrm{d}^3\xi\int\frac{\mathrm{d}\lambda}{2\pi}\,e^{\imath Mx\lambda}\left(\sum_{i=0}^{2}c_i\frac{\omega+\epsilon_\alpha}{\omega^2-\epsilon_\alpha^2-\Lambda_i^2+\imath\epsilon}\right)_{\mathrm{p}}\\
\times\langle N,\vec{s}\,|\bar{\Psi}_\alpha(\vec{\xi})\mathcal{Q}_A^2\gamma^\sigma\gamma^5\Psi_\alpha(\vec{\xi}+\lambda\hat{e}_3)e^{-\imath\omega\lambda}+\bar{\Psi}_\alpha(\vec{\xi})\mathcal{Q}_A^2\gamma^\sigma\gamma^5\Psi_\alpha(\vec{\xi}-\lambda\hat{e}_3)e^{\imath\omega\lambda}|N,\vec{s}\,\rangle. \qquad (5.2.35)
\end{aligned}
$$

For the cranking correction we obtain the symmetric piece as

$$
\begin{aligned}
S_{\mu\nu}^{(\Omega_1)}(q) = -\imath MN_c\frac{\pi}{4}S_{\mu\rho\nu\sigma}n^\rho\int\frac{\mathrm{d}\omega}{2\pi}\sum_\alpha\int\mathrm{d}^3\xi\int\frac{\mathrm{d}\lambda}{2\pi}\,e^{\imath Mx\lambda}\left(\frac{\omega+\epsilon_\alpha}{\omega^2-\epsilon_\alpha^2+\imath\epsilon}\right)_{\mathrm{p}}\\
\times\langle N,\vec{s}\,|\frac{\imath\lambda}{4}\Big[\bar{\Psi}_\alpha(\vec{\xi})\vec{\Omega}\cdot\vec{\tau}\mathcal{Q}_A^2\gamma^\sigma\Psi_\alpha(\vec{\xi}+\lambda\hat{e}_3)e^{-\imath\omega\lambda}+\bar{\Psi}_\alpha(\vec{\xi})\vec{\Omega}\cdot\vec{\tau}\mathcal{Q}_A^2\gamma^\sigma\Psi_\alpha(\vec{\xi}-\lambda\hat{e}_3)e^{\imath\omega\lambda}\Big]\\
+\sum_\beta\langle\alpha|\vec{\Omega}\cdot\vec{\tau}|\beta\rangle\left(\frac{(\omega+\epsilon_\alpha)(\omega+\epsilon_\beta)}{(\omega^2-\epsilon_\alpha^2+\imath\epsilon)(\omega^2-\epsilon_\beta^2+\imath\epsilon)}\right)_{\mathrm{p}}\\
\times\Big[\bar{\Psi}_\beta(\vec{\xi})\mathcal{Q}_A^2\gamma^\sigma\Psi_\alpha(\vec{\xi}+\lambda\hat{e}_3)e^{-\imath\omega\lambda}-\bar{\Psi}_\beta(\vec{\xi})\mathcal{Q}_A^2\gamma^\sigma\Psi_\alpha(\vec{\xi}-\lambda\hat{e}_3)e^{\imath\omega\lambda}\Big]|N,\vec{s}\,\rangle, \qquad (5.2.36)
\end{aligned}
$$

and the antisymmetric contribution as

$$
\begin{aligned}
A^{(\Omega_1)}_{\mu\nu}(q) = -MN_c\frac{\pi}{4}\epsilon_{\mu\rho\nu\sigma}n^\rho \int \frac{\mathrm{d}\omega}{2\pi}\sum_\alpha \int \mathrm{d}^3\xi \int \frac{\mathrm{d}\lambda}{2\pi}\, e^{\imath Mx\lambda}\left(\frac{\omega+\epsilon_\alpha}{\omega^2-\epsilon_\alpha^2+\imath\epsilon}\right)_{\mathrm{p}} \\
\times \langle N,\vec{s}\,|\frac{\imath\lambda}{4}\Big[\bar{\Psi}_\alpha(\vec{\xi})\vec{\Omega}\cdot\vec{\tau}\mathcal{Q}_A^2\gamma^\sigma\gamma^5\Psi_\alpha(\vec{\xi}+\lambda\hat{e}_3)e^{-\imath\omega\lambda} - \bar{\Psi}_\alpha(\vec{\xi})\vec{\Omega}\cdot\vec{\tau}\mathcal{Q}_A^2\gamma^\sigma\gamma^5\Psi_\alpha(\vec{\xi}-\lambda\hat{e}_3)e^{\imath\omega\lambda}\Big] \\
+\sum_\beta\langle\alpha|\vec{\Omega}\cdot\vec{\tau}|\beta\rangle\left(\frac{(\omega+\epsilon_\alpha)(\omega+\epsilon_\beta)}{(\omega^2-\epsilon_\alpha^2+\imath\epsilon)(\omega^2-\epsilon_\beta^2+\imath\epsilon)}\right)_{\mathrm{p}} \\
\times\Big[\bar{\Psi}_\beta(\vec{\xi})\mathcal{Q}_A^2\gamma^\sigma\gamma^5\Psi_\alpha(\vec{\xi}+\lambda\hat{e}_3)e^{-\imath\omega\lambda} + \bar{\Psi}_\beta(\vec{\xi})\mathcal{Q}_A^2\gamma^\sigma\gamma^5\Psi_\alpha(\vec{\xi}-\lambda\hat{e}_3)e^{\imath\omega\lambda}\Big]|N,\vec{s}\,\rangle. \qquad (5.2.37)
\end{aligned}
$$

It can be noted that the spectral functions of both the symmetric and the antisymmetric contribution of the leading order term are fully regularized with their pole contribution coming from $f_\alpha^+(\omega) - f_\alpha^-(-\omega)$ and hence are associated with the real part of the bosonized action. In the case of the cranking correction the spectral functions of the symmetric and antisymmetric contributions are not fully regularized as the pole contribution of the spectral functions associated with the quadratic spinor terms comes from $f_\alpha^+(\omega) + f_\alpha^-(-\omega)$, and that associated with the quartic spinor terms comes from $g^+_{\alpha\beta}(\omega) - g^-_{\alpha\beta}(-\omega)$. Note also that an additional factor $\frac{\pi}{2}$ appears in our formulas when compared to those of the authors in Refs.[24]. This factor results from the definitions of the Fourier transformation of equations (5.2.19) and (5.2.31).

Chapter 6

Calculations and Numerical Results for the Leading Order Contributions of the Structure Functions

In this chapter we compute the polarized and the unpolarized structure functions that stem from the leading order contribution in $\frac{1}{N_c}$ of the hadronic tensor. These functions are extracted from the symmetric and antisymmetric pieces (equations (5.2.34) and (5.2.35), respectively). We note that the rotated flavor quark charge matrix attains the form

$$\mathcal{Q}_A^2 = \frac{5}{18}\mathbf{1} + \frac{1}{6}D_{3i}\tau_i, \tag{6.0.1}$$

where D_{ij} is the adjoint representation of the collective rotation and τ_i are the isospin Pauli matrices.

In the first step we contract the leading order symmetric piece with the projection operator F_1 from Table 6.1. Making use of parity invariance and symmetry under grand-spin rotations, we find that only the flavor singlet piece of the rotated flavor quark charge matrix, i.e $\mathcal{Q}_A^2 \sim \frac{1}{18}\mathbf{1}$, contributes to the unpolarized structure function. Note that the Callan-Gross relation, $F_2(x) = 2xF_1(x)$ in order $\frac{1}{N_c}$ is fulfilled here. After generalizing the photon direction $\hat{e}_3$ into

F_1	F_2	g_1	$\mathrm{g}_T = \mathrm{g}_1 + \mathrm{g}_2$
$-\frac{1}{2}g^{\mu\nu}$	$-xg^{\mu\nu}$	$\frac{\imath}{2M_N}\epsilon^{\mu\nu\rho\sigma}\frac{q_\rho p_\sigma}{q\cdot s}$	$-\frac{\imath}{2M_N}\epsilon^{\mu\nu\rho\sigma}s_\rho p_\sigma$
spin independent	spin independent	$s \parallel q$	$s \perp q$

Table 6.1: Projection operators in the Bjorken limit which enable one to extract the nucleon structure functions from the hadronic tensor.

an arbitrary unit spherical direction $\hat{z}$ and taking its average $\int \frac{\mathrm{d}\Omega_z}{4\pi}\Big(\cdots\Big)$ [24, 49] we find

$$F_1^{I=0}(x) = \imath\frac{5\pi}{72}MN_c\int\frac{\mathrm{d}\Omega_z}{4\pi}\int\frac{\mathrm{d}\omega}{2\pi}\sum_\alpha\int\frac{\mathrm{d}\lambda}{2\pi}e^{\imath Mx\lambda}\left(\sum_{i=0}^{2}c_i\frac{\omega+\epsilon_\alpha}{\omega^2-\epsilon_\alpha^2-\Lambda_i^2+\imath\epsilon}\right)_{\mathrm{p}}$$
$$\times\int\mathrm{d}^3\xi\left\{\Psi_\alpha^\dagger(\vec{\xi})(1-\vec{\alpha}\cdot\hat{z})\Psi_\alpha(\vec{\xi}+\lambda\hat{z})e^{-\imath\omega\lambda}-\Psi_\alpha^\dagger(\vec{\xi})(1-\vec{\alpha}\cdot\hat{z})\Psi_\alpha(\vec{\xi}-\lambda\hat{z})e^{\imath\omega\lambda}\right\}. \tag{6.0.2}$$

Similarly contracting the antisymmetric piece of the leading order hadronic tensor with the projection operators for g_1 and g_T from Table 6.1 produces the polarized structure functions. When the nucleon is polarized along the positive $\hat{e}_3$ direction we obtain the longitudinal structure function. For the transverse polarized structure function it must be polarized within the $\hat{e}_1-\hat{e}_2$ plane. Making use of both parity invariance as well as the grand-spin reflection symmetry, we find that only the isovector part, i.e $\mathcal{Q}_A^2\sim\frac{1}{6}D_{3i}\tau_i$, contributes to both the longitudinal and transverse polarized structure functions. In the direction $\hat{e}_3$, the nucleon matrix elements cf. equation (4.4.27) becomes

$$\langle N,\frac{1}{2}\hat{e}_3|D_{3i}|N,\frac{1}{2}\hat{e}_3\rangle=-\frac{2}{3}I_3\delta_{3i}, \tag{6.0.3}$$

where $I_3=\pm\frac{1}{2}$ is the nucleon isospin. Generalizing the photon direction $\hat{e}_3$ into an arbitrary unit spherical direction $\hat{z}$, we find the leading order $\frac{1}{N_c}$ longitudinal polarized structure function

$$\mathrm{g}_1^{I=1}(x) = -\imath MN_c\frac{\pi}{72}\langle N|I_3|N\rangle\int\frac{\mathrm{d}\Omega_z}{4\pi}\int\frac{\mathrm{d}\omega}{2\pi}\sum_\alpha\int\frac{\mathrm{d}\lambda}{2\pi}e^{\imath Mx\lambda}\left(\sum_{i=0}^{2}c_i\frac{\omega+\epsilon_\alpha}{\omega^2-\epsilon_\alpha^2-\Lambda_i^2+\imath\epsilon}\right)_{\mathrm{p}}$$
$$\times\int\mathrm{d}^3\xi\left\{\Psi_\alpha^\dagger(\vec{\xi})\vec{\tau}\cdot\hat{z}(1-\vec{\alpha}\cdot\hat{z})\gamma_5\Psi_\alpha(\vec{\xi}+\lambda\hat{z})e^{-\imath\omega\lambda}+\Psi_\alpha^\dagger(\vec{\xi})\vec{\tau}\cdot\hat{z}(1-\vec{\alpha}\cdot\hat{z})\gamma_5\Psi_\alpha(\vec{\xi}-\lambda\hat{z})e^{\imath\omega\lambda}\right\}. \tag{6.0.4}$$

Similarly, singling out the $\hat{e}_1$ direction from the $\hat{e}_1-\hat{e}_2$ plane, the nucleon matrix elements become

$$\langle N,\frac{1}{2}\hat{e}_1|D_{3i}|N,\frac{1}{2}\hat{e}_1\rangle=-\frac{2}{3}I_3\delta_{1i}. \tag{6.0.5}$$

After generalizing the photon direction into an arbitrary unit spherical direction $\hat{z}$ we find the leading order $\frac{1}{N_c}$ transverse polarized structure function

$$\mathrm{g}_T^{I=1}(x) = -\imath MN_c\frac{\pi}{144}\langle N|I_3|N\rangle\int\frac{\mathrm{d}\Omega_z}{4\pi}\int\frac{\mathrm{d}\omega}{2\pi}\sum_\alpha\int\frac{\mathrm{d}\lambda}{2\pi}e^{\imath Mx\lambda}\left(\sum_{i=0}^{2}c_i\frac{\omega+\epsilon_\alpha}{\omega^2-\epsilon_\alpha^2-\Lambda_i^2+\imath\epsilon}\right)_{\mathrm{p}}$$
$$\times\int\mathrm{d}^3\xi\left\{\Psi_\alpha^\dagger(\vec{\xi})\left(\vec{\tau}\cdot\vec{\alpha}-\vec{\tau}\cdot\hat{z}\vec{\alpha}\cdot\hat{z}\right)\gamma_5\Psi_\alpha(\vec{\xi}+\lambda\hat{z})e^{-\imath\omega\lambda}\right.$$
$$\left.+\Psi_\alpha^\dagger(\vec{\xi})\left(\vec{\tau}\cdot\vec{\alpha}-\vec{\tau}\cdot\hat{z}\vec{\alpha}\cdot\hat{z}\right)\gamma_5\Psi_\alpha(\vec{\xi}-\lambda\hat{z})e^{\imath\omega\lambda}\right\}. \tag{6.0.6}$$

Note again that our calculations of the structure functions contains an extra factor of $\frac{\pi}{2}$ as compared to those of Ref.[24]. This extra factor results from using the definitions of the Fourier

transformations cf. equations (5.2.19) and (5.2.31). In the case of the transverse polarized structure function, the factor $\frac{\pi}{144}$ results from making use of the Fourier transformation as well as averaging over the $\hat{e}_1 - \hat{e}_2$ plane, as the transverse projector $\delta_{ij} - \hat{z}_i\hat{z}_j$ gives twice the desired result.

6.1 Numerical Calculations of the Iso-singlet Unpolarized Structure Function

In the next step, we take the Fourier transform of the eigenfunction into momentum space

$$F_1^{I=0}(x) = \imath\frac{5\pi}{72}MN_c\int\frac{\mathrm{d}\Omega_z}{4\pi}\int\frac{\mathrm{d}\omega}{2\pi}\sum_\alpha\int\frac{\mathrm{d}\lambda}{2\pi}\left(\sum_{i=0}^{2}c_i\frac{\omega+\epsilon_\alpha}{\omega^2-\epsilon_\alpha^2-\Lambda_i^2+\imath\epsilon}\right)_{\mathrm{p}}\int\frac{\mathrm{d}^3p}{2\pi^2}\int\frac{\mathrm{d}^3k}{2\pi^2}\int\mathrm{d}^3\xi$$
$$\times\left\{\tilde{\Psi}_\alpha^\dagger(\vec{p})(1-\vec{\alpha}\cdot\hat{z})\tilde{\Psi}_\alpha(\vec{k})e^{\imath\vec{\xi}\cdot(\vec{p}-\vec{k})}e^{\imath\lambda\left(Mx-\hat{z}\cdot\vec{k}\right)}e^{-\imath\omega\lambda}\right.$$
$$\left.-\tilde{\Psi}_\alpha^\dagger(\vec{p})(1-\vec{\alpha}\cdot\hat{z})\tilde{\Psi}_\alpha(\vec{k})e^{\imath\vec{\xi}\cdot(\vec{p}-\vec{k})}e^{\imath\lambda\left(Mx+\hat{z}\cdot\vec{k}\right)}e^{\imath\omega\lambda}\right\}. \tag{6.1.1}$$

Considering the pole contributions

$$\left(\sum_{i=0}^{2}c_i\frac{1}{\omega^2-\epsilon_\alpha^2-\Lambda_i^2+\imath\epsilon}\right)_{\mathrm{pole}}=\sum_{i=0}^{2}c_i\frac{-\imath\pi}{\omega_0}\left[\delta\left(\omega+\omega_0\right)+\delta\left(\omega-\omega_0\right)\right], \tag{6.1.2}$$

where (note that the labels α and i are not made explicit on ω_0)

$$\omega_0=\sqrt{\epsilon_\alpha^2+\Lambda_i^2}, \tag{6.1.3}$$

we have the following integral identity

$$\int\frac{\mathrm{d}\omega}{2\pi}\left(\sum_{i=0}^{2}c_i\frac{\omega+\epsilon_\alpha}{\omega^2-\epsilon_\alpha^2-\Lambda_i^2+\imath\epsilon}\right)_{\mathrm{pole}}e^{\mp\imath\omega\lambda}=\sum_{i=0}^{2}c_i\frac{1}{\omega_0}\left[\mp\omega_0\sin\omega_0\lambda-\imath\epsilon_\alpha\cos\omega_0\lambda\right]. \tag{6.1.4}$$

This then allows us to perform the integral over 'λ'

$$\int\frac{\mathrm{d}\lambda}{2\pi}\left(\mp\imath\omega_0\sin\omega_0\lambda+\epsilon_\alpha\cos\omega_0\lambda\right)e^{\imath\lambda(Mx\mp\hat{z}\cdot\vec{p})}=\mp\frac{\omega_0}{2}\left[\delta\left(Mx\mp\hat{z}\cdot\vec{p}+\omega_0\right)-\delta\left(Mx\mp\hat{z}\cdot\vec{p}-\omega_0\right)\right]$$
$$+\frac{\epsilon_\alpha}{2}\left[\delta\left(Mx\mp\hat{z}\cdot\vec{p}+\omega_0\right)+\delta\left(Mx\mp\hat{z}\cdot\vec{p}-\omega_0\right)\right], \tag{6.1.5}$$

At this stage the averaging procedure (over Ω_z) proves efficient because it copes with the Dirac-delta functions on the right-hand-side of equation (6.1.5). Details of this calculations are relegated to Appendix D. Furthermore we write the momentum integration variable in spherical coordinates, i.e

$$\int\mathrm{d}^3p\rightarrow\int\mathrm{d}p\,p^2\int\mathrm{d}\Omega_p. \tag{6.1.6}$$

We stress that, when constructing the soliton solution, a particular coordinate system had to be selected; the so-called rest frame (RF). Hence the computed structure structure functions will

Table 6.2: Matrix elements $\int \mathrm{d}\Omega_p \mathcal{Y}_{L'J'GM}(\vec{p})\hat{p}\cdot\vec{\sigma}\mathcal{Y}_{LJGM}(\vec{p})$.

$J'=G-\frac{1}{2}$		$J'=G+\frac{1}{2}$			
$L'=G-1$	$L'=G$	$L'=G$	$L'=G+1$		
0	-1	0	0	$L=G-1$	
					$J=G-\frac{1}{2}$
-1	0	0	0	$L=G$	
0	0	0	-1	$L=G$	
					$J=G+\frac{1}{2}$
0	0	-1	0	$L=G+1$	

have support for $|x|>1$. This seemingly Lorentz-violating effect will be cured by transforming to the infinite momentum frame (IMF)[61, 62] to be discussed later. This then gives the unpolarized structure function in the RF as

$$[F_1^{I=0}(x)]_{\mathrm{s}}^{\mp}=\frac{5MN_c}{144}\sum_{\alpha}\sum_{i=0}^{2}c_i\int_{|Mx_{\alpha}^{\pm}|}^{\infty}p\,\mathrm{d}p\int\mathrm{d}\Omega_p\left\{\pm\tilde{\Psi}_{\alpha}^{\dagger}(\vec{p})\tilde{\Psi}_{\alpha}(\vec{p})-\frac{\epsilon_{\alpha}}{\omega_0}\frac{Mx_{\alpha}^{\pm}}{p}\tilde{\Psi}_{\alpha}^{\dagger}(\vec{p})\hat{p}\cdot\vec{\alpha}\tilde{\Psi}_{\alpha}(\vec{p})\right\},\tag{6.1.7}$$

where

$$Mx_{\alpha}^{\pm}=Mx\pm\omega_0.\tag{6.1.8}$$

Keep in mind that ω_0 has hidden labels α and i. Here $[F_1^{I=0}(x)]_{\mathrm{s}}^{\pm}$ arises from the positive (negative) frequency components that are typically referred to as quark and antiquark distributions. The total unpolarized structure function is

$$[F_1^{I=0}(x)]_{\mathrm{s}}=[F_1^{I=0}(x)]_{\mathrm{s}}^{-}+[F_1^{I=0}(x)]_{\mathrm{s}}^{+}.\tag{6.1.9}$$

The subscript 's' denotes the sea (vacuum) contribution of this structure function as it is merely the part which is extracted from the vacuum part of the action. As for all previous applications we compute it by making use of the formula for single cut-off adopted from the Pauli-Villar's regularization (see Appendix B.1).

In the next step we consider the matrix elements of:

$$\int\mathrm{d}\Omega_p\tilde{\Psi}_{\alpha}^{\dagger}(\vec{p})\tilde{\Psi}_{\alpha}(\vec{p})\quad\text{and}\tag{6.1.10}$$

$$\int\mathrm{d}\Omega_p\tilde{\Psi}_{\alpha}^{\dagger}(\vec{p})\hat{p}\cdot\vec{\alpha}\tilde{\Psi}_{\alpha}(\vec{p})=\int\mathrm{d}\Omega_p\tilde{\Psi}_{\alpha}^{\dagger}(\vec{p})\hat{p}\cdot\vec{\sigma}\gamma_5\tilde{\Psi}_{\alpha}(\vec{p}).\tag{6.1.11}$$

The matrix elements of (6.1.10) are straightforward: For positive intrinsic parity we have

$$\int\mathrm{d}\Omega_p\tilde{\Psi}_{\alpha}^{\dagger(G,+)}(\vec{p})\tilde{\Psi}_{\alpha}^{(G,+)}(\vec{p})=(2G+1)\Big(\tilde{g}_{\alpha}^{(G,+;1)}(p)^2+\tilde{f}_{\alpha}^{(G,+;1)}(p)^2+\tilde{g}_{\alpha}^{(G,+;2)}(p)^2+\tilde{f}_{\alpha}^{(G,+;2)}(p)^2\Big),$$

and for negative intrinsic parity we have

$$\int\mathrm{d}\Omega_p\tilde{\Psi}_{\alpha}^{\dagger(G,-)}(\vec{p})\tilde{\Psi}_{\alpha}^{(G,-)}(\vec{p})=(2G+1)\Big(\tilde{g}_{\alpha}^{(G,-;1)}(p)^2+\tilde{f}_{\alpha}^{(G,-;1)}(p)^2+\tilde{g}_{\alpha}^{(G,-;2)}(p)^2+\tilde{f}_{\alpha}^{(G,-;2)}(p)^2\Big).$$

The overall factor $(2G+1)$ arises from summing the grand spin projection contained in $\sum_\alpha$. Singling out this part of $\sum_\alpha$ is permissible because the single quark energies ϵ_α (contained in ω_0) are degenerate with respect to this quantum number. The matrix element of (6.1.11) is computed from the matrix elements from Table 6.2: For positive intrinsic parity we have

$$\int \mathrm{d}\Omega_p\, \tilde{\Psi}_\alpha^{\dagger(G,+)}(\vec{p})\hat{p}\cdot\vec{\sigma}\gamma_5\tilde{\Psi}_\alpha^{(G,+)}(\vec{p}) = -2(2G+1)\Big(\tilde{g}_\alpha^{(G,+;1)}(p)\tilde{f}_\alpha^{(G,+;1)}(p) + \tilde{g}_\alpha^{(G,+;2)}(p)\tilde{f}_\alpha^{(G,+;2)}(p)\Big).$$

and for negative intrinsic parity we have

$$\int \mathrm{d}\Omega_p\, \tilde{\Psi}_\alpha^{\dagger(G,-)}(\vec{p})\hat{p}\cdot\vec{\sigma}\gamma_5\tilde{\Psi}_\alpha^{(G,-)}(\vec{p}) = -2(2G+1)\Big(\tilde{g}_\alpha^{(G,-;1)}(p)\tilde{f}_\alpha^{(G,-;1)}(p) + \tilde{g}_\alpha^{(G,-;2)}(p)\tilde{f}_\alpha^{(G,-;2)}(p)\Big).$$

In what follows, we consider the baryon number $B=1$ in the soliton sector. As indicated in chapter 4, the baryon number $B=1$ is carried by the valence quarks. The valence quark contribution to the nucleon structure functions is obtained by including the first-order rotational correction for the valence quark wave function:

$$\begin{aligned}\Psi_{\mathrm{v}}^{(\mathrm{rot})}(\vec{x},t) &= e^{-\imath\epsilon_{\mathrm{v}}t}A(t)\left\{\Psi_{\mathrm{v}}(\vec{x}) + \frac{1}{2}\sum_{\alpha\neq\mathrm{v}}\Psi_\alpha(\vec{x})\frac{\langle\alpha|\vec{\tau}\cdot\vec{\Omega}|\mathrm{v}\rangle}{\epsilon_{\mathrm{v}}-\epsilon_\alpha}\right\}\\ &=: e^{-\imath\epsilon_{\mathrm{v}}t}A(t)\psi_{\mathrm{v}}(\vec{x}).\end{aligned} \tag{6.1.12}$$

Here $\Psi_\alpha(\vec{x})$ and ϵ_α are the eigenfunctions and energy eigenvalues of the Dirac Hamiltonian h of equation (4.1.7). Also $\psi_{\mathrm{v}}(\vec{x})$ is the spatial part of the valence quark wave function with the rotational corrections included. Furthermore ϵ_{v} is the energy eigenvalue of the valence quark level. In what follows, the quark level in equation (6.0.2) is replaced by the cranked valence level of equation (6.1.12) and the sum over α is omitted. This produces the valence quark contribution to the structure function. Of course, this contribution does not undergo regularization and thus yields

$$\begin{aligned}\Big[F_1^{I=0}(x)\Big]_{\mathrm{v}} &= \imath\frac{5\pi}{72}MN_c\int\frac{\mathrm{d}\Omega_z}{4\pi}\int\frac{\mathrm{d}\omega}{2\pi}\int\frac{\mathrm{d}\lambda}{2\pi}e^{\imath Mx\lambda}\left(\frac{\omega+\epsilon_{\mathrm{v}}}{\omega^2-\epsilon_{\mathrm{v}}^2+\imath\epsilon}\right)_{\mathrm{p}}\\ &\quad\times\int\mathrm{d}^3\xi\left\{\Psi_{\mathrm{v}}^\dagger(\vec{\xi})(1-\vec{\alpha}\cdot\hat{z})\Psi_{\mathrm{v}}(\vec{\xi}+\lambda\hat{z})e^{-\imath\omega\lambda} - \Psi_{\mathrm{v}}^\dagger(\vec{\xi})(1-\vec{\alpha}\cdot\hat{z})\Psi_{\mathrm{v}}(\vec{\xi}-\lambda\hat{z})e^{\imath\omega\lambda}\right\}.\end{aligned} \tag{6.1.13}$$

Repeating the calculations above, using that the valence quark wave function has positive parity and the pole condition $f^{\pm}|_{\mathrm{pole}} = -4\imath\pi\delta(\omega\mp\epsilon_\alpha)$ gives

$$\Big[F_1^{I=0}(x)\Big]_{\mathrm{v}}^{\mp} = -\frac{5MN_c}{72}\times\int_{M|x_{\mathrm{v}}^{\pm}|}^{\infty}p\,\mathrm{d}p\int\mathrm{d}\Omega_p\left\{\pm\tilde{\Psi}_{\mathrm{v}}^\dagger(\vec{p})\tilde{\Psi}_{\mathrm{v}}(\vec{p}) - \frac{Mx_{\mathrm{v}}^{\pm}}{p}\tilde{\Psi}_{\mathrm{v}}^\dagger(\vec{p})\hat{p}\cdot\vec{\alpha}\tilde{\Psi}_{\mathrm{v}}(\vec{p})\right\}, \tag{6.1.14}$$

here

$$Mx_{\mathrm{v}}^{\pm} = Mx \pm \epsilon_{\mathrm{v}}. \tag{6.1.15}$$

Before computing the matrix element that arises from the valence contribution we note the following: The valence quark carries $G=0$; then only the components with $J=+\frac{1}{2}$ are

allowed for the eigenspinor

$$\Psi_{\alpha}^{0,+}(\vec{x}) = \Psi_{\mathrm{v}}(\vec{x}) = \begin{pmatrix} \imath g_{\mathrm{v}}(r)\mathcal{Y}_{0,\frac{1}{2},0,0}(\hat{x}) \\ f_{\mathrm{v}}(r)\mathcal{Y}_{1,\frac{1}{2},0,0}(\hat{x}) \end{pmatrix} \tag{6.1.16}$$

here $g_{\mathrm{v}}(r) = g_{\alpha}^{(0,+;1)}(r)$ etc, are the particular eigenwave functions. The cranking correction associated with the first order rotation (6.1.12) dwells in the channel with $G = 1$ and negative intrinsic parity

$$\Psi_{\alpha}^{(1,-)}(\vec{x}) = \begin{pmatrix} \imath g_{\alpha}^{(1)}(r)\mathcal{Y}_{2,\frac{3}{2},1,M}(\hat{x}) \\ -f_{\alpha}^{(1)}(r)\mathcal{Y}_{1,\frac{3}{2},1,M}(\hat{x}) \end{pmatrix} + \begin{pmatrix} \imath g_{\alpha}^{(2)}(r)\mathcal{Y}_{0,\frac{1}{2},1,M}(\hat{x}) \\ f_{\alpha}^{(2)}(r)\mathcal{Y}_{1,\frac{1}{2},1,M}(\hat{x}) \end{pmatrix}, \tag{6.1.17}$$

for convenience we have written $g_{\alpha}^{(1,-;1)}(r)$ as $g_{\alpha}^{(1)}(r)$ etc.

Taking the Fourier transform of equation (6.1.12) gives

$$\tilde{\psi}_{\mathrm{v}}(\vec{p}) = \tilde{\Psi}_{\mathrm{v}}(\vec{p}) + \sum_{\alpha}\langle H_{\alpha}\rangle\tilde{\Psi}_{\alpha}(\vec{p}), \tag{6.1.18}$$

where

$$\tilde{\Psi}_{\mathrm{v}}(\vec{p}) = \imath \begin{pmatrix} \tilde{g}_{\mathrm{val}}(p)\mathcal{Y}_{0,\frac{1}{2},0,0}(\hat{p}) \\ \tilde{f}_{\mathrm{val}}(p)\mathcal{Y}_{1,\frac{1}{2},0,0}(\hat{p}) \end{pmatrix} \tag{6.1.19}$$

and

$$\tilde{\Psi}_{\alpha}(\vec{p}) = -\imath \begin{pmatrix} \tilde{g}_{\alpha}^{(1)}(p)\mathcal{Y}_{2,\frac{3}{2},1,M}(\hat{p}) - \tilde{g}_{\alpha}^{(2)}(p)\mathcal{Y}_{0,\frac{1}{2},1,M}(\hat{p}) \\ \tilde{f}_{\alpha}^{(1)}(p)\mathcal{Y}_{1,\frac{3}{2},1,M}(\hat{p}) - \tilde{f}_{\alpha}^{(2)}(p)\mathcal{Y}_{1,\frac{1}{2},1,M}(\hat{p}) \end{pmatrix}. \tag{6.1.20}$$

The "matrix element" $\langle H_{\alpha}\rangle$ arises from perturbation treatment of the collective rotation

$$\langle H_{\alpha}\rangle = \frac{1}{2}\frac{\langle\alpha|\vec{\tau}\cdot\vec{\Omega}|\mathrm{v}\rangle}{\epsilon_{\mathrm{v}} - \epsilon_{\alpha}}. \tag{6.1.21}$$

The discussion of the cranked corrections will be relegated to the next chapter, where we will look at the sub-leading contributions of the hadronic tensor. Having clarified this we obtain the matrix elements

$$\int \mathrm{d}\Omega_p \tilde{\Psi}_{\mathrm{v}}^{\dagger}(\vec{p})\tilde{\Psi}_{\mathrm{v}}(\vec{p}) = \tilde{g}_{\mathrm{v}}(p)^2 + \tilde{f}_{\mathrm{v}}(p)^2 \quad \text{and} \tag{6.1.22}$$

$$\int \mathrm{d}\Omega_p \tilde{\Psi}_{\mathrm{v}}^{\dagger}(\vec{p})\hat{p}\cdot\vec{\sigma}\gamma_5\tilde{\Psi}_{\mathrm{v}}(\vec{p}) = -2\tilde{g}_{\mathrm{v}}(p)\tilde{f}_{\mathrm{v}}(p) \tag{6.1.23}$$

at leading order $\frac{1}{N_c}$.

6.1.1 Numerical Results for the Iso-singlet Unpolarized Structure Function

As discussed in section 4.3, the energy eigenvalues ϵ_{α} and the corresponding eigenvectors $\Psi_{\alpha}(\vec{x})$ are obtained by diagonalizing the Dirac Hamiltonian in coordinate space. Discrete eigenvalues

are obtained by imposing suitable boundary conditions at spatial infinity represented by a spherical box with large radius $D = 10\,\mathrm{fm}$.

In a second step we construct the Fourier transform of the coordinate space wave-function. This defines the momentum space radial functions $\tilde{g}_\alpha$ and $\tilde{f}_\alpha$ that appear in the formulas above. We compute this for $0 \leq p \leq p_{\max}$ on an equi-distant grid with n_p points. We verify the numerical accuracy of this construction by ensuring the normalization of the momentum space wave function. This requires values as large as $n_p = 22001$ and $p_{\max} = 25$ when ϵ_α and/or G are large.

Regularization typically removes/cures quadratic and logarithmic divergences. In some cases even quartic divergences emerge. A typical example is the action functional itself that includes the quartically divergent cosmological constant. Such divergences are removed by subtracting the non-solitonic counterpart, i.e. the same quantity computed for $F(r) = 0$.

For the example of the action functional this enforces subtracting the zeroth order energy in equations (4.1.31) and (4.1.35). Since the iso-scalar unpolarized structure functions are related to the energy (i.e. the classical mass) of the soliton via the momentum sum rule it is obvious that this subtraction is also required for $F_1(x)$:

$$\left[F_1^{I=0}\right]_{\text{vacuum}} = \left[F_1^{I=0}\right]_{\text{s}} - \left[F_1^{(0)\,I=0}\right]_{\text{s}}. \tag{6.1.24}$$

It must be emphasized that the calculations of the structure functions is done in the nucleon rest frame (RF).

As described in Refs [61, 62] calculating the structure functions from localized fields requires the transformation to the infinite momentum frame (IMF). On the level of these structure functions this transformation reads

$$f_{IMF}(x) = \frac{\Theta\,(1-x)}{1-x} f_{RF}\left(-\ln(1-x)\right), \tag{6.1.25}$$

where f_{RF} refers to any of structure functions from the soliton discussed above. Obviously this ensures that the structure function have support only in the kinematically allowed interval $x \in [0,1]$. However, the argument of f_{RF} ranges between zero and infinity. Numerically we take[1] $x_{RF} = -\ln(1-x) \in [0,12]$, discretized on 3505 points.

We have choosen the experimental value, 940 MeV, for the nucleon mass in all our computations. Note that for $M \neq M_{\text{sol}}$ this implies $\int \mathrm{d}x\, F_1(x) = \dfrac{M_{\text{sol}}}{M} \neq 1$ in our sum rule.

In using the Pauli-Villar's regularization (see Appendix B.1 with $\Lambda_1 = \Lambda_2 = \Lambda$), the term $\Lambda^2 \dfrac{\partial g(\Lambda^2)}{\partial \Lambda^2}$ contributes

$$\left[\pm \Lambda^2 \frac{1}{2\omega_\Lambda} M x_2^\pm \int \mathrm{d}\Omega_p \tilde{\Psi}_\alpha^\dagger(\vec{p}) \tilde{\Psi}_\alpha(\vec{p}) - \Lambda^2 \frac{\epsilon_\alpha}{2\omega_\Lambda^2} |M x_2^\pm| \int \mathrm{d}\Omega_p \int \mathrm{d}\Omega_p \tilde{\Psi}_\alpha^\dagger(\vec{p}) \hat{p}\cdot\vec{\alpha} \tilde{\Psi}_\alpha(\vec{p}) \right]_{p=|Mx_2^\pm|}, \tag{6.1.26}$$

[1] Unless otherwise noted, x in the formulas of this chapter refers to $x_{RF} = -\ln(1-x_{\text{Bj}})$ i.e the argument of f_{RF}, while x_{Bj} is the physical variable in the IMF.

m	$\frac{1}{M}E_{\rm v}$	$[\mathcal{M}^0_G]_v$	$\frac{1}{M}E_{\rm s}$	$[\mathcal{M}^0_G]_s$
400	0.708	0.708	0.628	0.633
450	0.612	0.613	0.715	0.712
500	0.523	0.524	0.789	0.798

Table 6.3: Comparison of the calculated momentum sum rule of the iso-scalar unpolarized structure function to that from the valence energy $E_{\rm v}$ and the vacuum energy $E_{\rm s}$ for different constituent quark masses m (in MeV).

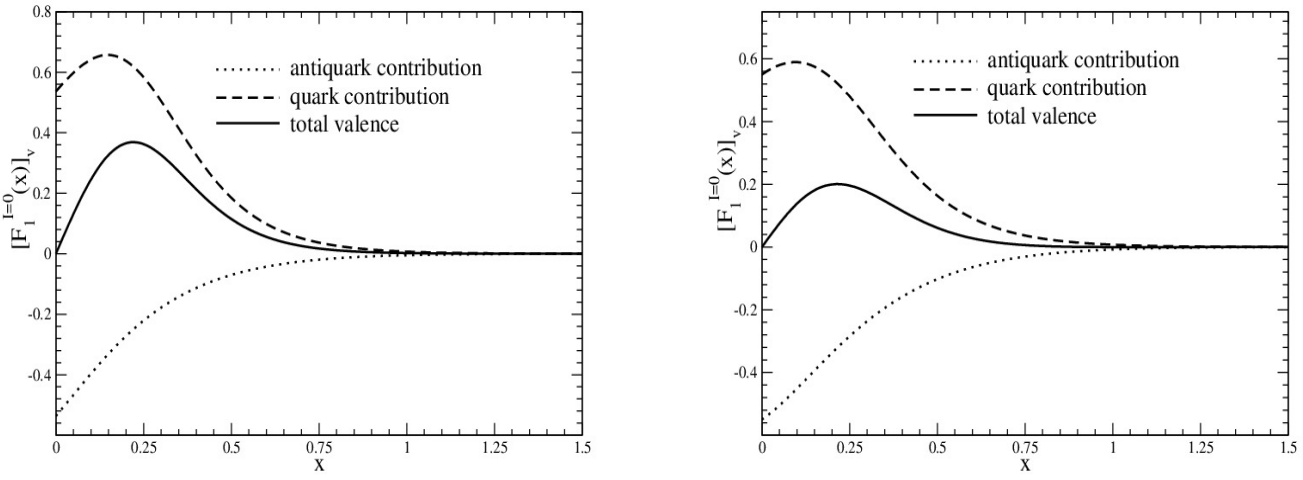

Figure 6.1: The numerical prediction for the valence part of the iso-scalar unpolarized structure function. Left panel: The case for $m = 400\,\text{MeV}$. Right panel: The case for $m = 450\,\text{MeV}$.

to the structure function which does not contain an integral over the radial momentum. We compute such terms by a linear interpolation between points on the momentum grid. Defining the right hand side of equation (6.1.26) as $y_i = y(p_i)$, for $i = 1 \cdots n_p$. Then for any given interval between p_j and p_{j+1}, the interpolation formula is given as [63]

$$y = y_j + \frac{(y_{j+1} - y_j)}{p_{j+1} - p_j}\left(|Mx^{\pm}| - p_j\right). \tag{6.1.27}$$

Also in computing the integral

$$I = \int_{|Mx^{\pm}|}^{\infty} \mathrm{d}p\, h(p), \tag{6.1.28}$$

that arises for the structure function, we first redefine the integral variable as

$$s(p) = \begin{cases} h(p), & \text{for} \quad p \geqslant |Mx^{\pm}|, \\ 0, & \text{otherwise}, \end{cases} \tag{6.1.29}$$

and then integrate this function

$$I = \int_0^{\infty} \mathrm{d}p\, s(p) \tag{6.1.30}$$

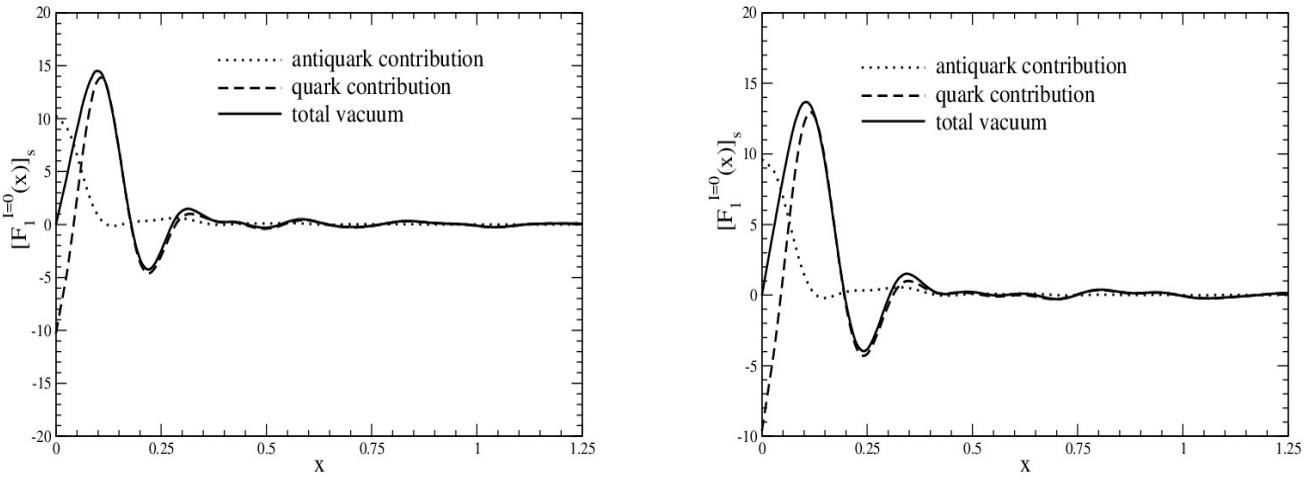

Figure 6.2: The numerical prediction for the vacuum part of the iso-scalar unpolarized structure function. Left panel: The case for $m = 400\,\text{MeV}$. Right panel: The case for $m = 450\,\text{MeV}$. This includes the subtraction of $F_1^{(0)\,I=0}$ (the case for $F(r) = 0$) as indicated in equation (6.1.24).

using Bode's algorithm, which combines the function values of four equi-distant subintervals defined by five points, $p_i = p_1 + h(i-1)$, with $i = 1, \cdots, 5$. Let $f(p)$ be the integrands of any of the structure functions. Then [63]

$$\int_{p_1}^{p_5} f(p)\,\mathrm{d}x = \frac{h}{45}\left(14f(p_1) + 64f(p_2) + 24f(p_3) + 64f(p_4) + 14f(p_5)\right), \tag{6.1.31}$$

where $h = p_2 - p_1$.

Before presenting our numerical results to the unpolarized structure function, we first look at the momentum sum rules for this structure function. We first integrate the scalar term[2] $(\tilde{\Psi}^\dagger_\alpha(\vec{p})\tilde{\Psi}_\alpha(\vec{p}))$

$$\begin{aligned}
\left[\mathcal{M}^0_G\right]_{\mathrm{s}} &= \frac{36}{5}\int_0^\infty \mathrm{d}x\, x\left[F_1^{I=0}(x)\right]_s = \frac{MN_c}{4}\sum_\alpha\sum_{i=0}^{2} c_i \int_0^\infty \mathrm{d}x\, x\left\{\left\langle\alpha|\alpha\right\rangle'_{|Mx^+|} - \left\langle\alpha|\alpha\right\rangle'_{|Mx^-|}\right\} \\
&= \frac{MN_c}{4}\sum_\alpha\sum_{i=0}^{2} c_i\left\{\int_{\frac{\omega_0}{M}}^\infty \mathrm{d}y\,\left(y - \frac{\omega_0}{M}\right)\left\langle\alpha|\alpha\right\rangle'_{My} - \int_{-\frac{\omega_0}{M}}^\infty \mathrm{d}y\,\left(y + \frac{\omega_0}{M}\right)\left\langle\alpha|\alpha\right\rangle'_{|My|}\right\}, \\
&= -\frac{N_c}{2}\sum_\alpha\sum_{i=0}^{2} c_i\,\omega_0\int_0^\infty \mathrm{d}y\left\langle\alpha|\alpha\right\rangle'_{My},
\end{aligned} \tag{6.1.32}$$

in the third line of the above equation we used the properties of integrals with symmetric boundaries. Finally, integrating by parts gives

$$\begin{aligned}
\left[\mathcal{M}^0_G\right]_{\mathrm{s}} &= \frac{N_c}{2}\sum_\alpha\sum_{i=0}^{2} c_i\,\omega_0\int_0^\infty \mathrm{d}y\, y\frac{\partial}{\partial y}\int_{My}^\infty \mathrm{d}p\, p\int \mathrm{d}\Omega\tilde{\Psi}^\dagger_\alpha(\vec{p})\tilde{\Psi}_\alpha(\vec{p}), \\
&= -\frac{MN_c}{2}\sum_\alpha\sum_{i=0}^{2} c_i\,\omega_0\int_0^\infty \mathrm{d}y\, y\left[p\int \mathrm{d}\Omega_p\Psi^\dagger_\alpha(\vec{p})\Psi_\alpha(\vec{p})\right]_{p=My} = -\frac{N_c}{2M}\sum_\alpha\sum_{i=0}^{2} c_i\sqrt{\epsilon_\alpha^2 + \Lambda_i^2},
\end{aligned} \tag{6.1.33}$$

[2]For convenience we have introduced the notation $\left\langle\alpha|\alpha\right\rangle'_a = \int_a^\infty \mathrm{d}p\, p\int \mathrm{d}\Omega\tilde{\Psi}^\dagger_\alpha(\vec{p})\tilde{\Psi}_\alpha(\vec{p})$.

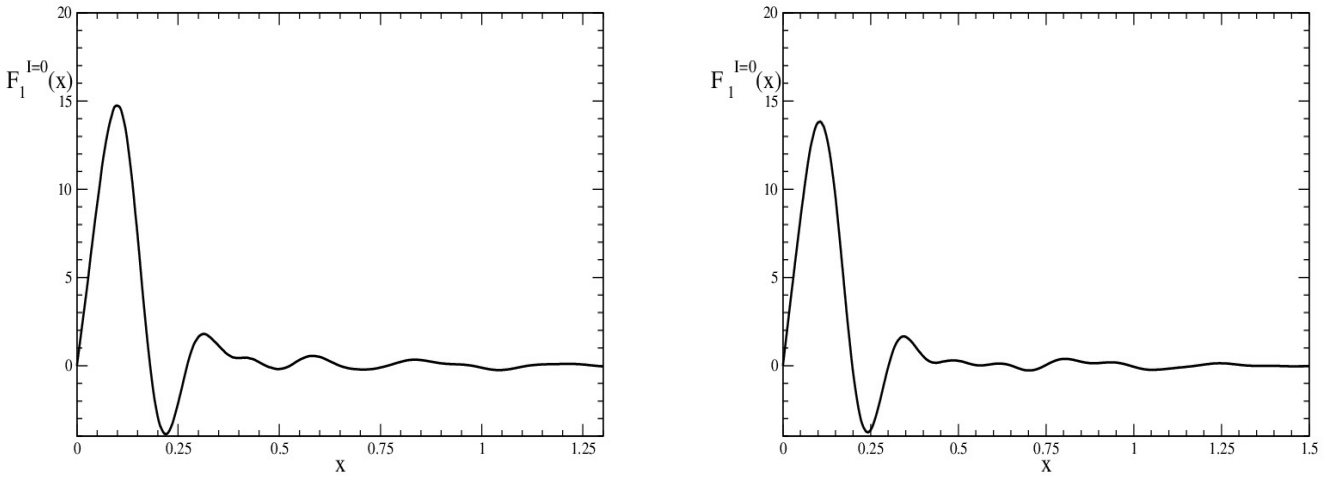

Figure 6.3: The numerical prediction to the iso-scalar unpolarized structure function. Left panel: The case for $m = 400\,\mathrm{MeV}$. Right panel: The case for $m = 450\,\mathrm{MeV}$.

which is $\frac{1}{M}$ times the vacuum contribution of the classical energy cf. equation (4.1.31), and hence necessitates the subtraction of the trivial meson equivalent to the structure function, as indicated earlier. Clearly, the momentum sum rule of the valence contribution becomes

$$\left[\mathcal{M}_G^0\right]_{\mathrm{v}} = \frac{36}{5}\int_0^\infty \mathrm{d}x\, x\left[F_1^{I=0}(x)\right]_{\mathrm{v}} \sim -\frac{N_c}{M}\epsilon_{\mathrm{v}}. \tag{6.1.34}$$

Similarly, integrating the term with the operator[3] $\hat{p}\cdot\vec{\alpha}$ gives

$$\begin{aligned}
\left[\mathcal{M}_G^1\right]_{\mathrm{s}} &= -\frac{MN_c}{4}\sum_\alpha\sum_{i=0}^{2} c_i\frac{\epsilon_\alpha}{\omega_0}\int_0^\infty \mathrm{d}x\, x\left\{Mx^+\left\langle\alpha|\hat{p}\cdot\vec{\alpha}|\alpha\right\rangle''_{|Mx^+|} + Mx^-\left\langle\alpha|\hat{p}\cdot\vec{\alpha}|\alpha\right\rangle''_{|Mx^-|}\right\},\\
&= -\frac{MN_c}{4}\sum_\alpha\sum_{i=0}^{2} c_i\frac{\epsilon_\alpha}{\omega_0}\left\{\int_{\frac{\omega_0}{M}}^\infty \mathrm{d}y\left(y-\frac{\omega_0}{M}\right)My\left\langle\alpha|\hat{p}\cdot\vec{\alpha}|\alpha\right\rangle''_{My} + \int_{-\frac{\omega_0}{M}}^\infty \mathrm{d}y\left(y+\frac{\omega_0}{M}\right)My\left\langle\alpha|\hat{p}\cdot\vec{\alpha}|\alpha\right\rangle''_{|My|}\right\},\\
&= -\frac{M^2N_c}{2}\sum_\alpha\sum_{i=0}^{2} c_i\frac{\epsilon_\alpha}{\omega_0}\int_0^\infty \mathrm{d}y\, y^2\left\langle\alpha|\hat{p}\cdot\vec{\alpha}|\alpha\right\rangle''_{My},
\end{aligned} \tag{6.1.35}$$

as before we used the properties of integrals with symmetric boundaries.

Again integrating by parts gives

$$\begin{aligned}
\left[\mathcal{M}_G^1\right]_{\mathrm{s}} &= -\frac{N_c}{6M}\sum_\alpha\sum_{i=0}^{2}\frac{\epsilon_\alpha}{\sqrt{\epsilon_\alpha+\Lambda_i^2}}\left\langle\alpha|\vec{\alpha}\cdot\hat{p}|\alpha\right\rangle_0 = \imath\frac{N_c}{6M}\sum_\alpha\sum_{i=0}^{2}\frac{\epsilon_\alpha}{\sqrt{\epsilon_\alpha+\Lambda_i^2}}\left\langle\alpha|\vec{\alpha}\cdot\vec{\partial}|\alpha\right\rangle_0,\\
&= -\frac{N_c}{6M}\sum_\alpha\sum_{i=0}^{2}\frac{\epsilon_\alpha}{\sqrt{\epsilon_\alpha+\Lambda_i^2}}\left\langle\alpha|\vec{x}\cdot\vec{\partial}\left\{U_H(\vec{x})\right\}^{\gamma_5}|\alpha\right\rangle_0,
\end{aligned} \tag{6.1.36}$$

[3] We have introduced the notation $\left\langle\alpha|\hat{p}\cdot\vec{\alpha}|\alpha\right\rangle''_a = \int_a^\infty \mathrm{d}p\int \mathrm{d}\Omega_p\tilde{\Psi}^\dagger_\alpha(\vec{p})\hat{p}\cdot\vec{\alpha}\tilde{\Psi}_\alpha(\vec{p})$.

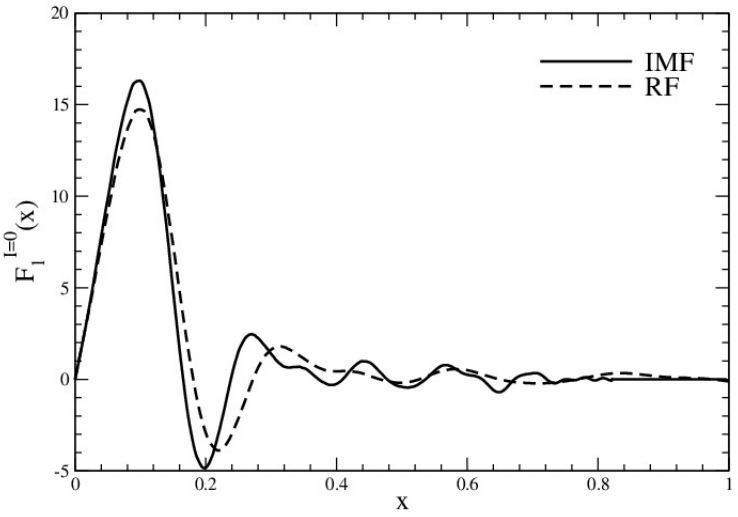

Figure 6.4: The effects of applying the IMF transformation to the iso-singlet unpolarized structure function for $m = 400\,\text{MeV}$. The curve labeled "RF" denote the result obtained from the nucleon rest frame and those labeled "IMF" denote the projection to the infinite momentum frame.

is the matrix element of the dilatation deformation of the soliton. Here we have use the notation

$$\langle\alpha|\hat{p}\cdot\vec{\alpha}|\alpha\rangle_0 = \int_0^\infty \mathrm{d}p\, p^2 \int \mathrm{d}\Omega_p \tilde{\Psi}^\dagger_\alpha(\vec{p})\hat{p}\cdot\vec{\alpha}\tilde{\Psi}_\alpha(\vec{p}).$$

Also using the Hamiltonian cf. equation (4.1.2) we have the relation

$$\left\langle\alpha|\vec{\alpha}\cdot\vec{\partial}|\alpha\right\rangle_0 \sim \left\langle\alpha|\left[\vec{x}\cdot\vec{\partial},h\right] - \left(\vec{x}\cdot\vec{\partial}\left\{U_H(\vec{x})\right\}^{\gamma_5}\right)|\alpha\right\rangle_0 = -\left\langle\alpha|\vec{x}\cdot\vec{\partial}\left\{U_H(\vec{x})\right\}^{\gamma_5}|\alpha\right\rangle_0. \quad (6.1.37)$$

The valence part has a similar contribution $\left[\mathcal{M}^1_G\right]_{\mathrm{v}} \sim -\dfrac{N_c}{6M}\left\langle \mathrm{v}|\vec{x}\cdot\vec{\partial}\left\{U_H(\vec{x})\right\}^{\gamma_5}|\mathrm{v}\right\rangle$. In total $[\mathcal{M}^1_G]_{\mathrm{s}} + [\mathcal{M}^1_G]_{\mathrm{v}}$ is the coefficient of $(s-1)$ in the expansion

$$E[U_H(s\vec{x})] = E_0 + (s-1)E_1 + \cdots (s-1)^l E_l + \cdots \quad (6.1.38)$$

of the classical energy. Since $U_H(\vec{x})$ is a stationary point, $E_1 = 0$ thus verifying the momentum sum rule. Note that the part of this sum rule that involves $\hat{p}\cdot\vec{\alpha}$ is not valid level by level; in contrast to the leading order with the unit matrix and other sum rules to be discussed later. Hence the momentum sum rule is very sensitive to details of the numerical simulation.

The sum rule will tell us, how accurate our numerical procedure is when evaluating this structure function. For example for constituent quark mass $m = 400\,\text{MeV}$, we have $[\mathcal{M}^0_G]_v = 0.708$ and from Table 4.1, we have $\dfrac{E_{\mathrm{v}}}{M} = 0.708$. In Table 6.3 we compare the calculated momentum sum rule with that from the energy contributions from Table 4.1.

In Figure 6.2 we present the numerical results for the vacuum contribution to the iso-scalar unpolarized structure function for constituent quark mass $m = 400\,\text{MeV}$ and $m = 450\,\text{MeV}$. We also separate the quark and antiquark distributions, respectively. One can see that the vacuum

contribution dominates over the valence contributions shown in Figure 6.1. This may be caused by the subtraction of the zero-solution counterpart $F_1^0(x)$ which could involve an alternative definition of x due to different kinematics. In Figure 6.3 we also present the total contribution[4] to the iso-scalar unpolarized structure function. Clearly, our numerical results show that the structure function have support for $x > 1$. To ensure the structure function have support in the kinematically allowed interval $0 \leq x \leq 1$, we transform to the infinite momentum frame, cf. equation (6.1.25). Figure 6.4 shows the results of using this transformation.

6.2 Numerical Calculations of the Isovector Longitudinal Polarized Structure Function

As before, we substitute the Fourier transform of the eigenfunctions into the relevant part of the hadronic tensor, equation (5.2.35) and project according to Table 6.1. Then the longitudinal polarized structure function in the RF at leading order $\dfrac{1}{N_c}$ (where it only contributes to the isovector ($I = 1$) component) reads

$$\begin{aligned}
\mathrm{g}_1^{I=1}(x) = -\imath\frac{MN_c\pi}{72}\langle N|I_3|N\rangle \int \frac{\mathrm{d}\Omega_z}{4\pi}\int\frac{\mathrm{d}\omega}{2\pi}\sum_\alpha\int\frac{\mathrm{d}\lambda}{2\pi}\left(\sum_{i=0}^{2} c_i \frac{\omega+\epsilon_\alpha}{\omega^2-\epsilon_\alpha^2-\Lambda_i^2+\imath\epsilon}\right)_{\mathrm{p}} \\
\times\int\frac{\mathrm{d}^3p}{2\pi^2}\int\frac{\mathrm{d}^3k}{2\pi^2}\int\mathrm{d}^3\xi\left[\tilde{\Psi}_\alpha^\dagger(\vec{p})\vec{\tau}\cdot\hat{z}(1-\vec{\alpha}\cdot\hat{z})\gamma_5\tilde{\Psi}_\alpha(\vec{k})e^{\imath\vec{\xi}\cdot(\vec{p}-\vec{k})}e^{\imath\lambda\left(Mx-\hat{z}\cdot\vec{k}\right)}e^{-\imath\omega\lambda}\right. \\
\left.+\,\tilde{\Psi}_\alpha^\dagger(\vec{p})\vec{\tau}\cdot\hat{z}(1-\vec{\alpha}\cdot\hat{z})\gamma_5\tilde{\Psi}_\alpha(\vec{k})e^{\imath\vec{\xi}\cdot(\vec{p}-\vec{k})}e^{\imath\lambda\left(Mx+\hat{z}\cdot\vec{k}\right)}e^{\imath\omega\lambda}\right]. \qquad (6.2.1)
\end{aligned}$$

Using the identities in equations (6.1.4) – (6.1.5), writing the integration variable into spherical coordinate cf. (6.1.6), and averaging over the photon direction gives

$$\begin{aligned}
\left[\mathrm{g}_1^{I=1}(x)\right]_{\mathrm{s}}^{\mp} = -\frac{MN_c}{72}\langle N|I_3|N\rangle\sum_\alpha\sum_{i=0}^{2}c_i\left\{\mp\int_{|Mx_\alpha^\pm|}^{\infty}\mathrm{d}p\,Mx_\alpha^\pm\int\mathrm{d}\Omega_p\tilde{\Psi}_\alpha^\dagger(\vec{p})\hat{p}\cdot\vec{\tau}\gamma_5\tilde{\Psi}_\alpha(\vec{p})\right. \\
\left.-\frac{\epsilon_\alpha}{\omega_0}\int_{|Mx_\alpha^\pm|}^{\infty}\mathrm{d}p\,p^2\left[A_\pm\int\mathrm{d}\Omega_p\tilde{\Psi}_\alpha^\dagger(\vec{p})\vec{\tau}\cdot\vec{\sigma}\tilde{\Psi}_\alpha(\vec{p})+B_\pm\int\mathrm{d}\Omega_p\tilde{\Psi}_\alpha^\dagger(\vec{p})\hat{p}\cdot\vec{\tau}\hat{p}\cdot\vec{\sigma}\tilde{\Psi}_\alpha(\vec{p})\right]\right\}, \qquad (6.2.2)
\end{aligned}$$

where $\left[\mathrm{g}_1^{I=1}(x)\right]_{\mathrm{s}}^{\pm}$ denotes the quark and antiquark distributions, respectively. The total distribution is given as the sum of the quark and antiquark distributions. Furthermore we have introduced the abbreviations, see also (6.1.8)

$$A_\pm = \frac{1}{2p}\left(1-\frac{(Mx_\alpha^\pm)^2}{p^2}\right), \quad B_\pm = \frac{1}{2p}\left(3\frac{(Mx_\alpha^\pm)^2}{p^2}-1\right). \qquad (6.2.3)$$

As before the subscript 's' denotes sea (vacuum) contribution of this structure function and is computed using the formula for single cut-off adopted from the Pauli-Villar's regularization

[4] By total we mean the sum of the vacuum and valence contributions.

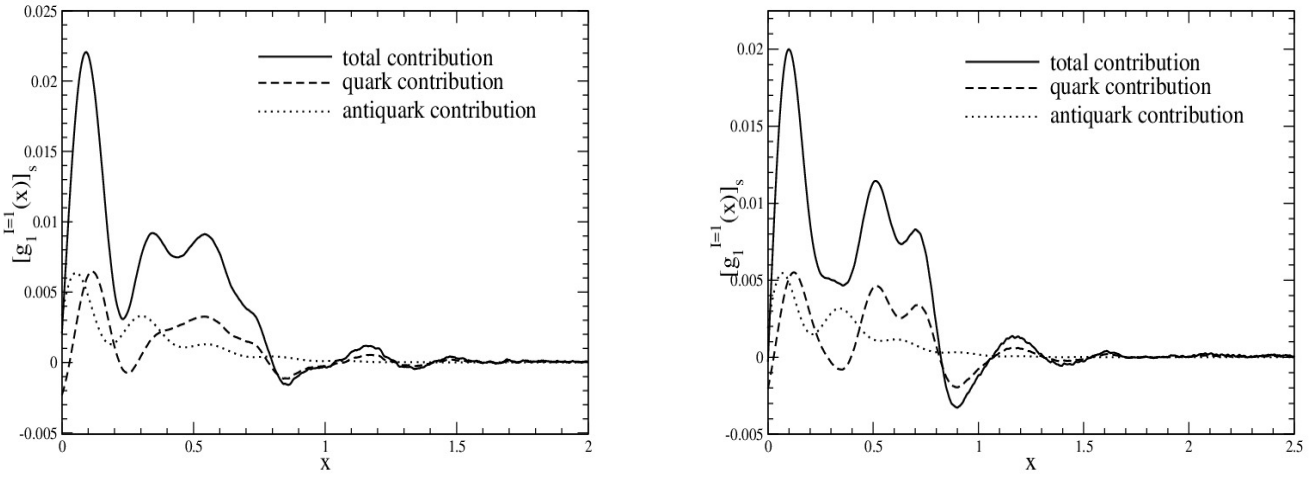

Figure 6.5: The numerical prediction for the vacuum part of the iso-vector polarized proton structure function. Left panel: The case for $m = 400\,\text{MeV}$. Right panel: The case for $m = 450\,\text{MeV}$.

Table 6.4: Matrix elements $\int \mathrm{d}\Omega_p \mathcal{Y}_{L'J'GM}(\vec{p})\hat{p}\cdot\vec{\tau}\mathcal{Y}_{LJGM}(\vec{p})$. Overall factor $\dfrac{1}{(2G+1)}$ needs to be multiplied.

$J' = G - \frac{1}{2}$		$J' = G + \frac{1}{2}$			
$L' = G-1$	$L' = G$	$L' = G$	$L' = G+1$		
0	-1	$-2\sqrt{G(G+1)}$	0	$L = G-1$	
					$J = G - \frac{1}{2}$
-1	0	0	$-2\sqrt{G(G+1)}$	$L = G$	
$-2\sqrt{G(G+1)}$	0	0	1	$L = G$	
					$J = G + \frac{1}{2}$
0	$-2\sqrt{G(G+1)}$	1	0	$L = G+1$	

(see Appendix B.1). In what follows, we consider the matrix elements:

$$\int \mathrm{d}\Omega_p \tilde{\Psi}^\dagger_\alpha(\vec{p})\hat{p}\cdot\vec{\tau}\gamma_5\tilde{\Psi}_\alpha(\vec{p}), \tag{6.2.4}$$

$$\int \mathrm{d}\Omega_p \tilde{\Psi}^\dagger_\alpha(\vec{p})\hat{p}\cdot\vec{\tau}\hat{p}\cdot\vec{\sigma}\tilde{\Psi}_\alpha(\vec{p}) \quad \text{and} \tag{6.2.5}$$

$$\int \mathrm{d}\Omega_p \tilde{\Psi}^\dagger_\alpha(\vec{p})\vec{\tau}\cdot\vec{\sigma}\tilde{\Psi}_\alpha(\vec{p}), \tag{6.2.6}$$

The matrix element (6.2.4) is computed from the matrix elements from Table 6.4: For positive intrinsic parity we have

$$\int \mathrm{d}\Omega_p\, \tilde{\Psi}^{\dagger(G,+)}_\alpha(\vec{p})\hat{p}\cdot\vec{\tau}\gamma_5\tilde{\Psi}^{(G,+)}_\alpha(\vec{p}) = 2\left(\tilde{g}^{(G,+;1)}_\alpha(p)\tilde{f}^{(G,+;1)}_\alpha(p) - \tilde{g}^{(G,+;2)}_\alpha(p)\tilde{f}^{(G,+;2)}_\alpha(p)\right) - 4\sqrt{G(G+1)}\left(\tilde{g}^{(G,+;1)}_\alpha(p)\tilde{f}^{(G,+;2)}_\alpha(p) + \tilde{g}^{(G,+;2)}_\alpha(p)\tilde{f}^{(G,+;1)}_\alpha(p)\right).$$

Table 6.5: Matrix elements $\int \mathrm{d}\Omega_p \mathcal{Y}_{L'J'GM}(\vec{p})\hat{p}\cdot\vec{\tau}\hat{p}\cdot\vec{\sigma}\mathcal{Y}_{LJGM}(\vec{p})$. Overall factor $\dfrac{1}{(2G+1)}$ needs to be multiplied.

$J'=G-\frac{1}{2}$		$J'=G+\frac{1}{2}$			
$L'=G-1$	$L'=G$	$L'=G$	$L'=G+1$		
1	0	0	$2\sqrt{G(G+1)}$	$L=G-1$	
					$J=G-\frac{1}{2}$
0	1	$2\sqrt{G(G+1)}$	0	$L=G$	
0	$2\sqrt{G(G+1)}$	-1	0	$L=G$	
					$J=G+\frac{1}{2}$
$2\sqrt{G(G+1)}$	0	0	-1	$L=G+1$	

Table 6.6: Matrix elements $\int \mathrm{d}\Omega_p \mathcal{Y}_{L'J'GM}(\vec{p})\vec{\tau}\cdot\vec{\sigma}\mathcal{Y}_{LJGM}(\vec{p})$. Overall factor $\dfrac{1}{(2G+1)}$ needs to be multiplied.

$J'=G-\frac{1}{2}$		$J'=G+\frac{1}{2}$			
$L'=G-1$	$L'=G$	$L'=G$	$L'=G+1$		
$2G+1$	0	0	0	$L=G-1$	
					$J=G-\frac{1}{2}$
0	$-(2G-1)$	$4\sqrt{G(G+1)}$	0	$L=G$	
0	$4\sqrt{G(G+1)}$	$-(2G+3)$	0	$L=G$	
					$J=G+\frac{1}{2}$
0	0	0	$2G+1$	$L=G+1$	

and for negative intrinsic parity we have

$$\int \mathrm{d}\Omega_p\, \tilde{\Psi}_\alpha^{\dagger(G,-)}(\vec{p})\hat{p}\cdot\vec{\tau}\gamma_5\tilde{\Psi}_\alpha^{(G,-)}(\vec{p}) = 2\left(\tilde{g}_\alpha^{(G,-;1)}(p)\tilde{f}_\alpha^{(G,-;1)}(p) - \tilde{g}_\alpha^{(G,-;2)}(p)\tilde{f}_\alpha^{(G,-;2)}(p)\right) + 4\sqrt{G(G+1)}\left(\tilde{g}_\alpha^{(G,-;1)}(p)\tilde{f}_\alpha^{(G,-;2)}(p) + \tilde{g}_\alpha^{(G,-;2)}(p)\tilde{f}_\alpha^{(G,-;1)}(p)\right).$$

Also the matrix element (6.2.5) is computed from the matrix elements from Table 6.5:

For positive intrinsic parity we have

$$\int \mathrm{d}\Omega_p\, \tilde{\Psi}_\alpha^{\dagger(G,+)}(\vec{p})\hat{p}\cdot\vec{\tau}\hat{p}\cdot\vec{\sigma}\tilde{\Psi}_\alpha^{(G,+)}(\vec{p}) = \left(-\tilde{g}_\alpha^{(G,+;1)}(p)^2 - \tilde{f}_\alpha^{(G,+;1)}(p)^2 + \tilde{g}_\alpha^{(G,+;2)}(p)^2 + \tilde{f}_\alpha^{(G,+;2)}(p)^2\right) + 4\sqrt{G(G+1)}\left(\tilde{g}_\alpha^{(G,+;1)}(p)\tilde{g}_\alpha^{(G,+;2)}(p) + \tilde{f}_\alpha^{(G,+;1)}(p)\tilde{f}_\alpha^{(G,+;2)}(p)\right).$$

and for negative intrinsic parity we have

$$\int \mathrm{d}\Omega_p\, \tilde{\Psi}_\alpha^{\dagger(G,-)}(\vec{p})\hat{p}\cdot\vec{\tau}\hat{p}\cdot\vec{\sigma}\tilde{\Psi}_\alpha^{(G,-)}(\vec{p}) = \left(-\tilde{g}_\alpha^{(G,-;1)}(p)^2 - \tilde{f}_\alpha^{(G,-;1)}(p)^2 + \tilde{g}_\alpha^{(G,-;2)}(p)^2 + \tilde{f}_\alpha^{(G,-;2)}(p)^2\right) - 4\sqrt{G(G+1)}\left(\tilde{g}_\alpha^{(G,-;1)}(p)\tilde{g}_\alpha^{(G,-;2)}(p) + \tilde{f}_\alpha^{(G,-;1)}(p)\tilde{f}_\alpha^{(G,-;2)}(p)\right).$$

Furthermore the matrix element (6.2.6) is computed from the matrix elements from Table 6.6: For positive intrinsic parity we have

$$\int \mathrm{d}\Omega_p\, \tilde{\Psi}^{\dagger(G,+)}_\alpha(\vec{p})\vec{\tau}\cdot\vec{\sigma}\tilde{\Psi}^{(G,+)}_\alpha(\vec{p}) = (2G+1)\left(\tilde{f}^{(G,+;1)}_\alpha(p)^2 + \tilde{f}^{(G,+;2)}_\alpha(p)^2\right) - (2G+3)\tilde{g}^{(G,+;1)}_\alpha(p)^2 + (2G-1)\tilde{g}^{(G,+;2)}_\alpha(p)^2 + 8\sqrt{G(G+1)}\tilde{g}^{(G,+;1)}_\alpha(p)\tilde{g}^{(G,+;2)}_\alpha(p).$$

and for negative intrinsic parity we have

$$\int \mathrm{d}\Omega_p\, \tilde{\Psi}^{\dagger(G,-)}_\alpha(\vec{p})\vec{\tau}\cdot\vec{\sigma}\tilde{\Psi}^{(G,-)}_\alpha(\vec{p}) = (2G+1)\left(\tilde{g}^{(G,-;1)}_\alpha(p)^2 + \tilde{g}^{(G,-;2)}_\alpha(p)^2\right) - (2G+3)\tilde{f}^{(G,-;1)}_\alpha(p)^2 - (2G-1)\tilde{f}^{(G,-;2)}_\alpha(p)^2 - 8\sqrt{G(G+1)}\tilde{f}^{(G,-;1)}_\alpha(p)\tilde{f}^{(G,-;2)}_\alpha(p).$$

Following the calculation of the valence contribution in section 6.1 the valence part of the longitudinal polarized structure function becomes

$$\begin{aligned}\left[\mathrm{g}_1^{I=1}(x)\right]_{\mathrm{v}} = \imath\frac{MN_c\pi}{72}\langle N|I_3|N\rangle \int\frac{\mathrm{d}\Omega_z}{4\pi}\int\frac{\mathrm{d}\omega}{2\pi}\int\frac{\mathrm{d}\lambda}{2\pi}e^{\imath Mx\lambda}\left(\frac{\omega+\epsilon_{\mathrm{v}}}{\omega^2-\epsilon_{\mathrm{v}}^2+\imath\epsilon}\right)_{\mathrm{p}} \\ \times\int \mathrm{d}^3\xi\left\{\Psi^\dagger_{\mathrm{v}}(\vec{\xi})\vec{\tau}\cdot\hat{z}(1-\vec{\alpha}\cdot\hat{z})\gamma_5\Psi_{\mathrm{v}}(\vec{\xi}+\lambda\hat{z})e^{-\imath\omega\lambda}\right. \\ \left. + \Psi^\dagger_{\mathrm{v}}(\vec{\xi})\vec{\tau}\cdot\hat{z}(1+\vec{\alpha}\cdot\hat{z})\gamma_5\Psi_{\mathrm{v}}(\vec{\xi}-\lambda\hat{z})e^{\imath\omega\lambda}\right\} \qquad (6.2.7)\end{aligned}$$

Repeating the calculations above and recalling that the valence quark carries positive parity we obtain the valence part of the longitudinal polarized structure function as

$$\begin{aligned}\left[\mathrm{g}_1^{I=1}(x)\right]^{\mp}_{\mathrm{v}} = \frac{MN_c}{36}\langle N|I_3|N\rangle\left\{\mp\int_{|Mx^\pm|}^\infty \mathrm{d}p\, Mx^\pm_{\mathrm{v}}\int\mathrm{d}\Omega_p\tilde{\Psi}^\dagger_{\mathrm{v}}(\vec{p})\hat{p}\cdot\vec{\tau}\gamma_5\tilde{\Psi}_{\mathrm{v}}(\vec{p})\right. \\ \left. -\int_{|Mx^\pm_{\mathrm{v}}|}^\infty \mathrm{d}p\, p^2\left[A_\pm\int\mathrm{d}\Omega_p\tilde{\Psi}^\dagger_{\mathrm{v}}(\vec{p})\vec{\tau}\cdot\vec{\sigma}\tilde{\Psi}_{\mathrm{v}}(\vec{p}) + B_\pm\int\mathrm{d}\Omega_p\tilde{\Psi}^\dagger_{\mathrm{v}}(\vec{p})\hat{p}\cdot\vec{\tau}\hat{p}\cdot\vec{\sigma}\tilde{\Psi}_{\mathrm{v}}(\vec{p})\right]\right\}. \qquad (6.2.8)\end{aligned}$$

In obtaining the above equation we have used the pole condition $f^\pm|_{\mathrm{pole}} = -4\imath\pi\delta(\omega\mp\epsilon_\alpha)$. Using the decomposition of the valence quark wavefunction in momentum (cf. equations (6.1.18)–(6.1.20)) space at leading order $\frac{1}{N_c}$ gives the valence part of the polarized structure function as

$$\left[\mathrm{g}_1^{I=1}(x)\right]^{\mp}_{\mathrm{v}} = \frac{MN_c}{36}\langle N|I_3|N\rangle\left[\mp\int_{|Mx^\pm_{\mathrm{v}}|}^\infty \mathrm{d}p\left\{2Mx^\pm_{\mathrm{v}}\tilde{g}_{\mathrm{v}}(p)\tilde{f}_{\mathrm{v}}(p) \pm p\left[\left(1-2\frac{(Mx^\pm_{\mathrm{v}})^2}{p^2}\right)\tilde{f}_{\mathrm{v}}(p)^2 - \tilde{g}_{\mathrm{v}}(p)^2\right]\right\}\right]. \qquad (6.2.9)$$

6.2.1 Bjorken Sum Rule

We conclude the discussion of $\mathrm{g}_1^{I=1}$ by verifying the Bjorken sum rule in our model, which relates the integrated isovector polarized structure function $\mathrm{g}_1^{I=1}$ to the axial charge, i.e the expectation value $\langle\gamma_3\gamma_5\tau_3\rangle$ [19, 24, 64]. Here we verify this sum rule for the explicit (regularized) expression

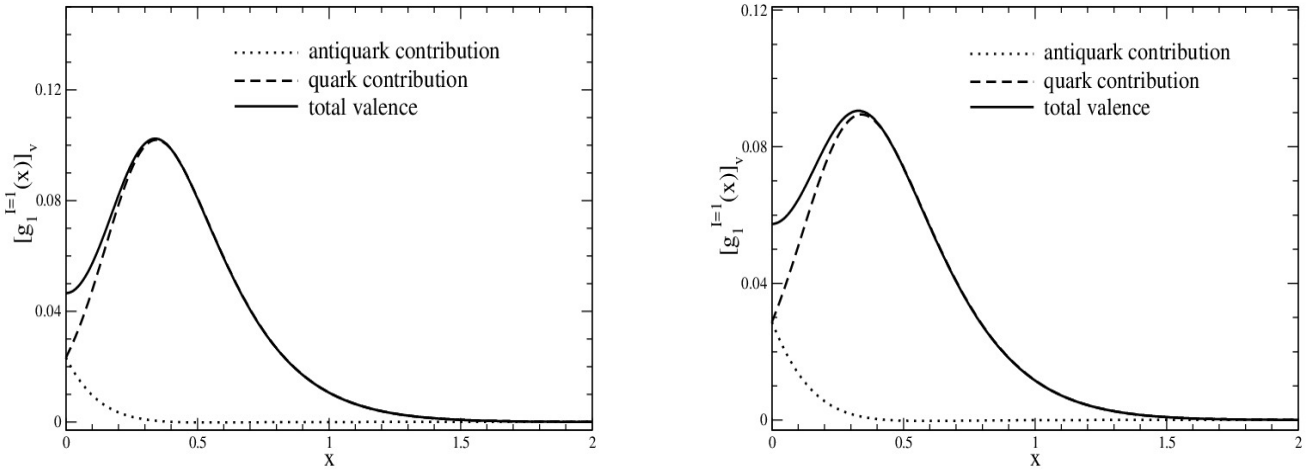

Figure 6.6: The numerical prediction for the valence part of the isovector polarized proton structure function. Left panel: The case for $m = 400\,\text{MeV}$. Right panel: The case for $m = 450\,\text{MeV}$.

for $\mathrm{g}_1^{I=1}$, equation (6.2.2) and first integrate the term with the operator $\hat{p}\cdot\vec{\tau}\gamma_5$ in the RF

$$\begin{aligned}
\int_0^\infty \mathrm{d}x\left[\mathrm{g}_1^{I=1}(x)\right]_{\mathrm{s}} &= -\frac{MN_cI_3}{72}\sum_\alpha\sum_{i=0}^{2}c_i\int_0^\infty \mathrm{d}x\left\{Mx^-\Big\langle\alpha|\hat{p}\cdot\vec{\tau}\gamma_5|\alpha\Big\rangle''_{|Mx^-|} - Mx^+\Big\langle\alpha|\hat{p}\cdot\vec{\tau}\gamma_5|\alpha\Big\rangle''_{|Mx^+|}\right\},\\
&= -\frac{MN_cI_3}{72}\sum_\alpha\sum_{i=0}^{2}c_i\left\{\int_{-\frac{\omega_0}{M}}^\infty \mathrm{d}y\,My\Big\langle\alpha|\hat{p}\cdot\vec{\tau}\gamma_5|\alpha\Big\rangle''_{|My|} - \int_{\frac{\omega_0}{M}}^\infty \mathrm{d}y\,My\Big\langle\alpha|\hat{p}\cdot\vec{\tau}\gamma_5|\alpha\Big\rangle''_{My}\right\},\\
&= -\frac{MN_cI_3}{72}\sum_\alpha\sum_{i=0}^{2}c_i\int_{-\frac{\omega_0}{M}}^{\frac{\omega_0}{M}}\mathrm{d}y\,My\Big\langle\alpha|\hat{p}\cdot\vec{\tau}\gamma_5|\alpha\Big\rangle''_{|My|} = 0, \qquad (6.2.10)
\end{aligned}$$

where we took advantage of the final integral being over a symmetric interval. For the contribution from the Dirac operator without γ_5 we get[5]

$$\begin{aligned}
\int_0^\infty \mathrm{d}x\,[\mathrm{g}_1^{I=1}(x)]_{\mathrm{s}} &= \frac{MN_cI_3}{72}\sum_\alpha\sum_{i=0}^{2}c_i\frac{\epsilon_\alpha}{\omega_0}\int_0^\infty \mathrm{d}x\left\{\left[A_+\Big\langle\alpha|\vec{\tau}\cdot\vec{\sigma}|\alpha\Big\rangle_{|Mx^+|} + B_+\Big\langle\alpha|\hat{p}\cdot\vec{\tau}\hat{p}\cdot\vec{\sigma}|\alpha\Big\rangle_{|Mx^+|}\right]\right.\\
&\quad\left.+\left[A_-\Big\langle\alpha|\vec{\tau}\cdot\vec{\sigma}|\alpha\Big\rangle_{|Mx^-|} + B_-\Big\langle\alpha|\hat{p}\cdot\vec{\tau}\hat{p}\cdot\vec{\sigma}|\alpha\Big\rangle_{|Mx^-|}\right]\right\},\\
&= \frac{MN_cI_3}{72}\sum_\alpha\sum_{i=0}^{2}c_i\frac{\epsilon_\alpha}{\omega_0}\left\{\int_{\frac{\omega_0}{M}}^\infty \mathrm{d}y\left[\Big\langle\alpha|\vec{\tau}\cdot\vec{\sigma}|\alpha\Big\rangle_{My}A_y + \Big\langle\alpha|\hat{p}\cdot\vec{\tau}\hat{p}\cdot\vec{\sigma}|\alpha\Big\rangle_{My}B_y\right]\right.\\
&\quad\left.+\int_{-\frac{\omega_0}{M}}^\infty \mathrm{d}y\left[\Big\langle\alpha|\vec{\tau}\cdot\vec{\sigma}|\alpha\Big\rangle_{|My|}A_y + \Big\langle\alpha|\hat{p}\cdot\vec{\tau}\hat{p}\cdot\vec{\sigma}|\alpha\Big\rangle_{|My|}B_y\right]\right\},\\
&= \frac{N_cI_3}{108}\sum_{i=0}^{2}c_i\frac{\epsilon_\alpha}{\omega_0}\Big\langle\alpha|\vec{\tau}\cdot\vec{\sigma}|\alpha\Big\rangle_0, \qquad (6.2.11)
\end{aligned}$$

where $A_y = \dfrac{1}{2p}\left(1-\dfrac{(My)^2}{p^2}\right)$ and $B_y = \dfrac{1}{2p}\left(3\dfrac{(My)^2}{p^2}-1\right)$. The term with $\hat{p}\cdot\vec{\tau}\hat{p}\cdot\vec{\sigma}$ disappeared

[5]Here we use the notation $\Big\langle\alpha|\vec{\tau}\cdot\vec{\sigma}|\alpha\Big\rangle_a = \displaystyle\int_a^\infty \mathrm{d}p\,p^2\int \mathrm{d}\Omega_p\tilde{\Psi}^\dagger_\alpha(\vec{p})\vec{\tau}\cdot\vec{\sigma}\tilde{\Psi}_\alpha(\vec{p})$.

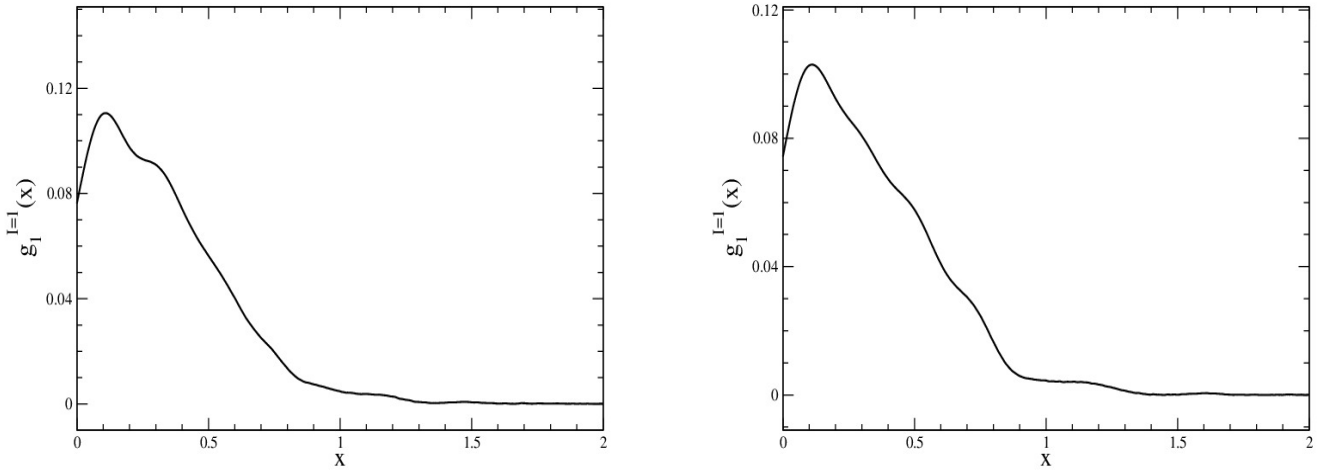

Figure 6.7: The sum of the vacuum and valence contribution to the isovector polarized proton structure function. Left panel: The case for $m = 400\,\mathrm{MeV}$. Right panel: The case for $m = 450\,\mathrm{MeV}$.

because

$$\int_0^\infty \mathrm{d}y\, B_y \int_{My}^\infty p^2 \mathrm{d}p \int \mathrm{d}\Omega_p \tilde{\Psi}_\alpha^\dagger(\vec{p})\hat{p}\cdot\vec{\tau}\hat{p}\cdot\vec{\sigma}\tilde{\Psi}_\alpha(\vec{p}) = -\int_0^\infty \mathrm{d}y \left(\frac{M^2y^3}{2p^2} - \frac{y}{2}\right)\frac{\partial}{\partial y}\int_{My}^\infty p\mathrm{d}p \int \mathrm{d}\Omega_p \tilde{\Psi}_\alpha^\dagger(\vec{p})\hat{p}\cdot\vec{\tau}\hat{p}\cdot\vec{\sigma}\tilde{\Psi}_\alpha(\vec{p})$$
$$= \int_0^\infty \mathrm{d}y \left(\frac{M^3y^3}{2p^2} - \frac{My}{2}\right)\left[p\int \mathrm{d}\Omega_p \tilde{\Psi}_\alpha^\dagger(\vec{p})\hat{p}\cdot\vec{\tau}\hat{p}\cdot\vec{\sigma}\tilde{\Psi}_\alpha(\vec{p})\right]_{p=My} = 0. \tag{6.2.12}$$

Hence the Bjorken sum rule for the vacuum contribution of the longitudinal polarized structure function becomes

$$\int \mathrm{d}x \left[\mathrm{g}_1^p(x) - \mathrm{g}_1^n(x)\right]_\mathrm{s} = \frac{N_c}{108}\sum_{i=0}^{2} c_i \frac{\epsilon_\alpha}{\omega_0}\Big\langle \alpha|\vec{\tau}\cdot\vec{\sigma}|\alpha\Big\rangle_0 = \frac{1}{6}\left[g_A\right]_\mathrm{s}, \tag{6.2.13}$$

where, by substituting $\omega_0 = \sqrt{\epsilon_\alpha^2 + \Lambda_i^2}$

$$\left[g_A\right]_\mathrm{s} = \frac{N_c}{18}\sum_\alpha\sum_{i=0}^{2} c_i \frac{\epsilon_\alpha}{\sqrt{\epsilon_\alpha^2 + \Lambda_i^2}}\langle\alpha|\gamma_3\gamma_5\tau_3|\alpha\rangle \tag{6.2.14}$$

is the vacuum contribution to the axial charge [24]. Similar calculations from equation (6.2.9) give the valence contribution as

$$\int \mathrm{d}x \left[\mathrm{g}_1^p(x) - \mathrm{g}_1^n(x)\right]_\mathrm{v} = -\frac{N_c}{54}\eta_\mathrm{v}\Big\langle \mathrm{v}|\vec{\tau}\cdot\vec{\sigma}|\mathrm{v}\Big\rangle_0 = \frac{1}{6}\left[g_A\right]_\mathrm{v}, \tag{6.2.15}$$

with

$$\left[g_A\right]_\mathrm{v} = -\frac{N_c}{9}\eta_\mathrm{v}\langle\mathrm{v}|\gamma_3\gamma_5\tau_3|\mathrm{v}\rangle. \tag{6.2.16}$$

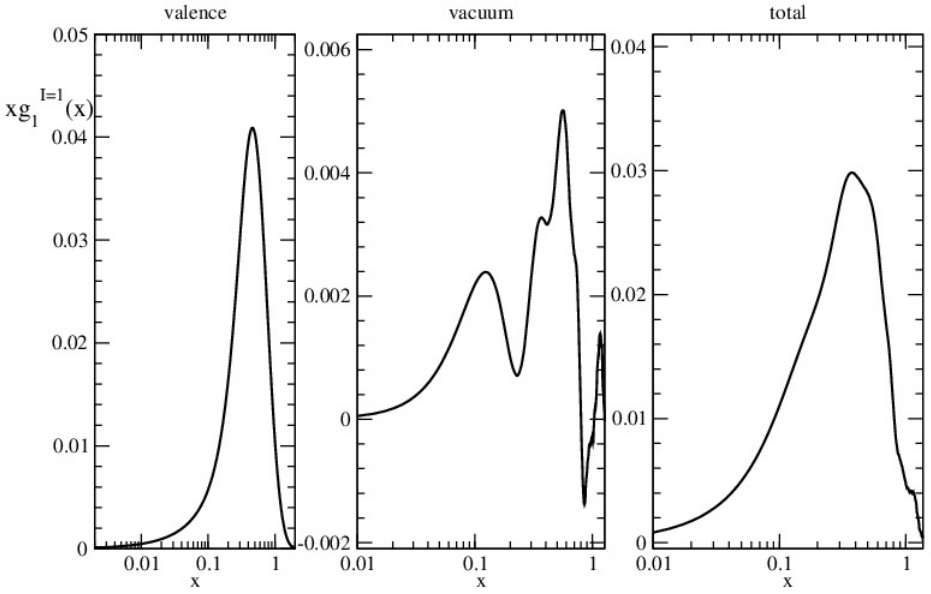

Figure 6.8: The model predictions for the longitudinal isovector proton polarized structure function, $x\mathrm{g}_1^{I=1}$ for $m = 400\,\mathrm{MeV}$.

m	$6\int \mathrm{d}x\,[\mathrm{g}_1^p - \mathrm{g}_1^n]_{\mathrm{v}}$	$[g_A]_{\mathrm{v}}$	$6\int \mathrm{d}x\,[\mathrm{g}_1^p - \mathrm{g}_1^n]_{\mathrm{s}}$	$[g_A]_{\mathrm{s}}$
400	0.734	0.731	0.0648	0.0637
450	0.715	0.715	0.0509	0.0496
500	0.704	0.704	0.0289	0.0293

Table 6.7: Verification of the Bjorken sum rule of our calculations cf. equation (6.2.11) to those of $g_A \sim \langle\gamma_3\gamma_5\tau_3\rangle$ cf. equation (6.2.17) for different constituent quark masses m (in MeV).

This indeed verifies the Bjorken sum rule with the total axial charge

$$g_A = -\frac{N_c}{3}\left[\frac{1}{3}\eta_{\mathrm{v}}\langle \mathrm{v}|\gamma_3\gamma_5\tau_3|\mathrm{v}\rangle - \frac{1}{6}\sum_{\alpha}\sum_{i=0}^{2} c_i \frac{\epsilon_\alpha}{\sqrt{\epsilon_\alpha^2 + \Lambda_i^2}}\langle\alpha|\gamma_3\gamma_5\tau_3|\alpha\rangle\right]. \tag{6.2.17}$$

Notice the difference between $\int \mathrm{d}x\,\mathrm{g}_1(x)$ and g_A, while the former depend on momentum coordinates the later involves integrals of the radial coordinate. The numerical verification of the Bjorken sum rule is depicted in Table 6.7 and reflects the accuracy of the numerical simulation for evaluating the structure functions. In this case the sum rule is saturated level by level of the α-sum. In Table 6.8 we compare our theoretical prediction of the axial charge for various constituent quark mass to that of the experimental value and we observe that it is under estimated by about 40%. This is a well known problem in chiral soliton models. There have been speculations that certain $\dfrac{1}{N_c}$ corrections might remedy the problem [65]; yet these are not necessarily consistent with the underlying symmetries such as PCAC [66]. Neither do they show up in the present calculation.

m	$6\int \mathrm{d}x\,[\mathrm{g}_1^p - \mathrm{g}_1^n]_{\mathrm{v}}$	$6\int \mathrm{d}x\,[\mathrm{g}_1^p - \mathrm{g}_1^n]_{\mathrm{s}}$	$6\int \mathrm{d}x\,[\mathrm{g}_1^p - \mathrm{g}_1^n]$	experimental value
400	0.734	0.0648	0.799	
450	0.715	0.0509	0.766	1.2601 ± 0.0025 [67]
500	0.704	0.0289	0.733	

Table 6.8: Comparison of the calculated axial charge of the nucleon for different constituent quark masses m (in MeV) to the experimental value.

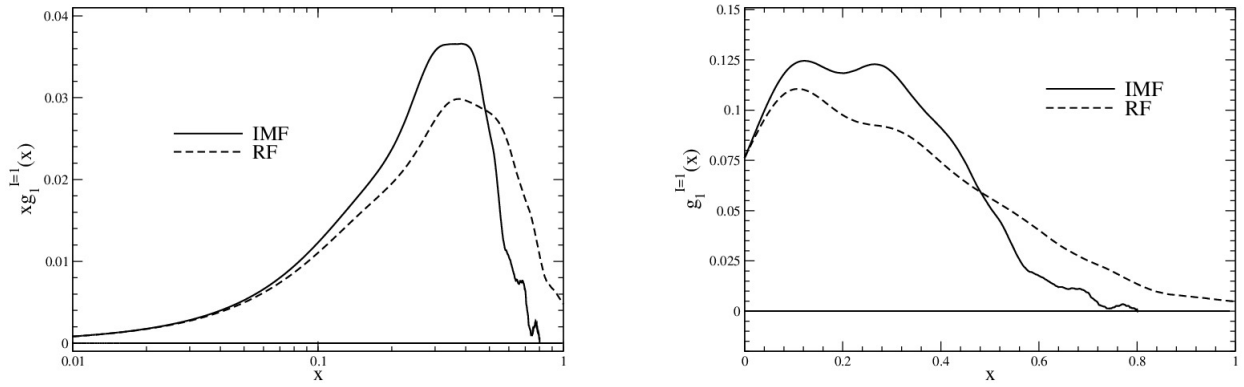

(a) (b)

Figure 6.9: (a) The sum of the valence and vacuum contributions for the longitudinal isovector proton polarized structure function, $x\mathrm{g}_1^{I=1}$, for $m = 400\,\mathrm{MeV}$ and (b) the sum of valence and vacuum contributions for the longitudinal iso-vector proton polarized structure function, $\mathrm{g}_1^{I=1}$, for $m = 400\,\mathrm{MeV}$. In both cases the curves labeled "RF" denote the results obtained from the nucleon rest frame and those labeled "IMF" denote the projection to the infinite momentum frame. Note that the horizontal coordinate of $x\mathrm{g}_1^{I=1}$ is on a logarithmic scale.

6.2.2 Discussion of the Numerical Results for the Isovector Longitudinal Polarized Structure Function

The results in Figures 6.5 and Figure 6.6 show that the valence contribution of the longitudinal polarized proton structure function dominates over those from the vacuum. We thus confirm the assumption underlying the approximation made in Ref.[47]. In other words, the vacuum is only moderately polarized.

While the valence contribution of the polarized proton structure function has a pronounced maximum around $x \sim 0.3$ [47] the vacuum contribution is pronounced around $x \sim 0.2$, which changes slightly as the constituent quark mass increases because the vacuum polarization slightly increases with the constituent quark mass. The vacuum contribution being pronounced at smaller x than the valence counterpart is consistent with the parton model picture that associates the vacuum with the sea of quark partons. We note, however, that the oscillatory behavior of the vacuum piece is not expected. Yet, the amplitude of that oscillation is small when compared to the maximum of the valence piece.

We also show the theoretical predictions for the sum of the vacuum and valence contribution

of the polarized proton structure function in Figure 6.7 and as well as the polarized proton structure function, $x\mathrm{g}_1^{I=1}$ in Figure 6.8. From the above numerical results, we notice that our solutions have non-zero support for $x > 1$. This effect is due to the fact that we are considering heavy nucleons in the large N_c limit and also because the meson field configuration is localized (non-relativistic). It must be emphasized that the non-zero local support of the numerical solutions for $x > 1$ contributes only about $(0.2-0.4)\%$ to axial charge of the nucleon. To restore the Lorentz covariance, we make use of equation (6.1.25). Obviously the (small) oscillations at large-x are mapped into the region just below $x = 1$. In Figure 6.9 we present the effects of this transformation on our predictions.

6.3 Numerical Calculations of the Transverse Polarized Structure Function

Similarly to the previous calculation we get the isovector component of the transverse polarized structure function. We first list the vacuum contribution (after substituting the Fourier transformation in momentum space)

$$\begin{aligned}\left[\mathrm{g}_T^{I=1}(x)\right]_{\mathrm{s}} = -\imath\frac{MN_c\pi}{144}\langle N|I_3|N\rangle\int\frac{\mathrm{d}\Omega_z}{4\pi}\int\frac{\mathrm{d}\omega}{2\pi}\sum_\alpha\int\frac{\mathrm{d}\lambda}{2\pi}\left(\sum_{i=0}^{2}c_i\frac{\omega+\epsilon_\alpha}{\omega^2-\epsilon_\alpha^2-\Lambda_i^2+\imath\epsilon}\right)_{\mathrm{p}}\\ \times\int\mathrm{d}^3p\int\mathrm{d}^3k\int\mathrm{d}^3\xi\left[\tilde{\Psi}_\alpha^\dagger(\vec{p})\left(\vec{\tau}\cdot\vec{\alpha}-(\vec{\tau}\cdot\hat{z})(\vec{\alpha}\cdot\hat{z})\right)\gamma_5\tilde{\Psi}_\alpha(\vec{k})e^{\imath\vec{\xi}\cdot(\vec{p}-\vec{k})}e^{\imath\lambda\left(Mx-\hat{z}\cdot\vec{k}\right)}e^{-\imath\omega\lambda}\right.\\ \left.+\,\tilde{\Psi}_\alpha^\dagger(\vec{p})\left(\vec{\tau}\cdot\vec{\alpha}-(\vec{\tau}\cdot\hat{z})(\vec{\alpha}\cdot\hat{z})\right)\gamma_5\tilde{\Psi}_\alpha(\vec{k})e^{\imath\vec{\xi}\cdot(\vec{p}-\vec{k})}e^{\imath\lambda\left(Mx+\hat{z}\cdot\vec{k}\right)}e^{\imath\omega\lambda}\right].\end{aligned}\tag{6.3.1}$$

Like before, using the identities in equations (6.1.4)– (6.1.5), writing the integration variable into spherical coordinate cf. (6.1.6) and averaging the photon direction gives

$$\begin{aligned}\left[\mathrm{g}_T^{I=1}(x)\right]_{\mathrm{s}}^{\mp} = \frac{MN_c}{144}\langle N|I_3|N\rangle\sum_\alpha\sum_{i=0}^{2}c_i\left\{\frac{\epsilon_\alpha}{\omega_0}\int_{|Mx_\alpha^\pm|}^{\infty}\mathrm{d}p\,p\int\mathrm{d}\Omega_p\tilde{\Psi}_\alpha^\dagger(\vec{p})\vec{\tau}\cdot\vec{\sigma}\tilde{\Psi}_\alpha(\vec{p})\right.\\ \left.-\frac{\epsilon_\alpha}{\omega_0}\int_{|Mx_\alpha^\pm|}^{\infty}\mathrm{d}p\,p^2\left[A_\pm\int\mathrm{d}\Omega_p\tilde{\Psi}_\alpha^\dagger(\vec{p})\vec{\tau}\cdot\vec{\sigma}\tilde{\Psi}_\alpha(\vec{p})+B_\pm\int\mathrm{d}\Omega_p\tilde{\Psi}_\alpha^\dagger(\vec{p})\hat{p}\cdot\vec{\tau}\hat{p}\cdot\vec{\sigma}\tilde{\Psi}_\alpha(\vec{p})\right]\right\},\end{aligned}\tag{6.3.2}$$

where the definitions of equation (6.2.3) have again been substituted. As before, $\left[\mathrm{g}_T^{I=1}(x)\right]_{\mathrm{s}}^{-}$ denotes the antiquark distribution and $\left[\mathrm{g}_T^{I=1}(x)\right]_{\mathrm{s}}^{+}$ denotes the quark distribution. They sum to total isovector transverse polarized structure function. The vacuum contribution is computed by using the single cut-off adopted from the Pauli-Villar's regularization. The valence quark approximation to the transverse polarized structure becomes

$$\begin{aligned}\left[\mathrm{g}_T^{I=1}(x)\right]_{\mathrm{v}} = -\imath\frac{MN_c\pi}{144}\langle N|I_3|N\rangle\int\frac{\mathrm{d}\Omega_z}{4\pi}\int\frac{\mathrm{d}\omega}{2\pi}\int\frac{\mathrm{d}\lambda}{2\pi}e^{\imath Mx\lambda}\left(\frac{\omega+\epsilon_{\mathrm{v}}}{\omega^2-\epsilon_{\mathrm{v}}^2+\imath\epsilon}\right)_{\mathrm{p}}\\ \times\int\mathrm{d}^3\xi\left\{\psi_{\mathrm{v}}^\dagger(\vec{\xi})\left(\vec{\tau}\cdot\vec{\alpha}-(\vec{\tau}\cdot\hat{z})(\vec{\alpha}\cdot\hat{z})\right)\gamma_5\psi_{\mathrm{v}}(\vec{\xi}+\lambda\hat{z})e^{-\imath\omega\lambda}\right.\\ \left.+\,\psi_{\mathrm{v}}^\dagger(\vec{\xi})\left(\vec{\tau}\cdot\vec{\alpha}-(\vec{\tau}\cdot\hat{z})(\vec{\alpha}\cdot\hat{z})\right)\gamma_5\psi_{\mathrm{v}}(\vec{\xi}-\lambda\hat{z})e^{\imath\omega\lambda}\right\}.\end{aligned}$$

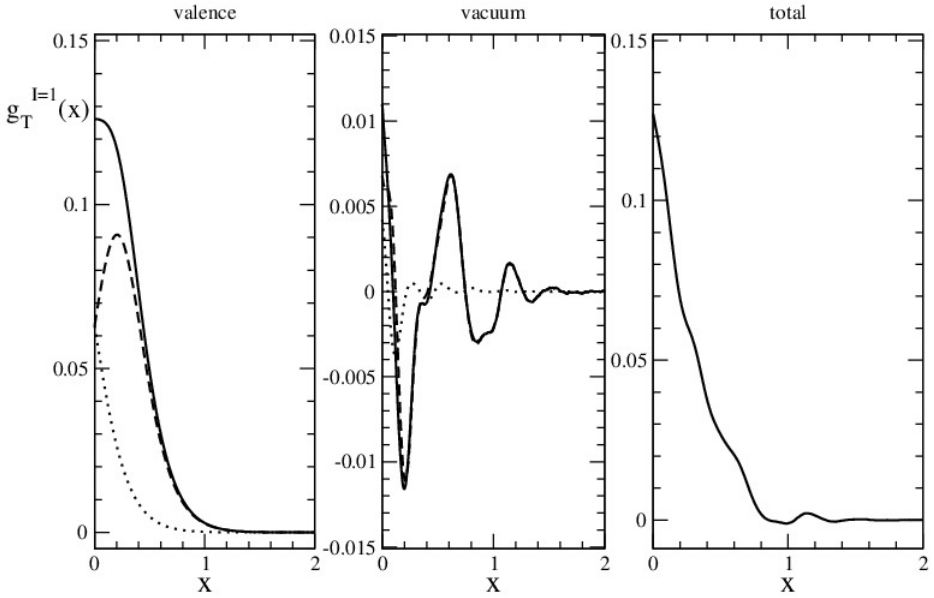

Figure 6.10: The model predictions for the transverse isovector polarized proton structure function for $m = 450\,\text{MeV}$. The dotted lines for the valence and vacuum contributions denotes the anti-quark distributions, the dashed lines denotes the quark distributions and the solid lines denotes the sum of quark and anti-quark distribution, respectively.

Repeating the above calculations and noting that $\left(\frac{\omega+\epsilon_{\text{v}}}{\omega^2-\epsilon_{\text{v}}^2+\imath\epsilon}\right)_p = -\imath\pi\delta\left(\omega-\epsilon_{\text{v}}\right)$ gives

$$\left[\text{g}_T^{I=1}(x)\right]_{\text{v}}^{\mp} = \frac{MN_c}{72}\langle N|I_3|N\rangle\left\{\int_{|Mx_{\text{v}}^{\pm}|}^{\infty}\text{d}p\,p\int\text{d}\Omega_p\tilde{\Psi}_{\text{v}}^{\dagger}(\vec{p})\vec{\tau}\cdot\vec{\sigma}\tilde{\Psi}_{\text{v}}(\vec{p})\right.$$
$$\left.-\int_{|Mx_{\text{v}}^{\pm}|}^{\infty}\text{d}p\,p^2\left[A_{\pm}\int\text{d}\Omega_p\tilde{\Psi}_{\text{v}}^{\dagger}(\vec{p})\vec{\tau}\cdot\vec{\sigma}\tilde{\Psi}_{\text{v}}(\vec{p})+B_{\pm}\int\text{d}\Omega_p\tilde{\Psi}_{\text{v}}^{\dagger}(\vec{p})\hat{p}\cdot\vec{\tau}\hat{p}\cdot\vec{\sigma}\tilde{\Psi}_{\text{v}}(\vec{p})\right]\right\}. \tag{6.3.3}$$

Using the decomposition of equations (6.1.19) and (6.1.20) produces the final result for the valence contribution as

$$\left[\text{g}_T^{I=1}(x)\right]_{\text{v}}^{\mp} = \frac{MN_c}{72}\langle N|I_3|N\rangle\int_{|Mx_{\text{v}}^{\pm}|}^{\infty}\text{d}p\,p\left[\tilde{g}_{\text{v}}(p)^2-\frac{(Mx_{\text{v}}^{\pm})^2}{p^2}\tilde{f}_{\text{v}}(p)^2\right]. \tag{6.3.4}$$

Note that the $\vec{\sigma}$ matrix that appears in the structure functions is a two-by-two component matrix that comes from the definition of the Dirac matrix

$$\vec{\sigma} = \vec{\alpha}\gamma_5 = (\vec{\sigma}\gamma_5)\gamma_5 = \begin{pmatrix}\vec{\sigma} & \mathbf{0}\\ \mathbf{0} & \vec{\sigma}\end{pmatrix}, \tag{6.3.5}$$

where $\mathbf{0}$ is a 2×2 zero matrix (see Appendix A.2).

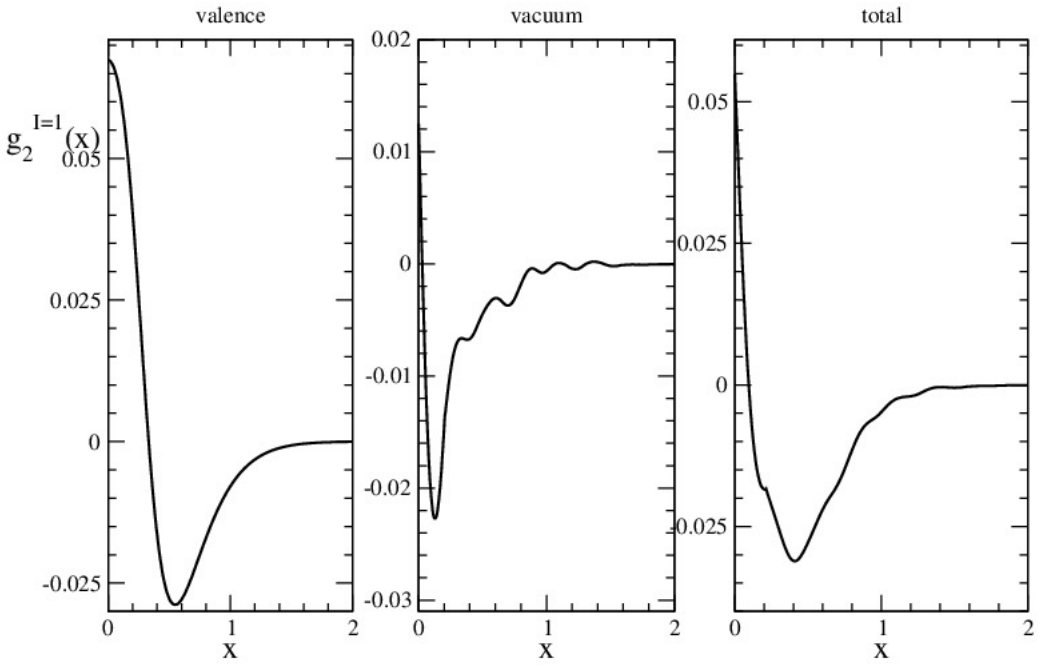

Figure 6.11: The model predictions for the isovector polarized proton structure function, $g_2^{I=1}(x)$, for $m = 400\,\text{MeV}$.

6.3.1 Numerical Results for the Isovector Transverse Polarized Structure Function

In this subsection, we discuss the numerical simulations for the iso-vector transverse polarized proton structure function as well as the iso-vector polarized proton structure function $g_2^{I=1}(x)$. In Figure 6.10 we show predictions for the transverse polarized proton spin structure function. It is worth noting that we observe regions in x-space where the vacuum contributions for $g_T^{I=1}(x)$ is negative. However, this has only a moderate effect on the total $g_T^{I=1}(x)$ which is dominated by the valence contribution. Also, again in consistency with the parton model picture, up to some small oscillations, the vacuum part vanishes more quickly than the valence part as x increases. In what follows, we extract the polarized structure function $g_2^{I=1}(x)$ from $g_T^{I=1}(x)$ [68]

$$g_2^{I=1}(x) = g_T^{I=1}(x) - g_1^{I=1}(x) \tag{6.3.6}$$

by subtracting $g_1^{I=1}(x)$ from it. Though we can obtain this difference directly from the above results it is illuminating to write it explicitly in order to study the respective sum rule. This gives the vacuum contribution as

$$\begin{aligned}\left[g_2^{I=1}(x)\right]_{\text{s}}^{\mp} = \frac{MN_c}{144}\langle N|I_3|N\rangle \sum_{\alpha}\sum_{i=0}^{2} c_i \Bigg\{ \pm 2 \int_{|Mx_\alpha^{\pm}|}^{\infty} \mathrm{d}p\, Mx_\alpha^{\pm} \int \mathrm{d}\Omega_p \tilde{\Psi}_\alpha^{\dagger}(\vec{p})\hat{p}\cdot\vec{\tau}\gamma_5\tilde{\Psi}_\alpha(\vec{p}) \\ + \frac{\epsilon_\alpha}{\omega_0}\int_{|Mx_\alpha^{\pm}|}^{\infty}\mathrm{d}p\, p^2\left[-B_\pm \int \mathrm{d}\Omega_p \tilde{\Psi}_\alpha^{\dagger}(\vec{p})\vec{\tau}\cdot\vec{\sigma}\tilde{\Psi}_\alpha(\vec{p}) + 3B_\pm \int \mathrm{d}\Omega_p \tilde{\Psi}_\alpha^{\dagger}(\vec{p})\hat{p}\cdot\vec{\tau}\hat{p}\cdot\vec{\sigma}\tilde{\Psi}_\alpha(\vec{p})\right]\Bigg\}.\end{aligned} \tag{6.3.7}$$

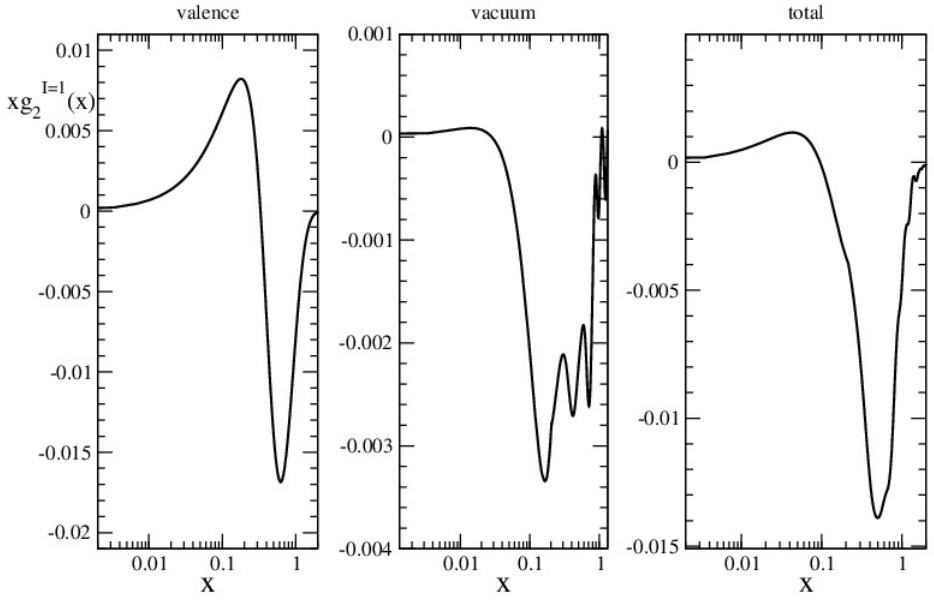

Figure 6.12: The model predictions for the isovector polarized proton structure function, $x\mathrm{g}_2^{I=1}(x)$, for $m = 400\,\mathrm{MeV}$.

After subtracting equation (6.2.9) from (6.3.4) the valence contribution reads

$$\left[\mathrm{g}_2^{I=1}(x)\right]_{\mathrm{v}}^{\mp} = \frac{MN_c}{72}\langle N|I_3|N\rangle \int_{|Mx_{\mathrm{v}}^{\pm}|}^{\infty} \mathrm{d}p \left[\pm 2Mx_{\mathrm{v}}^{\pm}\tilde{g}_{\mathrm{v}}(p)\tilde{f}_{\mathrm{v}}(p) + B_{\pm}\tilde{f}_{\mathrm{v}}(p)^2\right]. \tag{6.3.8}$$

In the next step, we verify analytically the Burkhardt-Cottingham sum rule[69]. The contribution from the operator $\hat{p}\cdot\vec{\tau}\gamma_5$ has already been discussed in equation (6.2.10). For the contribution from the Dirac operator without the explicit γ_5 we get

$$\begin{aligned}
\int_0^{\infty} \mathrm{d}x \left[\mathrm{g}_2^{I=1}(x)\right]_{\mathrm{s}} &= \frac{MN_cI_3}{144}\sum_{\alpha}\sum_{i=0}^{2} c_i\frac{\epsilon_\alpha}{\omega_0}\int_0^{\infty}\mathrm{d}x\left\{\left[-B_+\left\langle\alpha|\vec{\tau}\cdot\vec{\sigma}|\alpha\right\rangle_{|Mx^+|} + 3B_+\left\langle\alpha|\hat{p}\cdot\vec{\tau}\hat{p}\cdot\vec{\sigma}|\alpha\right\rangle_{|Mx^+|}\right]\right. \\
&\quad \left. + \left[-B_-\left\langle\alpha|\vec{\tau}\cdot\vec{\sigma}|\alpha\right\rangle_{|Mx^-|} + 3B_-\left\langle\alpha|\hat{p}\cdot\vec{\tau}\hat{p}\cdot\vec{\sigma}|\alpha\right\rangle_{|Mx^-|}\right]\right\}, \\
&= \frac{MN_cI_3}{144}\sum_{\alpha}\sum_{i=0}^{2} c_i\frac{\epsilon_\alpha}{\omega_0}\left\{\int_{\frac{\omega_0}{M}}^{\infty}\mathrm{d}y\left[-B_y\left\langle\alpha|\vec{\tau}\cdot\vec{\sigma}|\alpha\right\rangle_{My} + 3B_y\left\langle\alpha|\hat{p}\cdot\vec{\tau}\hat{p}\cdot\vec{\sigma}|\alpha\right\rangle_{My}\right]\right. \\
&\quad \left. + \int_{-\frac{\omega_0}{M}}^{\infty}\mathrm{d}y\left[-B_y\left\langle\alpha|\vec{\tau}\cdot\vec{\sigma}|\alpha\right\rangle_{|My|} + 3B_y\left\langle\alpha|\hat{p}\cdot\vec{\tau}\hat{p}\cdot\vec{\sigma}|\alpha\right\rangle_{|My|}\right]\right\} = 0.
\end{aligned} \tag{6.3.9}$$

In the last line we made use of the identity in equation (6.2.12). Thus, we have the Burkhardt-Cottingham sum rule for the vacuum contribution to the longitudinal polarized structure function as

$$[\Gamma_2^p - \Gamma_2^n]_{\mathrm{s}} = \int_0^{\infty}\mathrm{d}x\ [\mathrm{g}_2^p(x) - \mathrm{g}_2^n(x)]_{\mathrm{s}} = 0. \tag{6.3.10}$$

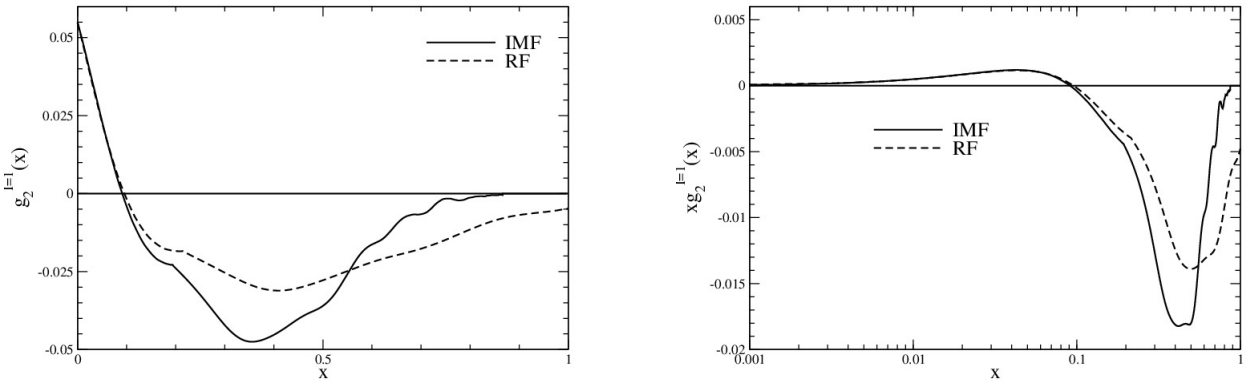

(a) (b)

Figure 6.13: The sum of valence and vacuum contributions for the isovector proton polarized structure function, $x\mathrm{g}_2^{I=1}$ and $\mathrm{g}_2^{I=1}(x)$ for $m = 400\,\mathrm{MeV}$. In both cases the curves labeled "RF" denote the results obtained from the nucleon rest frame and those labeled "IMF" denotes the projection to the infinite momentum frame. Note that the horizontal coordinate of $x\mathrm{g}_2^{I=1}$ is on a the logarithmic scale.

m	$[\Gamma_2^p - \Gamma_2^n]_{\mathrm{v}}$	$[\Gamma_2^p - \Gamma_2^n]_{\mathrm{s}}$	$\Gamma_2^p - \Gamma_2^n$
400	-6.00×10^{-9}	-2.71×10^{-4}	-2.71×10^{-4}
450	-8.00×10^{-8}	-4.84×10^{-5}	-4.84×10^{-5}
500	-2.20×10^{-8}	9.02×10^{-5}	9.02×10^{-5}

Table 6.9: Numerical verification of the Burkhardt-Cottingham sum rule for different constituent quark masses m (in MeV).

Similarly, we have the valence contribution as

$$[\Gamma_2^p - \Gamma_2^n]_{\mathrm{v}} = \int_0^\infty \mathrm{d}x\ [\mathrm{g}_2^p(x) - \mathrm{g}_2^n(x)]_{\mathrm{v}} = 0. \tag{6.3.11}$$

The numerical verification of this sum rule is shown in Table 6.9. Shown in Figure 6.11 and 6.12 are the theoretical predictions for the polarized proton spin-structure functions $\mathrm{g}_2^{I=1}(x)$ and $x\mathrm{g}_2^{I=1}(x)$ for the constituent quark mass, $m = 400\,\mathrm{MeV}$. In both figures, we display the valence and vacuum contributions as well as their sums. In addition to the direct model prediction (i.e RF results) we also display the kinematical corrections resulting from the transformation to the IMF in Figure 6.13. By construction it limits the support to $0 \leq x \leq 1$ and shifts the structure function towards lower x.

Chapter 7

Calculations and Numerical Results for the $\frac{1}{N_c}$ Corrections to the Structure Functions

In this chapter we compute the $\frac{1}{N_c}$ corrections to the polarized and the unpolarized structure functions, that stem from the sub-leading order (Ω_1) contribution of the hadronic tensor. They are extracted from the symmetric equation (5.2.36) and antisymmetric equation (5.2.37) using the projection operators in Table 6.1.

First, we consider the product $\vec{\Omega}\cdot\vec{\tau}\mathcal{Q}_A^2$ that appear in these formulas. Assuming symmetric ordering of this product and using equations (4.4.23) and (6.0.1) we have, when sandwiched between nucleon states

$$\frac{1}{2}\Big\{J_i,\mathcal{Q}_A^2\Big\}=\frac{1}{18}\left(5J_i-I_3\tau_i\right). \tag{7.0.1}$$

In the second step, we contract the symmetric piece (5.2.36) with the projection operator F_1 from Table 6.1. Using the grand-spin rotational invariance and parity properties, we find that only the isovector part of the rotated quark charge matrix i.e $\mathcal{Q}_A^2\sim\frac{1}{6}D_{3i}\tau_i$, contributes to the $\frac{1}{N_c}$ corrections for the unpolarized structure function. Formally we can write these contributions as

$$\begin{aligned}&\frac{1}{6}\langle\alpha|\vec{\Omega}\cdot\vec{\tau}|\beta\rangle\Psi_\beta^\dagger(\vec{\xi})D_{3i}\tau_i\Psi_\alpha(\vec{\xi}\pm\lambda\hat{e}_3)=\frac{1}{6\alpha^2}J_jD_{3i}\langle\alpha|\tau_j|\beta\rangle\Psi_\beta^\dagger(\vec{\xi})\tau_i\Psi_\alpha(\vec{\xi}\pm\lambda\hat{e}_3),\\&=-\frac{I_3}{18\alpha^2}\Big\{2\langle\alpha|\tau_1|\beta\rangle\Psi_\beta^\dagger(\vec{\xi})\tau_1\Psi_\alpha(\vec{\xi}\pm\lambda\hat{e}_3)+\langle\alpha|\tau_3|\beta\rangle\Psi_\beta^\dagger(\vec{\xi})\tau_3\Psi_\alpha(\vec{\xi}\pm\lambda\hat{e}_3)\Big\}.\end{aligned}$$

We then obtain the isovector unpolarized structure function after generalizing the photon di-

rection '$\hat{e}_3$' to an arbitrary unit spherical direction $\hat{z}$ over which we average

$$\begin{aligned} F_1^{I=1}(x) = \imath\frac{MN_c\pi}{72\alpha^2}I_3\int\frac{\mathrm{d}\Omega_z}{4\pi}\int\frac{\mathrm{d}\omega}{2\pi}\sum_\alpha\int\frac{\mathrm{d}\lambda}{2\pi}e^{\imath Mx\lambda}\int\mathrm{d}^3\xi\Bigg\{\left(\frac{\omega+\epsilon_\alpha}{\omega^2-\epsilon_\alpha^2+\imath\epsilon}\right)_{\mathrm{p}} \\ \times\frac{3\imath\lambda}{4}\Big[-\Psi_\alpha^\dagger(\vec{\xi})(1-\vec{\alpha}\cdot\hat{z})\Psi_\alpha(\vec{\xi}+\lambda\hat{z})e^{-\imath\omega\lambda}-\Psi_\alpha^\dagger(\vec{\xi})(1-\vec{\alpha}\cdot\hat{z})\Psi_\alpha(\vec{\xi}-\lambda\hat{z})e^{\imath\omega\lambda}\Big] \\ +\sum_\beta\left(\frac{(\omega+\epsilon_\alpha)(\omega+\epsilon_\beta)}{(\omega^2-\epsilon_\alpha^2+\imath\epsilon)(\omega^2-\epsilon_\beta^2+\imath\epsilon)}\right)_{\mathrm{p}} \\ \times\langle\alpha|\vec{\tau}|\beta\rangle\cdot\Big[\Psi_\beta^\dagger(\vec{\xi})\vec{\tau}(1-\vec{\alpha}\cdot\hat{z})\Psi_\alpha(\vec{\xi}+\lambda\hat{z})e^{-\imath\omega\lambda}-\Psi_\beta^\dagger(\vec{\xi})\vec{\tau}(1-\vec{\alpha}\cdot\hat{z})\Psi_\alpha(\vec{\xi}-\lambda\hat{z})e^{\imath\omega\lambda}\Big]\Bigg\}. \end{aligned} \tag{7.0.2}$$

Similarly, contracting the antisymmetric piece with the projection operators for g_1 and g_T from Table 6.1 produces the polarized structure functions. Using the grand-spin reflection symmetry and parity invariance, we find that only the flavor singlet piece of the rotated flavor quark charge matrix, i.e $\mathcal{Q}_A^2\sim\frac{1}{18}\mathbf{1}$, contributes to the polarized structure functions of this order. Using the quantization condition of equation (4.4.23) and noting that the nucleon is polarized along the positive $\hat{e}_3$ direction in the case of the longitudinal polarized structure function gives the matrix element

$$\langle N,\frac{1}{2}\hat{e}_3|J_3|N,\frac{1}{2}\hat{e}_3\rangle=\frac{1}{2}. \tag{7.0.3}$$

Generalizing the photon direction $\hat{e}_3$ into an arbitrary unit spherical direction $\hat{z}$, we find the $\frac{1}{N_c}$ corrections to the longitudinal polarized structure function

$$\begin{aligned} \mathrm{g}_1^{I=0}(x) = \frac{\imath 5MN_c\pi}{12\alpha^2}\int\frac{\mathrm{d}\Omega_z}{4\pi}\int\frac{\mathrm{d}\omega}{2\pi}\sum_\alpha\int\frac{\mathrm{d}\lambda}{2\pi}e^{\imath Mx\lambda}\int\mathrm{d}^3\xi\Bigg\{\left(\frac{\omega+\epsilon_\alpha}{\omega^2-\epsilon_\alpha^2+\imath\epsilon}\right)_{\mathrm{p}} \\ \times\frac{\imath\lambda}{4}\Big[\Psi_\alpha^\dagger(\vec{\xi})\vec{\tau}\cdot\hat{z}(1-\vec{\alpha}\cdot\hat{z})\gamma_5\Psi_\alpha(\vec{\xi}+\lambda\hat{z})e^{-\imath\omega\lambda}-\Psi_\alpha^\dagger(\vec{\xi})\vec{\tau}\cdot\hat{z}(1-\vec{\alpha}\cdot\hat{z})\gamma_5\Psi_\alpha(\vec{\xi}-\lambda\hat{z})e^{\imath\omega\lambda}\Big] \\ +\sum_\beta\left(\frac{(\omega+\epsilon_\alpha)(\omega+\epsilon_\beta)}{(\omega^2-\epsilon_\alpha^2+\imath\epsilon)(\omega^2-\epsilon_\beta^2+\imath\epsilon)}\right)_{\mathrm{p}}\langle\alpha|\vec{\tau}\cdot\hat{z}|\beta\rangle \\ \times\Big[\Psi_\beta^\dagger(\vec{\xi})(1-\vec{\alpha}\cdot\hat{z})\gamma_5\Psi_\alpha(\vec{\xi}+\lambda\hat{z})e^{-\imath\omega\lambda}+\Psi_\beta^\dagger(\vec{\xi})(1-\vec{\alpha}\cdot\hat{z})\gamma_5\Psi_\alpha(\vec{\xi}-\lambda\hat{z})e^{\imath\omega\lambda}\Big]\Bigg\}. \end{aligned} \tag{7.0.4}$$

For the transverse case the nucleon is polarized in the positive $\hat{e}_1$ direction. Then the quantization condition of equation (4.4.23) gives rise to matrix element

$$\langle N,\frac{1}{2}\hat{e}_1|J_1|N,\frac{1}{2}\hat{e}_1\rangle=\frac{1}{2}. \tag{7.0.5}$$

Again, generalizing the photon direction into an arbitrary unit spherical direction $\hat{z}$ we find the

$\frac{1}{N_c}$ corrections to the transverse polarized structure function

$$\begin{aligned}
\mathrm{g}_T^{I=0}(x) = \frac{\imath 5MN_c\pi}{24\alpha^2}\int\frac{\mathrm{d}\Omega_z}{4\pi}\int\frac{\mathrm{d}\omega}{2\pi}\sum_\alpha\int\frac{\mathrm{d}\lambda}{2\pi}e^{\imath Mx\lambda}\int\mathrm{d}^3\xi\Bigg\{\left(\frac{\omega+\epsilon_\alpha}{\omega^2-\epsilon_\alpha^2+\imath\epsilon}\right)_{\mathrm{p}}\\
\times\Big[\Psi_\alpha^\dagger(\vec{\xi})\left(\vec{\tau}\cdot\vec{\alpha}-\vec{\tau}\cdot\hat{z}\vec{\alpha}\cdot\hat{z}\right)\gamma_5\Psi_\alpha(\vec{\xi}+\lambda\hat{z})e^{-\imath\omega\lambda}\\
-\Psi_\alpha^\dagger(\vec{\xi})\left(\vec{\tau}\cdot\vec{\alpha}-\vec{\tau}\cdot\hat{z}\vec{\alpha}\cdot\hat{z}\right)\gamma_5\Psi_\alpha(\vec{\xi}-\lambda\hat{z})e^{\imath\omega\lambda}\Big]+\sum_\beta\left(\frac{(\omega+\epsilon_\alpha)(\omega+\epsilon_\beta)}{(\omega^2-\epsilon_\alpha^2+\imath\epsilon)(\omega^2-\epsilon_\beta^2+\imath\epsilon)}\right)_{\mathrm{p}}\\
\times\Bigg(\langle\alpha|\tau_i|\beta\rangle\Big[\Psi_\beta^\dagger(\vec{\xi})\alpha_i\gamma_5\Psi_\alpha(\vec{\xi}+\lambda\hat{z})e^{-\imath\omega\lambda}+\Psi_\beta^\dagger(\vec{\xi})\alpha_i\gamma_5\Psi_\alpha(\vec{\xi}-\lambda\hat{z})e^{\imath\omega\lambda}\Big]\\
-\langle\alpha|\vec{\tau}\cdot\hat{z}|\beta\rangle\Big[\Psi_\beta^\dagger(\vec{\xi})\vec{\alpha}\cdot\hat{z}\gamma_5\Psi_\alpha(\vec{\xi}+\lambda\hat{z})e^{-\imath\omega\lambda}+\Psi_\beta^\dagger(\vec{\xi})\vec{\alpha}\cdot\hat{z}\gamma_5\Psi_\alpha(\vec{\xi}-\lambda\hat{z})e^{\imath\omega\lambda}\Big]\Bigg)\Bigg\}. \quad (7.0.6)
\end{aligned}$$

Note the absence of regularization in these structure functions as they contain the spectral functions

$$f_\alpha^+(\omega)+f_\alpha^-(-\omega)=2\frac{\omega+\epsilon_\alpha}{\omega^2-\epsilon_\alpha^2+\imath\epsilon}\quad\text{and}\quad g_{\alpha\beta}^+(\omega)-g_{\alpha\beta}^-(-\omega)=2\frac{(\omega+\epsilon_\alpha)(\omega+\epsilon_\beta)}{(\omega^2-\epsilon_\alpha^2+\imath\epsilon)\left(\omega^2-\epsilon_\beta^2+\imath\epsilon\right)}. \quad (7.0.7)$$

7.1 Numerical Calculations of the Isovector Unpolarized Structure Function

In what follows, we substitute the Fourier transform of the eigenfunction into equation (7.0.2). In the RF the isovector unpolarized structure function at leading order $\frac{1}{N_c}$ then reads

$$\begin{aligned}
F_1^{I=1}(x) = \imath\frac{MN_c\pi}{72\alpha^2}I_3\int\frac{\mathrm{d}\Omega_z}{4\pi}\int\frac{\mathrm{d}\omega}{2\pi}\sum_\alpha\int\frac{\mathrm{d}\lambda}{2\pi}\int\frac{\mathrm{d}^3p}{2\pi^2}\int\frac{\mathrm{d}^3k}{2\pi^2}\int\mathrm{d}^3\xi\Bigg\{\left(\frac{\omega+\epsilon_\alpha}{\omega^2-\epsilon_\alpha^2+\imath\epsilon}\right)_{\mathrm{p}}\\
\times\frac{3\imath\lambda}{4}\Big[-\tilde{\Psi}_\alpha^\dagger(\vec{p})(1-\vec{\alpha}\cdot\hat{z})\tilde{\Psi}_\alpha(\vec{k})e^{\imath\vec{\xi}\cdot(\vec{p}-\vec{k})}e^{\imath\lambda\left(Mx-\vec{k}\cdot\hat{z}\right)}e^{-\imath\omega\lambda}\\
-\tilde{\Psi}_\alpha^\dagger(\vec{p})(1-\vec{\alpha}\cdot\hat{z})\tilde{\Psi}_\alpha(\vec{k})e^{\imath\vec{\xi}\cdot(\vec{p}-\vec{k})}e^{\imath\lambda\left(Mx+\vec{k}\cdot\hat{z}\right)}e^{\imath\omega\lambda}\Big]+\sum_\beta\left(\frac{(\omega+\epsilon_\alpha)(\omega+\epsilon_\beta)}{(\omega^2-\epsilon_\alpha^2+\imath\epsilon)(\omega^2-\epsilon_\beta^2+\imath\epsilon)}\right)_{\mathrm{p}}\\
\times\langle\alpha|\vec{\tau}|\beta\rangle\cdot\Big[\tilde{\Psi}_\beta^\dagger(\vec{p})\vec{\tau}(1-\vec{\alpha}\cdot\hat{z})\tilde{\Psi}_\alpha(\vec{k})e^{\imath\vec{\xi}\cdot(\vec{p}-\vec{k})}e^{\imath\lambda\left(Mx-\vec{k}\cdot\hat{z}\right)}e^{-\imath\omega\lambda}\\
-\tilde{\Psi}_\beta^\dagger(\vec{p})\vec{\tau}(1-\vec{\alpha}\cdot\hat{z})\tilde{\Psi}_\alpha(\vec{k})e^{\imath\vec{\xi}\cdot(\vec{p}-\vec{k})}e^{\imath\lambda\left(Mx+\vec{k}\cdot\hat{z}\right)}e^{\imath\omega\lambda}\Big]\Bigg\}. \quad (7.1.1)
\end{aligned}$$

Considering the pole contributions (in the quadratic spinor terms)

$$\left(\frac{1}{\omega^2-\epsilon_\alpha^2+\imath\epsilon}\right)_{\mathrm{p}}=-\frac{\imath\pi}{|\epsilon_\alpha|}\left[\delta\left(\omega+\epsilon_\alpha\right)+\delta\left(\omega-\epsilon_\alpha\right)\right],$$

we have the following integral identity

$$\int\frac{\mathrm{d}\omega}{2\pi}\left(\frac{\omega+\epsilon_\alpha}{\omega^2-\epsilon_\alpha^2+\imath\epsilon}\right)_{\mathrm{p}}e^{\mp\imath\omega\lambda}=\frac{\epsilon_\alpha}{|\epsilon_\alpha|}\Big(\mp\sin(\epsilon_\alpha\lambda)-\imath\cos(\epsilon_\alpha\lambda)\Big), \quad (7.1.2)$$

This then allows us to perform the integral over 'λ'

$$\imath\int\frac{\mathrm{d}\lambda}{2\pi}\lambda\left(\mp\imath\sin(\epsilon_\alpha\lambda)+\cos(\epsilon_\alpha\lambda)\right)e^{\imath\lambda(Mx\mp\hat{z}\cdot\vec{p})}=\frac{\partial}{\partial\epsilon_\alpha}\int\frac{\mathrm{d}\lambda}{2\pi}\left(\mp\cos(\epsilon_\alpha\lambda)+\imath\sin(\epsilon_\alpha\lambda)\right)e^{\imath\lambda(Mx\mp\hat{z}\cdot\vec{p})}$$
$$=\mp\frac{\partial}{\partial\epsilon_\alpha}\delta\left(Mx\mp\hat{z}\cdot\vec{p}\mp\epsilon_\alpha\right), \tag{7.1.3}$$

For the quartic spinor terms, the pole contributions are

$$\left(\frac{1}{(\omega^2-\epsilon_\alpha^2+\imath\epsilon)(\omega^2-\epsilon_\beta^2+\imath\epsilon)}\right)_{\mathrm{p}}=-\frac{\imath\pi}{\epsilon_\alpha^2-\epsilon_\beta^2}\left[\frac{1}{|\epsilon_\alpha|}\Big\{\delta\left(\omega+\epsilon_\alpha\right)+\delta\left(\omega-\epsilon_\alpha\right)\Big\}-\frac{1}{|\epsilon_\beta|}\Big\{\delta\left(\omega+\epsilon_\beta\right)+\delta\left(\omega-\epsilon_\beta\right)\Big\}\right],$$

yielding the following integral identity

$$\int\frac{\mathrm{d}\omega}{2\pi}\left(\frac{(\omega+\epsilon_\alpha)(\omega+\epsilon_\beta)}{(\omega^2-\epsilon_\alpha^2+\imath\epsilon)(\omega^2-\epsilon_\beta^2+\imath\epsilon)}\right)_{\text{pole}}e^{\mp\imath\omega\lambda}=-\frac{1}{\epsilon_\alpha-\epsilon_\beta}\left[\frac{\epsilon_\alpha}{|\epsilon_\alpha|}\Big(\pm\sin(\epsilon_\alpha\lambda)+\imath\cos(\epsilon_\alpha\lambda)\Big)\right.$$
$$\left.-\frac{\epsilon_\beta}{|\epsilon_\beta|}\Big(\pm\sin(\epsilon_\beta\lambda)+\imath\cos(\epsilon_\beta\lambda)\Big)\right], \tag{7.1.4}$$

which finally allows us to perform the integral over 'λ'

$$\int\frac{\mathrm{d}\lambda}{2\pi}\Big\{\frac{\epsilon_\alpha}{|\epsilon_\alpha|}\Big(\pm\imath\sin(\epsilon_\alpha\lambda)-\cos(\epsilon_\alpha\lambda)\Big)-\frac{\epsilon_\beta}{|\epsilon_\beta|}\Big(\pm\imath\sin(\epsilon_\beta\lambda)-\cos(\epsilon_\beta\lambda)\Big)\Big\}e^{\imath\lambda(Mx\mp\vec{p}\cdot\hat{z})}$$
$$=-\frac{\epsilon_\alpha}{|\epsilon_\alpha|}\delta\left(Mx\mp\hat{z}\cdot\vec{p}\mp\epsilon_\alpha\right)+\frac{\epsilon_\beta}{|\epsilon_\beta|}\delta\left(Mx\mp\hat{z}\cdot\vec{p}\mp\epsilon_\beta\right), \tag{7.1.5}$$

Writing the momentum integration variable into spherical coordinates cf, (6.1.6), and averaging over the photon direction gives the vacuum contribution

$$\Big[F_1^{I=1}(x)\Big]_{\mathrm{s}}^{\mp}=\frac{MN_cI_3}{72\alpha^2}\sum_\alpha\Bigg\{-\frac{3}{4}\frac{\epsilon_\alpha}{|\epsilon_\alpha|}\frac{\partial}{\partial\epsilon_\alpha}\int_{|Mx_\alpha^\pm|}^\infty p\,\mathrm{d}p\int\mathrm{d}\Omega_p\Big[\tilde{\Psi}_\alpha^\dagger(\vec{p})\tilde{\Psi}_\alpha(\vec{p})\pm\frac{Mx_\alpha^\pm}{p}\tilde{\Psi}_\alpha^\dagger(\vec{p})\hat{p}\cdot\vec{\alpha}\tilde{\Psi}_\alpha(\vec{p})\Big]$$
$$+\sum_\beta\frac{\langle\alpha|\tau_i|\beta\rangle}{\epsilon_\beta-\epsilon_\alpha}\left(\frac{\epsilon_\alpha}{|\epsilon_\alpha|}\int_{|Mx_\alpha^\pm|}^\infty p\,\mathrm{d}p\int\mathrm{d}\Omega_p\Big[\tilde{\Psi}_\beta^\dagger(\vec{p})\tau_i\tilde{\Psi}_\alpha(\vec{p})\pm\frac{Mx_\alpha^\pm}{p}\tilde{\Psi}_\beta^\dagger(\vec{p})\tau_i\hat{p}\cdot\vec{\alpha}\tilde{\Psi}_\alpha(\vec{p})\Big]\right.$$
$$\left.-\frac{\epsilon_\beta}{|\epsilon_\beta|}\int_{|Mx_\beta^\pm|}^\infty p\,\mathrm{d}p\int\mathrm{d}\Omega_p\Big[\tilde{\Psi}_\beta^\dagger(\vec{p})\tau_i\tilde{\Psi}_\alpha(\vec{p})\pm\frac{Mx_\beta^\pm}{p}\tilde{\Psi}_\beta^\dagger(\vec{p})\tau_i\hat{p}\cdot\vec{\alpha}\tilde{\Psi}_\alpha(\vec{p})\Big]\right)\Bigg\}, \tag{7.1.6}$$

where $\Big[F_1^{I=1}(x)\Big]_{\mathrm{s}}^-$ and $\Big[F_1^{I=1}(x)\Big]_{\mathrm{s}}^+$ denote the antiquark and quark distributions, respectively. The derivative $\dfrac{\partial}{\partial\epsilon_\alpha}$ acts on the lower boundary of the first integral. The total distribution is given as

$$\Big[F_1^{I=1}(x)\Big]_{\mathrm{s}}=\Big[F_1^{I=1}(x)\Big]_{\mathrm{s}}^+-\Big[F_1^{I=1}(x)\Big]_{\mathrm{s}}^-. \tag{7.1.7}$$

We have also defined $Mx_\alpha^\pm=Mx\pm\epsilon_\alpha$. The quadratic spinor matrix element

$$\int\mathrm{d}\Omega_p\tilde{\Psi}_\alpha^\dagger(\vec{p})\tilde{\Psi}_\alpha(\vec{p})\quad\text{and}\quad\int\mathrm{d}\Omega_p\tilde{\Psi}_\alpha^\dagger(\vec{p})\hat{p}\cdot\vec{\alpha}\tilde{\Psi}_\alpha(\vec{p}) \tag{7.1.8}$$

have already been discussed in section 6.1. Those involving the quartic terms

$$\Big\{\int \mathrm{d}\Omega_r \Psi^\dagger_\alpha(\vec{r})\tau_i\Psi_\beta(\vec{r})\Big\}\Big\{\int \mathrm{d}\Omega_p \tilde{\Psi}^\dagger_\beta(\vec{p})\tau_i\tilde{\Psi}_\alpha(\vec{p})\Big\} \quad \text{and}$$
$$\Big\{\int \mathrm{d}\Omega_r \Psi^\dagger_\alpha(\vec{r})\tau_i\Psi_\beta(\vec{r})\Big\}\Big\{\int \mathrm{d}\Omega_p \tilde{\Psi}^\dagger_\beta(\vec{p})\tau_i\hat{p}\cdot\vec{\alpha}\tilde{\Psi}_\alpha(\vec{p})\Big\} \tag{7.1.9}$$

are listed in Appendix E.

Following the calculations of the valence contributions in section 6.1 and noting that the cranking correction cf. (6.1.12) dwells in the channel with $G = 1$ and negative intrinsic parity(see equations (6.1.19) and (6.1.20)) we obtain the valence contribution of the isovector unpolarized structure function

$$\Big[F_1^{I=1}(x)\Big]^{\mp}_{\mathrm{v}} = -\frac{MN_cI_3}{12\alpha^2}\sum_{\alpha\neq\mathrm{v}}\frac{1}{\epsilon_{\mathrm{v}}-\epsilon_\alpha}N_\alpha$$
$$\times\int_{|Mx^\pm_{\mathrm{v}}|}^{\infty}\mathrm{d}p\Big[p\Big(\tilde{g}_{\mathrm{v}}(p)\tilde{g}^{(2)}_\alpha(p)+\tilde{f}_{\mathrm{v}}(p)\tilde{f}^{(2)}_\alpha(p)\Big)\mp Mx^\pm_{\mathrm{v}}\Big(\tilde{g}_{\mathrm{v}}(p)\tilde{f}^{(2)}_\alpha(p)+\tilde{f}_{\mathrm{v}}(p)\tilde{g}^{(2)}_\alpha(p)\Big)\Big], \tag{7.1.10}$$

where $Mx^\pm_{\mathrm{v}}$ is defined in equation (6.1.15). Also we have introduced the shorthand notation

$$N_\alpha = \int \mathrm{d}r\, r^2\Big\{g_{\mathrm{v}}(r)g^{(2)}_\alpha(r)+f_{\mathrm{v}}(r)f^{(2)}_\alpha(r)\Big\}. \tag{7.1.11}$$

7.1.1 Gottfried Sum Rule

In the following we formulate the relation of the Gottfried sum rule [19, 24, 64] $\mathcal{S}_G \sim \langle\tau_3\rangle\langle\tau_3\rangle$ and isovector unpolarized structure function within our model. We first integrate the quadratic spinor terms. The integration of the scalar term $(\tilde{\Psi}^\dagger_\alpha(\vec{p})\tilde{\Psi}_\alpha(\vec{p}))$ gives

$$2\int_0^\infty \mathrm{d}x\ \big[F_1^{I=1}(x)\big]_{\mathrm{s}} \sim \frac{MN_cI_3}{48\alpha^2}\sum_\alpha\frac{\epsilon_\alpha}{|\epsilon_\alpha|}\frac{\partial}{\partial\epsilon_\alpha}\int_0^\infty \mathrm{d}x\left\{\Big\langle\alpha|\alpha\Big\rangle'_{|Mx^+|}+\Big\langle\alpha|\alpha\Big\rangle'_{|Mx^-|}\right\}$$
$$= \frac{MN_cI_3}{48\alpha^2}\sum_\alpha\frac{\epsilon_\alpha}{|\epsilon_\alpha|}\frac{\partial}{\partial\epsilon_\alpha}\left\{\int_{\frac{\epsilon_\alpha}{M}}^\infty \mathrm{d}y\Big\langle\alpha|\alpha\Big\rangle'_{My}+\int_{-\frac{\epsilon_\alpha}{M}}^\infty \mathrm{d}y\Big\langle\alpha|\alpha\Big\rangle'_{|My|}\right\},$$
$$= -\frac{MN_cI_3}{24\alpha^2}\sum_\alpha\frac{\epsilon_\alpha}{|\epsilon_\alpha|}\frac{\partial}{\partial\epsilon_\alpha}\int_0^\infty \mathrm{d}y\int_{My}^\infty \mathrm{d}p\,p\int \mathrm{d}\Omega_p\tilde{\Psi}^\dagger_\alpha(\vec{p})\tilde{\Psi}_\alpha(\vec{p})$$
$$= \frac{N_cI_3}{24\alpha^2}\sum_\alpha\frac{\epsilon_\alpha}{|\epsilon_\alpha|}\frac{\partial}{\partial\epsilon_\alpha}\int_0^\infty \mathrm{d}^3p\tilde{\Psi}^\dagger_\alpha(\vec{p})\tilde{\Psi}_\alpha(\vec{p}) = 0. \tag{7.1.12}$$

Here we have made use of the properties of symmetric boundaries and the fact that the last integral is the normalization of the quark wave-function that does not depend on ϵ_α to obtain the above results. Similarly, integrating the quadratic operator term of $\hat{p}\cdot\vec{\alpha}$ gives

$$2\int_0^\infty \mathrm{d}x\ \big[F_1^{I=1}(x)\big]_{\mathrm{s}} \sim \frac{MN_cI_3}{48\alpha^2}\sum_\alpha\frac{\epsilon_\alpha}{|\epsilon_\alpha|}\frac{\partial}{\partial\epsilon_\alpha}\int_0^\infty \mathrm{d}x\left\{Mx^+\Big\langle\alpha|\hat{p}\cdot\vec{\alpha}|\alpha\Big\rangle''_{|Mx^+|}-Mx^-\Big\langle\alpha|\hat{p}\cdot\vec{\alpha}|\alpha\Big\rangle''_{|Mx^-|}\right\},$$
$$= \frac{MN_cI_3}{48\alpha^2}\sum_\alpha\frac{\epsilon_\alpha}{|\epsilon_\alpha|}\frac{\partial}{\partial\epsilon_\alpha}\left\{\int_{\frac{\epsilon_\alpha}{M}}^\infty \mathrm{d}y\,My\Big\langle\alpha|\hat{p}\cdot\vec{\alpha}|\alpha\Big\rangle''_{My}-\int_{-\frac{\epsilon_\alpha}{M}}^\infty \mathrm{d}y\,My\Big\langle\alpha|\hat{p}\cdot\vec{\alpha}|\alpha\Big\rangle''_{|My|}\right\},$$
$$= -\frac{MN_cI_3}{24\alpha^2}\sum_\alpha\frac{\epsilon_\alpha}{|\epsilon_\alpha|}\frac{\partial}{\partial\epsilon_\alpha}\int_{-\frac{\epsilon_\alpha}{M}}^{\frac{\epsilon_\alpha}{M}} \mathrm{d}y\,My\Big\langle\alpha|\hat{p}\cdot\vec{\alpha}|\alpha\Big\rangle''_{|My|} = 0, \tag{7.1.13}$$

m	$2\int_0^\infty \mathrm{d}x\ (F_1^p - F_1^n)_{\mathrm{v}}$	$[\mathcal{S}_G]_{\mathrm{v}}$	$2\int_0^\infty \mathrm{d}x\ (F_1^p - F_1^n)_{\mathrm{s}}$	$[\mathcal{S}_G]_{\mathrm{s}}$
400	0.214	0.214	0.000156	0.000157
450	0.225	0.225	0.000248	0.000285
500	0.236	0.236	0.000356	0.000444

Table 7.1: Verification of the Gottfried sum rule of our calculations cf. equation (7.1.15) to the exact calculations $\mathcal{S}_G \sim \langle\tau_3\rangle\langle\tau_3\rangle$ cf. equation (7.1.20) for different constituent quark masses m (in MeV).

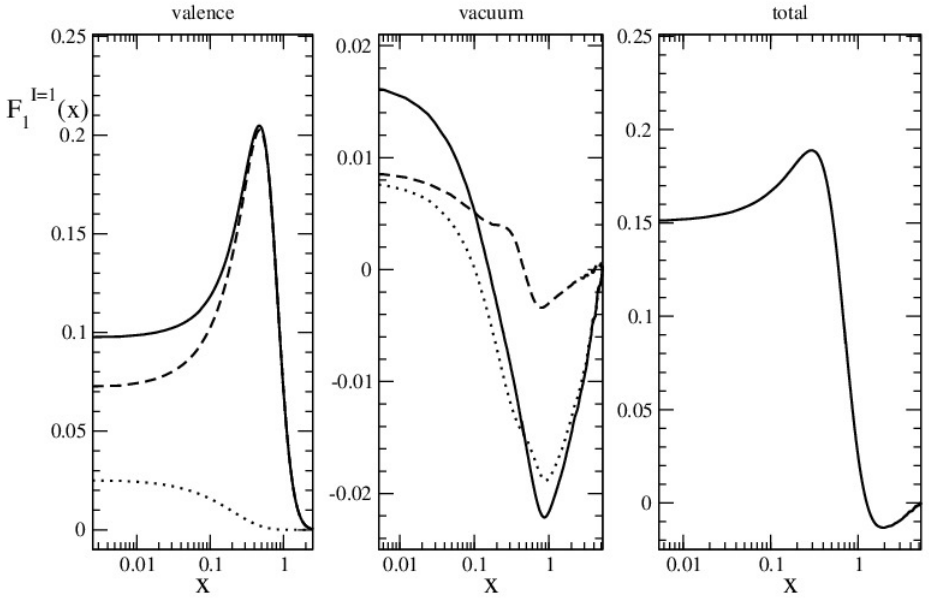

Figure 7.1: The numerical predictions for the isovector unpolarized proton structure function, $F_1^{I=1}(x)$, for $m = 400\,\mathrm{MeV}$. The dotted lines in the graphs for the valence and vacuum contributions denote the anti-quark distributions, the dashed lines denote the quark distributions and the solid lines denote the sum of quark and anti-quark distribution, respectively

since only symmetric integrals survive. In the next step we consider the quartic spinor contributions by first integrating the term with the matrix element $\left\{\int \mathrm{d}\Omega_r \Psi_\alpha^\dagger(\vec{r})\tau_i\Psi_\beta(\vec{r})\right\}\left\{\int \mathrm{d}\Omega_p \tilde{\Psi}_\beta^\dagger(\vec{p})\tau_i\hat{p}\cdot\vec{\alpha}\tilde{\Psi}_\alpha(\vec{p})\right\}$. We first consider the term involving $\dfrac{\epsilon_\alpha}{|\epsilon_\alpha|}$

$$
\begin{aligned}
2\int_0^\infty \mathrm{d}x\ \left[F_1^{I=1}(x)\right]_{\mathrm{s}} &\sim \frac{MN_cI_3}{36\alpha^2}\sum_{\alpha\beta}\frac{\langle\alpha|\tau_i|\beta\rangle}{\epsilon_\beta-\epsilon_\alpha}\frac{\epsilon_\alpha}{|\epsilon_\alpha|}\int_0^\infty \mathrm{d}x\left\{Mx_\alpha^+\left\langle\beta|\tau_i\hat{p}\cdot\vec{\alpha}|\alpha\right\rangle''_{|Mx_\alpha^+|} - Mx_\alpha^-\left\langle\beta|\tau_i\hat{p}\cdot\vec{\alpha}|\alpha\right\rangle''_{|Mx_\alpha^-|}\right\},\\
&= \frac{MN_cI_3}{36\alpha^2}\sum_{\alpha\beta}\frac{\langle\alpha|\tau_i|\beta\rangle}{\epsilon_\beta-\epsilon_\alpha}\frac{\epsilon_\alpha}{|\epsilon_\alpha|}\left\{\int_{\frac{\epsilon_\alpha}{M}}^\infty \mathrm{d}y\, My\left\langle\beta|\tau_i\hat{p}\cdot\vec{\alpha}|\alpha\right\rangle''_{My} - \int_{-\frac{\epsilon_\alpha}{M}}^\infty \mathrm{d}y\, My\left\langle\alpha|\tau_i\hat{p}\cdot\vec{\alpha}|\alpha\right\rangle''_{|My|}\right\},\\
&= \frac{MN_cI_3}{36\alpha^2}\sum_{\alpha\beta}\frac{\langle\alpha|\tau_i|\beta\rangle}{\epsilon_\beta-\epsilon_\alpha}\frac{\epsilon_\alpha}{|\epsilon_\alpha|}\int_{-\frac{\epsilon_\alpha}{M}}^{\frac{\epsilon_\alpha}{M}} \mathrm{d}y\, My\left\langle\beta|\tau_i\hat{p}\cdot\vec{\alpha}|\alpha\right\rangle''_{|My|} = 0. \qquad (7.1.14)
\end{aligned}
$$

Similar results hold for the term multiplying $\dfrac{\epsilon_\beta}{|\epsilon_\beta|}$. In what follows we consider the integration of

m	$2\int_0^\infty \mathrm{d}x\ (F_1^p - F_1^n)_{\mathrm{v}}$	$2\int_0^\infty \mathrm{d}x\ (F_1^p - F_1^n)_{\mathrm{s}}$	$2\int_0^\infty \mathrm{d}x\ (F_1^p - F_1^n)$	experimental value
400	0.214	0.000156	0.214	
450	0.225	0.000248	0.225	0.235 ± 0.026 [4]
500	0.236	0.000356	0.237	

Table 7.2: Comparison of the calculated Gottfried sum rule of the nucleon for different constituent quark masses m (in MeV) to that of experimental data. Here the subscripts 'v' and 's' denote the vacuum and sea contributions, respectively.

the matrix element of $\left\{\int \mathrm{d}\Omega_r \Psi^\dagger_\alpha(\vec{r})\tau_i\Psi_\beta(\vec{r})\right\}\left\{\int \mathrm{d}\Omega_p \tilde{\Psi}^\dagger_\beta(\vec{p})\tau_i\hat{p}\cdot\vec{\alpha}\tilde{\Psi}_\alpha(\vec{p})\right\}$. As before we commence with the term involving $\dfrac{\epsilon_\alpha}{|\epsilon_\alpha|}$

$$\begin{aligned}
2\int_0^\infty \mathrm{d}x\ \left[F_1^{I=1}(x)\right]_{\mathrm{s}} &\sim \frac{MN_cI_3}{36\alpha^2}\sum_{\alpha\beta}\frac{\langle\alpha|\tau_i|\beta\rangle}{\epsilon_\beta-\epsilon_\alpha}\frac{\epsilon_\alpha}{|\epsilon_\alpha|}\int_0^\infty \mathrm{d}x\left\{\left\langle\beta|\tau_i|\alpha\right\rangle'_{|Mx^+_\alpha|}+\left\langle\beta|\tau_i|\alpha\right\rangle'_{|Mx^-_\alpha|}\right\},\\
&= \frac{MN_cI_3}{36\alpha^2}\sum_{\alpha\beta}\frac{\langle\alpha|\tau_i|\beta\rangle}{\epsilon_\beta-\epsilon_\alpha}\frac{\epsilon_\alpha}{|\epsilon_\alpha|}\left\{\int_{\frac{\epsilon_\alpha}{M}}^\infty \mathrm{d}y\left\langle\beta|\tau_i|\alpha\right\rangle'_{My}+\int_{-\frac{\epsilon_\alpha}{M}}^\infty \mathrm{d}y\left\langle\alpha|\tau_i|\alpha\right\rangle'_{|My|}\right\},\\
&= -\frac{MN_cI_3}{18\alpha^2}\sum_{\alpha\beta}\frac{\langle\alpha|\tau_i|\beta\rangle}{\epsilon_\beta-\epsilon_\alpha}\frac{\epsilon_\alpha}{|\epsilon_\alpha|}\int_0^\infty \mathrm{d}y\left\langle\beta|\tau_i|\alpha\right\rangle'_{|My|}\\
&= \frac{N_cI_3}{18\alpha^2}\sum_{\alpha\beta}\frac{\epsilon_\alpha}{|\epsilon_\alpha|}\frac{\langle\alpha|\tau_i|\beta\rangle}{\epsilon_\beta-\epsilon_\alpha}\left\langle\beta|\tau_i|\alpha\right\rangle_0. \qquad (7.1.15)
\end{aligned}$$

Similar results also hold for the terms involving $\dfrac{\epsilon_\beta}{|\epsilon_\beta|}$. Combining results we obtain

$$2\int_0^\infty \mathrm{d}x\ (F_1^p - F_1^n)_{\mathrm{s}} = \frac{N_c}{18\alpha^2}\sum_{\alpha\beta}\left(\frac{\epsilon_\alpha}{|\epsilon_\alpha|}-\frac{\epsilon_\beta}{|\epsilon_\beta|}\right)\frac{\langle\alpha|\tau_i|\beta\rangle}{\epsilon_\beta-\epsilon_\alpha}\left\langle\beta|\tau_i|\alpha\right\rangle_0 = \Big[\mathcal{S}_G\Big]_{\mathrm{s}}, \qquad (7.1.16)$$

where F_1^p and F_1^n denote the unpolarized proton and neutron structure functions corresponding to the isospin $I_3 = \pm\dfrac{1}{2}$, respectively. Here

$$\Big[\mathcal{S}_G\Big]_{\mathrm{s}} = \frac{N_c}{18\alpha^2}\sum_{\alpha\beta}\left(\frac{\epsilon_\alpha}{|\epsilon_\alpha|}-\frac{\epsilon_\beta}{|\epsilon_\beta|}\right)\frac{\langle\alpha|\tau_3|\beta\rangle}{\epsilon_\beta-\epsilon_\alpha}\langle\beta|\tau_3|\alpha\rangle \qquad (7.1.17)$$

is the vacuum contribution to the Gottfried sum rule[24]. Our calculations reveal that the Gottfried sum rule is independent of the Pauli-Villar's regulators, thus it remains unregularized. Similar calculations from equation (7.1.10) give the valence contribution

$$2\int_0^\infty \mathrm{d}x\ (F_1^p - F_1^n)_{\mathrm{v}} = \frac{N_c}{9\alpha^2}\eta_{\mathrm{v}}\sum_{\mathrm{v}\neq\beta}\frac{\langle\mathrm{v}|\tau_i|\beta\rangle}{\epsilon_{\mathrm{v}}-\epsilon_\beta}\left\langle\beta|\tau_i|\mathrm{v}\right\rangle_0 = \Big[\mathcal{S}_G\Big]_{\mathrm{v}}, \qquad (7.1.18)$$

where

$$\Big[\mathcal{S}_G\Big]_{\mathrm{v}} = \frac{N_c}{9\alpha^2}\eta_{\mathrm{v}}\sum_{\mathrm{v}\neq\beta}\frac{\langle\mathrm{v}|\tau_3|\beta\rangle}{\epsilon_{\mathrm{v}}-\epsilon_\beta}\langle\beta|\tau_3|\mathrm{v}\rangle \qquad (7.1.19)$$

with the total Gottfried sum

$$\mathcal{S}_G = \frac{N_c}{9\alpha^2}\left[\eta_{\mathrm{v}}\frac{\langle\mathrm{v}|\tau_3|\beta\rangle}{\epsilon_{\mathrm{v}}-\epsilon_\beta}\langle\beta|\tau_3|\mathrm{v}\rangle+\frac{1}{2}\sum_{\alpha\beta}\left(\frac{\epsilon_\alpha}{|\epsilon_\alpha|}-\frac{\epsilon_\beta}{|\epsilon_\beta|}\right)\frac{\langle\alpha|\tau_3|\beta\rangle}{\epsilon_\beta-\epsilon_\alpha}\langle\beta|\tau_3|\alpha\rangle\right]. \qquad (7.1.20)$$

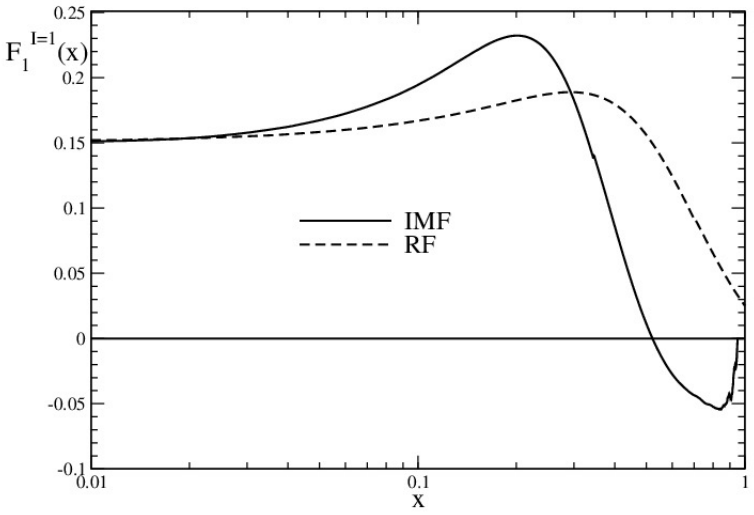

Figure 7.2: The effects of applying the IMF transformation to the isovector unpolarized proton structure function for $m = 400\,\text{MeV}$. The curve labeled "RF" denotes the result obtained from the nucleon rest frame and those labeled "IMF" denotes the projection to the infinite momentum frame.

We have verified the numerical evaluation of our results $2\int_0^\infty \mathrm{d}x\ (F_1^p - F_1^n)$ to that of the direct calculations $\mathcal{S}_G$ in Table 7.1. This reflects the accuracy of our numerical evaluation. In Table 7.2, we compare our numerical prediction of the Gottfried sum rule for various constituent quark mass to that of the experimental value [4] from NMC Collaboration. Note that, in computing the valence contribution we have made use of the total moment of inertia and also as pointed out earlier the vacuum contribution of the Gottfried sum rule is not regularized. It can be noticed from Table 7.2 that the valence quarks contribute about 99% to the Gottfried sum rule. The prediction from our results agrees reasonably well with the NMC observation [4]. Also, it is substantially lower than the parton model prediction [70] $\int_0^1 \mathrm{d}x\ (F_1^p - F_1^n) = \frac{1}{3}$ in agreement with the empirical data. This shows that our model well incorporates the chiral symmetry features of QCD.

7.1.2 Numerical Results for the Isovector Unpolarized Structure Function

In this subsection we discuss our numerical results for the isovector unpolarized proton structure function. In Figure 7.1 we display the numerical results of the unpolarized proton structure function for a constituent quark mass of $m = 400\,\text{MeV}$. We observe from Figure 7.1 that the valence contribution dominates over the vacuum contributions. The later being negative for $x \geq 0.2$. Nevertheless the vacuum part only has a moderate effect on the total $F_1^{I=1}(x)$. We see that the total $F_1^{I=1}(x)$ contribution is a smooth function and peaks around values of $x \sim \frac{1}{3}$. Also we observe from Figure 7.1 that the structure functions are not well localized in the Bjorken interval $0 \leq x \leq 1$. To account for this non-locality the structure functions are again projected using the transformation to the infinite momentum frame (IMF).

In Figure 7.2 we display the effect of projecting the structure function to the infinite momentum frame. At $x > 0.5$ [1], the vacuum contribution changes sign to account for the small vacuum value of the Gottfried sum rule. Nevertheless as we shall see in a moment it reproduce the gross features of the structure function that enters the Gottfried sum rule.

It should be pointed out that because of the large radial value of the spherical cavity which we have taken to be $r = D = 10\,\text{fm}$ and the maximal value of the grand spin $G_{\max} \approx 100$, it takes a long time to compute the isovector unpolarized structure function.

7.2 Numerical Calculations of the Flavor-Singlet Longitudinal Polarized Structure Function

As before, we substitute the Fourier transforms of the eigenfunctions into equation (7.0.4). Using the identities in equations (7.1.2)-(7.1.5), writing the integration variable into spherical coordinate cf. (6.1.6) and averaging over the photon direction gives the vacuum contribution of the flavor-singlet longitudinal polarized structure function in the RF at leading order $\frac{1}{N_c}$ as

$$\begin{aligned}
\Big[\mathrm{g}_1^{I=0}(x)\Big]_{\mathrm{s}}^{\mp} = \frac{5MN_c}{24\alpha^2}\sum_{\alpha}\Bigg\{ & \frac{1}{4}\frac{\epsilon_\alpha}{|\epsilon_\alpha|}\frac{\partial}{\partial\epsilon_\alpha}\Big[\mp\int_{|Mx_\alpha^\pm|}^{\infty}\mathrm{d}p\,Mx_\alpha^\pm\int\mathrm{d}\Omega_p\tilde{\Psi}_\alpha^\dagger(\vec{p})\hat{p}\cdot\vec{\tau}\gamma_5\tilde{\Psi}_\alpha(\vec{p}) \\
& -\int_{|Mx_\alpha^\pm|}^{\infty}\mathrm{d}p\,p^2\Big(A_\pm^\alpha\int\mathrm{d}\Omega_p\tilde{\Psi}_\alpha^\dagger(\vec{p})\vec{\tau}\cdot\vec{\sigma}\tilde{\Psi}_\alpha(\vec{p})+B_\pm^\alpha\int\mathrm{d}\Omega_p\tilde{\Psi}_\alpha^\dagger(\vec{p})\hat{p}\cdot\vec{\tau}\hat{p}\cdot\vec{\sigma}\tilde{\Psi}_\alpha(\vec{p})\Big)\Big] \\
& -\sum_{\beta}\frac{\langle\alpha|\tau_i|\beta\rangle}{\epsilon_\beta-\epsilon_\alpha}\Big[\pm\frac{\epsilon_\alpha}{|\epsilon_\alpha|}\int_{|Mx_\alpha^\pm|}^{\infty}\mathrm{d}p\,Mx_\alpha^\pm\int\mathrm{d}\Omega_p\tilde{\Psi}_\beta^\dagger(\vec{p})\hat{p}_i\gamma_5\tilde{\Psi}_\alpha(\vec{p}) \\
& +\frac{\epsilon_\alpha}{|\epsilon_\alpha|}\int_{|Mx_\alpha^\pm|}^{\infty}\mathrm{d}p\,p^2\Big(A_\pm^\alpha\int\mathrm{d}\Omega_p\tilde{\Psi}_\beta^\dagger(\vec{p})\sigma_i\tilde{\Psi}_\alpha(\vec{p})+B_\pm^\alpha\int\mathrm{d}\Omega_p\tilde{\Psi}_\beta^\dagger(\vec{p})\hat{p}_i\hat{p}\cdot\vec{\sigma}\tilde{\Psi}_\alpha(\vec{p})\Big) \\
& \mp\frac{\epsilon_\beta}{|\epsilon_\beta|}\int_{|Mx_\beta^\pm|}^{\infty}\mathrm{d}p\,Mx_\beta^\pm\int\mathrm{d}\Omega_p\tilde{\Psi}_\beta^\dagger(\vec{p})\hat{p}_i\gamma_5\tilde{\Psi}_\alpha(\vec{p}) \\
& -\frac{\epsilon_\beta}{|\epsilon_\beta|}\int_{|Mx_\beta^\pm|}^{\infty}\mathrm{d}p\,p^2\Big(A_\pm^\beta\int\mathrm{d}\Omega_p\tilde{\Psi}_\beta^\dagger(\vec{p})\sigma_i\tilde{\Psi}_\alpha(\vec{p})+B_\pm^\beta\int\mathrm{d}\Omega_p\tilde{\Psi}_\beta^\dagger(\vec{p})\hat{p}_i\hat{p}\cdot\vec{\sigma}\tilde{\Psi}_\alpha(\vec{p})\Big)\Big]\Bigg\}, \qquad (7.2.1)
\end{aligned}$$

where $\Big[\mathrm{g}_1^{I=0}(x)\Big]_{\mathrm{s}}^{-}$ denotes the antiquark distribution and $\Big[\mathrm{g}_1^{I=0}(x)\Big]_{\mathrm{s}}^{+}$ denotes the quark distribution. The total distribution is given as the sum of the quark and antiquark distributions. Here

$$A_\pm^\alpha = \frac{1}{2p}\left(1-\frac{(Mx_\alpha^\pm)^2}{p^2}\right) \quad \text{and} \quad B_\pm^\alpha = \frac{1}{2p}\left(3\frac{(Mx_\alpha^\pm)^2}{p^2}-1\right). \qquad (7.2.2)$$

[1] note that in the rest frame (RF) we have taken $x_{RF} \in [0, 12]$.

The matrix elements of the quadratic spinor terms

$$\begin{aligned}
&\int \mathrm{d}\Omega_p \tilde{\Psi}^\dagger_\alpha(\vec{p})\hat{p}\cdot\vec{\tau}\gamma_5\tilde{\Psi}_\alpha(\vec{p}),\\
&\int \mathrm{d}\Omega_p \tilde{\Psi}^\dagger_\alpha(\vec{p})\hat{p}\cdot\vec{\tau}\hat{p}\cdot\vec{\sigma}\tilde{\Psi}_\alpha(\vec{p}) \quad \text{and}\\
&\int \mathrm{d}\Omega_p \tilde{\Psi}^\dagger_\alpha(\vec{p})\vec{\tau}\cdot\vec{\sigma}\tilde{\Psi}_\alpha(\vec{p}),
\end{aligned} \tag{7.2.3}$$

have already been discussed in section 6.2. The matrix elements of the quartic spinor terms

$$\begin{aligned}
&\left\{\int \mathrm{d}\Omega_r \Psi^\dagger_\alpha(\vec{r})\tau_i\Psi_\beta(\vec{r})\right\}\left\{\int \mathrm{d}\Omega_p \tilde{\Psi}^\dagger_\beta(\vec{p})\hat{p}_i\gamma_5\tilde{\Psi}_\alpha(\vec{p})\right\},\\
&\left\{\int \mathrm{d}\Omega_r \Psi^\dagger_\alpha(\vec{r})\tau_i\Psi_\beta(\vec{r})\right\}\left\{\int \mathrm{d}\Omega_p \tilde{\Psi}^\dagger_\beta(\vec{p})\sigma_i\tilde{\Psi}_\alpha(\vec{p})\right\} \quad \text{and}\\
&\left\{\int \mathrm{d}\Omega_r \Psi^\dagger_\alpha(\vec{r})\tau_i\Psi_\beta(\vec{r})\right\}\left\{\int \mathrm{d}\Omega_p \tilde{\Psi}^\dagger_\beta(\vec{p})\hat{p}_i\hat{p}\cdot\vec{\sigma}\tilde{\Psi}_\alpha(\vec{p})\right\},
\end{aligned} \tag{7.2.4}$$

are listed Appendix E. The valence quark contribution to the isoscalar longitudinal structure function follows a similar calculation and reads

$$\begin{aligned}
\left[\mathrm{g}_1^{I=0}(x)\right]^{\mp}_{\mathrm{v}} = &-\frac{5MN_c}{12\alpha^2}\sum_{\alpha\neq \mathrm{v}}\frac{1}{\epsilon_{\mathrm{v}}-\epsilon_\alpha}N_\alpha\\
&\int_{|Mx^\pm_{\mathrm{v}}|}^\infty p\mathrm{d}p\left[\mp\frac{Mx^\pm_{\mathrm{v}}}{p}\tilde{g}_{\mathrm{v}}(p)\tilde{f}^2_\alpha(p)\mp\frac{Mx^\pm_{\mathrm{v}}}{p}\tilde{f}_{\mathrm{v}}(p)\tilde{g}^2_\alpha(p)\mp\frac{Mx^\pm_{\mathrm{v}}}{p}\sqrt{2}\tilde{g}_{\mathrm{v}}(p)\tilde{f}^1_\alpha(p)\right.\\
&\mp\frac{Mx^\pm_{\mathrm{v}}}{p}\sqrt{2}\tilde{f}_{\mathrm{v}}(p)\tilde{g}^1_\alpha(p)+\tilde{g}_{\mathrm{v}}(p)\tilde{g}^2_\alpha(p)-\left(1-2\frac{(Mx^\pm_{\mathrm{v}})^2}{p^2}\right)\tilde{f}_{\mathrm{v}}(p)\tilde{f}^2_\alpha(p)\\
&\left.-\sqrt{2}\left(1-3\frac{(Mx^\pm_{\mathrm{v}})^2}{p^2}\right)\tilde{g}_{\mathrm{v}}(p)\tilde{g}^1_\alpha(p)+\sqrt{2}\left(1+\frac{(Mx^\pm_{\mathrm{v}})^2}{p^2}\right)\tilde{f}_{\mathrm{v}}(p)\tilde{f}^1_\alpha(p)\right].
\end{aligned} \tag{7.2.5}$$

7.2.1 The Axial-Singlet Charge

In this subsection we discuss the relation of the axial-singlet charge $g^0_A \sim \langle\alpha_3\gamma_5\rangle$ and the iso-singlet longitudinal polarized structure function in our model. We first investigate the quadratic spinor terms. Integration of the matrix element $\hat{p}\cdot\vec{\tau}\gamma_5$ in the RF gives

$$\begin{aligned}
\int_0^\infty \mathrm{d}x\left[\mathrm{g}_1^{I=0}(x)\right]_{\mathrm{s}} &\sim \frac{5MN_c}{96\alpha^2}\sum_\alpha\frac{\epsilon_\alpha}{|\epsilon_\alpha|}\frac{\partial}{\partial\epsilon_\alpha}\int_0^\infty \mathrm{d}x\left\{Mx^-\left\langle\alpha|\hat{p}\cdot\vec{\tau}\gamma_5|\alpha\right\rangle''_{|Mx^-|}-Mx^+\left\langle\alpha|\hat{p}\cdot\vec{\tau}\gamma_5|\alpha\right\rangle''_{|Mx^+|}\right\},\\
&= \frac{5MN_c}{96\alpha^2}\sum_\alpha\frac{\epsilon_\alpha}{|\epsilon_\alpha|}\frac{\partial}{\partial\epsilon_\alpha}\left\{\int_{-\frac{\epsilon_\alpha}{M}}^\infty \mathrm{d}y\, My\left\langle\alpha|\hat{p}\cdot\vec{\tau}\gamma_5|\alpha\right\rangle''_{|My|}-\int_{\frac{\epsilon_\alpha}{M}}^\infty \mathrm{d}y\, My\left\langle\alpha|\hat{p}\cdot\vec{\tau}\gamma_5|\alpha\right\rangle''_{My}\right\},\\
&= \frac{5MN_c}{96\alpha^2}\sum_\alpha\frac{\epsilon_\alpha}{|\epsilon_\alpha|}\frac{\partial}{\partial\epsilon_\alpha}\int_{-\frac{\omega_0}{M}}^{\frac{\omega_0}{M}} \mathrm{d}y\, My\left\langle\alpha|\hat{p}\cdot\vec{\tau}\gamma_5|\alpha\right\rangle''_{|My|}=0.
\end{aligned} \tag{7.2.6}$$

Here we took advantage of the integral being on a symmetric interval and also made use of the

notations in (6.2.10). Similarly, the integral of the matrix element without (explicit) γ_5 gives

$$\begin{aligned}\int_0^\infty \mathrm{d}x\,[\mathrm{g}_1^{I=0}(x)]_{\mathrm{s}} &\sim \frac{5MN_c}{96\alpha^2}\sum_\alpha \frac{\epsilon_\alpha}{|\epsilon_\alpha|}\frac{\partial}{\partial\epsilon_\alpha}\int_0^\infty \mathrm{d}x\left\{\left[A_+^\alpha\Big\langle\alpha|\vec{\tau}\cdot\vec{\sigma}|\alpha\Big\rangle_{|Mx_\alpha^+|} + B_+^\alpha\Big\langle\alpha|\hat{p}\cdot\vec{\tau}\hat{p}\cdot\vec{\sigma}|\alpha\Big\rangle_{|Mx_\alpha^+|}\right]\right.\\ &\left.+\left[A_-^\alpha\Big\langle\alpha|\vec{\tau}\cdot\vec{\sigma}|\alpha\Big\rangle_{|Mx_\alpha^-|} + B_-^\alpha\Big\langle\alpha|\hat{p}\cdot\vec{\tau}\hat{p}\cdot\vec{\sigma}|\alpha\Big\rangle_{|Mx_\alpha^-|}\right]\right\},\\ &= \frac{5MN_c}{96\alpha^2}\sum_\alpha \frac{\epsilon_\alpha}{|\epsilon_\alpha|}\frac{\partial}{\partial\epsilon_\alpha}\left\{\int_{\frac{\epsilon_\alpha}{M}}^\infty \mathrm{d}y\left[\Big\langle\alpha|\vec{\tau}\cdot\vec{\sigma}|\alpha\Big\rangle_{My}A_y + \Big\langle\alpha|\hat{p}\cdot\vec{\tau}\hat{p}\cdot\vec{\sigma}|\alpha\Big\rangle_{My}B_y\right]\right.\\ &\left.+\int_{-\frac{\epsilon_\alpha}{M}}^\infty \mathrm{d}y\left[\Big\langle\alpha|\vec{\tau}\cdot\vec{\sigma}|\alpha\Big\rangle_{|My|}A_y + \Big\langle\alpha|\hat{p}\cdot\vec{\tau}\hat{p}\cdot\vec{\sigma}|\alpha\Big\rangle_{|My|}B_y\right]\right\},\\ &= \frac{5MN_c}{144\alpha^2}\sum_\alpha \frac{\epsilon_\alpha}{|\epsilon_\alpha|}\frac{\partial}{\partial\epsilon_\alpha}\Big\langle\alpha|\vec{\tau}\cdot\vec{\sigma}|\alpha\Big\rangle_0 = 0,\end{aligned} \tag{7.2.7}$$

where we made use of the integration condition of equation (6.2.12). In what follows, we consider the quartic operator contributions by first integrating the term with the matrix element $\left\{\int \mathrm{d}\Omega_r \Psi_\alpha^\dagger(\vec{r})\tau_i\Psi_\beta(\vec{r})\right\}\left\{\int \mathrm{d}\Omega_p \tilde{\Psi}_\beta^\dagger(\vec{p})\hat{p}_i\gamma_5\tilde{\Psi}_\alpha(\vec{p})\right\}$. We consider the term involving the factor $\frac{\epsilon_\alpha}{|\epsilon_\alpha|}$

$$\begin{aligned}\int_0^\infty \mathrm{d}x\left[\mathrm{g}_1^{I=0}(x)\right]_{\mathrm{s}} &\sim \frac{5MN_c}{24\alpha^2}\sum_{\alpha\beta}\frac{\epsilon_\alpha}{|\epsilon_\alpha|}\frac{\langle\alpha|\tau_i|\beta\rangle}{\epsilon_\beta-\epsilon_\alpha}\int_0^\infty \mathrm{d}x\left\{-Mx_\alpha^-\Big\langle\beta|\hat{p}_i\gamma_5|\alpha\Big\rangle''_{|Mx_\alpha^-|} + Mx_\alpha^+\Big\langle\beta|\hat{p}_i\gamma_5|\alpha\Big\rangle''_{|Mx_\alpha^+|}\right\},\\ &= \frac{5MN_c}{24\alpha^2}\sum_{\alpha\beta}\frac{\epsilon_\alpha}{|\epsilon_\alpha|}\frac{\langle\alpha|\tau_i|\beta\rangle}{\epsilon_\beta-\epsilon_\alpha}\left\{-\int_{-\frac{\epsilon_\alpha}{M}}^\infty \mathrm{d}y\,My\Big\langle\beta|\hat{p}_i\gamma_5|\alpha\Big\rangle''_{|My|} + \int_{\frac{\epsilon_\alpha}{M}}^\infty \mathrm{d}y\,My\Big\langle\beta|\hat{p}_i\gamma_5|\alpha\Big\rangle''_{My}\right\},\\ &= \frac{5MN_c}{24\alpha^2}\sum_{\alpha\beta}\frac{\epsilon_\alpha}{|\epsilon_\alpha|}\frac{\langle\alpha|\tau_i|\beta\rangle}{\epsilon_\beta-\epsilon_\alpha}\int_{-\frac{\epsilon_\alpha}{M}}^{\frac{\epsilon_\alpha}{M}}\mathrm{d}y\,My\Big\langle\beta|\hat{p}_i\gamma_5|\alpha\Big\rangle''_{|My|} = 0.\end{aligned} \tag{7.2.8}$$

A similar result hold for the term multiplying $\frac{\epsilon_\beta}{|\epsilon_\beta|}$. In the next step, we consider the integration of the matrix elements without γ_5 (considering again the term involving $\frac{\epsilon_\alpha}{|\epsilon_\alpha|}$)

$$\begin{aligned}\int_0^\infty \mathrm{d}x\left[\mathrm{g}_1^{I=0}(x)\right]_{\mathrm{s}} &\sim \frac{5MN_c}{24\alpha^2}\sum_{\alpha\beta}\frac{\epsilon_\alpha}{|\epsilon_\alpha|}\frac{\langle\alpha|\tau_i|\beta\rangle}{\epsilon_\beta-\epsilon_\alpha}\int_0^\infty \mathrm{d}x\left\{\left[A_+^\alpha\Big\langle\beta|\sigma_i|\alpha\Big\rangle_{|Mx_\alpha^+|} + B_+^\alpha\Big\langle\beta|\hat{p}_i\hat{p}\cdot\vec{\sigma}|\alpha\Big\rangle_{|Mx_\alpha^+|}\right]\right.\\ &\left.+\left[A_-^\alpha\Big\langle\beta|\sigma_i|\alpha\Big\rangle_{|Mx_\alpha^-|} + B_-^\alpha\Big\langle\beta|\hat{p}_i\hat{p}\cdot\vec{\sigma}|\alpha\Big\rangle_{|Mx_\alpha^-|}\right]\right\},\\ &= \frac{5MN_c}{24\alpha^2}\sum_{\alpha\beta}\frac{\epsilon_\alpha}{|\epsilon_\alpha|}\frac{\langle\alpha|\tau_i|\beta\rangle}{\epsilon_\beta-\epsilon_\alpha}\left\{\int_{\frac{\epsilon_\alpha}{M}}^\infty \mathrm{d}y\left[\Big\langle\beta|\sigma_i|\alpha\Big\rangle_{My}A_y + \Big\langle\beta|\hat{p}_i\hat{p}\cdot\vec{\sigma}|\alpha\Big\rangle_{My}B_y\right]\right.\\ &\left.+\int_{-\frac{\epsilon_\alpha}{M}}^\infty \mathrm{d}y\left[\Big\langle\beta|\sigma_i|\alpha\Big\rangle_{|My|}A_y + \Big\langle\beta|\hat{p}_i\hat{p}\cdot\vec{\sigma}|\alpha\Big\rangle_{|My|}B_y\right]\right\},\\ &= \frac{5N_c}{36\alpha^2}\sum_{\alpha\beta}\frac{\epsilon_\alpha}{|\epsilon_\alpha|}\frac{\langle\alpha|\tau_i|\beta\rangle}{\epsilon_\beta-\epsilon_\alpha}\Big\langle\beta|\sigma_i|\alpha\Big\rangle_0,\end{aligned} \tag{7.2.9}$$

Using the relation in equation (6.2.12), the quartic spinor term with $\hat{p}_i\hat{p}\cdot\vec{\sigma}$ vanishes. Combining the results from the terms involving $\frac{\epsilon_\beta}{|\epsilon_\beta|}$ we obtain the vacuum contribution to the axial-singlet charge

$$(\Gamma_1^p+\Gamma_1^n)_{\mathrm{s}} = \int \mathrm{d}x\,[\mathrm{g}_1^p(x)+\mathrm{g}_1^n(x)]_{\mathrm{s}} = -\frac{5N_c}{36\alpha^2}\sum_{\alpha\beta}\left(\frac{\epsilon_\alpha}{|\epsilon_\alpha|}-\frac{\epsilon_\beta}{|\epsilon_\beta|}\right)\frac{\langle\alpha|\tau_i|\beta\rangle}{\epsilon_\beta-\epsilon_\alpha}\Big\langle\beta|\sigma_i|\alpha\Big\rangle_0 = \left[g_A^0\right]_{\mathrm{s}}. \tag{7.2.10}$$

m	$(\Gamma_1^p+\Gamma_1^n)_{\rm v}$	$[g_A^0]_{\rm v}$	$(\Gamma_1^p+\Gamma_1^n)_{\rm s}$	$[g_A^0]_{\rm s}$
400	0.344	0.348	0.00157	0.00141
450	0.327	0.331	0.00214	0.00187
500	0.316	0.321	0.00282	0.00237

Table 7.3: Verification of the axial-singlet charge of our calculations cf. equation (7.2.9) to the exact calculations $g_A^0 \sim \langle\alpha_3\gamma_5\rangle$ cf. equation (7.2.12) for different constituent quark masses m (in MeV).

m	$(\Gamma_1^p+\Gamma_1^n)_{\rm v}$	$(\Gamma_1^p+\Gamma_1^n)_{\rm s}$	$\Gamma_1^p+\Gamma_1^n$
400	0.344	0.00157	0.345
450	0.327	0.00214	0.329
500	0.316	0.00282	0.318

Table 7.4: Numerical prediction of the axial singlet charge for various constituent quark masses m (in MeV).

A similar calculation starting from equation (7.2.5) gives the valence quark contribution

$$(\Gamma_1^p+\Gamma_1^n)_{\rm v} = \int {\rm d}x\,[{\rm g}_1^p(x)+{\rm g}_1^n(x)]_{\rm v} = -\frac{5N_c}{18\alpha^2}\eta_{\rm v}\sum_{{\rm v}\neq\beta}\frac{\langle {\rm v}|\tau_i|\beta\rangle}{\epsilon_{\rm v}-\epsilon_\beta}\Big\langle\beta|\sigma_i|{\rm v}\Big\rangle_0 = \Big[g_A^0\Big]_{\rm v}. \tag{7.2.11}$$

Then the total axial-singlet charge becomes

$$g_A^0 = -\frac{5N_c}{18\alpha^2}\left[\eta_{\rm v}\sum_{{\rm v}\neq\beta}\frac{\langle {\rm v}|\tau_3|\beta\rangle}{\epsilon_{\rm v}-\epsilon_\beta}\langle\beta|\sigma_3|{\rm v}\rangle + \frac{1}{2}\sum_{\alpha\beta}\left(\frac{\epsilon_\alpha}{|\epsilon_\alpha|}-\frac{\epsilon_\beta}{|\epsilon_\beta|}\right)\frac{\langle\alpha|\tau_3|\beta\rangle}{\epsilon_\beta-\epsilon_\alpha}\langle\beta|\sigma_3|\alpha\rangle\right]. \tag{7.2.12}$$

The comparison of the direct calculations of axial-singlet charge, cf. equation (7.2.12), to the numerical evaluation of $\Gamma_1^p+\Gamma_1^n$, is shown in Table 7.3. The agreement from this table reflects the accuracy of our numerical procedure in evaluating this structure function. Though $[g_A^0]_{\rm s}$ has sizeable relative deviations from the sum rule, the absolute error is tiny. We note that each level in sums like equation (7.2.5) contributes an amount of the order of the valence quark counterpart. In Table 7.4 we display our theoretical prediction for the axial singlet charge for various constituent quark mass. Our results are in good agreement with the empirical value for the singlet axial charge $\Delta\Sigma \sim 0.31 \pm 0.07$ [71]. One should note that, the authors of Refs. [71] base their analysis on $SU(3)$ flavor symmetry. As can be seen from the table the valence contribution is dominant.

7.3 Numerical Calculations of the Flavor-Singlet Transverse Polarized Structure Function

Similar to the previous calculations, we substitute the Fourier transforms of the eigenfunctions into equation (7.0.6). Then using the identities in equations (7.1.2)- (7.1.5), writing the integration variable into spherical coordinate cf. (6.1.6) and averaging over the photon direction gives the vacuum contribution of the flavor-singlet transverse polarized structure function in

the RF at leading order $\frac{1}{N_c}$ as

$$\begin{aligned}\left[\mathrm{g}_T^{I=0}(x)\right]_{\mathrm{s}}^{\mp} = -\frac{5MN_c}{48\alpha^2}\sum_{\alpha}\Bigg\{&\frac{\epsilon_\alpha}{|\epsilon_\alpha|}\frac{\partial}{\partial\epsilon_\alpha}\int_{|Mx_\alpha^{\pm}|}^{\infty}p^2\mathrm{d}p\left[C_{\pm}^{\alpha}\int\mathrm{d}\Omega_p\tilde{\Psi}_\alpha^\dagger(\vec{p})\vec{\tau}\cdot\vec{\sigma}\tilde{\Psi}_\alpha(\vec{p})-B_{\pm}^{\alpha}\int\mathrm{d}\Omega_p\tilde{\Psi}_\alpha^\dagger(\vec{p})\hat{p}\cdot\vec{\tau}\hat{p}\cdot\vec{\sigma}\tilde{\Psi}_\alpha(\vec{p})\right]\\
&-\sum_{\beta}\frac{\langle\alpha|\tau_i|\beta\rangle}{\epsilon_\beta-\epsilon_\alpha}\Bigg(\frac{\epsilon_\alpha}{|\epsilon_\alpha|}\int_{|Mx_\alpha^{\pm}|}^{\infty}p^2\mathrm{d}p\left[-C_{\pm}^{\alpha}\int\mathrm{d}\Omega_p\,\mathrm{tr}\,\tilde{\Psi}_\beta^\dagger(\vec{p})\sigma_i\tilde{\Psi}_\alpha(\vec{p})+B_{\pm}^{\alpha}\int\mathrm{d}\Omega_p\tilde{\Psi}_\beta^\dagger(\vec{p})\hat{p}_i\hat{p}\cdot\vec{\sigma}\tilde{\Psi}_\alpha(\vec{p})\right]\\
&-\frac{\epsilon_\beta}{|\epsilon_\beta|}\int_{|Mx_\beta^{\pm}|}^{\infty}p^2\mathrm{d}p\left[-C_{\pm}^{\beta}\int\mathrm{d}\Omega_p\tilde{\Psi}_\beta^\dagger(\vec{p})\sigma_i\tilde{\Psi}_\alpha(\vec{p})+B_{\pm}^{\beta}\int\mathrm{d}\Omega_p\tilde{\Psi}_\beta^\dagger(\vec{p})\hat{p}_i\hat{p}\cdot\vec{\sigma}\tilde{\Psi}_\alpha(\vec{p})\right]\Bigg)\Bigg\},\end{aligned}\tag{7.3.1}$$

where the definitions of equation (7.2.2) have been employed for $B_{\pm}^{\alpha}$ as well as

$$C_{\pm}^{\alpha}=\frac{1}{2p}\left(1+\frac{(Mx_\alpha^{\pm})^2}{p^2}\right)\quad\text{and}\quad C_{\pm}^{\beta}=\frac{1}{2p}\left(1+\frac{(Mx_\beta^{\pm})^2}{p^2}\right).\tag{7.3.2}$$

As before, $\left[\mathrm{g}_T^{I=0}(x)\right]_{\mathrm{s}}^{\mp}$ denotes the antiquark and quark distributions, respectively. Their sum gives the total distribution of the isoscalar transverse polarized structure function. Its valence quark counterpart reads

$$\begin{aligned}\left[\mathrm{g}_T^{I=0}(x)\right]_{\mathrm{v}}^{\mp} = \frac{5MN_c}{12\alpha^2}\sum_{\alpha\neq\mathrm{v}}\frac{1}{\epsilon_{\mathrm{v}}-\epsilon_\alpha}N_\alpha\int_{|Mx_{\mathrm{v}}^{\pm}|}^{\infty}p\mathrm{d}p\Bigg[&-\tilde{g}_{\mathrm{v}}(p)\tilde{g}_\alpha^{(2)}(p)+\frac{1}{\sqrt{8}}\left(3\frac{(Mx_{\mathrm{v}}^{\pm})^2}{p^2}-1\right)\tilde{g}_{\mathrm{v}}(p)\tilde{g}_\alpha^{(1)}(p)\\
&+\frac{(Mx_{\mathrm{v}}^{\pm})^2}{p^2}\tilde{f}_{\mathrm{v}}(p)\tilde{f}_\alpha^{(2)}(p)-\frac{1}{\sqrt{8}}\left(3-\frac{(Mx_{\mathrm{v}}^{\pm})^2}{p^2}\right)\tilde{f}_{\mathrm{v}}(p)\tilde{f}_\alpha^{(1)}(p)\Bigg].\end{aligned}\tag{7.3.3}$$

We note that the $\vec{\sigma}$ matrix that appears in the structure functions is a two-by-two Dirac component matrix as defined in equation (6.3.5).

Next, we extract the polarized structure function $\mathrm{g}_2^{I=0}(x)$ directly as $\mathrm{g}_T^{I=0}(x)-\mathrm{g}_1^{I=0}$ using equation (6.3.6). We write it explicitly in order to study the sum rules. Subtracting equation (7.2.1) from equation (7.3.1) gives the vacuum contribution

$$\begin{aligned}\left[\mathrm{g}_2^{I=0}(x)\right]_{\mathrm{s}}^{\mp} = \frac{5MN_c}{48\alpha^2}\sum_{\alpha}\Bigg\{&\frac{1}{4}\frac{\epsilon_\alpha}{|\epsilon_\alpha|}\frac{\partial}{\partial\epsilon_\alpha}\Bigg[\mp2\int_{|Mx_\alpha^{\pm}|}^{\infty}\mathrm{d}p\,Mx_\alpha^{\pm}\int\mathrm{d}\Omega_p\tilde{\Psi}_\alpha^\dagger(\vec{p})\hat{p}\cdot\vec{\tau}\gamma_5\tilde{\Psi}_\alpha(\vec{p})\\
&-\int_{|Mx_\alpha^{\pm}|}^{\infty}\mathrm{d}p\,p^2\left(-B_{\pm}^{\alpha}\int\mathrm{d}\Omega_p\tilde{\Psi}_\alpha^\dagger(\vec{p})\vec{\tau}\cdot\vec{\sigma}\tilde{\Psi}_\alpha(\vec{p})+3B_{\pm}^{\alpha}\int\mathrm{d}\Omega_p\tilde{\Psi}_\alpha^\dagger(\vec{p})\hat{p}\cdot\vec{\tau}\hat{p}\cdot\vec{\sigma}\tilde{\Psi}_\alpha(\vec{p})\right)\Bigg]\\
&-\sum_{\beta}\frac{\langle\alpha|\tau_i|\beta\rangle}{\epsilon_\beta-\epsilon_\alpha}\Bigg(\frac{\epsilon_\alpha}{|\epsilon_\alpha|}\Bigg[\pm2\int_{|Mx_\alpha^{\pm}|}^{\infty}\mathrm{d}p\,Mx_\alpha^{\pm}\int\mathrm{d}\Omega_p\tilde{\Psi}_\beta^\dagger(\vec{p})\hat{p}_i\gamma_5\tilde{\Psi}_\alpha(\vec{p})\\
&+\int_{|Mx_\alpha^{\pm}|}^{\infty}\mathrm{d}p\,p^2\left(-B_{\pm}^{\alpha}\int\mathrm{d}\Omega_p\tilde{\Psi}_\beta^\dagger(\vec{p})\sigma_i\tilde{\Psi}_\alpha(\vec{p})+3B_{\pm}^{\alpha}\int\mathrm{d}\Omega_p\tilde{\Psi}_\beta^\dagger(\vec{p})\hat{p}_i\hat{p}\cdot\vec{\sigma}\tilde{\Psi}_\alpha(\vec{p})\right)\Bigg]\\
&+\frac{\epsilon_\beta}{|\epsilon_\beta|}\Bigg[\mp2\int_{|Mx_\beta^{\pm}|}^{\infty}\mathrm{d}p\,Mx_\beta^{\pm}\int\mathrm{d}\Omega_p\tilde{\Psi}_\beta^\dagger(\vec{p})\hat{p}_i\gamma_5\tilde{\Psi}_\alpha(\vec{p})\\
&-\int_{|Mx_\beta^{\pm}|}^{\infty}\mathrm{d}p\,p^2\left(-B_{\pm}^{\beta}\int\mathrm{d}\Omega_p\tilde{\Psi}_\beta^\dagger(\vec{p})\sigma_i\tilde{\Psi}_\alpha(\vec{p})+3B_{\pm}^{\beta}\int\mathrm{d}\Omega_p\tilde{\Psi}_\beta^\dagger(\vec{p})\hat{p}_i\hat{p}\cdot\vec{\sigma}\tilde{\Psi}_\alpha(\vec{p})\right)\Bigg]\Bigg)\Bigg\}.\end{aligned}\tag{7.3.4}$$

m	$[\Gamma_2^p + \Gamma_2^n]_v$	$[\Gamma_2^p + \Gamma_2^n]_s$	$\Gamma_2^p + \Gamma_2^n$
400	4.58×10^{-7}	1.36×10^{-4}	1.37×10^{-4}
450	2.43×10^{-6}	2.53×10^{-4}	2.56×10^{-4}
500	3.37×10^{-7}	4.40×10^{-4}	4.41×10^{-4}

Table 7.5: Numerical verification of the Burkhardt-Cottingham sum rule for different constituent quark masses m (in MeV).

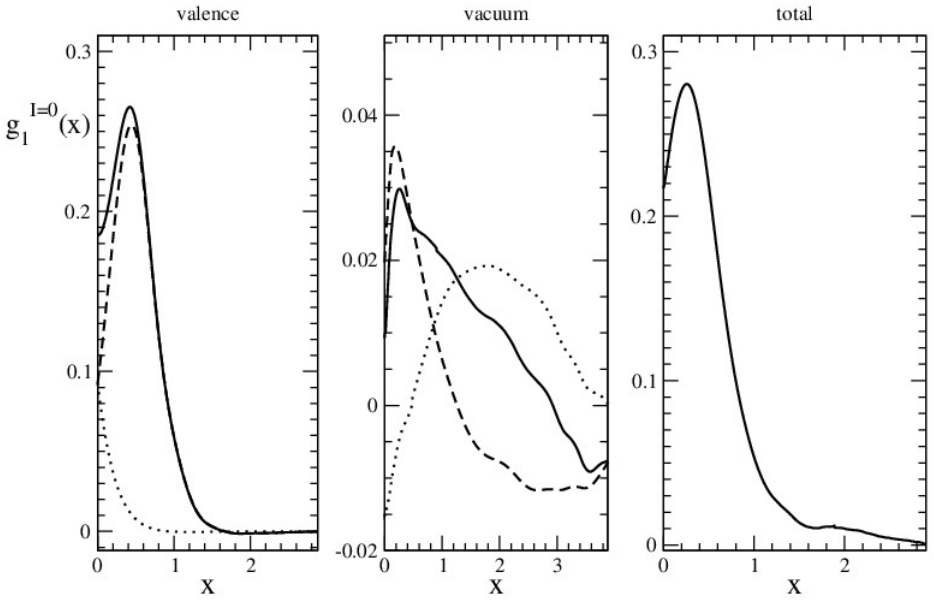

Figure 7.3: The numerical predictions for the flavor singlet longitudinal polarized structure function for $m = 400\,\text{MeV}$. The dotted lines in the graphs for the valence and vacuum contributions denote the anti-quark distributions, the dashed lines denote the quark distributions and the solid lines denote the sum of quark and anti-quark distribution, respectively.

Similarly subtracting equation (7.2.5) from equation (7.3.3) gives the valence contribution as

$$\begin{aligned}\left[g_2^{I=0}(x)\right]_{\rm v}^{\mp} = \frac{5MN_c}{24\alpha^2}\sum_{\alpha\neq {\rm v}}\frac{1}{\epsilon_{\rm v}-\epsilon_\alpha}N_\alpha\int_{|Mx_{\rm v}^{\pm}|}^{\infty}p{\rm d}p\Bigg[\\ \mp\frac{(Mx_{\rm v}^{\pm})^2}{p^2}\tilde{g}_{\rm v}(p)\tilde{f}_\alpha^2(p)\mp\frac{(Mx_{\rm v}^{\pm})^2}{p^2}\tilde{f}_{\rm v}(p)\tilde{g}_\alpha^2(p)\mp\sqrt{2}\frac{(Mx_{\rm v}^{\pm})^2}{p^2}\tilde{g}_{\rm v}(p)\tilde{f}_\alpha^1(p) \\ \mp\sqrt{2}\frac{(Mx_{\rm v}^{\pm})^2}{p^2}\tilde{f}_{\rm v}(p)\tilde{g}_\alpha^1(p)+2\left(3\frac{(Mx_{\rm v}^{\pm})^2}{p^2}-1\right)\tilde{f}_{\rm v}(p)\tilde{f}_\alpha^2(p) \\ +\frac{1}{\sqrt{2}}\left(3\frac{(Mx_{\rm v}^{\pm})^2}{p^2}-1\right)\tilde{f}_{\rm v}(p)\tilde{f}_\alpha^1(p)+\frac{3}{\sqrt{2}}\left(3\frac{(Mx_{\rm v}^{\pm})^2}{p^2}-1\right)\tilde{g}_{\rm v}(p)\tilde{g}_\alpha^1(p)\Bigg].\end{aligned} \tag{7.3.5}$$

In the next step, we verify the Burkhardt-Cottingham sum rule[69]. The contribution for the quadratic spinor terms has already been discussed in subsection 6.3.1. In what follows we consider the quartic spinor terms. The contribution from the matrix element $\hat{p}_i\gamma_5$ has already been discussed in equation (7.2.8). For the contribution from the matrix element without γ_5 (

explicitly) we get (considering the term involving $\frac{\epsilon_\alpha}{|\epsilon_\alpha|}$)

$$\begin{aligned}\int_0^\infty \mathrm{d}x \left[\mathrm{g}_2^{I=0}(x)\right]_{\mathrm{s}} &= -\frac{5MN_c}{48\alpha^2}\sum_{\alpha\beta}\frac{\epsilon_\alpha}{|\epsilon_\alpha|}\frac{\langle\alpha|\tau_i|\beta\rangle}{\epsilon_\beta-\epsilon_\alpha}\int_0^\infty \mathrm{d}x\left\{\left[-B_+^\alpha\Big\langle\beta|\sigma_i|\alpha\Big\rangle_{|Mx_\alpha^+|}+3B_+^\alpha\Big\langle\beta|\hat{p}_i\hat{p}\cdot\vec{\sigma}|\alpha\Big\rangle_{|Mx_\alpha^+|}\right]\right.\\ &\quad\left.+\left[-B_-^\alpha\Big\langle\beta|\sigma_i|\alpha\Big\rangle_{|Mx_\alpha^-|}+3B_-^\alpha\Big\langle\alpha|\hat{p}_i\hat{p}\cdot\vec{\sigma}|\alpha\Big\rangle_{|Mx_\alpha^-|}\right]\right\},\\ &= -\frac{5MN_c}{48\alpha^2}\sum_{\alpha\beta}\frac{\epsilon_\alpha}{|\epsilon_\alpha|}\frac{\langle\alpha|\tau_i|\beta\rangle}{\epsilon_\beta-\epsilon_\alpha}\left\{\int_{\frac{\epsilon_\alpha}{M}}^\infty \mathrm{d}y\left[-B_y\Big\langle\beta|\sigma_i|\alpha\Big\rangle_{My}+3B_y\Big\langle\beta|\hat{p}_i\hat{p}\cdot\vec{\sigma}|\alpha\Big\rangle_{My}\right]\right.\\ &\quad\left.+\int_{-\frac{\epsilon_\alpha}{M}}^\infty \mathrm{d}y\left[-B_y\Big\langle\beta|\sigma_i|\alpha\Big\rangle_{|My|}+3B_y\Big\langle\alpha|\hat{p}_i\hat{p}\cdot\vec{\sigma}|\alpha\Big\rangle_{|My|}\right]\right\}=0. \qquad (7.3.6)\end{aligned}$$

In the last line we made use of the identity in equation (6.2.12). Similar results hold for terms with $\frac{\epsilon_\beta}{|\epsilon_\beta|}$. Thus, we have the Burkhardt-Cottingham sum rule for the vacuum contribution to the longitudinal polarized structure function as

$$[\Gamma_2^p+\Gamma_2^n]_{\mathrm{s}}=\int_0^\infty \mathrm{d}x\ [\mathrm{g}_2^p(x)+\mathrm{g}_2^n(x)]_{\mathrm{s}}=0. \qquad (7.3.7)$$

Similarly, we have the valence contribution as

$$[\Gamma_2^p+\Gamma_2^n]_{\mathrm{v}}=\int_0^\infty \mathrm{d}x\ [\mathrm{g}_2^p(x)+\mathrm{g}_2^n(x)]_{\mathrm{v}}=0. \qquad (7.3.8)$$

The numerical verification of this sum rule is shown in Table 7.5.

7.3.1 Discussion of the Numerical Results for the Flavor-Singlet Polarized Structure Functions

In this section we discuss the numerical results of the flavor-singlet polarized structure functions. We note from our calculations that, the vacuum polarization contribution for these functions is unregularized. This indicates that they are associated with the imaginary part of the semi-bosonized effective action cf. equation (2.2.19) (when continuing to Euclidean space). In Figures 7.3, 7.4 and 7.5 we display the numerical results for the flavor-singlet longitudinal, transverse and that of the polarized structure function $\mathrm{g}_2^{I=0}$ respectively, for $m = 400\,\mathrm{MeV}$. For the flavor-singlet longitudinal polarized structure function, we observe a region in x-space where the vacuum contribution is negative. But this is negligible and has almost no effect on the total contribution, because the valence quark part dominates.

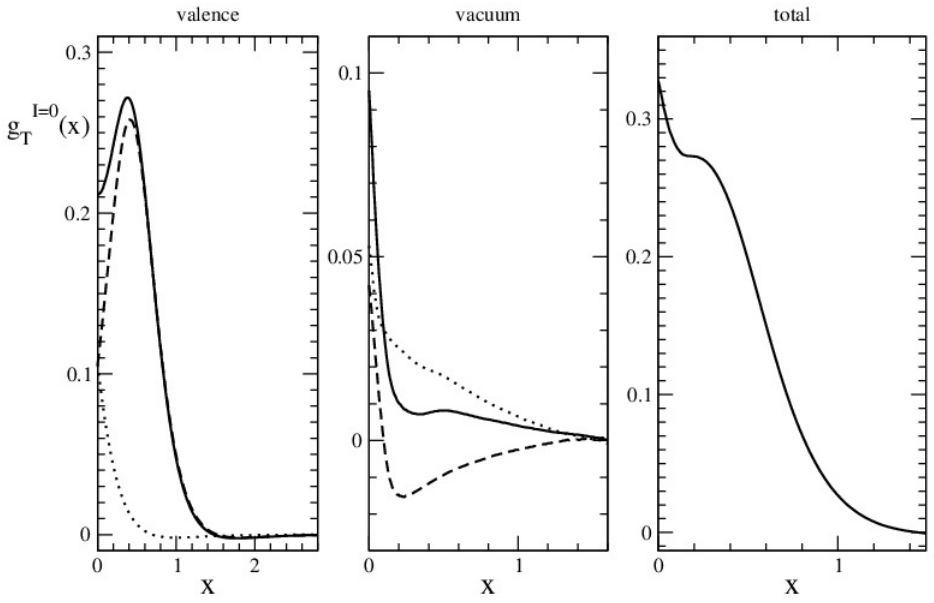

Figure 7.4: The numerical predictions for the flavor singlet transverse polarized structure function for $m = 400\,\text{MeV}$. The dotted lines in the graphs for the valence and vacuum contributions denote the anti-quark distributions, the dashed lines denote the quark distributions and the solid lines denote the sum of quark and anti-quark distribution, respectively.

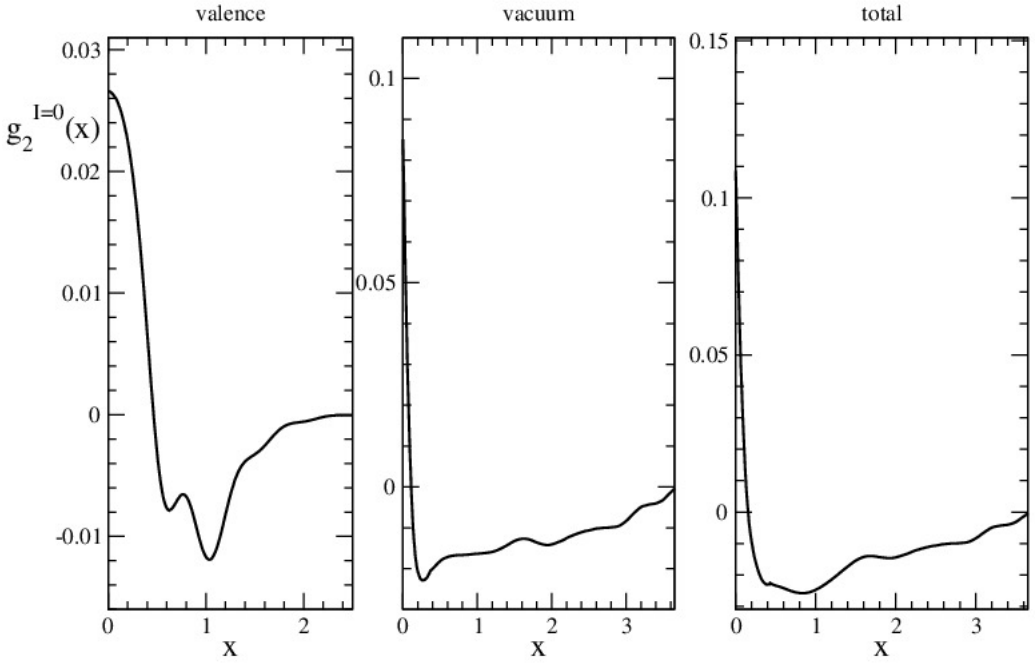

Figure 7.5: The numerical predictions for the flavor-singlet polarized proton structure function, $g_2^{I=0}(x)$, for $m = 400\,\text{MeV}$.

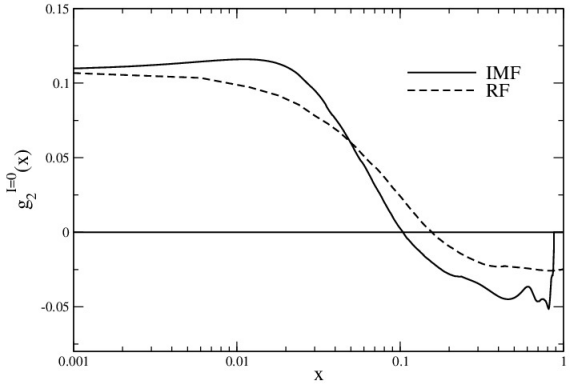

Figure 7.6: The sum of valence and vacuum contributions for the flavor-singlet polarized structure function, $\mathrm{g}_2^{I=0}(x)$ for $m = 400\,\mathrm{MeV}$. The curve labeled "RF" denotes the result obtained from the nucleon rest frame and the one labeled "IMF" denotes the projection to the infinite momentum frame equation (6.1.25).

For the flavor-singlet transverse polarized structure there is a significant contribution from the polarized vacuum thereby affecting the total $\mathrm{g}_T^{I=0}$ when compared to the isovector case. Similarly, the vacuum contribution to the flavor-singlet $\mathrm{g}_2^{I=0}$ structure function dominates over the valence counterpart.

The above results have non-zero local support for $x > 1$. This non-locality account about 0.2% to the axial-singlet charge of the longitudinal flavor-singlet polarized structure function. To restore Lorentz covariance, such that the structure functions are well localized in kinematical interval $0 \leq x \leq 1$, we transform to the infinite momentum frame. In Figure 7.6 we display the effects that this transformation has on the flavor-singlet structure function $\mathrm{g}_2^{I=0}(x)$.

Chapter 8

DGLAP Evolution and the Operator-Product-Expansion

So far we have computed the structure functions within the NJL soliton model. This model (presumably) approximates QCD at some low energy scale μ^2, which is different from the high energy scale Q^2 at which DIS data are available. In this chapter we adopt the (leading order) QCD evolution approach to evolve our NJL model structure functions perturbatively to the relevant Q^2 region. In this procedure μ^2 becomes an adjustable parameter. To be specific we will employ the Altarelli-Parisi evolution equation [72]. We then compare the evolved structure functions to the empirical DIS data. Though being only leading order, this procedure will sensibly test the relevance of our predictions. We will also discuss the operator-product-expansion (OPE) method for the spin-dependent structure functions. The OPE analysis will give qualitative information about the second-spin structure function $\mathrm{g}_2(x)$ and also identifies its twist-3 components. The twist-3 operators arise from the effects of quark-gluon correlations and quark masses [68, 73, 74].

8.1 Violation of Bjorken Scaling and Splitting Functions

In the NJL model calculations of DIS for hadrons gluons do not appear as force carrier of the associated colored quark interactions. That is, our model description for DIS processes ignores the possibility of the quarks to radiate gluons. To account for the collinear emission of gluons and quarks we consider three possibilities: In the first case the quark at a vertex can split into a quark and a gluon. Also there is a possibility of the gluon to split into a quark-antiquark pair. Furthermore, the gluon can split into two gluons. These possibilities are shown in Figure 8.1. One observable consequence of the above is that the Bjorken scaling is violated in the collinear emission processes. To account for this violation in our NJL model prediction we resort to the Altarelli-Parisi equations that are discussed below. This introduces a logarithmic dependence on Q^2. The appearance of this dependence signals the breaking of the Bjorken scaling, which is initiated by the emission of gluons. Incorporating these processes yields the evolution equations

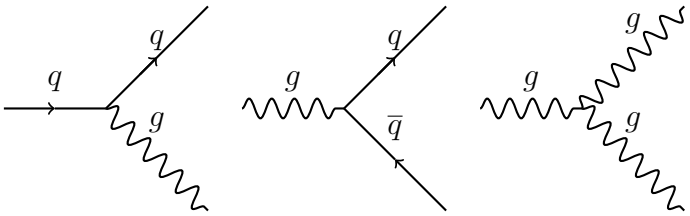

Figure 8.1: The three contributions to the leading order of the QCD evolution.

in terms of the splitting functions. This scaling violation provides a platform to compare our model results to experimental data. In normal practice, the Altarelli-Parisi equations are employed to evolve the model structure functions to larger Q^2 values causing it to decrease at large x. As such they are dominated by the leading order in $g_{QCD}(Q^2)$. Thus the probability of finding a quark at small x increases.

8.2 Evolution of the Longitudinal Polarized Structure Function

Let us first discuss the longitudinal polarized structure functions $\mathrm{g}_1(x)$. In the next step, we apply the leading order Altarelli-Parisi equations [72] to evolve this structure function perturbatively to the higher Q^2 region where the experiments of the functions are performed. Formally the evolution is performed by integrating [47]

$$h(x, t + \delta t) = h(x, t) + \delta t \frac{\mathrm{d}h(x, t)}{\mathrm{d}t}, \tag{8.2.1}$$

where $t = 2\ln\left(\dfrac{Q}{\Lambda_{QCD}}\right)$. Here $h(x, t)$ represents both isovector and isosinglet polarized and unpolarized functions. Now since in the DIS processes gluons are emitted, we take into account

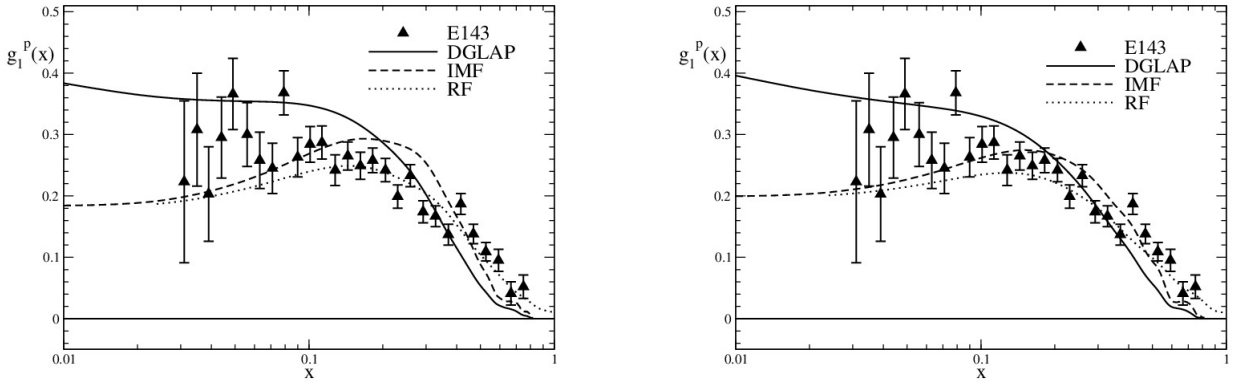

(a) (b)

Figure 8.2: The numerical prediction for the polarized proton structure function (a) $\mathrm{g}_1^{I=1}$ for $m = 400\,\mathrm{MeV}$, (b) $\mathrm{g}_1^{I=1}$ for $m = 450\,\mathrm{MeV}$ compared to experimental data from [1] E143 Collaborations. We have also displayed the statistical errors of those data. These functions are "DGLAP" evolved from $\mu^2 = 0.4\,\mathrm{GeV}^2$ to $Q^2 = 3\,\mathrm{GeV}^2$ after projected to the infinite momentum frame "IMF".

the gluon contributions for both structure functions. The second term on the right hand side of (8.2.1) emerges as an integro-differential equation in perturbation QCD. For isovector, isosinglet and gluon contributions they read[54]

$$\frac{\mathrm{d}h^{(I=1)}(x,t)}{\mathrm{d}t} = \frac{g_{QCD}(t)}{2\pi} C_R(F) \int_x^1 \frac{\mathrm{d}y}{y} P_{qq}(y) h^{(I=1)}\left(\frac{x}{y}, t\right), \tag{8.2.2}$$

$$\frac{\mathrm{d}h^{(I=0)}(x,t)}{\mathrm{d}t} = \frac{g_{QCD}(t)}{2\pi} C_R(F) \int_x^1 \frac{\mathrm{d}y}{y} \left\{ P_{qq}(y) h^{(I=0)}\left(\frac{x}{y}, t\right) + P_{qg}(y) g\left(\frac{x}{y}, t\right) \right\}, \tag{8.2.3}$$

$$\frac{\mathrm{d}g(x,t)}{\mathrm{d}t} = \frac{g_{QCD}(t)}{2\pi} C_R(F) \int_x^1 \frac{\mathrm{d}y}{y} \left\{ P_{gg}(y) g\left(\frac{x}{y}, t\right) + P_{gq}(y) h^{(I=0)}\left(\frac{x}{y}, t\right) \right\}, \tag{8.2.4}$$

respectively. Note that gluon and isosinglet pieces mix because of their identical quantum numbers. Also the splitting functions P_{nm} are different for the isovector, isosinglet and gluon contributions. They are given as [72, 75]

$$\begin{aligned} P_{qq}(z) &= \frac{1+z^2}{(1-z)_+}, \\ P_{qg}(z) &= \frac{1}{2C_R(F)} \left[z^2 + (1-z)^2\right], \\ P_{gq}(z) &= \frac{1+(1-z)^2}{z}, \\ P_{gg}(z) &= 2\left[\frac{1-z}{z} + \frac{z}{(1-z)_+} + z(1-z)\right]. \end{aligned} \tag{8.2.5}$$

These functions determine the probability for the parton n to emit a parton m such that the momentum of the parton n is reduced by the fraction z. The regularized function $(1-z)_+^{-1}$ is defined under the integral by [72]

$$\int_0^1 \mathrm{d}z \, \frac{f(z)}{(1-z)_+} = \int_0^1 \mathrm{d}z \, \frac{f(z) - f(1)}{1-z}. \tag{8.2.6}$$

The color factor $C_R(F)$ is defined as

$$C_R(F) = \frac{1}{N_f} \mathrm{tr}(t^a t^a) = \frac{\left(N_f^2 - 1\right)}{2N_f} \tag{8.2.7}$$

for N_f flavors and the running coupling constant in the leading order is given by

$$g_{QCD}(t) = \frac{4\pi}{\beta_0 t} \tag{8.2.8}$$

with $\beta_0 = \frac{11}{3} N_c - \frac{2}{3} N_f$ being the coefficient of the leading term of the QCD β-function. Using equations (8.2.5) and (8.2.6), the evolution equations for the isovector, isosinglet and gluon

contributions become [75]

$$\begin{aligned}
\frac{\mathrm{d}h^{(I=1)}(x,t)}{\mathrm{d}t} &= \frac{2C_R(F)}{9t}\Bigg\{\int_x^1 \frac{\mathrm{d}y}{y}\left(\frac{1+y^2}{1-y}\right)\left[\frac{1}{y}h^{(I=1)}\left(\frac{x}{y},t\right)-h^{(I=1)}(x,t)\right] \\
&\quad + \left[x+\frac{x^2}{2}+2\ln(1-x)\right]h^{(I=1)}(x,t)\Bigg\}, \\
\frac{\mathrm{d}h^{(I=0)}(x,t)}{\mathrm{d}t} &= \frac{2C_R(F)}{9t}\Bigg\{\int_x^1 \frac{\mathrm{d}y}{y}\Bigg(\left(\frac{1+y^2}{1-y}\right)\left[\frac{1}{y}h^{(I=0)}\left(\frac{x}{y},t\right)-h^{(I=0)}(x,t)\right] \\
&\quad + \frac{3}{4}\left(y^2+(1-y^2)\right)\frac{g(x,t)}{y}\Bigg) + \left[x+\frac{x^2}{2}+2\ln(1-x)\right]h^{I=0}(x,t)\Bigg\}, \\
\frac{\mathrm{d}g(x,t)}{\mathrm{d}t} &= \frac{2C_R(F)}{9t}\Bigg\{\int_x^1 \frac{\mathrm{d}y}{y}\Bigg(\left(\frac{1+(1-y)^2}{y}\right)h^{(I=0)}\left(\frac{x}{y},t\right) \\
&\quad + \frac{9}{2}\left(\frac{1-y}{y}+y^2(1-y)\right)\frac{g\left(\frac{x}{y},t\right)}{y} + \frac{9}{2}\frac{g\left(\frac{x}{y},t\right)-g(x,t)}{1-y}\Bigg) + \left[\frac{3}{2}+\frac{9}{2}\ln(1-x)\right]g(x,t)\Bigg\}. \qquad (8.2.9)
\end{aligned}$$

Now, since our NJL model calculations do not account for any gluon content in the nucleon, we assume in our numerical calculations that, at the initial boundary scale μ^2, the gluon content, $g(x,t_0)=0$ for both the polarized and unpolarized structure functions, where $t_0 = 2\ln\left(\frac{\mu}{\Lambda_{QCD}}\right)$ is the initial momentum from which the evolution equations are integrated.

In applying this evolution to the NJL structure functions, we have taken the QCD scale parameter Λ_{QCD} to be $0.2\,\mathrm{GeV}^2$. We achieve convergence of the integro-differential equations after performing 201 iterations. For the NJL model calculations to approximate QCD, we choose a reliable low-scale energy μ^2, so as to achieve a best fit to the experimental data (given at large Q^2) for the structure function. In doing so we obtain $\mu^2 = 0.4\,\mathrm{GeV}^2$. This approximate scale ($\mu^2 = 0.4\,\mathrm{GeV}^2$) has also been estimated by the authors in Refs.[46, 47, 76] to best fit the experimental data. The integration of the evolution equations to Q^2 is performed separately to both the isovector and isosinglet components of the NJL structure functions, which are later combined using

$$h^{(p,n)}(x) = h^{I=1}(x) \pm h^{I=0}(x), \qquad (8.2.10)$$

where the plus '(+)' term indicate the proton(p) contribution and the minus '(−)' term indicate the neutron(n) contributions, respectively. In the case of the polarized structure function, we focus our discussion on the proton contributions.

In Figures 8.2 and 8.3 , we presents the numerical results of the polarized proton structure functions $\mathrm{g}_1^p(x)$ and $x\mathrm{g}_1^p(x)$ using the evolution equation. We have compared our results to experimental results from [1, 2] E143 Collaboration. Here we solve the leading order evolution equation from the initial boundary scale $\mu^2 = 0.4\,\mathrm{GeV}^2$ to obtain the structure function at $Q^2 = 3\,\mathrm{GeV}^2$. One observes that after applying the DGLAP evolution our model predictions reproduce the qualitative features of the experimental data. Another remarkable feature of the evolution is that its enhances the structure function at small x region, thereby improving the agreement with the experimental data.

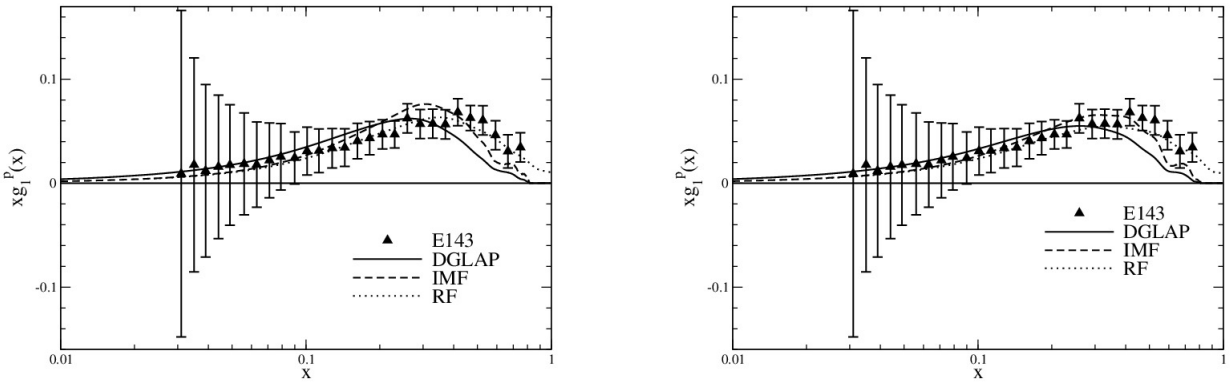

(a) (b)

Figure 8.3: The numerical prediction for the polarized proton structure function (a) $x\mathrm{g}_1^{I=1}$ for $m = 400\,\mathrm{MeV}$, (b) $x\mathrm{g}_1^{I=1}$ for $m = 450\,\mathrm{MeV}$ compared to experimental data from [2] E143 Collaboration. These functions are "DGLAP" evolved from $\mu^2 = 0.4\,\mathrm{GeV}^2$ to $Q^2 = 3\,\mathrm{GeV}^2$ after projected to the infinite momentum frame "IMF".

8.3 The Operator Product Expansion and Twist Operators

The OPE is normally used in studying the properties of structure functions in the DIS processes of QCD. The starting point is the expansion of the products of electromagnetic currents that appear in the Compton tensor, cf. equation (1.6.10), at light cone separations in terms of renormalized (at scale μ^2) operators [68, 73, 74]. In the Bjorken limit the importance of these operators is characterized by their twist (τ) or light-cone singularity of their coefficient functions. The twist-2 and twist-3 operators are given as $O_{2,i}^{\sigma\mu_1\cdots\mu_n}(\mu^2)$ and $O_{3,i}^{\sigma\mu_1\cdots\mu_n}(\mu^2)$, respectively. Where the Lorentz indices are symmetric in the case of the twist-2 operators but in the case of the twist-3 operators $\mu_1 \ldots \mu_n$ are symmetric with each other and antisymmetric with σ. Parametrizing the matrix element of these operators, the Compton tensor can be formulated as a power series in the inverse of the Bjorken variable x [47]

$$T_{\mu\nu}(p,q) = \sum_{n,i,\tau} \left(\frac{1}{x}\right)^n e^i_{\mu\nu}(q,p,s) C^n_{\tau,i}\left(\frac{Q^2}{\mu^2}, g^2_{QCD}(\mu^2)\right) a^n_{\tau,i}(\mu^2) \left(\frac{1}{Q^2}\right)^{\frac{\tau}{2}-1}. \tag{8.3.1}$$

Here $a^n_{\tau,i}(\mu^2)$ denote the scalar matrix elements and arises from the parametrized operators

$$\langle p,s|O^{\sigma\mu_1\cdots\mu_n}_{\tau,i}(\mu^2)|p,s\rangle = 2a^n_{\tau,i}(\mu^2)\Gamma_{\mathcal{SA}}\{s^\sigma p^{\mu_1}\cdots p^{\mu_n}\} - (\text{traces}), \tag{8.3.2}$$

where $\Gamma_{\mathcal{SA}} \in \{\mathcal{S}_1, \mathcal{SA}\}$ for twist-2 and twist-3 components of the Lorentz vectors s^σ and p^μ respectively [6]. In the case of twist-2, $\mathcal{S}_1$ symmetrizes all indices. For twist-3 piece, $\mathcal{A}$ antisymmetrizes σ and μ_1 and $\mathcal{S}$ symmetrizes $\mu_1, \mu_2 \cdots \mu_n$. The index i sums over all matrix elements with the same Lorentz structure and twist. These matrix elements describe the non-perturbative properties of the nucleon [77] and depend only on the renormalization scale. Also

$C^n_{\tau,i}\left(\frac{Q^2}{\mu^2}, g^2_{QCD}(\mu^2)\right)$ are the corresponding coefficient functions. They include all QCD radiative corrections, which contain the logarithmic large Q^2 behavior. From equations (1.6.9) and (1.6.12) one obtains the hadronic tensor as an infinite set of sum rules in terms of the form factors $W_i(\nu, Q^2)$

$$W_{\mu\nu}(p,q) = e^i_{\mu\nu} W_i(\nu, Q^2), \tag{8.3.3}$$

where the sum rules are given as

$$\int_0^1 x^{n-1} W_i(y, Q^2)\mathrm{d}x = \sum_\tau C^n_{\tau,i}\left(\frac{Q^2}{\mu^2}, g^2_{QCD}(\mu^2)\right) a^n_{\tau,i}(\mu^2)\left(\frac{1}{Q^2}\right)^{\frac{\tau}{2}-1}. \tag{8.3.4}$$

8.4 Evolution of the Polarized Structure Function $\mathsf{g}_2^p(x)$

In this section, we discuss the numerical results for the proton structure function $\mathsf{g}_2^p(x, Q^2)$ at $Q^2 = 5\,\mathrm{GeV}^2$ compared with the experimental data given by [3] SLAC-E143 Collaboration. But then, this structure function acquires contribution from both twist-two and -three operators. Under the standard impulse approximation [68, 73, 74] the set of sum rules in equation (8.3.4) simplifies to a set of sum rules for the structure functions (at leading order in $\frac{1}{Q^2}$)

$$\lim_{Q^2\to\infty}\int_0^1 x^n \mathsf{g}_1(x,Q^2)\mathrm{d}x = \frac{1}{2}\sum_i a^n_{2,i} C^n_{2,i}\Big(\frac{Q^2}{\mu^2}, g^2_{QCD}(\mu^2)\Big), \quad n = 0, 2, 4\cdots \tag{8.4.1}$$

$$\lim_{Q^2\to\infty}\int_0^1 x^n \mathsf{g}_2(x,Q^2)\mathrm{d}x = -\frac{n}{2(n+1)}\sum_i \left(a^n_{2,i} C^n_{2,i}\Big(\frac{Q^2}{\mu^2}, g^2_{QCD}(\mu^2)\Big) - a^n_{3,i} C^n_{3,i}\Big(\frac{Q^2}{\mu^2}, g^2_{QCD}(\mu^2)\Big)\right), n = 2, 4, \cdots \tag{8.4.2}$$

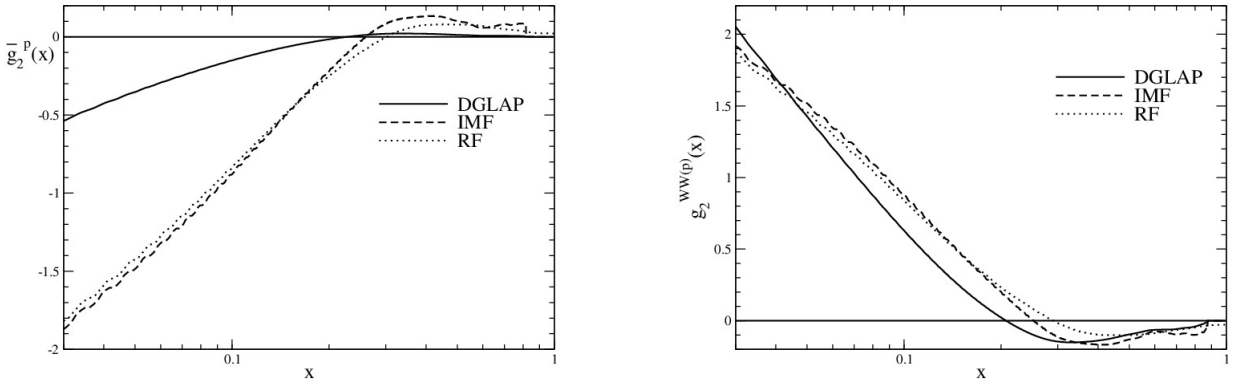

(a) (b)

Figure 8.4: (a) The numerical results for the polarized proton structure function, $\bar{\mathsf{g}}_2^p(x)$, for $m = 400\,\mathrm{MeV}$ and (b) the numerical results for the spin polarized proton structure function, $\mathsf{g}_2^{WW(p)}(x)$, for $m = 400\,\mathrm{MeV}$. In both cases the curves labeled "RF" denote the results obtained from the nucleon rest frame and those labeled "IMF" denote the projection to the infinite momentum frame. The latter are subsequently evolved (DGLAP) from $\mu^2 = 0.4\,\mathrm{GeV}^2$ to $Q^2 = 5.0\,\mathrm{GeV}$. Note that the horizontal coordinate for both functions is on a logarithmic scale.

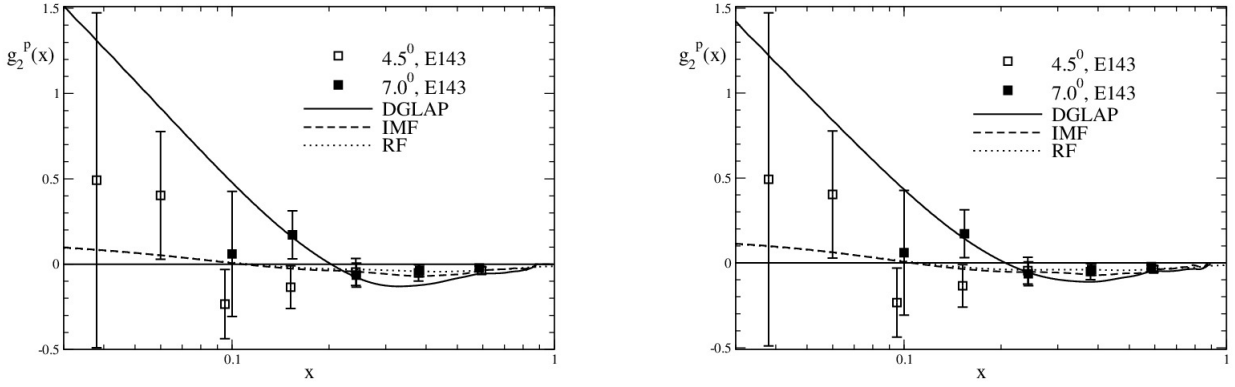

(a) (b)

Figure 8.5: The numerical prediction for the polarized proton structure function (a) $\mathrm{g}_2^p(x)$ for $m = 400\,\mathrm{MeV}$, (b) $\mathrm{g}_2^p(x)$ for $m = 450\,\mathrm{MeV}$ compared to experimental data from [3] SLAC-E143 Collaboration, with the 4.5^0 E143 and 7^0 E143 kinematics indicated by the open and black squared points. These functions are "DGLAP" evolved from $\mu^2 = 0.4\,\mathrm{GeV}^2$ to $Q^2 = 5\,\mathrm{GeV}^2$ after projected to the infinite momentum frame "IMF".

Equations (8.4.1) and (8.4.2) show that at leading order in $\dfrac{1}{Q^2}$, $\mathrm{g}_1(x, Q^2)$ only receives contribution from twist-two operators, while $\mathrm{g}_2(x, Q^2)$ receives contributions from both twist-two and twist-three operators [68, 73, 74]. The twist-two part of $\mathrm{g}_2(x, Q^2)$ is constructed from $\mathrm{g}_1(x, Q^2)$ as [78]

$$\mathrm{g}_2^{WW}(x, Q^2) = -\mathrm{g}_1(x, Q^2) + \int_0^1 \frac{1}{y}\mathrm{g}_1(y, Q^2)\mathrm{d}y. \tag{8.4.3}$$

In general we have

$$\mathrm{g}_2(x, Q^2) = \mathrm{g}_2^{WW}(x, Q^2) + \bar{\mathrm{g}}_2(x, Q^2), \tag{8.4.4}$$

where $\bar{\mathrm{g}}_2(x, Q^2)$ denotes twist-three contribution with the sum rule

$$\lim_{Q^2\to\infty} \int_0^1 x^n \bar{\mathrm{g}}_2(x, Q^2)\mathrm{d}x = \frac{2}{2(n+1)} \sum_i a_{3,i}^n C_{3,i}^n\left(\frac{Q^2}{\mu^2}, g_{QCD}^2(\mu^2)\right), \quad n = 2, 4, 6\cdots \tag{8.4.5}$$

Before presenting our solutions we comment on the twist-two and -three operators. Evolution of twist-two piece $\mathrm{g}_2^{WW}(x)$ is easily obtained using the Altarelli-Parisi equations above. That is, $\mathrm{g}_2^{WW}(x)$ is subject to the same differential equations as $\mathrm{g}_1(x)$. However, this evolution cannot be applied to the twist-three piece $\bar{\mathrm{g}}_2(x)$. This is because its contributing quark and quark-gluon operators with the same quantum numbers mix. As such, the number of contributing independent operators to $\bar{\mathrm{g}}_2(x)$ increases with the n^{th}-moment [79]. For this reason, we make use of the following approximation based on large-N_c arguments. In limit of $N_c \to \infty$, Jaffe[68] argues that the moments of $\mathrm{g}_2(x, \mu^2)$ evolves from μ^2 to Q^2 by the expression[1]

$$\int_0^1 x^{j-1}\bar{\mathrm{g}}_2(x, Q^2)\mathrm{d}x = \left(\frac{g_{QCD}(Q^2)}{g_{QCD}(\mu^2)}\right)^{\frac{\gamma_{j-1}}{b}} \int_0^1 x^{j-1}\bar{\mathrm{g}}_2(x, \mu^2)\mathrm{d}x, \tag{8.4.6}$$

[1] where μ^2 is the low energy scale parameter from above.

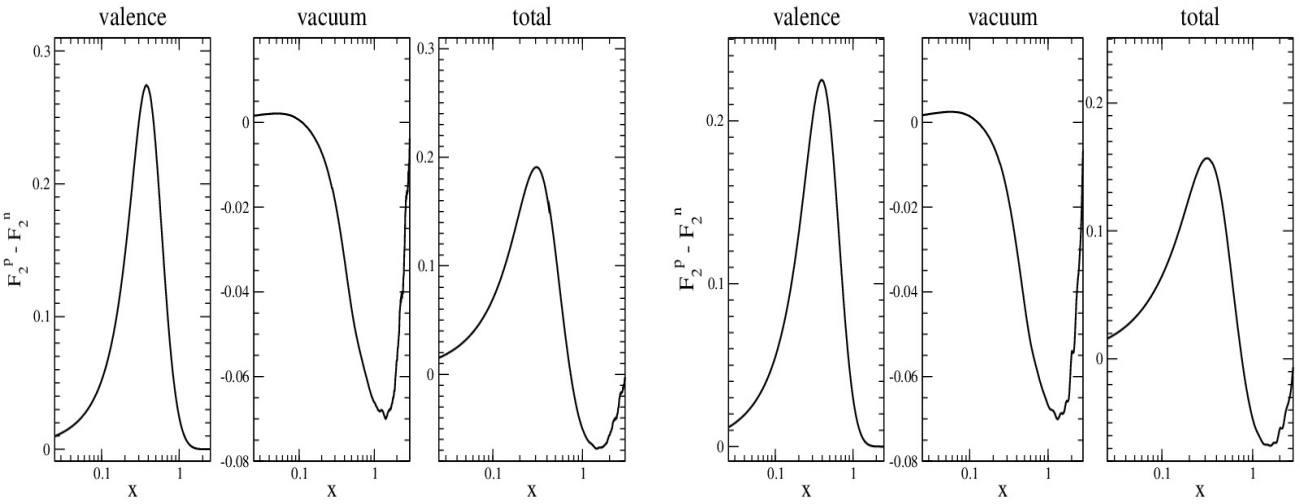

Figure 8.6: The unpolarized structure function $F_2^p(x) - F_2^n(x)$ in the nucleon rest frame. Left panel: The case for $m = 400\,\text{MeV}$. Right panel: The case for $m = 450\,\text{MeV}$.

where γ_{j-1} is the corresponding anomalous dimension given by

$$\gamma_{j-1} = 2N_c\left(\psi(j) + \gamma_E - \frac{1}{4} + \frac{1}{2j}\right) \tag{8.4.7}$$

with $\psi(y) = \dfrac{\mathrm{d}}{\mathrm{d}y}\ln\Gamma(y)$ and γ_E is the Euler constant. In what follows, we express the twist-three function $\overline{\mathsf{g}}_2(x,\mu^2)$ in terms of $\ln(x)$ and a power series in x [47]

$$\overline{\mathsf{g}}_2(x,\mu^2) = b_1(\mu^2)\ln(x) + \sum_{n=0}^{\infty} b_n(\mu^2)x^n. \tag{8.4.8}$$

This enables us to write the moment of $\overline{\mathsf{g}}_2(x,\mu^2)$ as

$$\int_0^1 x^{j-1}\overline{\mathsf{g}}_2(x,\mu^2)\mathrm{d}x = B_{jn}b_n(\mu^2). \tag{8.4.9}$$

After evolving the moment of $\overline{\mathsf{g}}_2(x,\mu^2)$ according to equation (8.4.6), we obtain the coefficient $b_n(Q^2)$ by inverting the matrix element B_{jn} which subsequently gives the evolved function $\overline{\mathsf{g}}_2(x,Q^2)$ using equation (8.4.8).

In Figure 8.4 we present the numerical results of the twist-two and -three pieces. One sees that our numerical results for $\mathsf{g}_2^{WW(p)}(x)$ and $\overline{\mathsf{g}}_2^p(x)$ are quite large when compared to the results of $\mathsf{g}_2(x)$ in subsection 6.3.1. Also we observe that in the nucleon rest frame (RF) for 400 MeV, the structure functions $\mathsf{g}_2^{WW(p)}(x)$ and $\overline{\mathsf{g}}_2^p(x)$ fall within the kinematically allowed interval $0 \leq x \leq 1$, in other words they are localized. However, they become smaller when evolved from $\mu^2 = 0.4\,\text{GeV}^2$ to $Q^2 = 5.0\,\text{GeV}$. The sum of the twist-two and -three contributions ($\mathsf{g}_2^p(x)$) are presented in Figure 8.5. We compare our results to that of empirical data from SLAC-E143 [3] collaborations. Our results are in good agreement with the experimental data, though their error bars are large at small x. This shows that the twist contributions cannot be neglected.

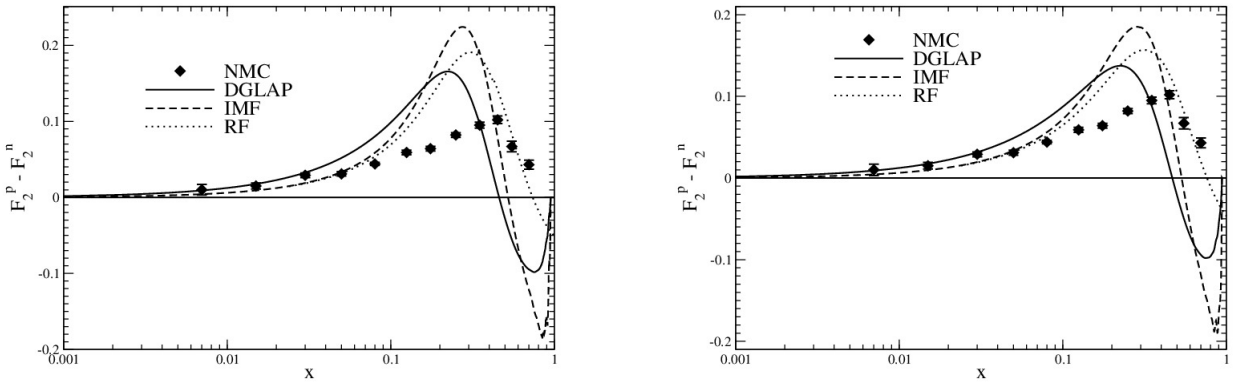

(a) (b)

Figure 8.7: The numerical results for the unpolarized structure function, $F_2^p - F_2^n$, (a)for $m = 400\,\text{MeV}$ and (b) for $m = 450\,\text{MeV}$ compared to experimental data from NMC [4]. These functions are "DGLAP" evolved to $Q^2 = 5\,\text{GeV}^2$ after being projected to the infinite momentum frame "IMF".

8.5 Evolution of the Unpolarized Structure Functions

In this section we discuss the evolution of the structure function that enters the Gottfried sum rule. We recall from chapter 6 that our NJL model unpolarized structure function obeys the Callan-Gross relation, i.e $F_2(x) = 2xF_1(x)$. Thus, the structure function that enters the Gottfried sum rule becomes $F_2^p(x) - F_2^n(x) = 2x(F_1^p(x) - F_1^n(x))$. In obtaining the proton $(F_1^p(x))$ and neutron $(F_1^n(x))$ contributions we first evolve the isosinglet and isovector pieces of the unpolarized structure functions from $\mu^2 = 0.4\,\text{GeV}^2$ to $Q^2 = 4\,\text{GeV}^2$ where experimental data are available. They are then recombined using equation (8.2.10) to obtain the relevant physical flavor.

In Figure 8.6 we display the numerical results of the unpolarized structure function $F_2^p(x) - F_2^n(x)$ in the nucleon rest frame. One observe that at $x \gtrsim 1.0$, the function becomes negative. This negative value results from the vacuum contribution cf. Figure 8.6. This changes slightly as the constituent quark mass increases. From Figure 8.7, one observes that this negative contribution from the vacuum becomes relatively large when transformed to the infinite momentum frame cf. equation (6.1.25). However, these negative pieces diminish when evolved from $\mu^2 = 0.4\,\text{GeV}^2$ to $Q^2 = 4\,\text{GeV}^2$. Thus, the DGLAP function improves the structure function, by minimizing the negative sea contribution. Otherwise, it shows good agreement with the experimental data from NMC [4] at $x \lesssim 6$. Furthermore, its maximal value is around $x \approx 0.22$ which is somewhat smaller than the position of the empirical maximum.

Chapter 9

Summary, Conclusion and Outlook

9.1 Summary of results

We have discussed the polarized and unpolarized structure functions within the bosonized Nambu-Jona-Lasino(NJL) soliton model. The main aim of this work is to compute the vacuum contributions to the structure function as the valence level contribution (which is assumed to dominate) was intensively investigated earlier [46, 47]. Hence a major objective of the current project has been to investigate whether or not the earlier omission of the vacuum contribution was a sensible approximation. As for any observable in the model, the full structure function is given by the sum of the valence and vacuum parts.

This project make ample use of large-N_c arguments. It has been conjectured that [10, 11] in such a limit baryons emerge as solitons. We have reviewed this discussion in chapter 1. In chapter 2 we have discussed QCD and its phenomenological implications that are also realized in the NJL model. Especially we have reflected on chiral symmetry in the limit that the quark mass m^0 vanishes and the breaking of this symmetry for $m^0 \neq 0$. This dynamical breaking produces the constituent quark mass m. The NJL model is subsequently bosonized into an action functional. This introduces the chiral field as the fundamental degree of freedom. The bosonized action requires regularization. We have adopted the Pauli-Villar's subtraction scheme whose additive structure is useful in the context of structure function calculations [24]. The model parameters such as the physical cut-off Λ, the coupling constant G and the current quark mass m^0 are determined by imposing the empirical values: the pion mass $m_\pi = 138\,\mathrm{MeV}$ and the pion decay constant $f_\pi = 93\,\mathrm{MeV}$. Essentially one parameter remains free which we take to be m.

In chapters 3 and 4, using the chiral field and the regularized action functional we construct the soliton solutions self-consistently. This calculation produces the energy eigenvalues and associated eigenfunctions of the corresponding Dirac Hamiltonian that contains the soliton profile. To this end the Hamiltonian is diagonalized in a large but finite spherical cavity of radius $r = D$, which we chose to be $D = 10\,\mathrm{fm}$ (ten times more the proton radius). The energy eigenvalues and associated eigenfunctions are stored in a file and later used to construct the

quark spinors for computing the structure functions.

The starting point of computing the structure functions is the absorptive part of the Compton amplitude, which relates the matrix elements of the hadronic tensor to those of the time-ordered correlation function of the symmetry currents. Using Cutkosky's rules the structure functions are extracted from the regularized NJL action functional. No further ad hoc assumption on regularization has been made. In doing this we have taken the propagator with infinitely large photon momentum to be that of non-interacting massless quarks. Within the Pauli-Villar's scheme this propagator then simplifies to that of a free massless fermion. We have formulated these discussions in chapter 5.

Because of the nature of the hedgehog chiral field, the quark spinor posses grand spin symmetry, which is caused by the coupling of the spin and isospin. In addition the cranking correction terms need to be included to generate good quantum numbers for the baryon states. These corrections cause the isovector piece of the polarized structure function as well as the isosinglet piece of the unpolarized structure function to be regularized.

We have discussed the NJL model results in chapters 6 and 7, as well as the sum rules for the structure functions. We observe from our results (except for the isosinglet unpolarized structure functions) that the vacuum contributes, however small, oscillates at large values of x. These oscillations do not cause inaccuracies for the sum rules that are obeyed level by level. The only exception being the energy sum rule that relies on the soliton minimizing the classical energy. Thus this sum rule is only obeyed when all grand spin channels are summed. Furthermore it requires the subtraction of the non-soliton counterpart in case of the isosinglet unpolarized structure function (the cosmological constant part in the quantum energy). This has a huge effect and may be due to modified kinematics in the absence of the soliton. Subsequently, this affect the flavor-singlet unpolarized structure function $F_1^{I=0}(x)$.

We found in our discussion that, depending on the constituent quark mass, the Bjorken sum rule remains roughly 40% below the experimental value. This is a known problem of chiral solitons, e.g. g_A is predicted to be small. It has been suggested that $\frac{1}{N_c}$ effects cure this [20]. However, it is unclear how they could be included in the present structure function calculations. We have observed that the vacuum contributions to both the axial singlet charge and the Gottfried sum rule do not depend on the regularized parameters. Our model prediction for the axial singlet charge shows good agreement with the one predicted by the authors of Refs.[71]. For the case of the Gottfried sum rule our model prediction agrees reasonably well with that of the experimental data from the NMC [4]; with 99% of the value coming from the valence quark contribution.

Note that because the structure functions are computed within the soliton model (with the quarks considered to be heavy) they also receive support outside the kinematically allowed interval $0 \leq x \leq 1$, where x is the Bjorken variable. To ensure the structure functions are well

localised:

- we first transform them to the infinite momentum frame cf. equation (6.1.25) [61, 62].
- this is subsequently evolved from a lower-energy scale μ^2 to higher Q^2 values for which the experimental data are obtained.

Finally, we have compared our NJL model structure functions to that of the experimental data. After evolving the NJL structure functions from a lower-energy boundary μ^2 to higher energy boundary Q^2 at which the experiment are performed, we obtained agreement of our model predictions with the experiment also at lower x-values.

9.2 Outlook

It will be interesting to investigate the gradient expansion of the matrix elements and its relation to the Skyrme model. This will give important information on how the topological structures of baryonic-solitons lead to fermions while maintaining the Callan-Gross relation. We anticipate that, extending the investigation to the $SU(3)$ flavor symmetry will improve the structure function agreement with that of the experimental data. Although such analysis has been applied before in the case of using the valence quark approximation by the authors in Refs.[58], that of the Pauli-Villar's regularization scheme is yet to be investigated. Such studies will be particularly interesting for the axial singlet structure function because its empirical analysis relies on assuming flavor $SU(3)$ symmetry.

There are many other distributions defined in the framework of QCD. In that context they are extracted from hadron matrix elements of bilocal quark operators

$$\langle H|q(0)\Gamma\bar{q}(x)|H\rangle \tag{9.2.1}$$

by performing appropriate Fourier transformations of the space time coordinate x. Example are the chiral odd structure functions of the nucleon [80–82] that features in the Drell-Yan dilepton production. More recently quasi-distribution functions, transverse momentum distribution as well as Ioffe-time distribution for the pion have been studied in the NJL model and compared to lattice measurement [83, 84]. Since the structure of (9.2.1) is related to the bilinears entering our structure functions (cf. curly bracket in equation (6.0.2)) it is tempting to apply our approach.

However there is an essential difference. The just mentioned calculations require to identify the quark fields from QCD with those from the model. Such an assumption maybe be questioned and in fact we did not use it for our calculations. All what we identified was the coupling of the fundamental fields (that eventually build the hadron) to the electromagnetic field. This is nothing but the gauge principle and is based on the symmetry properties of QCD and the model. Hence any attempt to compute those generalized distributions would first require a

formulation in terms of symmetry currents as the symmetries of QCD and the model may indeed be identified (which is the basis of chiral perturbation theory). Of course this will be an interesting and worthwhile program for future research.

Appendices

Appendix A

General conventions

In this appendix we will list the conventions relevant to the relativistic formulation of the NJL model.

A.1 Conventions

Throughout this work, unless otherwise stated, we will use the natural units with $\hbar = c = 1$ where $\hbar = \frac{h}{2\pi}$, h is referred to as the Planck constant and c is the speed of light. We will adopt the notations in special relativity. We represent space-time and energy-momentum coordinates by the contravariant four-vector

$$x^\mu = (x^0, \vec{x})^\mu \tag{A.1.1}$$

$$p^\mu = (p^0, \vec{p})^\mu, \tag{A.1.2}$$

where $x^0 = t$ and $\vec{x} = (x^1, x^2, x^3)$ represents the time and spatial components respectively and $p^0 = E$ and $\vec{p} = (p^1, p^2, p^3)$ are the energy and momentum. The covariant vectors are defined as

$$x_\mu = g_{\mu\nu} x^\nu = (x_0, -\vec{x})_\mu \tag{A.1.3}$$

$$p_\mu = g_{\mu\nu} p^\nu = (p_0, -\vec{p})_\mu \tag{A.1.4}$$

with

$$p \cdot x = p^\mu x_\mu = g_{\mu\nu} p^\mu x^\nu = p^0 x^0 - \vec{p} \cdot \vec{x}. \tag{A.1.5}$$

Here $g_{\mu\nu}$ is the Minkowskian metric tensor

$$g_{\mu\nu} = \begin{pmatrix} 1 & 0 & 0 & 0 \\ 0 & -1 & 0 & 0 \\ 0 & 0 & -1 & 0 \\ 0 & 0 & 0 & -1 \end{pmatrix}_{\mu\nu}. \tag{A.1.6}$$

In the above we have make use of Einstein summation convention for repeated Greek indices with the sum going from 0 to 3. In the case of Latin indices, the sum goes from 1 to 3. Apart from the Minkowskian metric tensor, the Cartesian isotropic tensors (the Kronecker δ and the Levi-Civita symbol) will also play an important role's in our discussions. The Kronecker δ function is defined as

$$\delta_{ij} = \begin{cases} 1, & \text{for} \quad i = j, \\ 0, & \text{otherwise}, \end{cases} \tag{A.1.7}$$

and the totally antisymmetric Levi-Civita symbol is defined as

$$\epsilon_{\mu\nu\rho\sigma} = \begin{cases} 1, & \text{if } \mu, \nu, \rho, \sigma = \text{an even permutation of } 1, 2, 3, 4; \\ -1, & \text{if } \mu, \nu, \rho, \sigma = \text{an odd permutation of } 1, 2, 3, 4; \\ 0, & \text{if any indices are repeated.} \end{cases} \tag{A.1.8}$$

Denoting the nabla operator as $\vec{\partial} = (\partial_x, \partial_y, \partial_y)$, the contravariant and covariant vector space and time derivatives are defined as

$$\frac{\partial}{\partial x^\mu} = \partial_\mu = (\partial_t, \vec{\partial})_\mu, \tag{A.1.9}$$

and

$$\frac{\partial}{\partial x_\mu} = \partial^\mu = (\partial_t, -\vec{\partial})^\mu, \tag{A.1.10}$$

respectively. From this, the d'Alembert operator ($\partial^2 = \Box$) becomes

$$\partial^2 = \partial_\mu \partial^\mu = g_{\mu\nu} \partial^\mu \partial^\nu = \partial_t^2 - \vec{\partial}^2. \tag{A.1.11}$$

Here ∂_t and ∂_t^2 are the first and second derivatives with respect to time respectively. Sometimes we will use the dot notation e.g $\dot{A}$ to denote time derivative and $\partial_x A$ to denote the derivative of A with respect to the space coordinate x.

Furthermore, whenever we use dagger e.g $A^\dagger$ we mean a hermitian conjugate of A and asterisk e.g A^* as complex conjugate of A.

A.2 Dirac Matrices

In our discussion we used Dirac gamma matrices $\gamma^\mu := (\gamma^0, \vec{\gamma})$ which satisfies the anticommutation relation (Cartan algebra)

$$\{\gamma^\mu, \gamma^\nu\} = 2g^{\mu\nu}. \tag{A.2.1}$$

Here, the symbol $\{A, B\}$ means the anticommutation of A and B: $\{A, B\} = AB + BA$. The commutator relation is defined as $[A, B] = AB - BA$.

The standard (or Dirac) representation matrices are given as

$$\gamma^0 = \beta = \begin{pmatrix} \mathbf{1} & \mathbf{0} \\ \mathbf{0} & \mathbf{-1} \end{pmatrix}, \quad \vec{\gamma} = \beta\vec{\alpha} = \beta\vec{\sigma}\gamma_5 = \begin{pmatrix} \mathbf{0} & \vec{\sigma} \\ -\vec{\sigma} & \mathbf{0} \end{pmatrix}, \quad \gamma_5 = \imath\gamma^0\gamma^1\gamma^2\gamma^3 = \begin{pmatrix} \mathbf{0} & \mathbf{1} \\ \mathbf{1} & \mathbf{0} \end{pmatrix}, \tag{A.2.2}$$

where **1** and **0** are 2×2 identity and zero matrices respectively. Also, $\vec{\sigma}$ are the Pauli matrices (see below). The Dirac matrices have the following properties

$$\gamma^{\mu\,\dagger} = \gamma^0\gamma^\mu\gamma^0, \quad \gamma_5^\dagger = \gamma_5, \quad (\gamma^0)^2 = 1, \quad (\gamma^i)^2 = -1, \tag{A.2.3}$$

where the Latin index i represents spatial indices $1, 2, 3$.

A.3 The Pauli Matrices

Here we discussed the Pauli matrices we employed in our discussion. These matrices are defined as

$$\sigma_1 = \begin{pmatrix} 0 & 1 \\ 1 & 0 \end{pmatrix}, \quad \sigma_2 = \begin{pmatrix} 0 & -\imath \\ \imath & 0 \end{pmatrix} \quad \text{and} \quad \sigma_3 = \begin{pmatrix} 1 & 0 \\ 0 & -1 \end{pmatrix}. \tag{A.3.1}$$

Their product can be compactly written as

$$\sigma_i\sigma_j = \delta_{ij} + \imath\epsilon_{ijk}\sigma_k. \tag{A.3.2}$$

Thus, any expression quadratic with respect to the Pauli matrices can be reduced to a linear form. For example

$$\begin{aligned} (\vec{a}\cdot\vec{\sigma})(\vec{b}\cdot\vec{\sigma}) &= a_i b_j \sigma_i\sigma_j \\ &= a_i b_j \left(\delta_{ij} + \imath\epsilon_{ijk}\sigma_k\right) \\ &= \vec{a}\cdot\vec{b} + \imath\left(\vec{a}\wedge\vec{b}\right)\cdot\vec{\sigma}. \end{aligned} \tag{A.3.3}$$

The isospin version of these matrices is denoted as $\vec{\tau}$ and has the same properties listed above.

Appendix B

Regularization Integrals

Here we detail the explicit calculations of the regularized dependent integrals using the formula for single cut-off in equation (2.2.22).

B.1 Single Cut-Off Formula

We want to find the regularization conditions, equation (2.2.21) supplemented by identical cut-offs $\Lambda = \Lambda_1 \to \Lambda_2$. Expanding the regularized function $\sum_{i=0}^{2} c_i g(\Lambda_i^2)$ gives

$$\begin{aligned}\sum_{i=0}^{2} c_i g(\Lambda_i^2) &= c_0 g(\Lambda_0^2) + c_1 g(\Lambda_1^2) + c_2 g(\Lambda_2^2), \\ &= g(0) + c_1 g(\Lambda_1^2) + c_2 g(\Lambda_2^2) \quad \text{using (2.2.21) gives} \\ &= g(0) + \frac{\Lambda_2^2}{\Lambda_1^2 - \Lambda_2^2} g(\Lambda_1^2) - \frac{\Lambda_1^2}{\Lambda_1^2 - \Lambda_2^2} g(\Lambda_2^2), \end{aligned} \tag{B.1.1}$$

since equation (2.2.21) implies $c_1 + c_2 = -1$ and $c_2 \Lambda_2^2 = -c_1 \Lambda_1^2$. We parametrize Λ_1 and Λ_2 as

$$\Lambda_1^2 = \Lambda^2 + \epsilon \quad \text{and} \quad \Lambda_2^2 = \Lambda^2, \tag{B.1.2}$$

and take the limit as $\epsilon \to 0$

$$\begin{aligned}\sum_{i=0}^{2} c_i g(\Lambda_i^2) &= g(0) + \frac{\Lambda^2}{\epsilon} g(\Lambda^2 + \epsilon) - \frac{(\Lambda^2 + \epsilon)}{\epsilon} g(\Lambda^2), \\ &= g(0) - g(\Lambda^2) + \lim_{\epsilon \to 0} \Lambda^2 \left[\frac{g(\Lambda^2 + \epsilon) - g(\Lambda^2)}{\epsilon} \right], \\ &= g(0) - g(\Lambda^2) + \Lambda^2 \frac{\partial g(\Lambda^2)}{\partial \Lambda^2}, \end{aligned} \tag{B.1.3}$$

which is equation (2.2.22).

B.2 Quark Condensate Function

The quark condensate function is given in equation (2.3.6) as

$$\langle \bar{q}q \rangle = -\imath 4mN_c \sum_{i=0}^{2} c_i \int \frac{\mathrm{d}^4k}{(2\pi)^4} \frac{1}{[-k^2 + m^2 + \Lambda_i^2 - \imath\epsilon]}. \tag{B.2.1}$$

The '$\imath\epsilon$' requires to perform Wick rotation with $k \to \imath k$ given

$$\begin{aligned} \langle \bar{q}q \rangle &= 4mN_c \sum_{i=0}^{2} c_i \int \frac{\mathrm{d}^4k}{(2\pi)^4} \frac{1}{[k^2 + m^2 + \Lambda_i^2]} \\ &= \frac{mN_c}{4\pi^2} \sum_{i=0}^{2} c_i (m^2 + \Lambda_i^2) \log(m^2 + \Lambda_i^2). \end{aligned} \tag{B.2.2}$$

Applying single cut-off prescription, equation (2.2.22) or (B.1.3) gives

$$\begin{aligned} \langle \bar{q}q \rangle &= \frac{mN_c}{4\pi^2} \left[m^2 \log m^2 - (m^2 + \Lambda^2) \log(m^2 + \Lambda^2) + \Lambda^2 \left[\log(m^2 + \Lambda^2) + 1 \right] \right] \\ &= \frac{mN_c}{4\pi^2} \left[\Lambda^2 - m^2 \log\left(1 + \frac{\Lambda^2}{m^2}\right) \right]. \end{aligned} \tag{B.2.3}$$

B.3 Polarization Function

The polarization function in sections 2.4 and 5.1 is given as

$$\Pi(q^2) = -\imath \sum_{i=0}^{2} c_i \int \frac{\mathrm{d}^4k}{(2\pi)^4} \int_0^1 \mathrm{d}x \; \frac{1}{[m^2 - k^2 - x(1-x)q^2 + \Lambda_i^2 - \imath\epsilon]^2}. \tag{B.3.1}$$

After performing Wick rotation with $k \to \imath k$ we have

$$\Pi(q^2) = \sum_{i=0}^{2} c_i \int \frac{\mathrm{d}^4k}{(2\pi)^4} \int_0^1 \mathrm{d}x \; \frac{1}{[m^2 + k^2 - x(1-x)q^2 + \Lambda_i^2]^2} = -\frac{1}{16\pi^2} \sum_{i=0}^{2} c_i \int_0^1 \mathrm{d}x \; \log\left(m^2 - x(1-x)q^2 + \Lambda_i^2\right). \tag{B.3.2}$$

Applying single cut-off as in equation (2.2.22) gives

$$\begin{aligned} \Pi(q^2) &= -\frac{1}{16\pi^2} \int_0^1 \mathrm{d}x \left\{ \log\left(m^2 - x(1-x)q^2\right) - \log\left(m^2 - x(1-x)q^2 + \Lambda^2\right) + \frac{\Lambda^2}{m^2 - x(1-x)q^2 + \Lambda^2} \right\}, \\ &= -\frac{1}{16\pi^2} \int_0^1 \mathrm{d}x \left\{ \frac{\Lambda^2}{m^2 - x(1-x)q^2 + \Lambda^2} - \log\left(\frac{m^2 - x(1-x)q^2 + \Lambda^2}{m^2 - x(1-x)q^2} \right) \right\}. \end{aligned} \tag{B.3.3}$$

Appendix C

Eigenspinors of the Dirac Hamiltonian

For the effective chirally invariant meson field theory, the soliton is given by the time-independent hedgehog field configuration

$$U_H(\vec{x}) = \exp\left(\imath\vec{\tau}\cdot\hat{x}F(r)\right), \quad r = |\vec{x}|. \tag{C.0.1}$$

The soliton profile, $F(r)$ is called the chiral angle. In the presence of this soliton configuration the one-particle Dirac Hamiltonian becomes

$$h = \vec{\alpha}\cdot\vec{p} + m\beta\exp\left(\imath\gamma_5\vec{\tau}\cdot\hat{x}F(r)\right). \tag{C.0.2}$$

It commutes with the grand spin operator

$$\vec{G} = \vec{J} + \frac{\vec{\tau}}{2} = \vec{L} + \frac{\vec{\sigma}}{2} + \frac{\vec{\tau}}{2}, \tag{C.0.3}$$

which is the operator sum of the total spin $\vec{J}$ and the isospin $\frac{\vec{\tau}}{2}$. The total spin is the operator sum of the orbital angular momentum $\vec{L}$ and the intrinsic spin $\frac{\vec{\sigma}}{2}$. The Dirac Hamiltonian is diagonalized

$$h\Psi_\alpha = \epsilon_\alpha\Psi_\alpha \tag{C.0.4}$$

yielding eigenfunctions Ψ_α and real energy eigenvalues ϵ_α. The eigenstates are also eigenstates of $\vec{G}^2 = G(G+1)$ and $G_3 = M$. The energy eigenstates are constructed as linear combinations

of the eigenstates Ψ^0_α of the free Hamiltonian ($F \equiv 0$):

$$
\begin{aligned}
&|1, n, J = G + \frac{1}{2}, M\rangle = \mathcal{N}_n^G \begin{pmatrix} \imath w^+_{nG} j_G(k_{nG} r) \mathcal{Y}_{GG+\frac{1}{2}GM} \\ w^-_{nG} j_{G+1}(k_{nG} r) \mathcal{Y}_{G+1G+\frac{1}{2}GM} \end{pmatrix}, \\
&e^0 = E_{nG} = \pm\sqrt{k^2_{nG} + m^2}, \quad \Pi = (-)^G. \\
\\
&|2, n, J = G - \frac{1}{2}, M\rangle = \mathcal{N}_n^G \begin{pmatrix} \imath w^+_{nG} j_G(k_{nG} r) \mathcal{Y}_{GG-\frac{1}{2}GM} \\ -w^-_{nG} j_{G-1}(k_{nG} r) \mathcal{Y}_{G-1G-\frac{1}{2}GM} \end{pmatrix}, \\
&e^0 = E_{nG} = \pm\sqrt{k^2_{nG} + m^2}, \quad \Pi = (-)^G. \\
\\
&|3, n, J = G + \frac{1}{2}, M\rangle = \mathcal{N}_n^{G+1} \begin{pmatrix} \imath w^+_{nG+1} j_{G+1}(k_{nG+1} r) \mathcal{Y}_{G+1G+\frac{1}{2}GM} \\ -w^-_{nG+1} j_G(k_{nG+1} r) \mathcal{Y}_{GG+\frac{1}{2}GM} \end{pmatrix}, \\
&e^0 = E_{nG+1} = \pm\sqrt{k^2_{nG+1} + m^2}, \quad \Pi = (-)^{G+1}. \\
\\
&|4, n, J = G - \frac{1}{2}, M\rangle = \mathcal{N}_n^{G-1} \begin{pmatrix} \imath w^+_{nG-1} j_{G-1}(k_{nG-1} r) \mathcal{Y}_{G-1G-\frac{1}{2}GM} \\ w^-_{nG-1} j_G(k_{nG-1} r) \mathcal{Y}_{GG-\frac{1}{2}GM} \end{pmatrix}, \\
&e^0 = E_{nG-1} = \pm\sqrt{k^2_{nG-1} + m^2}, \quad \Pi = (-)^{G+1}.
\end{aligned}
\tag{C.0.5}
$$

Here j_L represent the spherical Bessel functions. We have also listed the energy eigenvalues e^0 of the free Dirac Hamiltonian and the parity quantum numbers. $\mathcal{Y}_{LJGM}$ represent the grand spin states, where first the spin $\frac{\vec{\sigma}}{2}$ and orbital angular momentum $\vec{L}$ are coupled to the spin $\vec{J}$, which in turn is coupled with isopin $\frac{\vec{\tau}}{2}$ to the grand spin $\vec{G}$ with M as projection of the grand spin G [38]. This coupling scheme yields the selection rules

$$
J = \begin{cases} G + {}^1\!/_2, & L = \begin{cases} G+1, \\ G, \end{cases} \\ \\ G - {}^1\!/_2, & L = \begin{cases} G, \\ G-1. \end{cases} \end{cases}
\tag{C.0.6}
$$

The momentum eigenvalues k_{nL} are discretized by demanding the upper components to vanish at the boundary

$$
j_L(k_{nL} D) = 0. \tag{C.0.7}
$$

By this condition it is always the upper component of the spinor that vanishes at the box boundary $D \gg \Gamma_s$, where Γ_s is the soliton scale. This is different from the Kahana-Ripka bases[38] and avoid spurious contributions to the moment of inertia where D is finite[19]. The kinematical factors $w^\pm_{nL}$ are defined as

$$
w^+_{nL} = \sqrt{1 + \frac{m}{E_{nL}}}, \quad w^-_{nL} = \text{sign}(E_{nL}) \sqrt{1 - \frac{m}{E_{nL}}}, \tag{C.0.8}
$$

where m is the constituent quark mass and the normalization factor is given by

$$\mathcal{N}_n^L = \left[D^{\frac{3}{2}}|j_{L+1}(k_{nL}D)|\right]^{-1}. \tag{C.0.9}$$

In the numerical analyzes [85], the diagonalization of h requires an upper bound, $k_{\max}$ for the momenta k_{nL}. The quantum number L, then specifies the number of momentum eigenstates $N(L) : k_{1L}, \ldots, k_{NL}$. Because of charge conjugation each momentum has two energy eigenvalues $\pm e^0$. Hence for each grand spinor in equation (C.0.5) we have $2N(L)$ eigenfunctions of $h(F = 0)$. From this basis matrix elements of the Hamiltonian (C.0.2) are constructed. This matrix is diagonalized in each grand spin and parity sector.

The diagonalization of the Hamiltonian yields eigenenergies $\epsilon_G^{\pm}(\alpha)$ and the corresponding eigenvectors $V_G^{\pm}(n,\alpha)$ where the upper indices refers to the intrinsic parity. This eigenvectors are used to define the radial functions $g_\alpha^{(G,\pm;i)}$ and $f_\alpha^{(G,\pm;i)}(i = 1, 2)$ which appear in the coordinate space representation of the eigenstates of h

$$\Psi_\alpha^{(G,+)}(\vec{x}) = \begin{pmatrix} \imath g_\alpha^{(G,+;1)}(r)\mathcal{Y}_{GG+\frac{1}{2}GM}(\hat{x}) \\ f_\alpha^{(G,+;1)}(r)\mathcal{Y}_{G+1G+\frac{1}{2}GM}(\hat{x}) \end{pmatrix} + \begin{pmatrix} \imath g_\alpha^{(G,+;2)}(r)\mathcal{Y}_{GG-\frac{1}{2}GM}(\hat{x}) \\ -f_\alpha^{(G,+;2)}(r)\mathcal{Y}_{G-1G-\frac{1}{2}GM}(\hat{x}) \end{pmatrix} \tag{C.0.10}$$

$$\Psi_\alpha^{(G,-)}(\vec{x}) = \begin{pmatrix} \imath g_\alpha^{(G,-;1)}(r)\mathcal{Y}_{G+1G+\frac{1}{2}GM}(\hat{x}) \\ -f_\alpha^{(G,-;1)}(r)\mathcal{Y}_{GG+\frac{1}{2}GM}(\hat{x}) \end{pmatrix} + \begin{pmatrix} \imath g_\alpha^{(G,-;2)}(r)\mathcal{Y}_{G-1G-\frac{1}{2}GM}(\hat{x}) \\ f_\alpha^{(G,-;2)}(r)\mathcal{Y}_{GG-\frac{1}{2}GM}(\hat{x}) \end{pmatrix}, \tag{C.0.11}$$

where $r = |\vec{x}|$. The second superscript denotes intrinsic parity. The radial functions are obtain from diagonalization as

1. For positive intrinsic parity

$$\begin{aligned}
g_\alpha^{(G,+;1)}(r) &= \sum_{n=1}^{2N(G)} V_G^{(+)}(n,\alpha)\mathcal{N}_n^G w_{nG}^+ j_G(k_{nG}r) \\
g_\alpha^{(G,+;2)}(r) &= \sum_{n=1}^{2N(G)} V_G^{(+)}(n+2N(G),\alpha)\mathcal{N}_n^G w_{nG}^+ j_G(k_{nG}r) \\
f_\alpha^{(G,+;1)}(r) &= \sum_{n=1}^{2N(G)} V_G^{(+)}(n,\alpha)\mathcal{N}_n^G w_{nG}^- j_{G+1}(k_{nG}r) \\
f_\alpha^{(G,+;2)}(r) &= \sum_{n=1}^{2N(G)} V_G^{(+)}(n+2N(G),\alpha)\mathcal{N}_n^G w_{nG}^- j_{G-1}(k_{nG}r).
\end{aligned}$$

2. For negative intrinsic parity

$$
\begin{aligned}
g_\alpha^{(G,-;1)}(r) &= \sum_{n=1}^{2N(G+1)} V_{G+1}^{(-)}(n,\alpha)\mathcal{N}_n^{G+1} w_{nG+1}^{+} j_{G+1}(k_{nG+1}r) \\
g_\alpha^{(G,-;2)}(r) &= \sum_{n=1}^{2N(G-1)} V_{G-1}^{(-)}(n+2N(G-1),\alpha)\mathcal{N}_n^{G-1} w_{nG-1}^{+} j_{G-1}(k_{nG-1}r) \\
f_\alpha^{(G,-;1)}(r) &= \sum_{n=1}^{2N(G+1)} V_{G+1}^{(-)}(n,\alpha)\mathcal{N}_n^{G+1} w_{nG+1}^{-} j_{G}(k_{nG+1}r) \\
f_\alpha^{(G,-;2)}(r) &= \sum_{n=1}^{2N(G-1)} V_{G-1}^{(-)}(n+2N(G-1),\alpha)\mathcal{N}_n^{G-1} w_{nG-1}^{-} j_{G}(k_{nG-1}r),
\end{aligned}
$$

where $V_G^I(n,\alpha)$ is the n^{th} component of the eigenvector of $h(F \neq 0)$ for eigenvalue ϵ_α.

Taking the Fourier transform of these eigenspinors (for a general case) gives

$$
\tilde{\Psi}_\alpha(\vec{p}) = \int \frac{\mathrm{d}^3 r}{4\pi}\, e^{\imath \vec{p}\cdot\vec{r}} \Psi_\alpha(\vec{r}). \tag{C.0.12}
$$

This involves the generalised spherical harmonics and the radial functions, therefore can be written as

$$
\tilde{\Psi}_\alpha(\vec{p}) = \int \frac{\mathrm{d}^3 r}{4\pi}\, e^{\imath \vec{p}\cdot\vec{r}} \phi_\alpha(r)\mathcal{Y}_{L_\alpha JGM}(\hat{r}) = \sum_{m_\alpha, s_3, i_3, J_3} C^{GM}_{JJ_3,\frac{1}{2}i_3} C^{JJ_3}_{L_\alpha m_\alpha,\frac{1}{2}s_3} \chi_s(s_3)\chi_i(i_3) \int \frac{\mathrm{d}^3 r}{4\pi}\, e^{\imath \vec{p}\cdot\vec{r}} \phi_\alpha(r) Y_{L_\alpha m_\alpha}(\hat{r}),
$$

where $\phi_\alpha(r)$ is the radial function and $Y_{L_\alpha m_\alpha}(\hat{r})$ is the spherical harmonic function. In the next step, we expand the plane wave function in terms of spherical Bessel functions as

$$
e^{\imath \vec{p}\cdot\vec{r}} = 4\pi \sum_{Lm} (\imath)^L j_L(pr) Y^*_{Lm}(\hat{r}) Y_{Lm}(\hat{p}). \tag{C.0.13}
$$

This gives

$$
\tilde{\Psi}_\alpha(\vec{p}) = \sum_{m_\alpha, s_3, i_3, J_3} C^{GM}_{JJ_3,\frac{1}{2}i_3} C^{JJ_3}_{L_\alpha m_\alpha,\frac{1}{2}s_3} \chi_s(s_3)\chi_i(i_3) \sum_{Lm} (\imath)^L \int \mathrm{d}^3 r\, j_L(pr) Y^*_{Lm}(\hat{r}) Y_{Lm}(\hat{p}) \phi_\alpha(r) Y_{L_\alpha m_\alpha}(\hat{r}). \tag{C.0.14}
$$

Expressing the integral variable in spherical coordinates as

$$
\int \mathrm{d}^3 r \sim \int \mathrm{d}r\, r^2 \int \mathrm{d}\Omega_r,
$$

where Ω_r is the solid angle and using the orthogonal identity

$$
\int \mathrm{d}\Omega_r\, Y^*_{Lm}(\hat{r}) Y_{L'm'}(\hat{r}) = \delta_{LL'}\delta_{mm'}, \tag{C.0.15}
$$

gives

$$
\begin{aligned}
\tilde{\Psi}_\alpha(\vec{p}) &= \sum_{m_\alpha, s_3, i_3, J_3} C^{GM}_{JJ_3,\frac{1}{2}i_3} C^{JJ_3}_{L_\alpha m_\alpha,\frac{1}{2}s_3} \chi_s(s_3)\chi_i(i_3) \sum_{Lm} (\imath)^L \int \mathrm{d}r\, r^2 j_L(pr) \phi_\alpha(r) Y_{Lm}(\hat{p}) \delta_{LL_\alpha}\delta_{mm_\alpha}, \\
&= (\imath)^{L_\alpha} \tilde{\phi}_\alpha(p) \mathcal{Y}_{L_\alpha JGM}(\hat{p}),
\end{aligned} \tag{C.0.16}
$$

where

$$\mathcal{Y}_{L_\alpha JGM}(\hat{p}) = \sum_{m_\alpha, s_3, i_3, J_3} C^{GM}_{JJ_3,\frac{1}{2}i_3} C^{JJ_3}_{L_\alpha m_\alpha,\frac{1}{2}s_3} Y_{L_\alpha m_\alpha}(\hat{p})\chi_s(s_3)\chi_i(i_3)$$

is a generalised spherical harmonic function in momentum space and

$$\tilde{\phi}_\alpha(p) = \int \mathrm{d}r\, r^2 j_{L_\alpha}(pr)\phi_\alpha(r) \tag{C.0.17}$$

is the radial function in momentum space. Using the above results, we have the two eigenfunction in momentum space in full glory

1. For $(-)^L = (-)^G$ (positive intrinsic parity) as

$$\tilde{\Psi}^{(G,+)}_\alpha(\vec{p}) = \begin{pmatrix} (\imath)^{G+1}\tilde{g}^{(G,+;1)}_\alpha(p)\mathcal{Y}_{GG+\frac{1}{2}GM}(\hat{p}) \\ (\imath)^{G+1}\tilde{f}^{(G,+;1)}_\alpha(p)\mathcal{Y}_{G+1G+\frac{1}{2}GM}(\hat{p}) \end{pmatrix} + \begin{pmatrix} (\imath)^{G+1}\tilde{g}^{(G,+;2)}_\alpha(p)\mathcal{Y}_{GG-\frac{1}{2}GM}(\hat{p}) \\ -(\imath)^{G-1}\tilde{f}^{(G,+;2)}_\alpha(p)\mathcal{Y}_{G-1G-\frac{1}{2}GM}(\hat{p}) \end{pmatrix}. \tag{C.0.18}$$

2. For $(-)^L = (-)^{G+1}$ (negative intrinsic parity) as

$$\tilde{\Psi}^{(G,-)}_\alpha(\vec{p}) = \begin{pmatrix} (\imath)^{G+2}\tilde{g}^{(G,-;1)}_\alpha(p)\mathcal{Y}_{G+1G+\frac{1}{2}GM}(\hat{p}) \\ -(\imath)^{G}\tilde{f}^{(G,-;1)}_\alpha(p)\mathcal{Y}_{GG+\frac{1}{2}GM}(\hat{p}) \end{pmatrix} + \begin{pmatrix} (\imath)^{G}\tilde{g}^{(G,-;2)}_\alpha(p)\mathcal{Y}_{G-1G-\frac{1}{2}GM}(\hat{p}) \\ (\imath)^{G}\tilde{f}^{(G,-;2)}_\alpha(p)\mathcal{Y}_{GG-\frac{1}{2}GM}(\hat{p}) \end{pmatrix}. \tag{C.0.19}$$

Using equations (C.0.17) and (C.0.5) the radial functions in momentum space for equations (C.0.18) and (C.0.19)

1. For positive intrinsic parity becomes

$$\tilde{g}^{(G,+;1)}_\alpha(p) = \int_0^D \mathrm{d}r\, r^2 \left(\sum_{n=1}^{2N(G)} V^{(+)}_G(n,\alpha)\mathcal{N}^G_n w^+_{nG} j_G(k_{nG}r)\right) j_G(pr)$$

$$\tilde{g}^{(G,+;2)}_\alpha(p) = \int_0^D \mathrm{d}r\, r^2 \left(\sum_{n=1}^{2N(G)} V^{(+)}_G(n+2N(G),\alpha)\mathcal{N}^G_n w^+_{nG} j_G(k_{nG}r)\right) j_G(pr)$$

$$\tilde{f}^{(G,+;1)}_\alpha(p) = \int_0^D \mathrm{d}r\, r^2 \left(\sum_{n=1}^{2N(G)} V^{(+)}_G(n,\alpha)\mathcal{N}^G_n w^-_{nG} j_{G+1}(k_{nG}r)\right) j_{G+1}(pr)$$

$$\tilde{f}^{(G,+;2)}_\alpha(p) = \int_0^D \mathrm{d}r\, r^2 \left(\sum_{n=1}^{2N(G)} V^{(+)}_G(n+2N(G),\alpha)\mathcal{N}^G_n w^-_{nG} j_{G-1}(k_{nG}r)\right) j_{G-1}(pr).$$

2. For negative intrinsic parity becomes

$$\tilde{g}^{(G,-;1)}_\alpha(p) = \int_0^D \mathrm{d}r\, r^2 \left(\sum_{n=1}^{2N(G+1)} V^{(-)}_{G+1}(n,\alpha)\mathcal{N}^{G+1}_n w^+_{nG+1} j_{G+1}(k_{nG+1}r)\right) j_{G+1}(pr)$$

$$\tilde{g}^{(G,-;2)}_\alpha(p) = \int_0^D \mathrm{d}r\, r^2 \left(\sum_{n=1}^{2N(G-1)} V^{(-)}_{G-1}(n+2N(G-1),\alpha)\mathcal{N}^{G-1}_n w^+_{nG-1} j_{G-1}(k_{nG-1}r)\right) j_{G-1}(pr)$$

$$\tilde{f}^{(G,-;1)}_\alpha(p) = \int_0^D \mathrm{d}r\, r^2 \left(\sum_{n=1}^{2N(G+1)} V^{(-)}_{G+1}(n,\alpha)\mathcal{N}^{G+1}_n w^-_{nG+1} j_G(k_{nG+1}r)\right) j_G(pr)$$

$$\tilde{f}^{(G,-;2)}_\alpha(p) = \int_0^D \mathrm{d}r\, r^2 \left(\sum_{n=1}^{2N(G-1)} V^{(-)}_{G-1}(n+2N(G-1),\alpha)\mathcal{N}^{G-1}_n w^-_{nG-1} j_G(k_{nG-1}r)\right) j_G(pr).$$

Appendix D

Important Integrals for Structure Functions

Here we detail the calculations of the averaging integrals over ' Ω_z ' that appear in the structure functions, see also Ref.[49].

1. In the first case we consider the integral of the form

$$I_i' = \int \frac{\mathrm{d}\Omega_z}{4\pi}\, z_i\, \delta\left(M_N x \pm \hat{z}\cdot\vec{p}\right). \tag{D.0.1}$$

Here $\hat{z}$ is a unit vector in the direction of the photon. The solid angle element is written in spherical coordinates

$$\mathrm{d}\Omega_z = \sin(\theta_z)\mathrm{d}\theta_z\mathrm{d}\phi_z = \mathrm{d}\left(\cos(\theta_z)\right)\mathrm{d}\phi_z, \quad \text{for } \theta_z \in (0,\pi) \text{ and } \phi_z \in (0,2\pi).$$

We write $\hat{z}\cdot\vec{p} = z_k p_k$, and define $p_k = R_{k3}p_3$ where $p_3 = |\vec{p}\hat{e}_3| = |\vec{p}|$ and R_{k3} is an arbitrary rotation in the z-direction. Similarly we define $z_k = R_{kl}z_l'$. Then we have

$$z_k p_k = R_{k3}R_{kl}z_l' p_3 = \delta_{3l}z_l' p_3 = z_3' p_3, \quad \text{here } z_3' = \cos(\theta_{z'}).$$

Since the integration measure is rotationally invariant the integral becomes

$$I_i' = R_{im}\int \frac{\mathrm{d}\Omega_{z'}}{4\pi}\, z_m'\, \delta\left(M_N x \pm p_3 z_3'\right) = R_{im}\int_{-1}^{1}\frac{\mathrm{d}(\cos(\theta_{z'}))}{4\pi p_3}\int_0^{2\pi}\mathrm{d}\phi_{z'}\, z_m'\,\delta\left(\frac{M_N x}{p_3} \pm \cos(\theta_{z'})\right).$$

Let

$$I_m = \int_{-1}^{1}\frac{\mathrm{d}(\cos(\theta_{z'}))}{4\pi p_3}\int_0^{2\pi}\mathrm{d}\phi_{z'}\, z_m'\,\delta\left(\frac{M_N x}{p_3} \pm \cos(\theta_{z'})\right) \tag{D.0.2}$$

and noting that $\int_0^{2\pi}\mathrm{d}\phi_{z'}\,\sin\phi_{z'} = 0$ and $\int_0^{2\pi}\mathrm{d}\phi_{z'}\,\cos\phi_{z'} = 0$, we have

$$\begin{aligned}
&I_1 = I_2 = 0,\\
&I_3 = \int_{-1}^{1}\frac{\mathrm{d}(\cos(\theta_{z'}))}{4\pi p_3}\int_0^{2\pi}\mathrm{d}\phi_{z'}\cos\theta_{z'}\,\delta\left(\frac{M_N x}{p_3} \pm \cos(\theta_{z'})\right) = \mp\frac{1}{2p_3}\frac{M_N x}{p_3}\Theta\left(p_3 - |M_N x|\right),\\
&\quad = \mp\frac{1}{2|\vec{p}|}\frac{M_N x}{|\vec{p}|}\Theta\left(|\vec{p}| - |M_N x|\right),
\end{aligned}$$

where "Θ" is the heaviside step function. Thus we have

$$I'_i = R_{i1}I_1 + R_{i2}I_2 + R_{i3}I_3 = R_{i3}I_3 = \hat{p}_i I_3. \tag{D.0.3}$$

2. In the second case we consider the integral

$$I'_{ij} = \int \frac{\mathrm{d}\Omega_z}{4\pi}\, z_i z_j\, \delta\left(M_N x \pm \hat{z}\cdot\vec{p}\right). \tag{D.0.4}$$

Using the techniques from above the integral becomes

$$I'_{ij} = R_{im}R_{jn}\int \frac{\mathrm{d}\Omega_{z'}}{4\pi}\, z'_m z'_n\, \delta\left(M_N x + p_3 z'_3\right) = R_{im}R_{jn}\int_{-1}^{1}\frac{\mathrm{d}(\cos(\theta_{z'}))}{4\pi p_3}\int_0^{2\pi}\mathrm{d}\phi_{z'}\, z'_m z'_n\, \delta\left(\frac{M_N x}{p_3} \pm \cos(\theta_{z'})\right).$$

Let

$$I_{mn} = \int_{-1}^{1}\frac{\mathrm{d}(\cos(\theta_{z'}))}{4\pi p_3}\int_0^{2\pi}\mathrm{d}\phi_{z'}\, z'_m z'_n\, \delta\left(\frac{M_N x}{p_3} \pm \cos(\theta_{z'})\right). \tag{D.0.5}$$

With the identities

$$\int_0^{2\pi}\mathrm{d}\phi_{z'}\,\sin^2\phi_{z'} = \pi = \int_0^{2\pi}\mathrm{d}\phi_{z'}\,\cos^2\phi_{z'}.$$
$$\int_0^{2\pi}\mathrm{d}\phi_{z'}\,\sin\phi_{z'} = 0 = \int_0^{2\pi}\mathrm{d}\phi_{z'}\,\cos\phi_{z'}. \quad \text{and}$$
$$\int_0^{2\pi}\mathrm{d}\phi_{z'}\,\cos\phi_{z'}\sin\phi_{z'} = \frac{1}{2}\int_0^{2\pi}\mathrm{d}\phi_{z'}\,\sin 2\phi_{z'} = 0.$$

we have

$$\begin{aligned}
I_{11} = I_{22} &= \int_{-1}^{1}\frac{\mathrm{d}(\cos(\theta_{z'}))}{4\pi p_3}\int_0^{2\pi}\mathrm{d}\phi_{z'}\,\sin^2\theta_{z'}\cos^2\phi_{z'}\,\delta\left(\frac{M_N x}{p_3} \pm \cos(\theta_{z'})\right),\\
&= \frac{1}{4|\vec{p}|}\left(1 - \frac{(M_N x)^2}{|\vec{p}|^2}\right)\Theta\left(|\vec{p}| - |M_N x|\right),\\
I_{12} = I_{21} = I_{13} = I_{31} = I_{23} = I_{32} &= 0,\\
I_{33} &= \int_{-1}^{1}\frac{\mathrm{d}(\cos(\theta_{z'}))}{4\pi p_3}\int_0^{2\pi}\mathrm{d}\phi_{z'}\,\cos^2\theta_{z'}\,\delta\left(\frac{M_N x}{p_3} \pm \cos(\theta_{z'})\right) = \frac{1}{2|\vec{p}|}\frac{(M_N x)^2}{|\vec{p}|^2}\Theta\left(|\vec{p}| - |M_N x|\right).
\end{aligned}$$

From the results above we have

$$\begin{aligned}
I'_{ij} &= R_{im}R_{jn}I_{mn}\\
&= R_{i1}R_{j1}I_{11} + R_{i2}R_{j2}I_{22} + R_{13}R_{j3}I_{33}\\
&= \left(R_{i1}R_{j1} + R_{i2}R_{j2}\right)I_{11} + R_{i3}R_{j3}I_{33}.
\end{aligned}$$

But $\sum_{k=1}^{3} R_{ik}R_{jk} = \delta_{ij}$, which implies that $R_{i1}R_{j1} + R_{i2}R_{j2} = \delta_{ij} - R_{i3}R_{j3}$. Using this we have

$$I'_{ij} = \left(\delta_{ij} - \hat{p}_i\hat{p}_j\right)I_{11} + \hat{p}_i\hat{p}_j I_{33}. \tag{D.0.6}$$

Appendix E

Matrix Elements of some Dirac Operators

Here we discuss some of the matrix elements of some Dirac operators between eigenstates (Appendix C) of the single particle Dirac Hamiltonian.

E.1 Matrix Element of the Moment of Inertia

We first look at the matrix element that appears in the moment of inertia. We write the matrix element $\langle\alpha|\tau_3|\beta\rangle$ as $\int \mathrm{d}r\, r^2 \int \mathrm{d}\Omega_r \Psi_\alpha(\vec{r})\tau_3\Psi_\beta(\vec{r})$, where $\int \mathrm{d}\Omega_r$ is the solid angle integral. Then we have

$$\begin{aligned}
\langle\alpha|\tau_3|\beta\rangle\langle\beta|\tau_3|\alpha\rangle &= \Big\{\int \mathrm{d}r\, r^2 \int \mathrm{d}\Omega_r \Psi_\alpha(\vec{r})\tau_3\Psi_\beta(\vec{r})\Big\}\Big\{\int \mathrm{d}r\, r^2 \int \mathrm{d}\Omega_r \Psi_\beta(\vec{r})\tau_3\Psi_\alpha(\vec{r})\Big\} \\
&= \sum_M \Big\{\int \mathrm{d}r\, r^2 \int \mathrm{d}\Omega_r \mathcal{Y}_{L'J'GM}(\vec{r})\tau_3\mathcal{Y}_{LJGM}(\vec{r})\Big\}^2 \\
&+ \sum_M \Big\{\int \mathrm{d}r\, r^2 \int \mathrm{d}\Omega_r \mathcal{Y}_{L'J'G+1M}(\vec{r})\tau_3\mathcal{Y}_{LJGM}(\vec{r})\Big\}^2 \\
&+ \sum_M \Big\{\int \mathrm{d}r\, r^2 \int \mathrm{d}\Omega_r \mathcal{Y}_{L'J'G-1M}(\vec{r})\tau_3\mathcal{Y}_{LJGM}(\vec{r})\Big\}^2 .
\end{aligned}$$

After summing over all grand spin projections we obtain

$$\begin{aligned}
&\Big\{\int \mathrm{d}\Omega_r \Psi_\alpha^{\dagger(G,+)}(\vec{r})\tau_3\Psi_\beta^{(G,+)}(\vec{r})\Big\}^2 \\
&= (2G+1)\Bigg\{\frac{G}{3(G+1)}\Big(g_\alpha^{(G,+;1)}(r)g_\beta^{(G,+;1)}(r)\Big)^2 + \frac{G}{3(G+1)}\Big(f_\alpha^{(G,+;1)}(r)f_\beta^{(G,+;1)}(r)\Big)^2 \\
&+ \frac{G+1}{3G}\Big(g_\alpha^{(G,+;2)}(r)g_\beta^{(G,+;2)}(r)\Big)^2 + \frac{G+1}{3G}\Big(f_\alpha^{(G,+;2)}(r)f_\beta^{(G,+;2)}(r)\Big)^2\Bigg\},
\end{aligned}$$

$$\Big\{\int \mathrm{d}\Omega_r \Psi_\alpha^{\dagger(G+1,-)}(\vec{r})\tau_3\Psi_\beta^{(G,+)}(\vec{r})\Big\}^2$$
$$= (2G+1)\Bigg\{\frac{2G+3}{3(G+1)}\Big(g_\beta^{(G,+;1)}(r)g_\alpha^{(G+1,-;2)}(r)\Big)^2 + \frac{2G+3}{3(G+1)}\Big(f_\beta^{(G,+;1)}(r)f_\alpha^{(G+1,-;2)}(r)\Big)^2\Bigg\},$$
$$\Big\{\int \mathrm{d}\Omega_r \Psi_\alpha^{\dagger(G,-)}(\vec{r})\tau_3\Psi_\beta^{(G,-)}(\vec{r})\Big\}^2$$
$$= (2G+1)\Bigg\{\frac{G}{3(G+1)}\Big(g_\alpha^{(G,-;1)}(r)g_\beta^{(G,-;1)}(r)\Big)^2 + \frac{G}{3(G+1)}\Big(f_\alpha^{(G,-;1)}(r)f_\beta^{(G,-;1)}(r)\Big)^2$$
$$+ \frac{G+1}{3G}\Big(g_\alpha^{(G,-;2)}(r)g_\beta^{(G,-;2)}(r)\Big)^2 + \frac{G+1}{3G}\Big(f_\alpha^{(G,-;2)}(r)f_\beta^{(G,-;2)}(r)\Big)^2\Bigg\},$$
$$\Big\{\int \mathrm{d}\Omega_r \Psi_\alpha^{\dagger(G-1,-)}(\vec{r})\tau_3\Psi_\beta^{(G,+)}(\vec{r})\Big\}^2$$
$$= (2G+1)\Bigg\{\frac{2G-1}{3G}\Big(g_\beta^{(G,+;2)}(r)g_\alpha^{(G-1,-;1)}(r)\Big)^2 + \frac{2G-1}{3G}\Big(f_\beta^{(G,+;2)}(r)f_\alpha^{(G-1,-;1)}(r)\Big)^2\Bigg\}.$$

E.2 Matrix element of the Quartic Spinor Terms of the Isovector Unpolarized Structure Function

To discuss the matrix element of (7.1.9) we first express the vector τ_i into spherical components i.e

$$\tau_+ = -\frac{1}{\sqrt{2}}(\tau_1 + \imath\tau_2), \quad \tau_- = \frac{1}{\sqrt{2}}(\tau_1 - \imath\tau_2) \quad \text{and} \quad \tau_0 = \tau_3. \tag{E.2.1}$$

then we have

$$\Big\{\int \mathrm{d}\Omega_r \Psi_\alpha^\dagger(\vec{r})\tau_i\Psi_\beta(\vec{r})\Big\}\Big\{\int \mathrm{d}\Omega_p \tilde{\Psi}_\beta^\dagger(\vec{p})\tau_i\tilde{\Psi}_\alpha(\vec{p})\Big\}$$
$$= \sum_M \Big\{\int \mathrm{d}\Omega_r \mathcal{Y}_{L'J'G'M}(\vec{r})\tau_+\mathcal{Y}_{LJGM-1}(\vec{r})\Big\}\Big\{\int \mathrm{d}\Omega_p \mathcal{Y}_{LJGM-1}(\vec{p})\tau_-\mathcal{Y}_{L'J'G'M}(\vec{p})\Big\}$$
$$+ \sum_M \Big\{\int \mathrm{d}\Omega_r \mathcal{Y}_{L'J'G'M}(\vec{r})\tau_-\mathcal{Y}_{LJGM+1}(\vec{r})\Big\}\Big\{\int \mathrm{d}\Omega_p \mathcal{Y}_{LJGM+1}(\vec{p})\tau_+\mathcal{Y}_{L'J'G'M}(\vec{p})\Big\}$$
$$+ \sum_M \Big\{\int \mathrm{d}\Omega_r \mathcal{Y}_{L'J'G'M}(\vec{r})\tau_0\mathcal{Y}_{LJGM}(\vec{r})\Big\}\Big\{\int \mathrm{d}\Omega_p \mathcal{Y}_{LJGM}(\vec{p})\tau_0\mathcal{Y}_{L'J'G'M}(\vec{p})\Big\}.$$

Summing over the grand spin projections gives

$$\Big\{\int \mathrm{d}\Omega_r \Psi_\alpha^{\dagger(G,+)}(\vec{r})\tau_i\Psi_\beta^{(G,+)}(\vec{r})\Big\}\Big\{\int \mathrm{d}\Omega_p \tilde{\Psi}_\beta^{\dagger(G,+)}(\vec{p})\tau_i\Psi_\alpha^{(G,+)}(\vec{p})\Big\}$$
$$= M_{\alpha\beta}\Bigg\{-\sqrt{\frac{G(2G+1)}{3(G+1)}}\Big[\Big(\tilde{g}_\beta^{(G,+;1)}(p)\tilde{g}_\alpha^{(G,+;1)}(p)\Big) + \Big(\tilde{f}_\beta^{(G,+;1)}(p)\tilde{f}_\alpha^{(G,+;1)}(p)\Big)\Big]$$
$$+ \sqrt{\frac{(G+1)(2G+1)}{3G}}\Big[\Big(\tilde{g}_\beta^{(G,+;2)}(p)\tilde{g}_\alpha^{(G,+;2)}(p)\Big) + \Big(\tilde{f}_\beta^{(G,+;2)}(p)\tilde{f}_\alpha^{(G,+;2)}(p)\Big)\Big]\Bigg\},$$
$$\Big\{\int \mathrm{d}\Omega_r \Psi_\alpha^{\dagger(G+1,-)}(\vec{r})\tau_i\Psi_\beta^{(G,+)}(\vec{r})\Big\}\Big\{\int \mathrm{d}\Omega_p \tilde{\Psi}_\beta^{\dagger(G,+)}(\vec{p})\tau_i\Psi_\alpha^{(G+1,-)}(\vec{p})\Big\}$$

$$= N_{\alpha\beta}\left\{\sqrt{\frac{(2G+3)(2G+1)}{3(G+1)}}\left[\left(\tilde{g}_\beta^{(G,+;1)}(p)\tilde{g}_\alpha^{(G+1,-;2)}(p)\right)+\left(\tilde{f}_\beta^{(G,+;1)}(p)\tilde{f}_\alpha^{(G+1,-;2)}(p)\right)\right]\right\},$$

$$\left\{\int \mathrm{d}\Omega_r \Psi_\alpha^{\dagger\,(G,-)}(\vec{r})\tau_i\Psi_\beta^{(G,-)}(\vec{r})\right\}\left\{\int \mathrm{d}\Omega_p \tilde{\Psi}_\beta^{\dagger\,(G,-)}(\vec{p})\tau_i\Psi_\alpha^{(G,-)}(\vec{p})\right\}$$

$$= B_{\alpha\beta}\left\{-\sqrt{\frac{G(2G+1)}{3(G+1)}}\left[\left(\tilde{g}_\beta^{(G,-;1)}(p)\tilde{g}_\alpha^{(G,-;1)}(p)\right)+\left(\tilde{f}_\beta^{(G,-;1)}(p)\tilde{f}_\alpha^{(G,-;1)}(p)\right)\right]\right.$$

$$\left.+\sqrt{\frac{(G+1)(2G+1)}{3G}}\left[\left(\tilde{g}_\beta^{(G,-;2)}(p)\tilde{g}_\alpha^{(G,-;2)}(p)\right)+\left(\tilde{f}_\beta^{(G,-;2)}(p)\tilde{f}_\alpha^{(G,-;2)}(p)\right)\right]\right\},$$

$$\left\{\int \mathrm{d}\Omega_r \Psi_\alpha^{\dagger\,(G,+)}(\vec{r})\tau_i\Psi_\beta^{(G-1,-)}(\vec{r})\right\}\left\{\int \mathrm{d}\Omega_p \tilde{\Psi}_\beta^{\dagger\,(G,-)}(\vec{p})\tau_i\Psi_\alpha^{(G,+)}(\vec{p})\right\}$$

$$= Q_{\alpha\beta}\left\{-3\sqrt{\frac{(2G-1)(2G+1)}{3G}}\left[\left(\tilde{g}_\beta^{(G,+;2)}(p)\tilde{g}_\alpha^{(G-1,-;1)}(p)\right)+\left(\tilde{f}_\beta^{(G,+;2)}(p)\tilde{f}_\alpha^{(G-1,-;1)}(p)\right)\right]\right\},$$

where $M_{\alpha\beta}, N_{\alpha\beta}, B_{\alpha\beta}$ and $Q_{\alpha\beta}$ are defined as

$$M_{\alpha\beta} = \left\{-\sqrt{\frac{G(2G+1)}{3(G+1)}}\left[\left(g_\beta^{(G,+;1)}(r)g_\alpha^{(G,+;1)}(r)\right)+\left(f_\beta^{(G,+;1)}(r)f_\alpha^{(G,+;1)}(r)\right)\right]\right.$$
$$\left.+\sqrt{\frac{(G+1)(2G+1)}{3G}}\left[\left(g_\beta^{(G,+;2)}(r)g_\alpha^{(G,+;2)}(r)\right)+\left(f_\beta^{(G,+;2)}(r)f_\alpha^{(G,+;2)}(r)\right)\right]\right\},$$

$$N_{\alpha\beta} = \left\{-3\sqrt{\frac{(2G+3)(2G+1)}{3(G+1)}}\left[\left(g_\beta^{(G,+;1)}(r)g_\alpha^{(G+1,-;2)}(r)\right)+\left(f_\beta^{(G,+;1)}(r)f_\alpha^{(G+1,-;2)}(r)\right)\right]\right\},$$

$$B_{\alpha\beta} = \left\{-\sqrt{\frac{G(2G+1)}{3(G+1)}}\left[\left(g_\beta^{(G,-;1)}(r)g_\alpha^{(G,-;1)}(r)\right)+\left(f_\beta^{(G,-;1)}(r)f_\alpha^{(G,-;1)}(r)\right)\right]\right.$$
$$\left.+\sqrt{\frac{(G+1)(2G+1)}{3G}}\left[\left(g_\beta^{(G,-;2)}(r)g_\alpha^{(G,-;2)}(r)\right)+\left(f_\beta^{(G,-;2)}(r)f_\alpha^{(G,-;2)}(r)\right)\right]\right\},$$

$$Q_{\alpha\beta} = \left\{\sqrt{\frac{(2G-1)(2G+1)}{3G}}\left[\left(g_\beta^{(G,+;2)}(r)g_\alpha^{(G-1,-;1)}(r)\right)+\left(f_\beta^{(G,+;2)}(r)f_\alpha^{(G-1,-;1)}(r)\right)\right]\right\},$$

In the next step, we consider matrix element of

$$\tilde{\Psi}_\beta^\dagger(\vec{p})\vec{\tau}(\hat{p}\cdot\vec{\alpha})\tilde{\Psi}_\alpha(\vec{p}) = \tilde{\Psi}_\beta^\dagger(\vec{p})\vec{\tau}\tilde{\varphi}_\alpha(\vec{p}),$$

where $\tilde{\varphi}_\alpha(\vec{p}) = \hat{p}\cdot\vec{\alpha}\tilde{\Psi}_\alpha(\vec{p})$. Now since $\hat{p}\cdot\vec{\alpha}$ is even in parity transformation we have

$$\tilde{\varphi}_\alpha^{(G',+)}(\vec{p}) = \begin{pmatrix}(\imath)^{G'+1}\bar{g}_\alpha^{(G',+;1)}(p)\mathcal{Y}_{G'G'+\frac{1}{2}G'M'}(\hat{p})\\(\imath)^{G'+1}\bar{f}_\alpha^{(G',+;1)}(p)\mathcal{Y}_{G'+1G'+\frac{1}{2}G'M'}(\hat{p})\end{pmatrix}+\begin{pmatrix}(\imath)^{G'+1}\bar{g}_\alpha^{(G',+;2)}(p)\mathcal{Y}_{G'G'-\frac{1}{2}G'M'}(\hat{p})\\-(\imath)^{G'-1}\bar{f}_\alpha^{(G',+;2)}(p)\mathcal{Y}_{G'-1G'-\frac{1}{2}G'M'}(\hat{p})\end{pmatrix}, \quad \text{(E.2.2)}$$

and

$$\tilde{\varphi}_\alpha^{(G',-)}(\vec{p}) = \begin{pmatrix}(\imath)^{G'+2}\bar{g}_\alpha^{(G',-;1)}(p)\mathcal{Y}_{G'+1G'+\frac{1}{2}G'M'}(\hat{p})\\-(\imath)^{G'}\bar{f}_\alpha^{(G',-;1)}(p)\mathcal{Y}_{G'G'+\frac{1}{2}G'M'}(\hat{p})\end{pmatrix}+\begin{pmatrix}(\imath)^{G'}\bar{g}_\alpha^{(G',-;2)}(p)\mathcal{Y}_{G'-1G'-\frac{1}{2}G'M'}(\hat{p})\\(\imath)^{G'}\bar{f}_\alpha^{(G',-;2)}(p)\mathcal{Y}_{G'G'-\frac{1}{2}G'M'}(\hat{p})\end{pmatrix}, \quad \text{(E.2.3)}$$

where

$$\bar{g}_\alpha^{(G',+;1)}(p) = -\tilde{f}_\alpha^{(G',+;1)}(p), \quad \bar{f}_\alpha^{(G',+;1)}(p) = -\tilde{g}_\alpha^{(G',+;1)}(p),$$
$$\bar{g}_\alpha^{(G',+;2)}(p) = -\tilde{f}_\alpha^{(G',+;2)}(p), \quad \bar{f}_\alpha^{(G',+;2)}(p) = -\tilde{g}_\alpha^{(G',+;2)}(p),$$

and

$$\bar{g}_\alpha^{(G',-;1)}(p) = -\tilde{f}_\alpha^{(G',-;1)}(p), \quad \bar{f}_\alpha^{(G',-;1)}(p) = -\tilde{g}_\alpha^{(G',-;1)}(p)$$
$$\bar{g}_\alpha^{(G',-;2)}(p) = -\tilde{f}_\alpha^{(G',-;2)}(p), \quad \bar{f}_\alpha^{(G',-;2)}(p) = -\tilde{g}_\alpha^{(G',-;2)}(p).$$

E.3 Matrix element of the Quartic Spinor Terms of the Isoscalar Longitudinal Polarized Structure Function

In this section we discuss the matrix elements of equation (7.2.4). We first consider the matrix element of

$$\Big\{\int \mathrm{d}\Omega_r \Psi_\alpha^\dagger(\vec{r})\tau_i\Psi_\beta(\vec{r})\Big\}\Big\{\int \mathrm{d}\Omega_p \tilde{\Psi}_\beta^\dagger(\vec{p})\sigma_i\tilde{\Psi}_\alpha(\vec{p})\Big\}. \tag{E.3.1}$$

Expressing the vector σ_i into spherical components

$$\sigma_+ = -\frac{1}{\sqrt{2}}\left(\sigma_1 + \imath\sigma_2\right), \quad \sigma_- = \frac{1}{\sqrt{2}}\left(\sigma_1 - \imath\sigma_2\right) \quad \text{and} \quad \sigma_0 = \sigma_3, \tag{E.3.2}$$

we have

$$\begin{aligned}
&\Big\{\int \mathrm{d}\Omega_r \Psi_\alpha^\dagger(\vec{r})\tau_i\Psi_\beta(\vec{r})\Big\}\Big\{\int \mathrm{d}\Omega_p \tilde{\Psi}_\beta^\dagger(\vec{p})\sigma_i\tilde{\Psi}_\alpha(\vec{p})\Big\}\\
&= \sum_M \Big\{\int \mathrm{d}\Omega_r \mathcal{Y}_{L'J'G'M}(\vec{r})\tau_+\mathcal{Y}_{LJGM-1}(\vec{r})\Big\}\Big\{\int \mathrm{d}\Omega_p \mathcal{Y}_{LJGM-1}(\vec{p})\sigma_-\mathcal{Y}_{L'J'G'M}(\vec{p})\Big\}\\
&+ \sum_M \Big\{\int \mathrm{d}\Omega_r \mathcal{Y}_{L'J'G'M}(\vec{r})\tau_-\mathcal{Y}_{LJGM+1}(\vec{r})\Big\}\Big\{\int \mathrm{d}\Omega_p \mathcal{Y}_{LJGM+1}(\vec{p})\sigma_+\mathcal{Y}_{L'J'G'M}(\vec{p})\Big\}\\
&+ \sum_M \Big\{\int \mathrm{d}\Omega_r \mathcal{Y}_{L'J'G'M}(\vec{r})\tau_0\mathcal{Y}_{LJGM}(\vec{r})\Big\}\Big\{\int \mathrm{d}\Omega_p \mathcal{Y}_{LJGM}(\vec{p})\sigma_0\mathcal{Y}_{L'J'G'M}(\vec{p})\Big\}.
\end{aligned}$$

Summing over the grand spin projections gives

$$\begin{aligned}
&\Big\{\int \mathrm{d}\Omega_r \Psi_\alpha^{\dagger(G,+)}(\vec{r})\tau_i\Psi_\beta^{(G,+)}(\vec{r})\Big\}\Big\{\int \mathrm{d}\Omega_p \tilde{\Psi}_\beta^{\dagger(G,+)}(\vec{p})\sigma_i\Psi_\alpha^{(G,+)}(\vec{p})\Big\}\\
&= M_{\alpha\beta}\Bigg\{\frac{2G+3}{2G+1}\sqrt{\frac{G(2G+1)}{3(G+1)}}\Big(\tilde{g}_\beta^{(G,+;1)}(p)\tilde{g}_\alpha^{(G,+;1)}(p)\Big) - \sqrt{\frac{G(2G+1)}{3(G+1)}}\Big(\tilde{f}_\beta^{(G,+;1)}(p)\tilde{f}_\alpha^{(G,+;1)}(p)\Big)\\
&- \frac{2G-1}{2G+1}\sqrt{\frac{(G+1)(2G+1)}{3G}}\Big(\tilde{g}_\beta^{(G,+;2)}(p)\tilde{g}_\alpha^{(G,+;2)}(p)\Big) + \sqrt{\frac{(G+1)(2G+1)}{3G}}\Big(\tilde{f}_\beta^{(G,+;2)}(p)\tilde{f}_\alpha^{(G,+;2)}(p)\Big)\\
&+ \frac{2}{3(2G+1)}\Big[\Big(\tilde{g}_\beta^{(G,+;2)}(p)\tilde{g}_\alpha^{(G,+;1)}(p)\Big) + \Big(\tilde{g}_\beta^{(G,+;1)}(p)\tilde{g}_\alpha^{(G,+;2)}(p)\Big)\Big]\Bigg\},\\
&\Big\{\int \mathrm{d}\Omega_r \Psi_\alpha^{\dagger(G+1,-)}(\vec{r})\tau_i\Psi_\beta^{(G,+)}(\vec{r})\Big\}\Big\{\int \mathrm{d}\Omega_p \tilde{\Psi}_\beta^{\dagger(G,+)}(\vec{p})\sigma_i\Psi_\alpha^{(G+1,-)}(\vec{p})\Big\}
\end{aligned}$$

$$
\begin{aligned}
&= N_{\alpha\beta}\Bigg\{-\sqrt{\frac{2G+3}{3(G+1)(2G+1)}}\Big(\tilde{g}_\beta^{(G,+;1)}(p)\tilde{g}_\alpha^{(G+1,-;2)}(p)\Big)\\
&+\sqrt{\frac{2G+1}{3(G+1)(2G+3)}}\Big(\tilde{f}_\beta^{(G,+;1)}(p)\tilde{f}_\alpha^{(G+1,-;2)}(p)\Big)\\
&-2\sqrt{\frac{(G+2)(2G+1)}{3(2G+3)}}\Big(\tilde{f}_\beta^{(G,+;1)}(p)\tilde{f}_\alpha^{(G+1,-;1)}(p)\Big)+2\sqrt{\frac{G(2G+3)}{3(2G+1)}}\Big(\tilde{g}_\beta^{(G,+;2)}(p)\tilde{g}_\alpha^{(G+1,-;2)}(p)\Big)\Bigg\},\\
&\Big\{\int \mathrm{d}\Omega_r \Psi_\alpha^{\dagger\,(G,-)}(\vec{r})\tau_i\Psi_\beta^{(G,-)}(\vec{r})\Big\}\Big\{\int \mathrm{d}\Omega_p \tilde{\Psi}_\beta^{\dagger\,(G,-)}(\vec{p})\sigma_i\Psi_\alpha^{(G,-)}(\vec{p})\Big\}\\
&= B_{\alpha\beta}\Bigg\{\frac{2G+3}{2G+1}\sqrt{\frac{G(2G+1)}{3(G+1)}}\Big(\tilde{f}_\beta^{(G,-;1)}(p)\tilde{f}_\alpha^{(G,-;1)}(p)\Big)-\sqrt{\frac{G(2G+1)}{3(G+1)}}\Big(\tilde{g}_\beta^{(G,-;1)}(p)\tilde{g}_\alpha^{(G,-;1)}(p)\Big)\\
&-\frac{2G-1}{2G+1}\sqrt{\frac{(G+1)(2G+1)}{3G}}\Big(\tilde{f}_\beta^{(G,-;2)}(p)\tilde{f}_\alpha^{(G,-;2)}(p)\Big)+\sqrt{\frac{(G+1)(2G+1)}{3G}}\Big(\tilde{g}_\beta^{(G,-;2)}(p)\tilde{g}_\alpha^{(G,-;2)}(p)\Big)\\
&-\frac{2}{3(2G+1)}\Big[\Big(\tilde{f}_\beta^{(G,-;2)}(p)\tilde{f}_\alpha^{(G,-;1)}(p)\Big)-\Big(\tilde{f}_\beta^{(G,-;1)}(p)\tilde{f}_\alpha^{(G,-;2)}(p)\Big)\Big]\Bigg\},\\
&\Big\{\int \mathrm{d}\Omega_r \Psi_\alpha^{\dagger\,(G,+)}(\vec{r})\tau_i\Psi_\beta^{(G-1,-)}(\vec{r})\Big\}\Big\{\int \mathrm{d}\Omega_p \tilde{\Psi}_\beta^{\dagger\,(G,-)}(\vec{p})\sigma_i\Psi_\alpha^{(G,+)}(\vec{p})\Big\}\\
&= Q_{\alpha\beta}\Bigg\{-\sqrt{\frac{3(2G-1)}{G(2G+1)}}\Big(\tilde{g}_\beta^{(G,+;2)}(p)\tilde{g}_\alpha^{(G-1,-;1)}(p)\Big)+6\sqrt{\frac{(G-1)(2G+1)}{3(2G-1)}}\Big(\tilde{f}_\beta^{(G,+;2)}(p)\tilde{f}_\alpha^{(G-1,-;2)}(p)\Big)\\
&+3\sqrt{\frac{2G+1}{3G(2G-1)}}\Big(\tilde{f}_\beta^{(G,+;2)}(p)\tilde{f}_\alpha^{(G-1,-;1)}(p)\Big)-6\sqrt{\frac{(G+1)(2G-1)}{3(2G+1)}}\Big(\tilde{g}_\beta^{(G,+;1)}(p)\tilde{g}_\alpha^{(G-1,-;1)}(p)\Big)\Bigg\}. \qquad \text{(E.3.3)}
\end{aligned}
$$

Next, we consider the matrix element of $\Big\{\int \mathrm{d}\Omega_r \Psi_\alpha^\dagger(\vec{r})\tau_i\Psi_\beta(\vec{r})\Big\}\Big\{\int \mathrm{d}\Omega_p \tilde{\Psi}_\beta^\dagger(\vec{p})\hat{p}_i\gamma_5\tilde{\Psi}_\alpha(\vec{p})\Big\}$.

For convenience we write

$$
\int \mathrm{d}\Omega_p \tilde{\Psi}_\beta^\dagger(\vec{p})\hat{p}_i\gamma_5\tilde{\Psi}_\alpha = \frac{1}{2}\int \mathrm{d}\Omega_p\Big\{\tilde{\Psi}_\beta^\dagger(\vec{p})\tau_i\hat{p}\cdot\vec{\tau}\gamma_5\tilde{\Psi}_\alpha(\vec{p})+\tilde{\Psi}_\beta^\dagger(\vec{p})\hat{p}\cdot\vec{\tau}\tau_i\gamma_5\tilde{\Psi}_\alpha(\vec{p})\Big\}, \qquad \text{(E.3.4)}
$$

here we have made use of the definition

$$
\hat{p}_i = \frac{1}{2}\left\{\tau_i, \hat{p}\cdot\vec{\tau}\right\}. \qquad \text{(E.3.5)}
$$

(a) In what follows, we consider the matrix element of

$$
\int \mathrm{d}\Omega_p \tilde{\Psi}_\beta^\dagger(\vec{p})\tau_i\hat{p}\cdot\vec{\tau}\gamma_5\tilde{\Psi}_\alpha(\vec{p}) = \int \mathrm{d}\Omega_p \tilde{\Psi}_\beta^\dagger(\vec{p})\tau_i\tilde{\phi}_\alpha(\vec{p}), \qquad \text{(E.3.6)}
$$

where $\tilde{\phi}_\alpha(\vec{p}) = \hat{p}\cdot\vec{\tau}\gamma_5\tilde{\Psi}_\alpha(\vec{p})$. But since the matrix $\hat{p}\cdot\vec{\tau}\gamma_5$ is even in parity transformation we have

$$
\tilde{\phi}_\alpha^{(G',+)}(\vec{p}) = \begin{pmatrix}(\imath)^{G'+1}\overleftarrow{g}_\alpha^{(G',+;1)}(p)\mathcal{Y}_{G'G'+\frac{1}{2}G'M'}(\hat{p})\\ (\imath)^{G'+1}\overleftarrow{f}_\alpha^{(G',+;1)}(p)\mathcal{Y}_{G'+1G'+\frac{1}{2}G'M'}(\hat{p})\end{pmatrix}+\begin{pmatrix}(\imath)^{G'+1}\overleftarrow{g}_\alpha^{(G',+;2)}(p)\mathcal{Y}_{G'G'-\frac{1}{2}G'M'}(\hat{p})\\ -(\imath)^{G'-1}\overleftarrow{f}_\alpha^{(G',+;2)}(p)\mathcal{Y}_{G'-1G'-\frac{1}{2}G'M'}(\hat{p})\end{pmatrix}, \qquad \text{(E.3.7)}
$$

and

$$
\tilde{\phi}_\alpha^{(G',-)}(\vec{p}) = \begin{pmatrix}(\imath)^{G'+2}\overleftarrow{g}_\alpha^{(G',-;1)}(p)\mathcal{Y}_{G'+1G'+\frac{1}{2}G'M'}(\hat{p})\\ -(\imath)^{G'}\overleftarrow{f}_\alpha^{(G',-;1)}(p)\mathcal{Y}_{G'G'+\frac{1}{2}G'M'}(\hat{p})\end{pmatrix}+\begin{pmatrix}(\imath)^{G'}\overleftarrow{g}_\alpha^{(G',-;2)}(p)\mathcal{Y}_{G'-1G'-\frac{1}{2}G'M'}(\hat{p})\\ (\imath)^{G'}\overleftarrow{f}_\alpha^{(G',-;2)}(p)\mathcal{Y}_{G'G'-\frac{1}{2}G'M'}(\hat{p})\end{pmatrix}. \qquad \text{(E.3.8)}
$$

Here we have defined

$$\begin{aligned}
\overleftarrow{g}_{\alpha}^{(G',+;1)}(p) &= -\frac{2\sqrt{G'(G'+1)}}{2G'+1}\tilde{f}_{\alpha}^{(G',+;2)}(p) + \frac{1}{2G'+1}\tilde{f}_{\alpha}^{(G',+;1)}(p)\\
\overleftarrow{f}_{\alpha}^{(G',+;1)}(p) &= -\frac{2\sqrt{G'(G'+1)}}{2G'+1}\tilde{g}_{\alpha}^{(G',+;2)}(p) + \frac{1}{2G'+1}\tilde{g}_{\alpha}^{(G',+;1)}(p)\\
\overleftarrow{g}_{\alpha}^{(G',+;2)}(p) &= -\frac{2\sqrt{G'(G'+1)}}{2G'+1}\tilde{f}_{\alpha}^{(G',+;1)}(p) - \frac{1}{2G'+1}\tilde{f}_{\alpha}^{(G',+;2)}(p)\\
\overleftarrow{f}_{\alpha}^{(G',+;2)}(p) &= -\frac{2\sqrt{G'(G'+1)}}{2G'+1}\tilde{g}_{\alpha}^{(G',+;1)}(p) - \frac{1}{2G'+1}\tilde{g}_{\alpha}^{(G',+;2)}(p),
\end{aligned}$$

and

$$\begin{aligned}
\overleftarrow{g}_{\alpha}^{(G',-;1)}(p) &= \frac{2\sqrt{G'(G'+1)}}{2G'+1}\tilde{f}_{\alpha}^{(G',-;2)}(p) + \frac{1}{2G'+1}\tilde{f}_{\alpha}^{(G',-;1)}(p)\\
\overleftarrow{f}_{\alpha}^{(G',-;1)}(p) &= \frac{2\sqrt{G'(G'+1)}}{2G'+1}\tilde{g}_{\alpha}^{(G',-;2)}(p) + \frac{1}{2G'+1}\tilde{g}_{\alpha}^{(G',-;1)}(p)\\
\overleftarrow{g}_{\alpha}^{(G',-;2)}(p) &= \frac{2\sqrt{G'(G'+1)}}{2G'+1}\tilde{f}_{\alpha}^{(G',-;1)}(p) - \frac{1}{2G'+1}\tilde{f}_{\alpha}^{(G',-;2)}(p)\\
\overleftarrow{f}_{\alpha}^{(G',-;2)}(p) &= \frac{2\sqrt{G'(G'+1)}}{2G'+1}\tilde{g}_{\alpha}^{(G',-;1)}(p) - \frac{1}{2G'+1}\tilde{g}_{\alpha}^{(G',-;2)}(p).
\end{aligned}$$

(b) Furthermore, we consider the matrix element

$$\int \mathrm{d}\Omega_p \tilde{\Psi}_{\beta}^{\dagger}(\vec{p})\hat{p}\cdot\vec{\tau}\tau_i\gamma_5\tilde{\Psi}_{\alpha}(\vec{p}) = \int \mathrm{d}\Omega_p \tilde{\Phi}_{\beta}^{\dagger}(\vec{p})\tau_i\tilde{\Phi}_{\alpha}(\vec{p}), \tag{E.3.9}$$

where $\tilde{\Phi}_{\beta}(\vec{p}) = \hat{p}\cdot\vec{\tau}\tilde{\Psi}_{\beta}(\vec{p})$ and $\tilde{\Phi}_{\alpha}(\vec{p}) = \gamma_5\tilde{\Psi}_{\alpha}(\vec{p})$. But since the matrix $\hat{p}\cdot\vec{\tau}$ is odd under parity we have

$$\tilde{\Phi}_{\beta}^{(G,+)}(\vec{p}) = \begin{pmatrix} (\imath)^{G+2}\widetilde{g}_{\beta}^{(G,+;1)}(p)\mathcal{Y}_{G+1G+\frac{1}{2}GM}(\hat{p}) \\ -(\imath)^{G}\widetilde{f}_{\beta}^{(G,+;1)}(p)\mathcal{Y}_{GG+\frac{1}{2}GM}(\hat{p}) \end{pmatrix} + \begin{pmatrix} (\imath)^{G}\widetilde{g}_{\beta}^{(G,+;2)}(p)\mathcal{Y}_{G-1G-\frac{1}{2}GM}(\hat{p}) \\ (\imath)^{G}\widetilde{f}_{\beta}^{(G,+;2)}(p)\mathcal{Y}_{GG-\frac{1}{2}GM}(\hat{p}) \end{pmatrix}, \tag{E.3.10}$$

and

$$\tilde{\Phi}_{\beta}^{(G,-)}(\vec{p}) = \begin{pmatrix} (\imath)^{G+1}\widetilde{g}_{\beta}^{(G,-;1)}(p)\mathcal{Y}_{GG+\frac{1}{2}GM}(\hat{p}) \\ (\imath)^{G+1}\widetilde{f}_{\beta}^{(G,-;1)}(p)\mathcal{Y}_{G+1G+\frac{1}{2}GM}(\hat{p}) \end{pmatrix} + \begin{pmatrix} (\imath)^{G+1}\widetilde{g}_{\beta}^{(G,-;2)}(p)\mathcal{Y}_{GG-\frac{1}{2}GM}(\hat{p}) \\ -(\imath)^{G-1}\widetilde{f}_{\beta}^{(G,-;2)}(p)\mathcal{Y}_{G-1G-\frac{1}{2}GM}(\hat{p}) \end{pmatrix}, \tag{E.3.11}$$

with

$$\begin{aligned}
\widetilde{g}_{\beta}^{(G,+;1)}(p) &= \frac{2\sqrt{G(G+1)}}{2G+1}\tilde{g}_{\beta}^{(G,+;2)}(p) - \frac{1}{2G+1}\tilde{g}_{\beta}^{(G,+;1)}(p)\\
\widetilde{f}_{\beta}^{(G,+;1)}(p) &= \frac{2\sqrt{G(G+1)}}{2G+1}\tilde{f}_{\beta}^{(G,+;2)}(p) - \frac{1}{2G+1}\tilde{f}_{\beta}^{(G,+;1)}(p)\\
\widetilde{g}_{\beta}^{(G,+;2)}(p) &= -\frac{2\sqrt{G(G+1)}}{2G+1}\tilde{g}_{\beta}^{(G,+;1)}(p) - \frac{1}{2G+1}\tilde{g}_{\beta}^{(G,+;2)}(p)\\
\widetilde{f}_{\beta}^{(G,+;2)}(p) &= -\frac{2\sqrt{G(G+1)}}{2G+1}\tilde{f}_{\beta}^{(G,+;1)}(p) - \frac{1}{2G+1}\tilde{f}_{\beta}^{(G,+;2)}(p),
\end{aligned}$$

and

$$\begin{aligned}
\widetilde{g}_\beta^{(G,-;1)}(p) &= \frac{2\sqrt{G(G+1)}}{2G+1}\tilde{g}_\beta^{(G,-;2)}(p) + \frac{1}{2G+1}\tilde{g}_\beta^{(G,-;1)}(p)\\
\widetilde{f}_\beta^{(G,-;1)}(p) &= \frac{2\sqrt{G(G+1)}}{2G+1}\tilde{f}_\beta^{(G,-;2)}(p) + \frac{1}{2G+1}\tilde{f}_\beta^{(G,-;1)}(p)\\
\widetilde{g}_\beta^{(G,-;2)}(p) &= -\frac{2\sqrt{G(G+1)}}{2G+1}\tilde{g}_\beta^{(G,-;1)}(p) + \frac{1}{2G+1}\tilde{g}_\beta^{(G,-;2)}(p)\\
\widetilde{f}_\beta^{(G,-;2)}(p) &= -\frac{2\sqrt{G(G+1)}}{2G+1}\tilde{f}_\beta^{(G,-;1)}(p) + \frac{1}{2G+1}\tilde{f}_\beta^{(G,-;2)}(p).
\end{aligned}$$

Similarly, since γ_5 is odd under parity we have

$$\tilde{\Phi}_\alpha^{(G',+)}(\vec{p}) = \begin{pmatrix} (\imath)^{G'+2}\breve{g}_\alpha^{(G',+;1)}(p)\mathcal{Y}_{G'+1G'+\frac{1}{2}G'M'}(\hat{p}) \\ -(\imath)^{G'}\breve{f}_\alpha^{(G',+;1)}(p)\mathcal{Y}_{G'G'+\frac{1}{2}G'M'}(\hat{p}) \end{pmatrix} + \begin{pmatrix} (\imath)^{G'}\breve{g}_\alpha^{(G',+;2)}(p)\mathcal{Y}_{G'-1G'-\frac{1}{2}G'M'}(\hat{p}) \\ (\imath)^{G'}\breve{f}_\alpha^{(G',+;2)}(p)\mathcal{Y}_{G'G'-\frac{1}{2}G'M'}(\hat{p}) \end{pmatrix}, \tag{E.3.12}$$

and

$$\tilde{\Phi}_\alpha^{(G',-)}(\vec{p}) = \begin{pmatrix} (\imath)^{G'+1}\breve{g}_\alpha^{(G',-;1)}(p)\mathcal{Y}_{G'G'+\frac{1}{2}G'M'}(\hat{p}) \\ (\imath)^{G'+1}\breve{f}_\alpha^{(G',-;1)}(p)\mathcal{Y}_{G'+1G'+\frac{1}{2}G'M'}(\hat{p}) \end{pmatrix} + \begin{pmatrix} (\imath)^{G'+1}\breve{g}_\alpha^{(G',-;2)}(p)\mathcal{Y}_{G'G'-\frac{1}{2}G'M'}(\hat{p}) \\ -(\imath)^{G'-1}\breve{f}_\alpha^{(G',-;2)}(p)\mathcal{Y}_{G'-1G'-\frac{1}{2}G'M'}(\hat{p}) \end{pmatrix}. \tag{E.3.13}$$

Here we have define

$$\begin{aligned}
\breve{g}_\alpha^{(G',+;1)}(p) &= -\tilde{f}_\alpha^{(G',+;1)}(p), \quad \breve{f}_\alpha^{(G',+;1)}(p) = -\tilde{g}_\alpha^{(G',+;1)}(p),\\
\breve{g}_\alpha^{(G',+;2)}(p) &= \tilde{f}_\alpha^{(G',+;2)}(p), \quad \breve{f}_\alpha^{(G',+;2)}(p) = \tilde{g}_\alpha^{(G',+;2)}(p),
\end{aligned}$$

and

$$\begin{aligned}
\breve{g}_\alpha^{(G',-;1)}(p) &= \tilde{f}_\alpha^{(G',-;1)}(p), \quad \breve{f}_\alpha^{(G',-;1)}(p) = \tilde{g}_\alpha^{(G',-;1)}(p)\\
\breve{g}_\alpha^{(G',-;2)}(p) &= -\tilde{f}_\alpha^{(G',-;2)}(p), \quad \breve{f}_\alpha^{(G',-;2)}(p) = -\tilde{g}_\alpha^{(G',-;2)}(p).
\end{aligned}$$

Lastly, we consider the matrix element of $\Big\{\int \mathrm{d}\Omega_r \Psi_\alpha^\dagger(\vec{r})\tau_i\Psi_\beta(\vec{r})\Big\}\Big\{\int \mathrm{d}\Omega_p \tilde{\Psi}_\beta^\dagger(\vec{p})\hat{p}_i\hat{p}\cdot\vec{\sigma}\tilde{\Psi}_\alpha(\vec{p})\Big\}$.

Making use of equation (E.3.5), we write

$$\int \mathrm{d}\Omega_p \tilde{\Psi}_\beta^\dagger(\vec{p})\hat{p}_i\hat{p}\cdot\vec{\alpha}\gamma_5\tilde{\Psi}_\alpha = \int \mathrm{d}\Omega_p \frac{1}{2}\Big\{\tilde{\Psi}_\beta^\dagger(\vec{p})\tau_i\hat{p}\cdot\vec{\tau}\hat{p}\cdot\vec{\alpha}\gamma_5\tilde{\Psi}_\alpha(\vec{p}) + \tilde{\Psi}_\beta^\dagger(\vec{p})\hat{p}\cdot\vec{\tau}\tau_i\hat{p}\cdot\vec{\alpha}\gamma_5\tilde{\Psi}_\alpha(\vec{p})\Big\}. \tag{E.3.14}$$

(a) In the first step, we consider the matrix element of

$$\int \mathrm{d}\Omega_p \tilde{\Psi}_\beta^\dagger(\vec{p})\tau_i\hat{p}\cdot\vec{\tau}\hat{p}\cdot\vec{\alpha}\gamma_5\tilde{\Psi}_\alpha(\vec{p}) = \int \mathrm{d}\Omega_p \tilde{\Psi}_\beta^\dagger(\vec{p})\tau_i\tilde{\psi}_\alpha(\vec{p}), \tag{E.3.15}$$

where $\tilde{\psi}_\alpha(\vec{p}) = \hat{p}\cdot\vec{\tau}\hat{p}\cdot\vec{\alpha}\gamma_5\tilde{\Psi}_\alpha(\vec{p})$. But since the matrix $\hat{p}\cdot\vec{\tau}\hat{p}\cdot\vec{\alpha}\gamma_5$ is even in parity transformation we have

$$\tilde{\psi}_\alpha^{(G',+)}(\vec{p}) = \begin{pmatrix} (\imath)^{G'+1}\widehat{g}_\alpha^{(G',+;1)}(p)\mathcal{Y}_{G'G'+\frac{1}{2}G'M'}(\hat{p}) \\ (\imath)^{G'+1}\widehat{f}_\alpha^{(G',+;1)}(p)\mathcal{Y}_{G'+1G'+\frac{1}{2}G'M'}(\hat{p}) \end{pmatrix} + \begin{pmatrix} (\imath)^{G'+1}\widehat{g}_\alpha^{(G',+;2)}(p)\mathcal{Y}_{G'G'-\frac{1}{2}G'M'}(\hat{p}) \\ -(\imath)^{G'-1}\widehat{f}_\alpha^{(G',+;2)}(p)\mathcal{Y}_{G'-1G'-\frac{1}{2}G'M'}(\hat{p}) \end{pmatrix}, \tag{E.3.16}$$

and

$$\tilde{\psi}_\alpha^{(G',-)}(\vec{p}) = \begin{pmatrix} (\imath)^{G'+2}\widehat{g}_\alpha^{(G',-;1)}(p)\mathcal{Y}_{G'+1G'+\frac{1}{2}G'M'}(\hat{p}) \\ -(\imath)^{G'}\widehat{f}_\alpha^{(G',-;1)}(p)\mathcal{Y}_{G'G'+\frac{1}{2}G'M'}(\hat{p}) \end{pmatrix} + \begin{pmatrix} (\imath)^{G'}\widehat{g}_\alpha^{(G',-;2)}(p)\mathcal{Y}_{G'-1G'-\frac{1}{2}G'M'}(\hat{p}) \\ (\imath)^{G'}\widehat{f}_\alpha^{(G',-;2)}(p)\mathcal{Y}_{G'G'-\frac{1}{2}G'M'}(\hat{p}) \end{pmatrix}, \tag{E.3.17}$$

with the radial functions defined as

$$\begin{aligned}
\widehat{g}_\alpha^{(G',+;1)}(p) &= \frac{2\sqrt{G'(G'+1)}}{2G'+1}\tilde{g}_\alpha^{(G',+;2)}(p) - \frac{1}{2G'+1}\tilde{g}_\alpha^{(G',+;1)}(p)\\
\widehat{f}_\alpha^{(G',+;1)}(p) &= \frac{2\sqrt{G'(G'+1)}}{2G'+1}\tilde{f}_\alpha^{(G',+;2)}(p) - \frac{1}{2G'+1}\tilde{f}_\alpha^{(G',+;1)}(p)\\
\widehat{g}_\alpha^{(G',+;2)}(p) &= \frac{2\sqrt{G'(G'+1)}}{2G'+1}\tilde{g}_\alpha^{(G',+;1)}(p) + \frac{1}{2G'+1}\tilde{g}_\alpha^{(G',+;2)}(p)\\
\widehat{f}_\alpha^{(G',+;2)}(p) &= \frac{2\sqrt{G'(G'+1)}}{2G'+1}\tilde{f}_\alpha^{(G',+;1)}(p) + \frac{1}{2G'+1}\tilde{f}_\alpha^{(G',+;2)}(p),
\end{aligned}$$

and

$$\begin{aligned}
\widehat{g}_\alpha^{(G',-;1)}(p) &= -\frac{2\sqrt{G'(G'+1)}}{2G'+1}\tilde{g}_\alpha^{(G',-;2)}(p) - \frac{1}{2G'+1}\tilde{g}_\alpha^{(G',-;1)}(p)\\
\widehat{f}_\alpha^{(G',-;1)}(p) &= -\frac{2\sqrt{G'(G'+1)}}{2G'+1}\tilde{f}_\alpha^{(G',-;2)}(p) - \frac{1}{2G'+1}\tilde{f}_\alpha^{(G',-;1)}(p)\\
\widehat{g}_\alpha^{(G',-;2)}(p) &= -\frac{2\sqrt{G'(G'+1)}}{2G'+1}\tilde{g}_\alpha^{(G',-;1)}(p) + \frac{1}{2G'+1}\tilde{g}_\alpha^{(G',-;2)}(p)\\
\widehat{f}_\alpha^{(G',-;2)}(p) &= -\frac{2\sqrt{G'(G'+1)}}{2G'+1}\tilde{f}_\alpha^{(G',-;1)}(p) + \frac{1}{2G'+1}\tilde{f}_\alpha^{(G',-;2)}(p).
\end{aligned}$$

(b) In the second step, we consider the matrix element of

$$\int \mathrm{d}\Omega_p \tilde{\Psi}_\beta^\dagger(\vec{p})\hat{p}\cdot\vec{\tau}\tau_i\hat{p}\cdot\vec{\alpha}\gamma_5\tilde{\Psi}_\alpha(\vec{p}) = \int \mathrm{d}\Omega_p \tilde{\Phi}_\beta^\dagger(\vec{p})\tau_i\tilde{\varphi}_\alpha(\vec{p}), \tag{E.3.18}$$

where $\tilde{\Phi}_\beta(\vec{p}) = \hat{p}\cdot\vec{\tau}\tilde{\Psi}_\beta(\vec{p})$, which we have already discussed above and $\tilde{\varphi}_\alpha(\vec{p}) = \hat{p}\cdot\vec{\alpha}\gamma_5\tilde{\Psi}_\alpha(\vec{p})$. But since $\hat{p}\cdot\vec{\alpha}\gamma_5$ is odd in parity transformation we have

$$\tilde{\varphi}_\alpha^{(G',+)}(\vec{p}) = \begin{pmatrix} (\imath)^{G'+2}\check{g}_\alpha^{(G',+;1)}(p)\mathcal{Y}_{G'+1G'+\frac{1}{2}G'M'}(\hat{p}) \\ -(\imath)^{G'}\check{f}_\alpha^{(G',+;1)}(p)\mathcal{Y}_{G'G'+\frac{1}{2}G'M'}(\hat{p}) \end{pmatrix} + \begin{pmatrix} (\imath)^{G'}\check{g}_\alpha^{(G',+;2)}(p)\mathcal{Y}_{G'-1G'-\frac{1}{2}G'M'}(\hat{p}) \\ (\imath)^{G'}\check{f}_\alpha^{(G',+;2)}(p)\mathcal{Y}_{G'G'-\frac{1}{2}G'M'}(\hat{p}) \end{pmatrix}, \tag{E.3.19}$$

and

$$\tilde{\varphi}_\alpha^{(G',-)}(\vec{p}) = \begin{pmatrix} (\imath)^{G'+1}\check{g}_\alpha^{(G',-;1)}(p)\mathcal{Y}_{G'G'+\frac{1}{2}G'M'}(\hat{p}) \\ (\imath)^{G'+1}\check{f}_\alpha^{(G',-;1)}(p)\mathcal{Y}_{G'+1G'+\frac{1}{2}G'M'}(\hat{p}) \end{pmatrix} + \begin{pmatrix} (\imath)^{G'+1}\check{g}_\alpha^{(G',-;2)}(p)\mathcal{Y}_{G'G'-\frac{1}{2}G'M'}(\hat{p}) \\ -(\imath)^{G'-1}\check{f}_\alpha^{(G',-;2)}(p)\mathcal{Y}_{G'-1G'-\frac{1}{2}G'M'}(\hat{p}) \end{pmatrix}. \tag{E.3.20}$$

Here the radial functions becomes

$$\begin{aligned}
\check{g}_\alpha^{(G',+;1)}(p) &= \tilde{g}_\alpha^{(G',+;1)}(p), \quad \check{f}_\alpha^{(G',+;1)}(p) = \tilde{f}_\alpha^{(G',+;1)}(p),\\
\check{g}_\alpha^{(G',+;2)}(p) &= -\tilde{g}_\alpha^{(G',+;2)}(p), \quad \check{f}_\alpha^{(G',+;2)}(p) = -\tilde{f}_\alpha^{(G',+;2)}(p),
\end{aligned}$$

and

$$\begin{aligned}
\check{g}_\alpha^{(G',-;1)}(p) &= -\tilde{g}_\alpha^{(G',-;1)}(p), \quad \check{f}_\alpha^{(G',-;1)}(p) = -\tilde{f}_\alpha^{(G',-;1)}(p)\\
\check{g}_\alpha^{(G',-;2)}(p) &= \tilde{g}_\alpha^{(G',-;2)}(p), \quad \check{f}_\alpha^{(G',-;2)}(p) = \tilde{f}_\alpha^{(G',-;2)}(p).
\end{aligned}$$

Bibliography

[1] Abe, K., Akagi, T., Anthony, P., Antonov, R., Arnold, R., Averett, T., Band, H., Bauer, J., Borel, H., Bosted, P. *et al.*: Precision measurement of the proton spin structure function g_1^p. *Phys. Rev. Lett.*, vol. 74, no. 3, p. 346, 1995.

[2] Abe, K., Akagi, T., Anthony, P., Antonov, R., Arnold, R., Averett, T., Band, H., Bauer, J., Borel, H., Bosted, P. *et al.*: Measurements of the proton and deuteron spin structure functions g_1 and g_2. *Phys. Rev. D*, vol. 58, no. 11, p. 112003, 1998.

[3] Abe, K., Akagi, T., Anthony, P., Antonov, R., Arnold, R., Averett, T., Band, H., Bauer, J., Borel, H., Bosted, P. *et al.*: Measurements of the proton and deuteron spin structure function g_2 and asymmetry A_2. *Phys. Rev. Lett.*, vol. 76, no. 4, p. 587, 1996.

[4] Arneodo, M., Arvidson, A., Badelek, B., Ballintijn, M., Baum, G., Beaufays, J., Bird, I., Björkholm, P., Botje, M., Broggini, C. *et al.*: Reevaluation of the Gottfried sum. *Phys. Rev. D*, vol. 50, no. 1, p. R1, 1994.

[5] Itzykson, C. and Zuber, J.-B.: *Quantum field theory.* McGraw-Hill, New York, 1985.

[6] Muta, T.: *Foundations of quantum chromodynamics: an introduction to perturbative methods in gauge theories.* World Scientific, 2010.

[7] Chen, H.-X., Chen, W., Liu, X. and Zhu, S.-L.: The hidden-charm pentaquark and tetraquark states. *arXiv preprint arXiv:1601.02092*, 2016.

[8] Tanabashi, M., Richardson, P., Bettini, A., Vogt, A., Garren, L., Schwartz, A.J., Terashi, K., Karliner, M., Chivukula, R.S., Sjöstrand, T. *et al.*: Aps: Review of particle physics. *Phys. Rev. D*, vol. 98, p. 030001, 2018.

[9] Weigel, H.: *Chiral soliton models for baryons, Springer Lecture Notes Physics*, vol. 743. Berlin: Springer Verlag, 2008.

[10] Witten, E.: Baryons in the $\frac{1}{N}$ expansion. *Nucl. Phys. B*, vol. 160, no. 1, p. 57, 1979.

[11] t Hooft, G.: A planar diagram theory for strong interactions. *Nucl. Phys. B*, vol. 72, no. CERN-TH-1786, p. 461, 1973.

[12] Cheng, T.-P., Li, L.-F. and Cheng, T.-P.: *Gauge theory of elementary particle physics.* Clarendon press: Oxford, 1984.

[13] Lampe, B. and Reya, E.: Spin physics and polarized structure functions. *Phys. Rep*, vol. 332, no. 1, p. 1, 2000.

[14] Nambu, Y. and Jona-Lasinio, G.: Dynamical model of elementary particles based on an analogy with superconductivity. I. *Phys. Rev.*, vol. 122, no. 1, p. 345, 1961.

[15] Alkofer, R. and Reinhardt, H.: *Chiral quark dynamics, Springer Lecture Notes Physics*, vol. 33. Springer, Berlin, 1995.

[16] Adler, S.L.: Axial-vector vertex in spinor electrodynamics. *Phys. Rev.*, vol. 177, no. 5, p. 2426, 1969.

[17] Bell, J.S. and Jackiw, R.: A pcac puzzle: $\pi \to \gamma\gamma$ in the σ-model. In: *Quantum Mechanics, High Energy Physics And Accelerators: Selected Papers Of John S Bell (With Commentary)*, p. 367. World Scientific, 1995.

[18] Ebert, D. and Reinhardt, H.: Effective chiral hadron Lagrangian with anomalies and Skyrme terms from quark flavour dynamics. *Nucl. Phys. B*, vol. 271, no. 1, p. 188, 1986.

[19] Alkofer, R., Reinhardt, H. and Weigel, H.: Baryons as chiral solitons in the Nambu-Jona-Lasinio model. *Phys. Rep.*, vol. 265, no. 3, p. 139, 1996.

[20] Christov, C.V., Blotz, A., Kim, H.-C., Pobylitsa, P., Watabe, T., Meissner, T., Ruiz-Arriola, E. and Goeke, K.: Baryons as non-topological chiral solitons. *Prog. Part. Nucl. Phys.*, vol. 37, p. 91, 1996.

[21] Vogl, U. and Weise, W.: The Nambu and Jona-Lasinio model: its implications for hadrons and nuclei. *Prog. Part. Nucl. Phys*, vol. 27, p. 195, 1991.

[22] Rajaraman, R.: *Instantons and solitons.* Amsterdam: North Holland, 1982.

[23] Pauli, W. and Villars, F.: On the invariant regularization in relativistic quantum theory. *Rev. Mod. Phys.*, vol. 21, no. 3, p. 434, 1949.

[24] Weigel, H., Ruiz-Arriola, E. and Gamberg, L.: Hadron structure functions in a chiral quark model: Regularization, scaling and sum rules. *Nucl. Phys. B*, vol. 560, no. 1, p. 383, 1999.

[25] Davidson, R. and Ruiz-Arriola, E.: Structure functions of pseudoscalar mesons in the $SU(3)$ NJL model. *Phys. Lett. B*, vol. 348, no. 1, p. 163, 1995.

[26] Ruiz-Arriola, E. and Salcedo, L.: Chiral anomaly and nucleon properties in the Nambu-Jona-Lasinio model with vector mesons. *Nucl. Phys. A*, vol. 590, no. 3, p. 703, 1995.

[27] Doering, F., Schueren, C., E, R.-A., Watabe, T. and Goeke, K.: Analytical continuation of the fermion determinant with a finite cut-off. *Nucl. Phys. A*, vol. 603, no. 3, p. 415, 1996.

[28] Fujikawa, K. and Suzuki, H.: *Path integrals and quantum anomalies*, vol. 122. Oxford: Oxford University Press, 2004.

[29] Schüren, C., Ruiz-Arriola, E. and Goeke, K.: Explicit chiral symmetry breaking in the Nambu-Jona-Lasinio model. *Nucl. Phys. A*, vol. 547, no. 4, p. 612, 1992.

[30] Halzen, F. and Martin, A.D.: *Quark and Leptons: An introductory course in modern particle physics*. John Wiley and Sons, 2008.

[31] Döring, F., Blotz, A., Schüren, C., Meissner, T., Ruiz-Arriola, E. and Goeke, K.: The Connection between soliton and vacuum regularization in the Nambu-Jona-Lasinio model. *Nucl. Phys. A*, vol. 536, no. 3, p. 548, 1992.

[32] Pauli, W.: *Meson theory of nuclear forces*. Interscience Publishers, 1948.

[33] Derrick, G.: Comments on nonlinear wave equations as models for elementary particles. *J. Math. Phys.*, vol. 5, no. 9, p. 1252, 1964.

[34] Skyrme, T.H.R.: A non-linear field theory. *Proc. Roy. Soc. Lond.*, vol. 260, no. 1300, p. 127, 1961.

[35] Manton, N. and Sutcliffe, P.: *Topological solitons*. Cambridge: Cambridge University Press, 2004.

[36] Reinhardt, H.: The chiral soliton in the proper-time regularization scheme. *Nucl. Phys. A*, vol. 503, no. 3, p. 825, 1989.

[37] Dashen, R.F., Hasslacher, B. and Neveu, A.: Semiclassical bound states in an asymptotically free theory. *Phys. Rev. D*, vol. 12, no. 8, p. 2443, 1975.

[38] Kahana, S. and Ripka, G.: Baryon density of quarks coupled to a chiral field. *Nucl. Phys. A*, vol. 429, no. 3, p. 462, 1984.

[39] Alkofer, R., Reinhardt, H., Weigel, H. and Zuckert, U.: Supporting the Skyrmion from the Nambu-Jona-Lasinio model with vector and axial vector mesons. *Phys. Rev. Lett.*, vol. 69, p. 1874, 1992.

[40] Reinhardt, H. and Wünsch, R.: Topological solitons of the Nambu-Jona-Lasinio model. *Phys. Lett. B*, vol. 230, no. 1, p. 93, 1989.

[41] Meissner, T., Grümmer, F. and Goeke, K.: Solitons in the Nambu-Jona-Lasinio Model. *Phys. Lett. B*, vol. 227, no. 3, p. 296, 1989.

[42] Alkofer, R.: The soliton of the Nambu-Jona-Lasinio model. *Phys. Lett. B*, vol. 236, no. 3, p. 310, 1990.

[43] Ring, P. and Schuck, P.: *The nuclear many-body problem*. Berlin: Springer Verlag, 2004.

[44] Holzwarth, G. and Schwesinger, B.: Baryons in the Skyrme model. *Rep. Prog. Phys.*, vol. 49, no. 8, p. 825, 1986.

[45] Adkins, G.S., Nappi, C.R. and Witten, E.: Static properties of nucleons in the Skyrme model. *Nucl. Phys. B*, vol. 228, no. 3, p. 552, 1983.

[46] Weigel, H., Gamberg, L. and Reinhardt, H.: Nucleon structure functions from a chiral soliton. *Phys. Lett. B*, vol. 399, no. 3, p. 287, 1997.

[47] Weigel, H., Gamberg, L. and Reinhardt, H.: Polarized nucleon structure functions within a chiral soliton model. *Phys. Rev. D*, vol. 55, no. 11, p. 6910, 1997.

[48] Diakonov, D., Petrov, V., Pobylitsa, P., Polyakov, M. and Weiss, C.: Nucleon parton distributions at low normalization point in the large N_c limit. *Nucl. Phys. B*, vol. 480, no. 1, p. 341, 1996.

[49] Diakonov, D., Petrov, V.Y., Pobylitsa, P., Polyakov, M.V. and Weiss, C.: Unpolarized and polarized quark distributions in the large-N_c limit. *Phys. Rev. D*, vol. 56, no. 7, p. 4069, 1997.

[50] Wakamatsu, M. and Kubota, T.: Chiral symmetry and the nucleon spin structure functions. *Phys. Rev. D*, vol. 60, no. 3, p. 034020, 1999.

[51] Wakamatsu, M.: Light-flavor sea-quark distributions in the nucleon in the $SU(3)$ chiral quark soliton model. I. Phenomenological predictions. *Phys. Rev. D*, vol. 67, no. 3, p. 034005, 2003.

[52] Frederico, T. and Miller, G.: Deep-inelastic structure function of the pion in the null-plane phenomenology. *Phys. Rev. D*, vol. 50, no. 1, p. 210, 1994.

[53] Gross, F.: *Relativistic quantum mechanics and field theory.* John Wiley & Sons, 2008.

[54] Peskin, M.E. and Schroeder, D.V.: An introduction to quantum field theory. 1995.

[55] Gervals, J., Jevicki, A. and Sakita, B.: Collective coordinate method for quantization of extended systems. *Phys. Rep.*, vol. 23, no. 3, p. 281, 1976.

[56] Wakamatsu, M. and Kubota, T.: Chiral symmetry and the nucleon structure functions. *Phys. Rev. D*, vol. 57, no. 9, p. 5755, 1998.

[57] Pobylitsa, P., Polyakov, M.V., Goeke, K., Watabe, T. and Weiss, C.: Isovector unpolarized quark distribution in the nucleon in the large-N_c limit. *Phys. Rev. D*, vol. 59, no. 3, p. 034024, 1999.

[58] Schröder, O., Reinhardt, H. and Weigel, H.: Nucleon structures functionsin the three-flavor NJL soliton model. *Nucl. Phys. A*, vol. 651, no. 2, p. 174, 1999.

[59] Jaffe, R.L.: Deep-inelastic structure functions in an approximation to the bag theory. *Phys. Rev. D*, vol. 11, no. 7, p. 1953, 1975.

[60] Weigel, H., Gamberg, L. and Reinhardt, H.: Unpolarized nucleon structure functions in the Nambu-Jona-Lasinio chiral soliton model. *Mod. Phys. Lett. A*, vol. 11, no. 38, p. 3021, 1996.

[61] Jaffe, R.L.: Operators in a translation invariant two-dimensional bag model. *Ann. Phys.*, vol. 132, no. 1, p. 32, 1981.

[62] Gamberg, L., Reinhardt, H. and Weigel, H.: Nucleon structure functions from a chiral soliton in the infinite momentum frame. *Int. J. Mod. Phys. A*, vol. 13, no. 32, p. 5519, 1998.

[63] Press, W.H., Teukolsky, S.A., Vetterling, W.T. and Flannery, B.P.: *Numerical recipes in Fortran 77 and Fortran 90.* Cambridge: Cambridge University Press, 1996.

[64] Wakamatsu, M.: Sea-quark effects on g_A in a chiral quark model. *Phys. Lett. B*, vol. 234, no. 3, p. 223, 1990.

[65] Christov, C.V., Blotz, A., Goeke, K., Pobilitsa, P., Petrov, V., Wakamatsu, M. and Watabe, T.: $\frac{1}{N_c}$ rotational corrections to g_A and isovector magnetic moment of the nucleon. *Phys. Lett. B*, vol. 325, no. 3-4, p. 467, 1994.

[66] Alkofer, R. and Weigel, H.: $\frac{1}{N_c}$ corrections to g_A in the light of PCAC. *Phys. Lett. B*, vol. 319, no. 1, p. 1, 1993.

[67] Barnett, R.M., Carone, C., Groom, D., Trippe, T., Wohl, C., Armstrong, B., Gee, P., Wagman, G., James, F., Mangano, M. *et al.*: Review of particle physics. *Phys. Rev. D*, vol. 54, no. 1, p. 1, 1996.

[68] Jaffe, R.L.: $\mathtt{g}_2$-the nucleon's other spin-dependent structure function. *Comments Nucl. Part. Phys.*, vol. 19, p. 239, 1989.

[69] Burkhardt, H. and Cottingham, W.: Sum rules for forward virtual compton scattering. *Ann. Phys.*, vol. 56, no. 2, p. 453, 1970.

[70] Gottfried, K.: Sum rule for high-energy electron-proton scattering. *Phys. Rev. Lett.*, vol. 18, no. 25, p. 1174, 1967.

[71] Ellis, J. and Karliner, M.: Determination of α_S and the nucleon spin decomposition using recent polarized structure function data. *Phys. Lett. B*, vol. 341, no. 3, p. 397, 1995.

[72] Altarelli, G. and Parisi, G.: Asymptotic freedom in parton language. *Nucl. Phys. B*, vol. 126, no. 2, p. 298, 1977.

[73] Ji, X. and Chou, C.: QCD radiative corrections to the transverse spin structure function $\mathtt{g}_2(x, Q^2)$: Nonsinglet operators. *Phys. Rev. D*, vol. 42, no. 11, p. 3637, 1990.

[74] Jaffe, R.L. and Ji, X.: Studies of the transverse spin-dependent structure function $\mathtt{g}_2(x, Q^2)$. *Phys. Rev. D*, vol. 43, no. 3, p. 724, 1991.

[75] Altarelli, G., Nason, P. and Ridolfi, G.: On the Q^2 dependence of the measured polarized structure functions. *Phys. Lett. B*, vol. 320, p. 152, 1994.

[76] Weigel, H.: Nucleon structure functions in a chiral soliton model. *Nucl. Phys. A*, vol. 670, no. 1, p. 92, 2000.

[77] Anselmino, M., Efremov, A. and Leader, E.: The theory and phenomenology of polarized deep inelastic scattering. *Phys. Rep.*, vol. 261, no. 1, p. 1, 1995.

[78] Wandzura, S. and Wilczek, F.: Sum rules for spin-dependent electroproduction-test of relativistic constituent quarks. *Phys. Lett. B*, vol. 72, no. 2, p. 195, 1977.

[79] Ali, A., Braun, V. and Hiller, G.: Asymptotic solutions of the evolution equation for the polarized nucleon structure function $\mathrm{g}_2(x, Q^2)$. *Phys. Lett. B*, vol. 266, p. 117, 1991.

[80] Ralston, J.P. and Soper, D.E.: Production of dimuons from high-energy polarized proton-proton collisions. *Nucl. Phys. B*, vol. 152, no. 1, p. 109, 1979.

[81] Gamberg, L.P., Reinhardt, H. and Weigel, H.: Chiral odd structure functions from a chiral soliton. *Phys. Rev. D*, vol. 58, p. 054014, 1998.

[82] Wakamatsu, M.: Chiral odd distribution functions in the chiral quark soliton model. *Phys. Lett. B*, vol. 509, p. 59, 2001.

[83] Broniowski, W. and Ruiz-Arriola, E.: Partonic quasidistributions of the proton and pion from transverse-momentum distributions. *Phys. Rev. D*, vol. 97, no. 3, p. 034031, 2018.

[84] Broniowski, W. and Ruiz-Arriola, E.: Nonperturbative partonic quasidistributions of the pion from chiral quark models. *Phys. Lett. B*, vol. B773, p. 385, 2017.

[85] Alkofer, R. and Weigel, H.: Self-consistent solution to a fermion determinant with space dependent fields. *Comput. phys. commun.*, vol. 82, no. 1, p. 30, 1994.